Through the Horizon and Back: Lifting the Veil on Black Hole Thermodynamics

DISSERTATION

Presented in Partial Fulfillment of the Requirements
for the Degree Doctor of Philosophy
in the Graduate School of The Ohio State University

By

Madhur Mehta, B.S.,M.S.,M.S.

Graduate Program in Physics
The Ohio State University
2025

Dissertation Committee:

Samir D. Mathur, Ph.D., Advisor
Eric Braaten, Ph.D.
Richard J. Furnstahl, Ph.D.
Antonio Boveia, Ph.D.

Do not go gentle into that good night,
Old age should burn and rave at close of day;
Rage, rage against the dying of the light.

Though wise men at their end know dark is right,
Because their words had forked no lightning they
Do not go gentle into that good night...

Rage, rage against the dying of the light.

— D. Thomas

Abstract

Black holes provide a unique setting where the fundamental forces of nature intersect, offering a natural laboratory for novel physical phenomena and posing significant challenges to our understanding of quantum gravity.

This thesis investigates the thermodynamic and microscopic structure of black holes and their horizonless counterparts, Extremely Compact Objects (ECOs). We demonstrate that any ECO—defined as an object with radius $s_{\rm ECO}$ just outside the Schwarzschild radius of a black hole with mass M in d+1 dimensions, such that $s_{\rm ECO} \ll (M/m_p)^{2/(d-2)(d+1)} l_p$—exhibits thermodynamic behavior identical to black holes, despite lacking an event horizon. This result, derived using the back-reaction formalism via the Tolman-Oppenheimer-Volkoff (TOV) equation, establishes the universality of black hole thermodynamics independent of horizon formation or string-theoretic assumptions such as supersymmetry or extra dimensions.

In parallel, we investigate black hole microstates in the context of the 2D D1D5 conformal field theory (CFT). We present the conformal perturbation theoretic techniques developed to compute the lifting of superconformal primaries, their descendants and other states in the 2D CFT as the theory is deformed away from the orbifold point. We find a universal scaling law, lift $\sim \sqrt{h}$, where h is the conformal dimension and these results provide strong evidence for a universal structure in the second-order behavior of operator lifting, offering insight into how black hole microstates encode entropy in the dual CFT. Together, these lines of research contribute to a deeper understanding of horizonless black hole models, quantum gravity, and the microscopic origins of black hole thermodynamics.

The thesis concludes by addressing open questions across string theory, quantum gravity, and observational astrophysics, particularly concerning the implications of horizonless microstructure for gravitational wave signals and near-horizon structure in ECOs.

Dedicated to Didima...

Acknowledgments

My journey toward physics has been inspired, shaped, and propelled by countless individuals. It feels almost unjust to name only a few, knowing how many have nudged me forward, knowingly or unknowingly. Like a particle in Brownian motion, I have stumbled, collided, and been redirected—each encounter pushing me a little further along the path. But if I must name a few, I present them below. The names that follow are in no particular order—each has shaped my journey in their own meaningful way.

First and foremost, I would like to thank Didima. She remains the purest soul I have ever known. True to her nature, she would accept nothing more than a simple "thank you." May she rest in peace.

Next, I would like to thank my advisor, Prof. Samir D. Mathur. More than anyone and among many other things, he taught me how to think physics—not by getting lost in the technical machinery, but by seeking clarity about the heart of a problem before reaching for equations. His way of approaching deep questions with both simplicity and depth has left a lasting imprint on how I see the world. I do not know if I've fully learned this art yet, but I carry his lessons forward with deep gratitude and a determination to keep learning.

I would like to thank my family, especially my grandmother Choti Dadu, whose stories of Hindu mythology sparked in me a lifelong fascination with time, chaos, and the hidden science behind nature's mysteries. Those childhood debates lit the path that led me to the wonder and clarity of physics. To Papa and Mummy, whose entire lives have been a silent, tireless devotion to their children. In a world where selflessness is rare, they have always placed the three of us above their own needs and dreams. Every step I have taken, every milestone I've reached, rests on the foundation of their love, sacrifice, and unyielding belief in us. To Tanvi jija and Manvi jija—my sisters, my rivals, my unwavering support. Whether in laughter or debate, they have always stood by me, ready with love, wisdom, and strength whenever I needed them.

I would like to thank all my friends who have walked with me through different chapters of life. Your companionship, laughter, late-night debates, and quiet encouragement have made this journey not only bearable but beautiful. I would like to thank Obada Nairat, Harish Moni Prakash, Qazi Zulqurnain, Suriyaa Valliapan, Nagananda Krishnamurthy, Ayush Dhittal, Sang-Eon Bak, Seolhwa Kim, Richard Myers, Ranveer Kumar Singh, Gela Patashuri, Soumangsu Chakraborty, Manami Roy, Hosea Merritt, Savy Mudgal, Saisha

Singh, Mayank Choudhry, Apala Joshi, Sanchit Maheshwari, Devesh Dhamor, Mahesh Kotana, Arundhati Khenwar, Sonal, Sagar Meena, Tejas Somvanshi, V. Sresta, Keshav Das Agarwal, Shobhna Singh, Nupur Khatu, Kunal Suri, Avnip Kapur, Zardo Becker, Brian Sun, Jeremy Borden, Fareed Alasiri and Justin Pickett. A special thanks to Ayan Gupta, who has patiently and wholeheartedly engaged with my endless stream of questions, ideas, and theories since we were kids—his curiosity and friendship have meant more than words can say. To Abhijeet Mishra, whose quiet strength and unwavering support have carried me through some of the toughest moments—thank you for always being there. To Brandon Manley, for our daily philosophical and technical duels that pushed me to think sharper and deeper. To Naeem Bharmal, whose ambition, clarity, and drive have been both inspiring and grounding. And to Shreyas Samaga, whose quiet brilliance, discipline, and meticulous care have been nothing short of extraordinarily inspiring.

I would also like to thank all my teachers since childhood. I would especially like to thank Neelu Ma'am, Neeta Ma'am, Rita Ma'am, Sindhu Ma'am, Arundhati Ma'am, Neelam Ma'am, Dheeraj Sir, Seema Ma'am, Karuna Ma'am, Madhubala Ma'am, Arshi Ma'am, Udipt Sir, Nitesh Sir, Hemant Sir, and Shivbala Ma'am. In my academic journey, I would like to thank Prof. Suhas Gangadhariah, Prof. Auditya Sharma, Prof. Surajit Saha, Prof. Shuji Hasegawa, Prof. Sebastian Boeser, Prof. Sukanta Panda, Prof. Nabamita Banerjee, Prof. Ambar Jain, Prof. Romie Banerjee, Prof. Subhash Chaturvedi, Prof. Yuri Kovchegov, Prof. Brian Skinner, and Prof. Mohit Randeria. Also, my committee members Prof. Eric Braaten, Prof. Richard J. Furnstahl and Prof. Antonio Boveia.

I would also like to thank Prof. John Beacom. Though our fields within physics are quite different, his advice and support throughout my PhD journey have been nothing short of that of an advisor. Our discussions—thoughtful, generous, and filled with clarity—have taught me invaluable lessons, and I owe a great deal to his guidance and kindness.

I would also like to thank my collaborators—Prof. Pierre Heidmann, Bin Guo, Marcel Hughes, and Suvendu Giri—for their invaluable insights, mentorship, and the many things they have taught me along the way. I am especially grateful to Pierre, whose guidance helped me grow both intellectually and personally, and whose support during difficult times meant more than I can express.

I would also like to thank Prof. Steven B. Giddings for his generous support and for sharing the opportunity of the Heising-Simons Fellowship. His encouragement has been deeply meaningful to me. I look forward to working with Prof. Giddings and Prof. Kathryn Zurek during my postdoc.

Lastly, I would like to thank you, Katie. I don't know if words can truly capture how grateful I am for you. Your presence has been a constant source of motivation and inspiration, pushing me to become not just a better physicist, but a better human being. In my moments of pain and struggle, your smile and support have always made the burden lighter. Thank you—always and forever.

Vita

Date of Birth ..... November 17, 1995

Place of Birth ..... Jaipur, Rajasthan, India

B.S.-M.S. in Physics ..... IISER Bhopal, India, (2015-2020)

Graduate Teaching Assistant ..... The Ohio State University,
Columbus, OH, USA, (2021–2022)

M.S. in Physics ..... The Ohio State University,
Columbus, OH, USA, (2021-2022)

Summer Research Advisor ..... The Ohio State University,
Columbus, OH, USA, (May–July 2024)

Graduate Research Associate ..... The Ohio State University,
Columbus, OH, USA, (2021-2024)

Presidential Fellow ..... The Ohio State University,
Columbus, OH, USA, (2024-present)

Ph.D. in Physics ..... The Ohio State University,
Columbus, OH, USA,
(2021-2025 (expected))

Heising-Simons Fellow ..... UC Santa Barbara, CA, USA, (Fall 2025)

Publications

Peer-Reviewed Articles

1. *The Fuzzball Paradigm*
   Samir D. Mathur, **Madhur Mehta** - arxiv: 2412.09495 [hep-th] (Submitted as a book chapter in "The Black Hole Information Paradox", to be published by Springer Singapore in July 2025.)

2. *The universal thermodynamic properties of Extremely Compact Objects*
   Samir D. Mathur, **Madhur Mehta** - Classical and Quantum Gravity, Volume 41, Number 23, arxiv: 2402.13166 [hep-th]

3. *Electromagnetic Entrapment in Gravity*
   Pierre Heidmann, **Madhur Mehta** - JHEP 03 (2024) 046, arXiv: 2312.11607 [hep-th]

4. *Lifting of superconformal descendants in the D1-D5 CFT*
   Marcel R.R. Hughes, Samir D. Mathur, **Madhur Mehta** - JHEP 04 (2024) 129, arXiv: 2311.00052 [hep-th]

5. *Lifting of two-mode states in the D1-D5 CFT*
   Marcel R.R. Hughes, Samir D. Mathur, **Madhur Mehta** - JHEP 01 (2024) 183, arxiv: 2309.03321 [hep-th]

6. *The universality of black hole thermodynamics*
   Samir D. Mathur, **Madhur Mehta** - Int.J.Mod.Phys.D 32 (2023) 14, 2341003, arxiv: 2305.12003 [hep-th]

7. *Universal lifting in the D1-D5 CFT*
   Bin Guo, Marcel R.R. Hughes, Samir D. Mathur, **Madhur Mehta** - JHEP 10 (2022) 148, arxiv: 2208.07409 [hep-th]

8. *Contrasting the fuzzball and wormhole paradigms for black holes*
   Bin Guo, Marcel R.R. Hughes, Samir D. Mathur, **Madhur Mehta** - Turk.J.Phys. 45 (2021) 6, 281-365, arxiv: 2111.05295 [hep-th]

Preprints

1. *Extreme Compactness, Extreme Gravity: Higher-Derivative Corrections to ECOs*
   Madhur Mehta - arXiv:2505.09049 [hep-th]

2. *Redefining entanglement entropy - can it solve the information paradox?*
   Madhur Mehta - arxiv:2204.00192 [hep-th]

Contents

Abstract iii

Acknowledgments v

Vita vii

Publications viii

Contents ix

List of Figures xiii

List of Tables xv

1 Introduction 1

2 Black Holes in General Relativity 7

2.1 Preliminaries 8

2.1.1 Postulates of General Relativity 8

2.1.2 Einstein's field equations 8

2.2 Schwarzschild Black Hole 9

2.2.1 Tortoise Coordinate 10

2.2.2 Eddington-Finkelstein Coordinates 10

2.2.3 Kruskal-Szekeres Coordinates 11

2.2.4 Near-Horizon Limit: Rindler space 12

2.3 Reissner-Nordström Black Hole 13

2.3.1 Extremal black holes 14

2.4 Kerr Black Hole 16

2.4.1 Ergosphere for the Kerr metric 17

2.4.2 Penrose process: Spinning black holes can radiate 17

2.5 The AdS Spacetime 18

2.5.1 Basics 18

2.5.2 BTZ Black Hole 18

2.6 Black Hole theorems . . . 19
2.6.1 Birkhoff's theorem . . . 19
2.6.2 Israel's Uniqueness theorem . . . 19
2.6.3 No hair theorem . . . 20
2.6.4 Hawking's Area theorem . . . 20

3 Black Hole Thermodynamics . . . 21
3.1 Quantum Field Theory in Curved Spacetime . . . 21
3.1.1 Scalar field in curved spacetime . . . 22
3.1.2 Bogoliubov transformations and particle production . . . 23
3.2 Hawking Radiation . . . 24
3.2.1 Original style derivation . . . 24
3.2.2 Near horizon derivation . . . 29
3.2.3 Different vacua in curved spacetime . . . 32
3.3 The Four Laws of Black Hole Thermodynamics . . . 32
3.4 The Black Hole Information Paradox . . . 34

4 Black Holes in String Theory . . . 36
4.1 The Geometric Description of the D1D5 System . . . 37
4.2 The CFT Description of the D1D5 System . . . 38
4.3 The Fuzzball Paradigm . . . 39
4.3.1 The *naive* NS1-P solution . . . 39
4.3.2 The *true* NS1-P solution . . . 40
4.3.3 The D1D5 versions . . . 40
4.4 The Black Hole Information Paradox: Revisited . . . 42

5 Lifting in D1D5P system . . . 44
5.1 Conformal perturbation theory on the cylinder . . . 45
5.1.1 CFT Setup . . . 45
5.1.2 Degenerate states and perturbation . . . 46
5.1.3 Extraction of anomalous dimensions . . . 47
5.2 General expression for lifting at second order . . . 49
5.2.1 The lifting method . . . 52
5.3 Lifting of Superconformal Primaries . . . 55
5.3.1 Superconformal Primaries: Definition . . . 55
5.3.2 Superconformal Primaries: Building the state . . . 56
5.3.3 Superconformal Primaries: Simplifying the set . . . 58
5.3.4 Lift for superconformal primaries . . . 59
5.4 Lifting of Superconformal Descendants . . . 61
5.4.1 Superconformal Descendants: Definition and states . . . 61

5.4.2 Lift for G descendant . . . 62
5.4.3 Lift for J descendant . . . 64
5.5 Analytic form and asymptotic behavior . . . 66
5.5.1 Analytic expressions . . . 66
5.5.2 Asymptotic behavior . . . 68
5.6 Lifting of single-copy two-mode states . . . 69
5.6.1 The states . . . 69
5.6.2 Lifting of $|\alpha\alpha\rangle_{B\dot{B}A\dot{A}(m,n)}$ . . . 70
5.6.3 Lifting of $|\alpha d\rangle^{\alpha A}_{B\dot{B}(m,s)}$ . . . 74
5.6.4 Lifting of $|dd\rangle^{\beta B\alpha A}_{(r,s)}$ . . . 77
5.7 Relations between lifts . . . 80
5.7.1 L_{-1} relations . . . 80
5.7.2 $G^{\alpha}_{\dot{A},-\frac{1}{2}}$ relations . . . 82
5.7.3 Using lifting relations to perform checks . . . 84
5.8 Chapter Summary . . . 89

6 The Universality of Black Hole Thermodynamics . . . 91
6.1 Extremely Compact Objects . . . 92
6.1.1 Geometric Setup and the First ECO Condition . . . 92
6.1.2 Gravitational Redshift and the Second ECO Condition . . . 94
6.1.3 Minimal Exterior Energy and the Third ECO Condition . . . 94
6.2 The vacuum stress-energy near an ECO . . . 96
6.2.1 The vacuum stress-tensor near a black hole horizon . . . 97
6.2.2 The stress tensor near an ECO . . . 98
6.2.3 The ECO at a general temperature T . . . 100
6.3 Using the Tolman-Oppenheimer-Volkoff equation . . . 101
6.3.1 Assumptions for the TOV equation . . . 101
6.3.2 Approximating the TOV equation . . . 102
6.3.3 Analyzing the approximate TOV solution . . . 108
6.3.4 Checking the consistency of condition ECO3 . . . 112
6.4 Chapter Summary . . . 114

7 Future Outlook and Discussion . . . 116
7.1 Charged ECOs . . . 116
7.2 ECOs in Higher Derivative Gravity . . . 117
7.3 Electromagnetic Entrapment in Different Spacetimes . . . 118
7.4 The VECRO Hypothesis . . . 118
7.5 Lifting and Chaos . . . 119
7.6 Rotating ECOs, Kerr Uniqueness and Observations . . . 119

7.7 Closing Remarks . . . 120

A Gravity Appendix . . . 121

A.1 Surface gravity κ . . . 121

A.2 A relation following from condition ECO 1 . . . 122

A.3 A heuristic argument for the relation $T_{\mathrm{ECO}} \approx T_{\mathrm{H}}$ . . . 123

A.3.1 The energy of radiation near the ECO . . . 123

A.3.2 An outline of the argument . . . 126

A.3.3 Defining a useful scale Δr_{crit} . . . 128

A.3.4 The argument for $T_{\mathrm{ECO}} < T_{\mathrm{H}}$ . . . 129

A.3.5 The estimate for $T_{\mathrm{ECO}} > T_{\mathrm{H}}$ . . . 129

B CFT Appendix . . . 132

B.1 The $\mathcal{N} = 4$ superconformal algebra . . . 132

B.1.1 Commutation relations . . . 132

B.1.2 Relations involving the twist operator $\sigma_2^{\alpha\dot{\alpha}}$ . . . 133

B.1.3 Rules for Hermitian conjugation . . . 133

B.2 Transformation rules under spectral flow . . . 135

B.2.1 Operators on the cylinder . . . 135

B.2.2 Operators on the plane . . . 138

B.3 Choice of the deformation operator . . . 143

B.4 Choice of ground states . . . 144

B.5 Mapping amplitude relations to lift relations . . . 145

Bibliography . . . 148

List of Figures

1.1 Schematic idea of fuzzballs 3

2.1 The figure represents the Penrose diagram of the Schwarzschild black hole in Kruskal-Szekeres coordinates. Various important locations have been marked. 12

2.2 The figure represents an extremal black hole depicting its salient features. 15

3.1 The figure shows a collapsing shell of null quanta moving radially inwards at $v = v_0$. The figure also labels the different spacetime regions as mentioned in the text of this Section. 24

4.1 Naive vs true string geometry 41

5.1 The lifting problem setup 50

5.2 Contour integrals for lifting in D1D5 CFT 51

5.3 Plot of the lifts of superconformal primaries as a function of h 60

5.4 Plot of the lifts $E^{(2)}\left(|G\phi\rangle^{+}_{+(1,s)}\right)/\lambda^2$ for varying s 63

5.5 Plot of the lifts $E^{(2)}\left(|G\phi\rangle^{+}_{+(h,1/2)}\right)/\lambda^2$ for varying h 63

5.6 Plot of the lifts $E^{(2)}\left(|G\phi\rangle^{+}_{+(h,h-1/2)}\right)/\lambda^2$ for varying h 64

5.7 Plot of the lifts $E^{(2)}\left(|J\phi\rangle^{+}_{(1,n)}\right)/\lambda^2$ for varying n 65

5.8 Plot of the lifts $E^{(2)}\left(|J\phi\rangle^{+}_{(h,1)}\right)/\lambda^2$ for varying h 65

5.9 Plot of the lifts $E^{(2)}\left(|J\phi\rangle^{+}_{(h,h)}\right)/\lambda^2$ for varying n 65

5.10 Schematic description of the use of Ward identities in lift derivation . . . 66

5.11 Plot of the lifts $E^{(2)}(|\alpha\alpha\rangle_{++++(1,n)})/\lambda^2$ for varying n 73

5.12 Plot of the lifts $E^{(2)}(|\alpha\alpha\rangle_{++++(2,n)})/\lambda^2$ for varying n 73

5.13 Plot of the lifts $E^{(2)}(|\alpha\alpha\rangle_{++++(n,n)})/\lambda^2$ for varying n 74

5.14 Plot of the lifts $E^{(2)}\left(|\alpha d\rangle^{--}_{++(1,s)}\right)/\lambda^2$ for varying s 76

5.15 Plot of the lifts $E^{(2)}\left(|\alpha d\rangle^{--}_{++(n,1/2)}\right)/\lambda^2$ for varying n 77
5.16 Plot of the lifts $E^{(2)}\left(|dd\rangle^{----}_{(3/2,s)}\right)/\lambda^2$ for varying s 79
5.17 Schematic description of the derivation of lift relations 81

6.1 Wave modes in a highly redshifted geometry 100
6.2 $T_{\rm ECO} < T_{\rm H}$ argument 109
6.3 $T_{\rm ECO} > T_{\rm H}$ argument 110

List of Tables

2.1 Comparison of various coordinate systems used in Schwarzschild spacetime. 13

Chapter 1

Introduction

> *Of all the conceptions of the human mind from unicorns to gargoyles to the hydrogen bomb perhaps the most fantastic is the black hole: a hole in space with a definite edge over which anything can fall and nothing can escape; a hole with a gravitational field so strong that even light is caught and held in its grip; a hole that curves space and warps time.*
>
> — Kip Thorne

A Brief History

Black holes represent the frontier of our understanding of gravity and quantum mechanics, lying at the intersection where both theories must be invoked. In classical general relativity, black holes arise as solutions to Einstein's equations describing regions of spacetime with an event horizon—a boundary beyond which signals cannot escape. Formed through the gravitational collapse of massive stars, these objects are characterized solely by their mass, charge, and angular momentum, as dictated by the no-hair theorem.

Traditionally, black holes were believed to be purely absorptive: any matter or radiation that crossed the horizon would be lost forever. However, this view was radically altered by Hawking's discovery [1] that black holes emit thermal radiation—now known as *Hawking radiation*—due to quantum effects near the horizon. This radiation lacks any imprint of the initial state that formed the black hole, leading to the celebrated *black hole information paradox*: if black holes evaporate completely, the information about their initial state appears lost, violating unitarity—a foundational principle of quantum mechanics.

Further deepening the puzzle, Bekenstein had earlier proposed that black holes possess entropy proportional to the area of their event horizon [2]. This relation, later supported

by Hawking's calculation, takes the form:

$$S_{\text{Bek}} = \frac{A_{\text{hor}}}{4G_N}\,, \tag{1.1}$$

where A_{hor} is the horizon area and G_N is Newton's constant. Entropy, as understood in statistical mechanics, counts the number of microstates consistent with a given macroscopic configuration. Yet black holes, in the classical picture, lack any internal degrees of freedom, making this entropy enigmatic.

Attempts to resolve the paradox using semiclassical physics have been shown insufficient. The no-hair theorem and the small-corrections theorem indicate that perturbative or small corrections to Hawking's calculation cannot restore unitarity or encode information in the radiation. A dramatic departure from the conventional picture appears necessary.

These issues raise foundational questions:

> *How can black holes radiate in a unitary manner while maintaining thermodynamic consistency? Where do the microstates responsible for entropy reside, and how can they be described in a complete theory of quantum gravity?*

These challenges have positioned black holes as powerful probes into the nature of spacetime, thermodynamics, and quantum information, and have catalyzed much of the modern development in quantum gravity.

Toward a Resolution

One of the most promising candidates for a complete theory of quantum gravity is string theory. General relativity, while successful at macroscopic scales, is plagued by ultraviolet divergences that render it non-renormalizable at high energies. String theory naturally resolves these issues: the extended nature of fundamental strings introduces an intrinsic ultraviolet cutoff at the string length scale l_s, smoothing out short-distance singularities. Moreover, in the low-energy limit—at length scales much larger than l_s—the Einstein-Hilbert action emerges as an effective description, thereby recovering general relativity.

Remarkably, certain classes of black holes in string theory allow for precise microstate counting. These computations [3] provide a statistical explanation for the Bekenstein-Hawking entropy and offer deep insights into the microscopic origin of black hole thermodynamics. In particular, the *fuzzball paradigm* [4,5] offers a compelling resolution to the black hole information paradox. According to this proposal, black hole microstates are described by horizonless, smooth geometries composed of strings and branes—fuzzballs—which are indistinguishable from classical black holes at large distances. This framework challenges the conventional notion of an event horizon and suggests that the quantum structure of

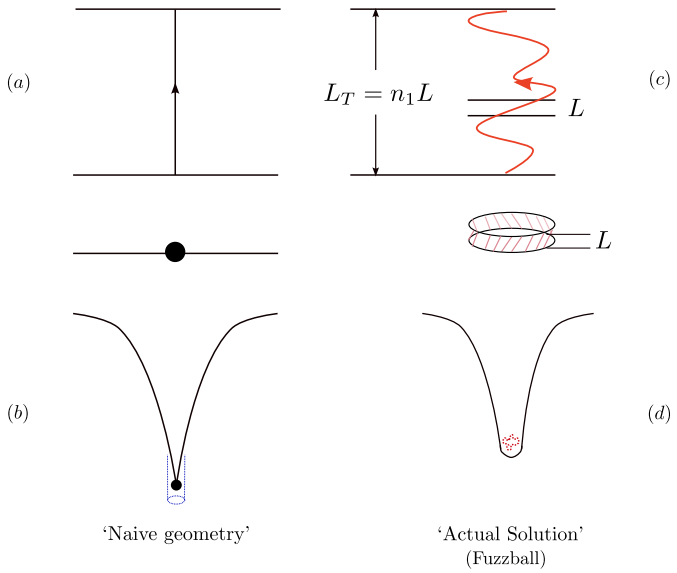

Figure 1.1: (a) If a string could carry momentum as a longitudinal wave, then it would generate a spherically symmetric geometry. (b) This 'naive' geometry would have a singular horizon at leading order, but α' corrections turn this singularity into a regular horizon. (c) The actual string of string theory has only transverse vibrations, which break spherical symmetry and cause the string to spread out over these transverse directions. (d) The resulting geometry is a 'fuzzball' with no horizon.

black holes is far richer than the classical picture implies. Some of the salient features of this paradigm are

1. **Absence of a horizon**: Analysis of the 2 charge construction as seen in section 4.3 that none of the microstates (4.14) have a horizon. There are regions in the solution where the redshift goes to infinity, but there is no closed trapped surface, and light rays can escape to infinity from any point in these geometries. In [6–9], simple examples of extremal solutions were constructed with NS1, NS5 and P charges; i.e. these solutions carried the charges of the Strominger-Vafa black hole. In each case, the solution was a fuzzball; i.e, there was no horizon.

2. **Lack of spherical symmetry**: The 2 charge fuzzball solutions are not spherically symmetric. If we impose spherical symmetry on the low energy gravity solution, then we get the *naive* metric as shown in Figure 1.1 below. We will return to a more detailed explanation of the figure in section 4.3. This naive metric is not realized in string theory, because it is not possible to add a momentum carrying wave to the string without breaking spherical symmetry. This in turn follows from the fact that the fundamental string has no longitudinal vibration mode; it only allows transverse vibrations, and the polarization of this vibration at any point along the string must break the spherical symmetry in the angular S^3 directions or the symmetry in the T^4.

3. **The microscopic count of black hole entropy** Given that there is no horizon, one might wonder what happens to the Bekenstein entropy relation (1.1). The microstates have the structure of flat space at infinity, then a *neck* which leads to a *throat*, and this throat ends in a *cap*. The geometries are almost identical everywhere except in the cap; thus this cap contains the detailed information of the choice of microstate. The Bekenstein entropy relation for fuzzballs tells us the number of orthogonal gravity solutions that we can fit in a given cap region. The area of the surface that encloses this region satisfies the relation

$$\frac{A}{G} \sim \sqrt{n_1 n_p} \sim S_{micro}\,. \tag{1.2}$$

   The computations of S_{micro} like in the works of [3] were performed at weak coupling using the dual CFT description, while the fuzzball solutions are constructed at strong coupling. In [10], the moduli space of regular D1-D5 microstates was quantized, directly from Type IIB SUGRA *i.e.*, the solutions obtained at strong coupling, was quantized and still shown to yield the entropy S_{micro}.

4. **Non-extremal fuzzballs and Hawking radiation**: Extremal holes do not radiate. Thus while extremal fuzzballs tell us something about the structure of black holes, we should construct non-extremal microstates to understand radiation from the hole and the resolution of the information paradox.

   In [11] a family of non-extremal D1D5P microstates were constructed. These solutions were again found to be fuzzballs; i.e., they had no horizon. They did have an ergoregion, and the emission from this ergoregion was computed in [12]. In [13–15] it was found that this emission spectrum was exactly the spectrum of Hawking radiation that was expected from these very non-generic microstates.

Questions Still Remain

Despite these promising advances, several fundamental questions in black hole physics remain unresolved. Most notably, while fuzzball constructions have demonstrated the existence of horizonless microstates for certain supersymmetric and extremal black holes, it remains unclear whether a complete basis of such solutions exists that fully accounts for black hole entropy in the non-extremal and astrophysical regime. Furthermore, the mechanism by which semiclassical thermodynamics—particularly the universality of the Bekenstein-Hawking entropy and Hawking radiation—emerges from a statistical ensemble of horizonless microstates is still under active investigation. From a dual CFT perspective, the lifting of BPS states as one moves away from the orbifold point in moduli space introduces additional complexity in identifying the full microstate spectrum.

These open questions motivate the exploration of generic, non-supersymmetric black hole analogues—such as Extremely Compact Objects (ECOs)—and call for new tools to study horizon-scale structure, information recovery, and quantum gravity signatures in a broader class of systems.

Some Contributions

In this thesis, we investigate how black hole thermodynamics can be understood without invoking classical event horizons. In a series of works with S. D. Mathur [16, 17], we demonstrated that any *Extremely Compact Object (ECO)*—an entity with a radius a small distance outside the Schwarzschild radius—exhibits the same thermodynamic properties as classical black holes. Using a semiclassical back-reaction analysis based on the Tolman-Oppenheimer-Volkoff (TOV) equation, we showed that quantum vacuum polarization forces any such object to have the same thermodynamics as a black hole of the same mass. These results provide compelling evidence for the *universality of black hole thermodynamics* even in the absence of horizons. Notably, this analysis does not rely on string-theoretic features such as supersymmetry or extra dimensions, thereby offering a model-independent testbed for quantum gravitational effects in semiclassical astrophysical systems. We present the details in Chapter 6.[1]

In parallel, we have studied the microscopic structure of a special class of black holes called the D1D5 black holes within the framework of string theory and the AdS/CFT correspondence. Specifically, in the D1-D5 conformal field theory, we have explored the phenomenon of BPS state lifting away from the free orbifold point. In our works [18–20] on universal lifting, we discovered that the lifting of the class of superconformal primary states depends solely on their conformal dimension h, with the lifting following a universal scaling: lift $\sim \sqrt{h}$. Subsequent investigations expanded this analysis to include two-mode states and descendants of superconformal primaries within a two-parameter deformation space. These results reinforce the conjecture that the second-order expectation value of operator lifts scales universally as $\sim \sqrt{h}$ in the large h limit. This scaling behavior has deep implications for understanding which states remain BPS and how the semiclassical geometry emerges from the dual CFT, thereby shedding light on the microscopic origins of black hole entropy. We present this direction in Chapter 5

Together, these investigations bridge the macroscopic thermodynamic properties of black holes and ECOs with the microscopic structure described by quantum field theory and string theory, advancing our understanding of black hole microphysics and the information paradox.

[1] It should be noted that only static ECOs have been constructed here and work on charged and/or rotating ECOs is still in progress.

Plan of the Thesis

This thesis is organized as follows. In Chapter 2, we review the classical theory of black holes within general relativity, including key solutions such as Schwarzschild, Reissner-Nordström, and Kerr black holes. We also introduce anti-de Sitter spacetimes and important theorems such as the no-hair theorem and Birkhoff's theorem. Chapter 3 covers black hole thermodynamics, beginning with quantum field theory in curved spacetime and progressing to Hawking radiation, the four laws of black hole thermodynamics, and the black hole information paradox. Chapter 4 presents the string-theoretic perspective, focusing on the D1-D5 system and the fuzzball paradigm as a candidate resolution to the information paradox. In Chapter 5, we examine the lifting of states in the D1-D5-P conformal field theory, providing a detailed computation of anomalous dimensions, including for superconformal primaries, descendants, and two-mode states. Chapter 6 introduces the concept of Extremely Compact Objects (ECOs) and demonstrates their thermodynamic equivalence with black holes using semiclassical back-reaction analysis. Finally, the thesis ends with Chapter 7 discussing possible future directions and providing a general discussion.

Chapter 2

Black Holes in General Relativity

> *Black holes are macroscopic objects with masses varying from a few solar masses to millions of solar masses. To the extent they may be considered as stationary and isolated, to that extent, they are all, every single one of them, described exactly by the Kerr solution. This is the only instance we have of an exact description of a macroscopic object. Macroscopic objects, as we see them all around us, are governed by a variety of forces, derived from a variety of approximations to a variety of physical theories. In contrast, the only elements in the construction of black holes are our basic concepts of space and time. They are, thus, almost by definition, the most perfect macroscopic objects there are in the universe. And since the general theory of relativity provides a unique two-parameter family of solutions for their description, they are the simplest objects as well.*
>
> — Subrahmanyan Chandrasekhar

General relativity extends the principles of special relativity to include gravity, marking a profound departure from Newtonian gravitation. This theoretical leap introduced the radical notions of black holes and spacetime singularities, fundamentally reshaping our understanding of the gravitational interaction.

In this chapter, we provide a concise review of classical black hole solutions and the geometric structures they exhibit. Our goal is to equip the reader with essential tools and concepts that serve as a foundation for the thermodynamic properties of black holes, which will be the focus of the next chapter. In this context, we also present the laws of black hole mechanics and their eventual formulation into thermodynamic laws.

2.1 Preliminaries

2.1.1 Postulates of General Relativity

Einstein was guided by a set of profound physical principles in formulating general relativity. We list below the set of principles that, in my view, not only guided him but also deepen our appreciation of the theory's conceptual foundation.[1]

P1. Mach's Principle:
The local inertial properties of a system are influenced by the global distribution of matter in the universe. Inertia arises from interactions with the mass-energy content of the cosmos, emphasizing the relational nature of motion.

P2. Principle of Equivalence:
No local experiment can distinguish between uniform acceleration and a uniform gravitational field. A freely falling observer in a gravitational field experiences physics identical to that in inertial motion in absence of gravitation.

This realization is what Einstein famously described as "*the happiest thought of my life.*"

P3. Principle of General Covariance:
The laws of physics must take the same mathematical form in all coordinate systems. No coordinate system is physically privileged, and all laws must be expressed in generally covariant form.

2.1.2 Einstein's field equations

Building on these principles, one is naturally led to the Einstein field equations of general relativity,[2] which relate spacetime curvature to the distribution of matter and energy:

$$G_{\mu\nu} + \Lambda g_{\mu\nu} = 8\pi G_N T_{\mu\nu} \ , \tag{2.1}$$

where $G_{\mu\nu}$ is the Einstein tensor, $g_{\mu\nu}$ is the metric tensor, $T_{\mu\nu}$ is the stress–energy tensor, Λ is the cosmological constant and G_N is the Newton's gravitational constant. The Einstein tensor $G_{\mu\nu}$ is defined as

$$G_{\mu\nu} = R_{\mu\nu} - \frac{1}{2} g_{\mu\nu} R \, , \tag{2.2}$$

[1] For a detailed analysis see [21]
[2] For standard references on general relativity, see [22–26].

where $R_{\mu\nu}$ is the Ricci curvature tensor, and R is the Ricci scalar curvature. The Ricci curvature tensor $R_{\mu\nu}$ is the contracted Riemann tensor $R^{\rho}{}_{\mu\rho\nu}$ defined as

$$\begin{aligned} R^{\alpha}{}_{\beta\mu\nu} &= \partial_\mu \Gamma^{\alpha}{}_{\beta\nu} - \partial_\nu \Gamma^{\alpha}{}_{\beta\mu} + \Gamma^{\alpha}{}_{\sigma\mu}\Gamma^{\sigma}{}_{\beta\nu} - \Gamma^{\alpha}{}_{\sigma\nu}\Gamma^{\sigma}{}_{\beta\mu} \\ \Gamma^{\alpha}{}_{\beta\nu} &= \frac{g^{\alpha\gamma}}{2}\left(\partial_\beta g_{\gamma\nu} + \partial_\nu g_{\gamma\beta} - \partial_\gamma g_{\beta\nu}\right) . \end{aligned} \tag{2.3}$$

in terms of Christoffel symbols $\Gamma^{\alpha}{}_{\beta\nu}$ and the Christoffel symbols $\Gamma^{\alpha}{}_{\beta\nu}$ are given in terms of the metric tensor $g_{\gamma\nu}$.

2.2 Schwarzschild Black Hole

One of the simplest solutions[3] to Einstein's equations is the vacuum solution of the Schwarzschild metric [27]. The solution is characterized by parameter M, which is the total energy in the spacetime as seen by an observer at infinity. The line element of the solution has the form

$$ds^2 = -\left(1 - \frac{2M}{r}\right) dt^2 + \left(1 - \frac{2M}{r}\right)^{-1} dr^2 + r^2\left(d\theta^2 + \sin\theta d\phi^2\right) . \tag{2.4}$$

One can model such a black hole using the Oppenheimer–Snyder model of gravitational collapse[4] [29], where a spherically symmetric dust cloud collapses under its own gravity to form a Schwarzschild black hole. This idealized scenario provides valuable insights into the formation of horizons and singularities in general relativity.

It is easy to see that the Ricci scalar $R = 0$ for the solution above as expected from a vacuum solution. The Schwarzschild black hole has a real spacelike singularity at $r = 0$ as seen by calculating the Kretschmann scalar:

$$\mathcal{R} \equiv R_{abcd}R^{abcd} = \frac{48M^2}{r^6} , \tag{2.5}$$

which blows up at only $r = 0$.

Clearly, the surface $r = 2M$ is not pathological and thus the solution only has a coordinate singularity at $r = 2M$. The Schwarzschild coordinates (t, r) do not cover the whole spacetime because of this coordinate singularity and it is unclear if we can trust the spacetime for $r < 2M$. We can circumvent the need to find another patch for $r < 2M$ by finding a "good" coordinate system that is smooth everywhere in the following way:

[3] Unless explicitly stated otherwise, we will set the cosmological constant $\Lambda = 0$ throughout this work.
[4] See [28] for a good review on the Oppenheimer-Snyder model of gravitational collapse.

2.2.1 Tortoise Coordinate

We start by defining the Regge-Wheeler coordinate [30] or more commonly known as the tortoise coordinate r^* by

$$dr^{*2} = \left(1 - \frac{2M}{r}\right)^{-2} dr^2 \,, \tag{2.6}$$

which gives

$$r^* = r + 2M \ln\left(\frac{r}{2M} - 1\right), \tag{2.7}$$

defined for $-\infty < r^* < \infty$. So, we have practically shifted the horizon $g^{rr} = 0 \implies r = 2M$ to $r^* = -\infty$. In this new coordinate system we see that the line element takes a form which is well suited to describe the path of light rays traveling in the radial direction

$$ds^2 = 0 \implies \frac{dr^*}{dt} = \pm 1 \implies t \pm r^* = const \,. \tag{2.8}$$

2.2.2 Eddington-Finkelstein Coordinates

If one defines the radial null geodesics by coordinates v, u, we get the Eddington-Finkelstein coordinate system [31, 32].

Ingoing EF coordinates

We define the ingoing coordinate by $v = t + r^*$. The ingoing coordinates are (v, r), then we find the line element takes the form

$$ds^2 = -\left(1 - \frac{2M}{r}\right) dv^2 + 2dvdr + r^2\left(d\theta^2 + \sin\theta d\phi^2\right) \,. \tag{2.9}$$

This coordinate system is regular across the future event horizon at $r = 2M$ and is adapted to infalling observers. It covers the black hole exterior and interior up to the singularity, smoothly crossing the future horizon.

Outgoing EF coordinates

Similarly we define the outgoing coordinate by $u = t - r^*$ and in the outgoing coordinates (u, r), we find the line element takes the form

$$ds^2 = -\left(1 - \frac{2M}{r}\right) du^2 - 2dudr + r^2\left(d\theta^2 + \sin\theta d\phi^2\right) \,. \tag{2.10}$$

This form is regular across the past event horizon and is adapted to outgoing null geodesics. It describes white hole regions—time-reverses of black holes—and again covers both the

interior and exterior, but now across the past horizon.

These two coordinate systems reflect two different extensions of Schwarzschild spacetime. The ingoing EF chart naturally includes the future horizon and black hole interior, while the outgoing EF chart encompasses the past horizon and white hole interior. Each provides a partial extension of the original Schwarzschild patch.

But this naturally raises the question: can we do better? Is there a way to extend the spacetime maximally, including both horizons and both interiors in a single, unified coordinate system? The answer is yes—and it leads us to the Kruskal-Szekeres coordinates, which describe the maximal analytic extension of the Schwarzschild solution[5].

2.2.3 Kruskal-Szekeres Coordinates

While EF coordinates extend the Schwarzschild metric across either the future or past horizon, they remain singular at one side of the horizon. Kruskal-Szekeres coordinates [33, 34] offer a maximal analytic extension, covering both regions smoothly.

Starting with the EF outgoing and ingoing coordinates (u, v), we find

$$ds^2 = -\left(1 - \frac{2M}{r}\right) du dv + r^2 \left(d\theta^2 + \sin\theta d\phi^2\right) . \tag{2.11}$$

To remove the metric degeneracy at $r = 2M$, we can introduce the coordinates

$$U = -e^{-\frac{u}{4M}} , \quad V = e^{\frac{v}{4M}} , \tag{2.12}$$

with which the line element becomes

$$ds^2 = -\frac{32\, M^3}{r} e^{-\frac{r}{2M}} dU dV + r^2 \left(d\theta^2 + \sin\theta d\phi^2\right) . \tag{2.13}$$

The radial and time coordinates are then defined as

$$UV = -\left(\frac{r}{2M} - 1\right) e^{\frac{r}{2M}} , \quad \frac{U}{V} = -e^{-\frac{t}{2M}} . \tag{2.14}$$

This form of the metric is manifestly regular at the Schwarzschild horizon $r = 2M$, removing the coordinate singularity present in Schwarzschild and EF coordinates. The only true singularity occurs at $r = 0$, as evidenced by the divergence of the Kretschmann scalar. We depict the Penrose diagram for the Kruskal extension of the Schwarzschild black hole in Figure 2.1.

[5] Simply writing the metric in u, v coordinates does not help as can be readily checked!

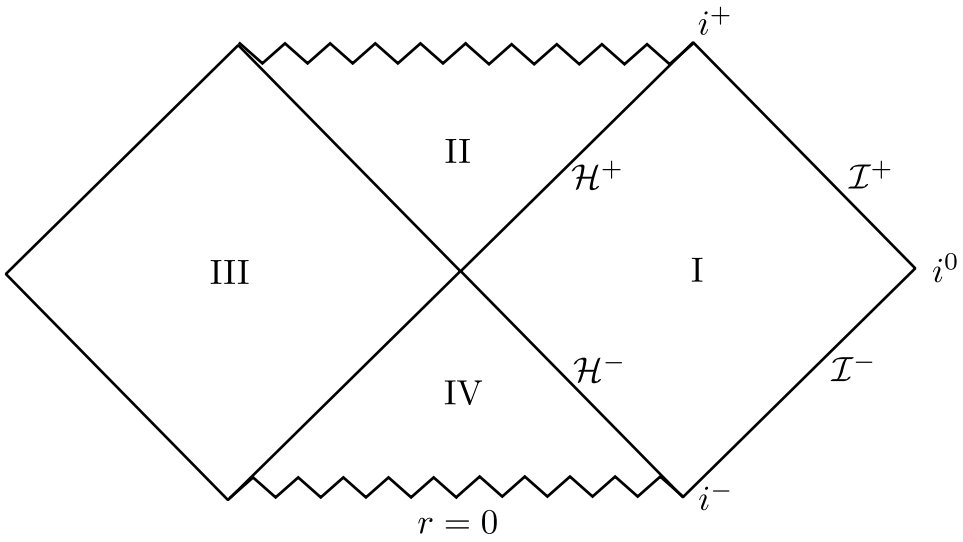

Figure 2.1: The figure represents the Penrose diagram of the Schwarzschild black hole in Kruskal-Szekeres coordinates. Various important locations have been marked.

2.2.4 Near-Horizon Limit: Rindler space

Another useful patch of spacetime is the near horizon region of the Schwarzschild metric. In the near horizon limit $r \approx 2M$, the angular part of the Schwarzschild metric separates as S^2 of radius $2M$ and the remaining metric takes a very interesting and important form, as we shall see in the later Section 3.2.2, known as the Rindler space

$$ds_2^2 = -\rho^2 d\eta^2 + d\rho^2 \,, \tag{2.15}$$

where s_2 is the two dimensional interval and, (ρ, η) are Rindler coordinates with $\rho = \sqrt{8M(r-2M)}$ and $\eta = \frac{t}{4M}$. Note that the Rindler metric is just the $(1,1)$ Minkowski metric if one redefines the coordinates as

$$X = \rho \cosh \eta \,, \quad T = \rho \sinh \eta \,, \tag{2.16}$$

after which the metric becomes

$$ds^2 = -dT^2 + dX^2 \,. \tag{2.17}$$

These are the same coordinates as seen by an observer experiencing a constant acceleration of $a = \frac{1}{4M}$ which is nothing but the surface gravity κ of the Schwarzschild black hole at $r = 2M$ (see Appendix A.1). We present the different coordinate systems used in Schwarzschild as a table below 2.2.4 for reference.

Coordinates	**Variables**	**Region Covered**	**Singularity at $r = 2M$?**	**Useful For**
Schwarzschild	(t, r)	$r > 2M$	Yes (coordinate)	Static observers
Tortoise (Regge-Wheeler)	(t, r^*)	$r > 2M$	Yes ($r^* \to -\infty$)	Wave equations
Eddington-Finkelstein (Ingoing)	(v, r)	$r > 0$	No	Infalling light
Eddington-Finkelstein (Outgoing)	(u, r)	$r > 0$	No	Outgoing light
Kruskal-Szekeres	(U, V)	Full extended spacetime	No	Penrose diagrams/local inertial frame
Rindler (near-horizon)	(η, ρ)	Near $r = 2M$	Approx. regular	Near-horizon physics

Table 2.1: Comparison of various coordinate systems used in Schwarzschild spacetime.

Next, we quickly review the other black hole solutions of general relativity and mention their salient features.

2.3 Reissner-Nordström Black Hole

One could construct another simple black hole solution of general relativity by adding a $U(1)$ charge Q. These charged black holes arise as a solution to Einstein-Maxwell theory, with action

$$S = \int d^4x\sqrt{-g}\left(\frac{R}{16\pi G} - \frac{1}{4}F^{\mu\nu}F_{\mu\nu}\right), \tag{2.18}$$

solution to which is the Reissner-Nordström metric [35, 36]

$$ds^2 = -\left(1 - \frac{2M}{r} + \frac{Q^2}{r^2}\right)dt^2 + \left(1 - \frac{2M}{r} + \frac{Q^2}{r^2}\right)^{-1}dr^2 + r^2\left(d\theta^2 + \sin\theta d\phi^2\right), \tag{2.19}$$

where $Q = \sqrt{Q_e^2 + Q_m^2}$ and it reduces to the Schwarzschild metric for $Q = 0$. Setting $g^{rr} = 0$ and restricting our focus to $M \geq Q$, we readily find that the RN solution has two horizons

$$r_\pm = M \pm \sqrt{M^2 - Q^2}, \tag{2.20}$$

with surface gravity(Appendix A.1)

$$\kappa_{\pm} = \frac{r_{\pm} - r_{\mp}}{2r_{\pm}^2}\,, \tag{2.21}$$

at the two horizons. The region $r > r_+$ is similar to the Schwarzschild $r > 2M$ and all our coordinates work from section 2.2 outside the outer horizon r_+. $r = r_-$ is a Cauchy horizon and the singularity at $r = 0$ is a timelike singularity unlike its Schwarzschild cousin.

2.3.1 Extremal black holes

We now turn to the interesting extremal case, $M = Q$. These black holes are called extremal black holes with the metric

$$ds^2 = -\left(1 - \frac{M}{r}\right)^2 dt^2 + \left(1 - \frac{M}{r}\right)^{-2} dr^2 + r^2\left(d\theta^2 + \sin\theta d\phi^2\right)\,. \tag{2.22}$$

The horizon is now located at $r = M$ and the surface gravity at this location is $\kappa = 0$. We can employ similar techniques as in section 2.2 to find "good" coordinate patches and construct the global causal structure using Kruskal-like coordinates. Two important features of the extremal black holes are the spacelike distance from the horizon and the near horizon geometry. We look at both in turn.

Spacelike distance from the horizon

Let us compute the spacelike distance s from the horizon of a point radially placed at R. We find

$$s = \int_M^R \frac{dr}{\left(1 - \frac{M}{r}\right)} = \infty\,. \tag{2.23}$$

For comparison, we perform a similar computation for the Schwarzschild black hole and find

$$s = \int_{2M}^R \frac{dr}{\sqrt{1 - \frac{2M}{r}}} = finite\,. \tag{2.24}$$

So, the horizon of an extremal black hole lies at infinite spatial distance in contrast to the Schwarzschild black hole. The integral measures the proper radial distance along a $t =$ const. hypersurface. This is a key geometric signature of extremality.

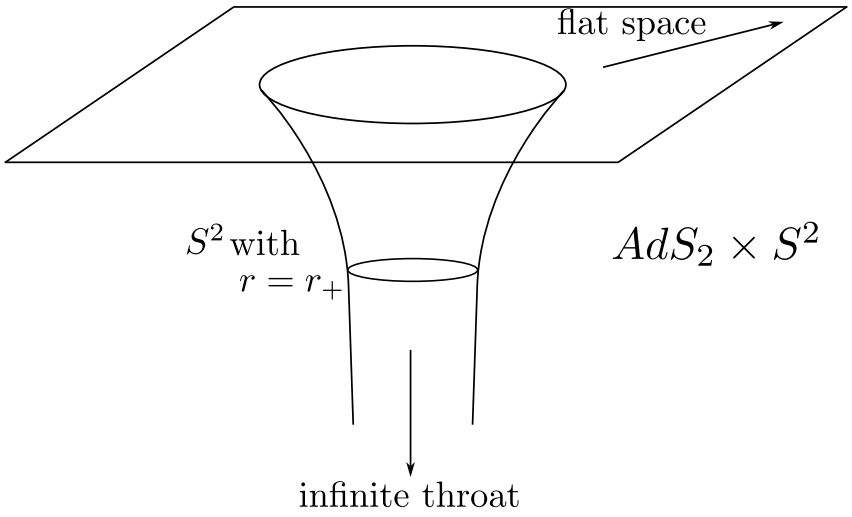

Figure 2.2: The figure represents an extremal black hole depicting its salient features.

Near-horizon geometry

Let us now zoom in near the horizon by defining $\rho = r - M$. In the limit $\rho \ll M$. We find that near $\rho \sim 0$, one can write the metric as

$$ds^2 = -\frac{\rho^2}{r_+^2}dt^2 + r_+^2\frac{d\rho^2}{\rho^2} + r_+^2\left(d\theta^2 + \sin\theta d\phi^2\right) , \tag{2.25}$$

which can be readily identified as the $AdS_2 \times S^2$ geometry, also known as the Robinson-Bertotti metric. A schematic description of the extremal infinite throat can be found in Figure 2.2. With these two features, the extremal black hole develops a semi-infinite throat structure. Note the striking difference between the near-horizon geometry of Schwarzschild (Section 2.2.4) and extremal Reissner-Nordström black holes.

This near-horizon geometry isn't just geometrically interesting—it plays a central role in quantum gravity as we will see in later sections. The AdS_2 factor gives rise to an emergent conformal symmetry and controls the low-energy dynamics. Extremal black holes are especially important in string theory and quantum gravity due to their zero temperature, infinite throat, and in many cases, supersymmetric structure.

The appearance of a semi-infinite throat indicates that low-energy modes get trapped near the horizon, experiencing extreme redshift. This decoupling mechanism lies at the heart of many extremal black hole microstate constructions (see Sections 4) and underpins their importance in holography.

2.4 Kerr Black Hole

We now turn to the Kerr metric [37], which is a solution to Einstein's equations describing an uncharged rotating black hole.[6] The solution written in Boyer-Lindquist coordinates (t, r, θ, ϕ) is

$$ds^2 = -\left(\frac{\Delta - a^2 \sin^2\theta}{\Sigma}\right) dt^2 - \frac{4aMr \sin^2\theta}{\Sigma} dt d\phi + \left(\frac{(r^2+a^2)^2 - \Delta a^2 \sin^2\theta}{\Sigma}\right) \sin^2\theta d\phi^2 + \frac{\Sigma}{\Delta} dr^2 + \Sigma d\theta^2 \,, \quad (2.26)$$

where

$$\Delta \equiv r^2 - 2Mr + a^2 \,, \quad \Sigma \equiv r^2 + a^2 \cos^2\theta \,. \quad (2.27)$$

This solution breaks spherical symmetry and is only axially symmetric. The parameter M is the mass of the black hole as seen from the g_{tt} component as $r \to \infty$:

$$\lim_{r\to\infty} g_{tt} = \lim_{r\to\infty} \frac{\Delta - a^2 \sin^2\theta}{\Sigma} \to 1 - \frac{2M}{r} \,. \quad (2.28)$$

Moreover, the off-diagonal term $g_{t\phi}$ gives meaning to the parameter a as the angular momentum per unit mass:

$$\lim_{r\to\infty} g_{t\phi} = \lim_{r\to\infty} -\frac{4aMr \sin^2\theta}{\Sigma} \to -4aM \frac{\sin^2\theta}{r} \,. \quad (2.29)$$

The curvature invariant or the Kretschmann scalar:

$$\mathcal{R} \equiv R_{abcd} R^{abcd} = \frac{48M^2 (r^2 - a^2\cos^2\theta)\,(\Sigma^2 - 16 r^2 a^2 \cos^2\theta)}{\Sigma^6} \,, \quad (2.30)$$

which diverges only at

$$r = 0, \;\; \theta = \frac{\pi}{2} \quad (2.31)$$

meaning that it is actually a curvature singularity. Setting $g^{rr} = 0$, one finds the location of the event horizon as

$$r_\pm = M \pm \sqrt{M^2 - a^2} \,, \quad (2.32)$$

which indicates coordinate singularity as seen from (2.30).

[6] For a brief review of the Kerr metric, see [38]. One may also add a $U(1)$ charge to the rotating black hole, resulting in the Kerr–Newman solution which we do not present here.

2.4.1 Ergosphere for the Kerr metric

An interesting feature of the Kerr black hole is the region where any observer is necessarily rotationally dragged along with the rotating black hole. This region is called the ergoregion or the ergosphere. Outside the event horizon r_+ in the region $r_+ < r < M + \sqrt{M^2 - a^2 \cos^2\theta}$ one find that all timelike curves have a minimum rotational velocity given by

$$\frac{a \sin\theta - \sqrt{\Delta}}{(r^2 + a^2)\sin\theta - \sqrt{\Delta}\, a \sin^2\theta} \leq \frac{d\phi}{dt}\,, \tag{2.33}$$

for any particle or light ray at a fixed r and θ.

2.4.2 Penrose process: Spinning black holes can radiate

In [39], Penrose pointed out an interesting property of spinning black holes: an energy extraction process. We briefly review this process to emphasize that Hawking radiation is not the sole mechanism by which black holes can emit energy.

Consider a particle a with four momenta p_a^μ, in the ergosphere with Killing vector ξ^μ following a geodesic trajectory with energy E

$$E_a = -p_{a\mu}\xi^\mu\,. \tag{2.34}$$

If particle a decays into two particles, b and c, with c falling through the horizon and b escapes to the exterior region outside the ergosphere, then conservation laws tell us

$$p_a^\mu = p_b^\mu + p_c^\mu\,, \quad E_a = E_b + E_c\,. \tag{2.35}$$

But, as the product $E_c = -p_{c\mu}\xi^\mu$ is not positive definite (as ξ^μ is spacelike), E_c can be less than zero which implies

$$E_a < E_b\,, \tag{2.36}$$

and we would have extracted some of the energy of the black hole. It is important to note that the energy extracted via the Penrose process is bounded, unlike Hawking radiation, which proceeds continuously—ultimately leading to complete evaporation of the black hole, unless a remnant scenario is considered (see Section 4.4 for details). The wave analog of this process is known as superradiance [40].

2.5 The AdS Spacetime

We now briefly review Anti-de Sitter (AdS) spacetime, a maximally symmetric solution to Einstein's equations with a negative cosmological constant $\Lambda < 0$. AdS spacetime plays a central role in string theory and quantum gravity, particularly due to its appearance in the AdS/CFT correspondence. Throughout this section, we work in units where the AdS radius ℓ is related to the cosmological constant by

$$\Lambda = -\frac{(d-1)(d-2)}{2\ell^2}\,, \tag{2.37}$$

in d spacetime dimensions.

2.5.1 Basics

The AdS_d spacetime is a maximally symmetric, constant negative curvature solution to the vacuum Einstein equations with $\Lambda < 0$. Its metric can be written in global coordinates (t, ρ, Ω) as:

$$ds^2 = -\left(1 + \frac{\rho^2}{\ell^2}\right) dt^2 + \left(1 + \frac{\rho^2}{\ell^2}\right)^{-1} d\rho^2 + \rho^2 d\Omega_{d-2}^2\,. \tag{2.38}$$

This geometry exhibits a timelike boundary at spatial infinity ($\rho \to \infty$), in contrast to asymptotically flat or de Sitter spacetimes. As a result, signals can reach the boundary in finite proper time, making boundary conditions and holographic duals physically significant.

Another commonly used coordinate system is the Poincaré patch, which covers only a portion of global AdS but is particularly useful in holography:

$$ds^2 = \frac{\ell^2}{z^2}\left(-dt^2 + d\vec{x}^2 + dz^2\right), \tag{2.39}$$

where $z > 0$ is the bulk radial coordinate, with the boundary at $z \to 0$.

2.5.2 BTZ Black Hole

A particularly important black hole solution in AdS_3 is the BTZ black hole, discovered by Bañados, Teitelboim, and Zanelli [41]. Unlike higher-dimensional black holes, the BTZ solution arises from identifying points in AdS_3 under discrete isometries, and it exists despite the absence of local gravitational degrees of freedom in three dimensions.

The metric of the non-rotating BTZ black hole is:

$$ds^2 = -\left(-M + \frac{r^2}{\ell^2}\right) dt^2 + \left(-M + \frac{r^2}{\ell^2}\right)^{-1} dr^2 + r^2 d\phi^2 \,, \tag{2.40}$$

where M is the ADM mass and the angular coordinate ϕ is periodically identified, $\phi \sim \phi + 2\pi$.

For $M > 0$, this geometry describes a black hole with event horizon at

$$r_+ = \ell\sqrt{M} \,, \tag{2.41}$$

and with no curvature singularity at $r = 0$—the singularity is instead of topological origin.

The BTZ black hole provides a useful toy model for black hole thermodynamics and information in a quantum gravity context, particularly in the study of AdS/CFT duality in $2 + 1$ dimensions.

2.6 Black Hole theorems

In the last century, several powerful theorems concerning black holes were developed, laying the groundwork for the emergence of black hole thermodynamics as a distinct field. In this section, we review these foundational theorems without proof and highlight how some of them set the stage for the thermodynamic formulation presented in the next chapter.

2.6.1 Birkhoff's theorem

The theorem presented by Birkhoff [42] states that

> *Any spherically symmetric solution of the vacuum Einstein field equations must be static and asymptotically flat.*

This means that the exterior solution of a *spherical, nonrotating,* gravitating body must be given by the Schwarzschild metric (2.4). A similar theorem can be extended to vacuum Einstein-Maxwell field equations to give the Reissner-Nordstörm solution. Unfortunately, such a theorem does not exist for the Kerr or Kerr-Newman solution.[7]

2.6.2 Israel's Uniqueness theorem

Presented by Israel [43] and then later improved in [44–46], this theorem states that

[7] We revisit this issue in the Section 7 and present some speculations.

The only static and asymptotically flat solution, with a regular event horizon, to the Einstein's field equations is a spherically symmetric solution, the Schwarzschild solution.

This is the converse of the Birkhoff's theorem. A similar theorem applies to the Reissner-Nordstörm solution and Kerr-Newman solution.

2.6.3 No hair theorem

This theorem remains unproven in full generality and is therefore often referred to as the *no-hair conjecture*. The idea was originally anticipated by Wheeler [47], inspired by the uniqueness results of Israel, Carter, and Wald [48–51]. In some sense, it is a culmination of the efforts for the uniqueness theorems. The conjecture posits that:

A black hole, after gravitational collapse, can be described by just a few externally observable parameters—M, J, and Q—and has no additional "hair" (i.e., no other independent degrees of freedom).

It should be noted that this theorem is not true in higher dimensional theories of gravity, in the presence of non-abelian Yang-Mills fields or some theories of gravity other than Einstein's general relativity [52].

2.6.4 Hawking's Area theorem

In the end, we present Hawking's area theorem [53] that states

Under general conditions like the absence of naked singularities and weak energy condition, the cross-sectional area of the future event horizon never decreases.

This growth of horizon area bears a striking resemblance to the second law of thermodynamics. It was Bekenstein who first recognized this resemblance. In his seminal paper [2], he conjectured that Hawking's area theorem might hold deeper significance for the nature of a quantum theory of gravity. He proposed a thought experiment and asked what happens to the entropy of a hot cup of coffee once it is thrown into a black hole? Does the universe lose entropy—in violation of the second law of thermodynamics?

To resolve this paradox, Bekenstein introduced the idea of a *generalized second law*, which asserts that the sum of black hole entropy (proportional to the area of the black hole horizon) and entropy of matter never decreases. This profound insight laid the groundwork for the development of the laws of black hole thermodynamics which we review in the next chapter.

Chapter 3

Black Hole Thermodynamics

If you feel you are in a black hole, don't give up. There's a way out.

— S.W. Hawking

Having surveyed the fundamental properties of classical black holes, we now turn to their quantum aspects. Specifically, we enter the semiclassical regime, where matter fields are quantized on a fixed classical spacetime background.

This chapter presents key developments that established black hole thermodynamics as a cornerstone of modern theoretical physics. We begin by introducing the essential ideas of quantum field theory in curved spacetime and then derive Hawking's prediction of black hole evaporation. Finally, we examine the conceptual challenges posed by this phenomenon—including various formulations of the information paradox—and explore proposed resolutions.

3.1 Quantum Field Theory in Curved Spacetime

The key difference between quantum field theory in flat Minkowski spacetime and in curved spacetime lies in the absence of a preferred notion of positive and negative frequency modes. In Minkowski space, the symmetries of the spacetime are encoded in the Poincaré group, and in particular, the existence of a global timelike Killing vector allows a natural definition of positive frequency modes—those that oscillate as $e^{-i\omega t}$ with $\omega > 0$. These modes define a unique vacuum state, the Minkowski vacuum, and the division between positive and negative frequencies is preserved under Lorentz transformations. Consequently, the Fock space constructed on top of this vacuum is invariant under inertial coordinate transformations and provides an observer-independent particle interpretation.

By contrast, in curved spacetime, such a global time translation symmetry typically does not exist. Without a global timelike Killing vector, there is no unique way to decompose solutions into positive and negative frequency parts that all observers agree

upon. Different observers—or even different coordinate choices—may adopt different mode decompositions, leading to distinct definitions of vacuum and, consequently, inequivalent Fock spaces.

This fundamental ambiguity in curved spacetime is one of the most striking conceptual departures from quantum field theory in flat spacetime. It gives rise to remarkable physical phenomena such as gravitational particle production, the Unruh effect, and Hawking radiation.[1] We focus our attention on the Hawking effect and review the field of black hole thermodynamics.

3.1.1 Scalar field in curved spacetime

We consider the simplest case of a scalar field in curved spacetime. The action for a scalar in $d+1$ dimensions is

$$S = \int d^{d+1}x\sqrt{-g}\left(\nabla_\mu\Phi(x^\mu)\nabla^\mu\Phi(x^\mu) - m^2\Phi^2(x^\mu)\right) . \tag{3.1}$$

We can solve the scalar field equation and expand the field into orthonormal positive and negative frequency modes as

$$\Phi(x^\mu) = \sum_i \left(a_i f_i(x^\mu) + a_i^\dagger f_i^*(x^\mu)\right) , \tag{3.2}$$

where the positive modes $\{f_i\}$ are defined using a timelike Killing vector ξ_1^μ as

$$\xi_1^\mu\nabla_\mu f_i(x^\mu) = -iw_i\, f_i(x^\mu)\,, \quad w_i > 0\,. \tag{3.3}$$

Using these one can construct Fock states and a notion of particles by applying the standard QFT techniques. The Klein-Gordon inner product in curved spacetime is defined as[2]

$$(\Phi_1, \Phi_2) = -i\int d\Sigma^\mu \left(\Phi_1\partial_\mu\Phi_2^* - \Phi_2^*\partial_\mu\Phi_1\right) , \tag{3.4}$$

where Σ is an *initial data* Cauchy hypersurface and $d\Sigma^\mu = d\Sigma\, n^\mu$, with $d\Sigma$ being the volume element and n^μ a future-directed unit normal vector to Σ. Using Gauss's theorem, one can show that the inner product is indeed independent of the choice of hypersurface. (See [58] for a good derivation.)

[1] For comprehensive treatments of quantum field theory in curved spacetime, see [28, 54–57].
[2] Suppressing the (x^μ) dependence.

3.1.2 Bogoliubov transformations and particle production

In the absence of a global timelike Killing vector, the notion of positive frequency modes becomes observer-dependent, and the mode decomposition of the scalar field is not unique. In addition to the expansion (3.2), one could equally well expand the field as

$$\Phi(x^\mu) = \sum_i \left(b_i g_i(x^\mu) + b_i^\dagger g_i^*(x^\mu) \right) , \tag{3.5}$$

where the $\{g_i\}$ are positive frequency modes defined with respect to a different timelike vector field ξ_2^μ.

In general, the two sets of mode functions $\{f_i\}$ and $\{g_i\}$ are related by a linear transformation that mixes positive and negative frequency components. This implies that the vacuum defined by the f_i modes is not empty of particles when viewed in the g_i basis. The mathematical framework that captures this mixing is known as the *Bogoliubov transformation*, which we now describe.

If the two sets of modes $\{f_i\}$ and $\{g_i\}$ are related by a linear transformation of the form

$$g_j = \sum_i \left(\alpha_{ji} f_i + \beta_{ji} f_i^* \right) , \tag{3.6}$$

then by substituting this relation into the expansion of Φ and using the KG product (3.4), we find that the operators $\{a_i, a_i^\dagger\}$ and $\{b_i, b_i^\dagger\}$ are related via

$$b_j = \sum_i \left(\alpha_{ji}^* a_i - \beta_{ji}^* a_i^\dagger \right) , \tag{3.7}$$

and equivalently,

$$a_i = \sum_j \left(\alpha_{ji} b_j + \beta_{ji}^* b_j^\dagger \right) . \tag{3.8}$$

These relations are known as *Bogoliubov transformations*.

Physically, nonzero β_{ji} coefficients signal mixing between positive and negative frequencies. In particular, the vacuum $|0_a\rangle$ defined by the f_i modes appears populated with particles when measured using the g_j modes. The expectation value of the number operator $b_j^\dagger b_j$ in the $|0_a\rangle$ vacuum is given by

$$\langle 0_a | \, b_j^\dagger b_j \, | 0_a \rangle = \sum_i |\beta_{ji}|^2 . \tag{3.9}$$

Thus, the modulus squared of the β coefficients tells us the number of particles detected by the g-observer in the f-vacuum.

3.2 Hawking Radiation

Hawking radiation arises from the fundamental fact that, in the presence of a black hole, no observer can define a consistent vacuum state across the entire spacetime. This lack of a unique vacuum leads to a mismatch in particle definitions between infalling and asymptotic observers, resulting in observable particle flux at infinity.

In this section, we will derive Hawking radiation using two complementary approaches. First, we present the derivation in Hawking's original style of mode matching, which offers deep physical insight into the mechanism of black hole evaporation. Then, we outline a more concise derivation based on the near-horizon geometry and conformal symmetry. While the former provides detailed intuition, the latter highlights the universal features of the radiation process while being quick to remember. We also present a third way, the Euclidean approach to calculate the Hawking temperature, later in the next chapter, see Section 4.

3.2.1 Original style derivation

Hawking's original derivation [1] of the black hole radiation computed Bogoliubov coefficients to relate scalar field modes in different coordinate frames.

Geometric setup

Consider the collapsing shell of null quanta moving radially inwards at $v = v_0$ in the EF coordinates (Section 2.2.2). There are three regions to consider for the spacetime as depicted in the Figure 3.1:

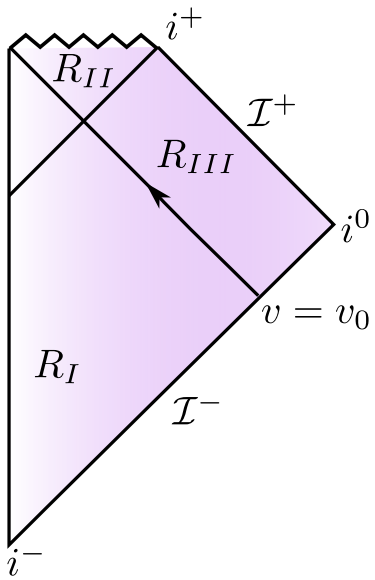

Figure 3.1: The figure shows a collapsing shell of null quanta moving radially inwards at $v = v_0$. The figure also labels the different spacetime regions as mentioned in the text of this Section.

1. **Inside the shell** (R_I): At all times, inside the shell the metric is the Minkowski metric give by[3]

$$\begin{aligned} ds^2 &= -du_{in}dv_{in} + r^2\left(d\theta^2 + \sin\theta d\phi^2\right) , \\ u_{in} &= t_{in} - r\,, v_{in} = t_{in} + r\,. \end{aligned} \tag{3.10}$$

   We can use the freedom of setting the origin by setting $v_i = 0$ to get

$$r = -\frac{u_{in}}{2}\,. \tag{3.11}$$

2. **Outside the shell, outside the horizon** (R_{II}): Outside the shell, the metric is given by the Schwarzschild metric for $r > 2M$:

$$\begin{aligned} ds^2 &= -\left(1 - \frac{2M}{r}\right)du_{out}dv_{out} + +r^2\left(d\theta^2 + \sin\theta d\phi^2\right) , \\ u_{out} &= t_{out} - r^*\,, v_{out} = t_{out} + r^*\,. \end{aligned} \tag{3.12}$$

   Again, we can set $v_{out} = 0$ to get $u_{out} = -2r^*$ where r^* is the tortoise coordinate. (Section 2.2.1.)

3. **Outside the shell, inside the horizon** (R_{III}): Once the shell has passed its horizon, the region inside the horizon bu outside the shell can be written in terms of the Kruskal metric for $r < 2M$ (Section 2.2.3):

$$\begin{aligned} ds^2 &= -\frac{32\,M^3}{r}e^{-\frac{r}{2M}}dU_{out}dV_{out} + r^2\left(d\theta^2 + \sin\theta d\phi^2\right) , \\ U_{out} &= e^{\frac{\tilde{u}_{out}}{4M}}\,, V_{out} = e^{\frac{\tilde{v}_{out}}{4M}} \quad \text{for } U < 0\,. \end{aligned} \tag{3.13}$$

   As in previous cases, we can set $\tilde{v}_{out} = 0$ to get $V_{out} = 1$.

Matching conditions

To ensure smoothness, we match the inside R_I and the outside of the shell R_{II} at radial coordinate $r = r$. We find

$$\begin{aligned} u_{out} = -2r^* &= -2\left(r + 2M\ln\left(\frac{r}{2M} - 1\right)\right) \\ &= u_{in} - 4M\ln\left(-\frac{u_{in} + 4M}{4M}\right), \end{aligned} \tag{3.14}$$

using $r = -u_{in}/2$ from above (3.11).

[3]We will use r, θ, ϕ as the same for both inside and outside. As they carry geometric meaning so we do not give them subscript *in*.

Wave modes and the Eikonal approximation

Having set up the geometry, we now look into the solution of a massless (setting $m = 0$ in (3.1)) scalar field equation in the black hole geometry. The Euler-Lagrange field equation is

$$\Box\Phi(x^\mu) = 0\,, \tag{3.15}$$

solution to which, Φ is a sum of positive and negative frequency modes depending on region and its timelike Killing vector. In the spherically symmetric spacetimes, the scalar field can be expanded as

$$\Phi(x^\mu) = \sum_{\ell,m} \int dk \left(a_k f_{\ell,k} + a_k^\dagger f_{\ell,k}^*\right) Y_\ell^m(\theta,\phi)\,. \tag{3.16}$$

where for $\ell = 0$ modes, in the Eikonal approximation, we find $f_{\ell,k}$ to take the following form[4]

$$f_{\ell,k} = \frac{\chi_\ell(u,r)}{r} = \frac{1}{4\pi r\sqrt{k}} e^{-iku}\,. \tag{3.17}$$

For our case, we expand the field in three regions and define the modes as follows

1. **Inside the shell** (R_I): Modes f_{k_a} defined as positive frequency modes at $\mathcal{I}^-$ with respect to the flat coordinate u_{in}. These modes get reflected at $r = 0$ and reach at $r \sim 2M$ where they can be written as

$$f(r, u_{in}) = \frac{1}{4\pi r\sqrt{k_a}} e^{-ik_a(u_{in}+4M)}\,, \tag{3.18}$$

   where we have used $u_{in}(2M) = -4M$ using the $r = -u_{in}/2$ at the horizon $2M$.

2. **Outside the shell, outside the horizon** (R_{II}): Modes g_{k_b} defined as positive frequency modes at $\mathcal{I}^+$ with respect to the coordinate u_{out}

$$g_{k_b}(r, u_{out}) = \frac{1}{4\pi r\sqrt{k_b}} e^{-ik_b u_{out}}\,, \tag{3.19}$$

   which using the matching conditions 3.2.1 become

$$g_{k_b}(r, u_{out}(u_{in})) = \frac{1}{4\pi r\sqrt{k_b}} e^{-ik_b\left(u_{in} - 4M\ln\left(-\frac{u_{in}+4M}{4M}\right)\right)}\,. \tag{3.20}$$

   This logarithmic divergence in the matching condition at $r = 2M$ is what ultimately

[4]We define χ_ℓ for a later use in chapter 6. Physically, in the Eikonal approximation, one assumes that the wavelength of the field modes is very short compared to the curvature scale of the background spacetime which leads to the form above.

leads to the thermal spectrum as we shall see below.

3. **Outside the shell, inside the horizon** (R_{III}): Modes g_{k_b} defined as positive frequency modes at $\mathcal{H}^+$ with respect to the coordinate $\tilde{u}_{out}$

$$h_{k_c}(r, \tilde{u}_{out}) = \frac{1}{4\pi r\sqrt{k_c}} e^{-ik_c\tilde{u}_{out}} \,. \tag{3.21}$$

Bogoliubov coefficients

With all the modes correctly defined, we are ready to compute the Bogoliubov coefficients. We begin by noting the following inner products (suppressing functional dependence for brevity) which can be easily verified using the above functions:

$$\begin{aligned}
&(f_{k_a}, f_{k'_a}) = \delta(k_a - k'_a)\,, \;\; (g_{k_b}, g_{k'_b}) = \delta(k_b - k'_b)\,, \;\; (h_{k_c}, h_{k'_c}) = \delta(k_c - k'_c)\,, \\
&(f^*_{k_a}, f^*_{k'_a}) = \delta(k_a - k'_a)\,, \;\; (g^*_{k_b}, g^*_{k'_b}) = \delta(k_b - k'_b)\,, \;\; (h^*_{k_c}, h^*_{k'_c}) = \delta(k_c - k'_c)\,.
\end{aligned} \tag{3.22}$$

We also note that as the functions g_{k_b}, h_{k_c} are spacelike separated they have vanishing cross-inner products

$$(g_{k_b}, h_{k_c}) = 0\,, \;\; (g_{k_b}, h^*_{k_c}) = 0\,, \;\; (g^*_{k_b}, h_{k_c}) = 0\,, \;\; (g^*_{k_b}, h^*_{k_c}) = 0\,. \tag{3.23}$$

Recall that the scalar field can be defined as

$$\Phi(x^\mu) = \int dk_a \left(a_{k_a} f_{k_a} + a^\dagger_{k_a} f^*_{k_a}\right) \,, \tag{3.24}$$

or as

$$\Phi(x^\mu) = \int dk_b \left(b_{k_b} g_{k_b} + b^\dagger_{k_b} g^*_{k_b}\right) + \int dk_c \left(c_{k_c} h_{k_c} + c^\dagger_{k_c} h^*_{k_c}\right) \,. \tag{3.25}$$

Taking inner product (Φ, g_{k_b}) and equating the above two equations, we find

$$b_{k_b} = \int dk_a \left(a_{k_a}\alpha_{k_a k_b} + a^\dagger_{k_a}\beta_{k_a k_b}\right) \,, \tag{3.26}$$

where

$$\alpha_{k_a k_b} = (f_{k_a}, g_{k_b}) \,, \quad \beta_{k_a k_b} = \left(f^*_{k_a}, g_{k_b}\right) \,, \tag{3.27}$$

and similarly we define the other coefficients.

Inner products

To find the coefficients we find the various inner products which we evaluate on $v = const$ slice using (3.4) to get

$$\begin{aligned}
\alpha_{k_a k_b} &= (f_{k_a}, g_{k_b}) \\
&= -i \int du_{in} d\Omega \left(f_{k_a} \partial_{u_{in}} g^*_{k_b} - g^*_{k_b} \partial_{u_{in}} f_{k_a} \right) \\
&= -i \int 4\pi r^2 du_{in} \left(-2 g^*_{k_b} \partial_{u_{in}} f_{k_a} \right) \\
&= 8\pi i r^2 \int du_{in} \, \frac{-i}{16\pi^2 r^2} \sqrt{\frac{k_a}{k_b}} e^{ik_b\left(u_{in} - 4M \ln\left(-\frac{u_{in}+4M}{4M}\right)\right) - ik_a(u_{in}+4M)} \\
&= \frac{1}{2\pi} \sqrt{\frac{k_a}{k_b}} \int_{-\infty}^{-4M} du_{in} \, e^{ik_b\left(u_{in} - 4M \ln\left(-\frac{u_{in}+4M}{4M}\right)\right) - ik_a(u_{in}+4M)} \\
&= \frac{1}{2\pi} \sqrt{\frac{k_a}{k_b}} \int_0^{\infty} d\omega \, e^{ik_b\left(-\omega - 4M - 4M \ln\left(\frac{\omega}{4M}\right)\right) + ik_a\omega} \,, \\
&= \frac{1}{2\pi} \sqrt{\frac{k_a}{k_b}} (4M)^{ik_b(4M)} e^{-ik_b(4M)} \Gamma(1 - ik_b(4M)) (-i(k_b - k_a))^{-(1 - ik_b(4M))} \\
&= \frac{1}{2\pi} \sqrt{\frac{k_a}{k_b}} \left(\frac{1}{\kappa}\right)^{i\frac{k_b}{\kappa}} e^{-i\frac{k_b}{\kappa}} \Gamma(1 - i\frac{k_b}{\kappa}) (-i(k_b - k_a))^{-(1 - i\frac{k_b}{\kappa})} \,,
\end{aligned} \tag{3.28}$$

where we made the change $\omega = -\left(u_{in} + 4M\right)$ and replaced $\kappa = 1/4M$ as surface gravity. Similarly, we compute

$$\begin{aligned}
\beta_{k_a k_b} &= \left(f^*_{k_a}, g_{k_b}\right) \\
&= -\frac{1}{2\pi} \sqrt{\frac{k_a}{k_b}} \int_{-\infty}^{-4M} du_{in} \, e^{ik_b\left(u_{in} - 4M \ln\left(-\frac{u_{in}+4M}{4M}\right)\right) + ik_a(u_{in}+4M)} \\
&= -\frac{1}{2\pi} \sqrt{\frac{k_a}{k_b}} \int_{-\infty}^{0} d\omega \, e^{ik_b\left(\omega - 4M - 4M \ln\left(-\frac{\omega}{4M}\right)\right) + ik_a\omega} \,, \\
&= -\frac{1}{2\pi} \sqrt{\frac{k_a}{k_b}} \int_0^{\infty} d\omega \, e^{ik_b\left(-\omega - 4M - 4M \ln\left(\frac{\omega}{4M}\right)\right) - ik_a\omega} \,, \\
&= -\frac{1}{2\pi} \sqrt{\frac{k_a}{k_b}} \left(\frac{1}{\kappa}\right)^{i\frac{k_b}{\kappa}} e^{-i\frac{k_b}{\kappa}} \Gamma(1 - i\frac{k_b}{\kappa}) (-i(k_b + k_a))^{-(1 - i\frac{k_b}{\kappa})} \,,
\end{aligned} \tag{3.29}$$

from which we find

$$|\alpha_{k_a k_b}| = e^{\frac{\pi k_b}{\kappa}} |\beta_{k_a k_b}| \,. \tag{3.30}$$

Radiation distribution

Suppose we define the absorptivity of the black hole as

$$\Gamma(k_b) = \int_0^{\infty} dk_a \left(|\alpha_{k_a k_b}|^2 - |\beta_{k_a k_b}|^2 \right) \,, \tag{3.31}$$

which is the fraction of particles absorbed by the black hole that were emitted at past null infinity, then from (3.30) we get

$$\Gamma(k_b) = \left(e^{\frac{2\pi k_b}{\kappa}} - 1\right) \int_0^\infty dk_a |\beta_{k_a k_b}|^2 \,. \tag{3.32}$$

Using the expectation of the number operator $\langle n_k \rangle = \int_0^\infty dk_a |\beta_{k_a k_b}|^2$ we find

$$\langle n_k \rangle = \frac{\Gamma(k_b)}{e^{\frac{2\pi k_b}{\kappa}} - 1} \,, \tag{3.33}$$

which for a massless field ($\omega = |\vec{k}_b|$) gives the familiar Planck distribution

$$\langle n_\omega \rangle = \frac{\Gamma(\omega)}{e^{8\pi M\omega} - 1} \,, \tag{3.34}$$

where we have set the surface gravity $\kappa = 1/4M$ for a Schwarzschild black hole. (See Appendix A.1.) After reinstating all the physical constants, we can extract the Hawking temperature

$$T_H = \frac{\hbar c^3}{8\pi G_N M k_B} \,. \tag{3.35}$$

3.2.2 Near horizon derivation

We review the Hawking effect by interpreting it as the dynamical formation of Rindler space from Minkowski spacetime. In this derivation we show the presence of an outward thermal energy flux from the black hole precisely at the Hawking temperature. While Hawking's original derivation considers a quantum scalar field in a fixed Schwarzschild background [1], here we present a rapid derivation that leverages the power of the near-horizon approximation and conformal field theory techniques.

Near horizon geometric setup

We again consider the collapse geometry modeled by the Vaidya metric as in (3.12) with $M = M\Theta(v - v_0)$ representing a shockwave. The shockwave divides the spacetime into regions. We focus on the two regions which we describe as "in" (R_I) and "out" (R_{II}) as seen in the Figure 3.1. We will zoom into the region $r \sim 2M$ while focusing on the $1+1$D spacetime and understand the mode expansion across the shockwave. The "in" region is Minkowski spacetime with metric

$$ds_2^2 = -du_{in} dv \,, \quad v < v_0 \,, \tag{3.36}$$

and the "out" region in the near horizon approximation has the Rindler metric

$$ds^2 = -\kappa^2\rho^2 dv^2 + 2\kappa\rho\, dv d\rho\,, \quad v > v_0\,, \tag{3.37}$$

where $\rho = \sqrt{8M(r-2M)}$ is the proper distance and κ is the surface gravity $\kappa = 1/4M$. The tortoise coordinate r^* is

$$r^* \sim \frac{1}{\kappa}\ln\kappa\rho\,, \tag{3.38}$$

which gives the outgoing null coordinate in the out region as u_{out}

$$u_{out} = v - 2r^* \sim v - \frac{2}{\kappa}\ln\kappa\rho\,. \tag{3.39}$$

In terms of the null coordinates, the metric becomes

$$ds_2^2 = -e^{\kappa(v-u_{out})}du_{out}dv\,. \tag{3.40}$$

Matching conditions

At the location of the shockwave $v = v_0$, for smoothness, we demand the two metrics to match. The u_{in} coordinate in terms of ρ is

$$u_{in} = v_0 - 2r \sim v_0 - 2(2M + \frac{\kappa\rho^2}{2})\,, \tag{3.41}$$

where we have used the near horizon expansion $r \sim 2M + \frac{\kappa\rho^2}{2}$. Substituting ρ in terms of the u_{out} from (3.39), we find

$$u_{in} = v_0 - 4M - \frac{1}{\kappa}e^{\kappa(v_0-u_{out})}\,. \tag{3.42}$$

Conformal transformations and the Schwarzian

We now return to the dynamics of a scalar field in this background. As in Section 3.2.1, we consider the scalar field equation but this time in the near-horizon limit. In the null coordinates (u, v) appropriate to this region, the wave equation for the (t, r) part simplifies as

$$\partial_u\partial_v\chi_\ell(t,r) = 0\,, \tag{3.43}$$

which we recognize as two dimensional conformal field equation.[5]

To compute the radiation flux, we need the vacuum expectation value of the stress energy tensor. We define the normal ordered stress energy tensor for a conformal field f

[5]For standard references of CFT, see [59–62].

using the point splitting [55][6]

$$: T_{\pm\pm}(x^{\pm}) := \lim_{x'^{\pm}\to x^{\pm}} \partial_{\pm} f(x^{\pm})\partial'_{\pm} f(x'^{\pm}) + \frac{\hbar}{4\pi}\frac{1}{(x^{\pm}-x'^{\pm})^2}\,. \tag{3.44}$$

In a $2D$ CFT, a normal ordered stress energy tensor transforms under a conformal transformation $x^{\pm} \to y^{\pm}$ as

$$: T_{\pm\pm}(y^{\pm}) := \left(\frac{dx^{\pm}}{dy^{\pm}}\right)^2 : T_{\pm\pm}(x^{\pm}) : -\frac{\hbar}{24\pi}\{x^{\pm}, y^{\pm}\}_S\,, \tag{3.45}$$

where $\{x^{\pm}, y^{\pm}\}_S$ is the Schwarzian operator.

The Hawking effect

At last, we are now ready to find the Hawking effect using the machinery developed above. Similar to the previous section 3.2.1, we consider a massless scalar field initially prepared in the "in" Minkowski region $v < v_0$ with a natural ground state $|in\rangle$ with respect to the (u_{in}, v) coordinates. Let this have the stress tensor $T_{u_{in}\,u_{in}}$. And the "out" Rindler region has the vacuum state $|out\rangle$ with respect to the (u_{out}, v) coordinates and stress tensor $T_{u_{out}\,u_{out}}$. So, the question becomes

> *How does a Rindler "out" observer, with coordinates (u_{out}, v) perceive the Minkowski $|in\rangle$ state?*

And to find this, we calculate $\langle in| : T_{u_{out}\,u_{out}} : |in\rangle$ using CFT techniques. We start by noting

$$\langle in| : T_{u_{in}\,u_{in}} : |in\rangle = 0\,, \tag{3.46}$$

as it is the Minkowski vacuum and the observer sees its own vacuum empty. Then from (3.45),

$$\langle in| : T_{u_{out}\,u_{out}} : |in\rangle = \left(\frac{du_{in}}{du_{out}}\right)^2 \langle in| : T_{u_{in}\,u_{in}} : |in\rangle - \frac{\hbar}{24\pi}\{u_{in}, u_{out}\}_S\,, \tag{3.47}$$

$$= -\frac{\hbar}{24\pi}\{u_{in}, u_{out}\}_S = \frac{\hbar\kappa^2}{48\pi}\,, \tag{3.48}$$

where in the last line we have used (3.42) to calculate the Schwarzian. Note the simplicity of the derivation! This derivation, relying solely on conformal symmetry and smooth gluing of coordinate patches, elegantly reproduces Hawking's result without requiring detailed mode analysis.

[6] Here, $x^{\pm}$ refer to any general orthonormal basis, for our case, we will use $x^{\pm} = (v, u)$.

The ingoing sector $\langle in| : T_{v\,v} : |in\rangle$ can be found to vanish. This tells us that an observer in the Rindler vacuum perceives the Minkowski vacuum populated by positive frequency modes with a thermal flux of $\frac{\hbar\kappa^2}{48\pi}$ which is precisely what Hawking had found as shown in the previous Section 3.2.1.

3.2.3 Different vacua in curved spacetime

Throughout the analysis of black hole evaporation, we have encountered various vacuum states, each reflecting a different observer perspective or spacetime region. We summarize these vacua in curved spacetime[7] here for conceptual clarity.

1. Minkowski vacuum $|0_M\rangle$: This vacuum is defined by requiring the normal modes f to be positive frequency with respect to the static timelike coordinate t.

2. Boulware vacuum $|0_B\rangle$: Defined by requiring normal modes to be positive frequency with respect to the Killing vector $\partial/\partial t$ with respect to which the exterior region of a black hole is static *i.e.* the Schwarzschild coordinate t.

3. Unruh vacuum $|0_U\rangle$: Defined by taking modes that are incoming from $\mathcal{I}^-$ to be positive frequency with respect to $\partial/\partial t$ with t being the Schwarzschild coordinate, while those that emanate from the past horizon are taken to be positive frequency with respect to the Kruskal coordinate U, the canonical affine parameter on the past horizon.

4. Hartle-Hawking vacuum $|0_{HH}\rangle$: This vacuum is defined by taking incoming modes to be positive frequency with respect to the Kruskal coordinate V, the canonical affine parameter on the future horizon, and outgoing modes to be positive frequency with respect to the Kruskal coordinate U, the canonical affine parameter on the past horizon.

5. Rindler vacuum $|0_R\rangle$: In flat spacetime, the metric is static with respect to both t (Minkowski timelike coordinate) and η (Rindler timelike coordinate) and hence one can find mode functions which are positive frequency with respect to t or with respect to η. The Rindler vacuum is defined using η.

3.3 The Four Laws of Black Hole Thermodynamics

The classical theorems of black hole mechanics—particularly the area theorem discussed in Section 2.6—led to a compelling analogy with the laws of thermodynamics. Initially,

[7]While additional vacua can be defined in other curved spacetimes—such as those describing expanding universes or (anti-)de Sitter geometries—we restrict our focus here to vacua relevant for black hole spacetimes.

this analogy was purely formal: within the classical framework of general relativity, the similarities were mathematical rather than physical. However, the discovery of Hawking radiation, emerging from semiclassical gravity, transformed this analogy into a deep physical equivalence, thereby establishing the foundations of black hole thermodynamics [63–66].

There is, in fact, a remarkably simple way to trace how quantum effects are essential in elevating this analogy from formality to physical law. Let us, for a moment, set aside Hawking's black hole radiation result. As discussed in Section 2.6, Bekenstein proposed that the second law of thermodynamics must be generalized in the presence of a black hole. He conjectured that the total entropy; the sum of entropy of matter and the area of a black hole never decreases:

$$S_{gen} = S_{matter} + \frac{A_h}{\alpha}\,, \tag{3.49}$$

where α is a proportionality constant which can also be used to formally define a temperature of a classical black hole to be

$$T_{BH} = \alpha \frac{c^2 \kappa}{G}\,. \tag{3.50}$$

While elegant, this proposal quickly got into trouble; Imagine immersing the black hole with temperature T_{BH} in a thermal bath with temperature $T_{bath} < T_{BH}$. The classical black hole would absorb the radiation without emitting anything, leading to a net transfer of heat from a colder body to a hotter one violating the generalized second law!

Bekenstein's formal analogy between the area of a black hole and its entropy required a physical input and needed black holes to radiate. A subtle hint comes from dimensional analysis: the product αk_B must have units of area, $[L]^2$. However, general relativity alone, with its constants G_N and c, cannot furnish a length scale. Only by mixing Planck's constant $\hbar$ into the recipe can one cook up an area scale, suggesting that quantum mechanics must be a necessary ingredient.

This is precisely what Hawking demonstrated: by incorporating quantum field theory in curved spacetime, he showed that black holes emit thermal radiation with a temperature proportional to $\hbar\kappa$, thus confirming Bekenstein's insight and establishing the physical foundation for the laws of black hole thermodynamics which we describe below:

Zeroth Law

For a stationary black hole, the surface gravity κ is constant over the entire event horizon.

First Law

For perturbations of stationary black holes, the change in mass is related to changes in horizon area, angular momentum, and charge as

$$dM = \kappa dA + \Omega_H dJ + \Phi_H dQ\,, \tag{3.51}$$

where M is the mass, A is the horizon area, Ω_H is the angular velocity, J is the angular momentum, Φ_H is the electrostatic potential and Q is the electric charge.

Second Law

The horizon area A of a classical black hole event horizon never decreases in any classical process:

$$\frac{dA}{dt} \geq 0\,. \tag{3.52}$$

Third Law

It is impossible, through any physical process, to reduce the surface gravity κ of a black hole to zero in a finite number of steps.

3.4 The Black Hole Information Paradox

The discovery of Hawking radiation revealed that black holes emit thermal radiation at a temperature

$$T_{\rm H} = \frac{\hbar\kappa}{2\pi c k_{\rm B}} = \frac{\hbar c^3}{8\pi G M k_{\rm B}}, \tag{3.53}$$

where κ is the surface gravity and M is the mass of the black hole. This result confirmed that black holes behave as thermodynamic objects, possessing an entropy

$$S_{\rm BH} = \frac{k_{\rm B} A}{4G\hbar}, \tag{3.54}$$

and obeying the laws of thermodynamics. However, this thermodynamic behavior leads to a fundamental puzzle when combined with the principles of quantum mechanics.

Hawking's original derivation shows that black holes radiate as perfect black bodies, with the outgoing radiation in a thermal, mixed state. Consider a black hole formed from a pure quantum state $|\Psi\rangle$. In semiclassical gravity, the evolution of this state leads to the emission of Hawking radiation entangled with interior modes, resulting in a reduced density matrix for the radiation:

$$\rho_{\rm rad} = {\rm Tr}_{\rm int}|\Psi\rangle\langle\Psi| \approx \rho_{\rm thermal}. \tag{3.55}$$

As the black hole evaporates completely, only the radiation remains. This implies an evolution of the form:

$$|\Psi\rangle \quad \longrightarrow \quad \rho_{\text{thermal}}, \tag{3.56}$$

a transformation from a pure to a mixed state, which contradicts unitary evolution:

$$|\Psi(t)\rangle = U(t)|\Psi(0)\rangle \quad \Rightarrow \quad \rho(t) = U\rho(0)U^{\dagger}. \tag{3.57}$$

Such non-unitary evolution is incompatible with the standard framework of quantum mechanics and raises the central question of the black hole information paradox:

Can black hole evaporation be consistent with unitary quantum evolution?

Various proposals have been made in response:

- **Information loss:** Hawking originally proposed that quantum gravity may allow non-unitary evolution, leading to a fundamental loss of information.
- **Remnants:** A stable Planck-scale remnant might store information, but such scenarios typically require an infinite number of internal states, leading to theoretical inconsistencies.
- **Information recovery:** A widely favored view is that Hawking's semiclassical treatment misses quantum gravitational corrections that restore unitarity. In particular, the entanglement entropy of the radiation, $S_{\text{rad}}(t)$, should follow the *Page curve*, rising until the Page time and then decreasing as information is recovered:

$$S_{\text{rad}}(t) \sim \begin{cases} t & t < t_{\text{Page}}, \\ S_{\text{BH}}(t) & t > t_{\text{Page}}. \end{cases} \tag{3.58}$$

This behavior cannot be captured within semiclassical gravity, which predicts a monotonically increasing entropy. Resolving the paradox therefore requires a deeper understanding of the quantum structure of black holes.

In the chapters that follow, we explore how string theory—and in particular the fuzzball paradigm—offers a framework in which the information paradox is resolved. In this approach, black hole microstates are described by horizonless, smooth geometries that emit radiation in a unitary manner. These solutions reproduce the Bekenstein-Hawking entropy and bypass the central assumptions leading to the paradox, providing a compelling resolution within a consistent theory of quantum gravity.

Chapter 4

Black Holes in String Theory

String theory is a part of twenty-first century physics that fell by chance into the twentieth century.

— E. Witten

String theory is a framework in which the fundamental constituents of nature are not point particles, but one-dimensional extended objects called strings. At low energies, string theory reduces to the Einstein field equations, but it also provides a microscopic description of black holes, revealing rich structures—such as branes and dualities—that go beyond classical general relativity. These features make it a powerful setting for exploring the issue of the black hole information paradox we discussed in the last section of the previous chapter, Section 2.6.

To make concrete progress on the black hole information paradox within string theory, it is useful to examine specific, tractable examples where black hole microstates can be constructed explicitly. Among the various systems studied over the past two decades, the D1D5 brane configuration has emerged as a particularly rich and well-understood setup [67]. It captures the essential features of black hole microphysics while offering analytic control over both geometric and CFT descriptions.

Rather than surveying the full landscape of string-theoretic black hole solutions[1], we focus on a single representative system and present a lightning review. This chapter provides the foundational framework and motivation for the subsequent investigations into the lifting of D1D5P states (Section 5) and the emergence of thermodynamic behavior in horizonless geometries (Section 6).

[1] For standard references, see [3, 68–70]

4.1 The Geometric Description of the D1D5 System

In a certain type of String theory, namely type IIB string theory compactified on[2] $M^5 \times S^1 \times T^4$, one encounters an interesting configuration known as the D1D5 system. This system can be constructed in M theory using intersecting $M2$ branes or in type IIB string theory as a bound state of n_5 D5-branes wrapped on $S^1 \times T^4$, n_1 D1-branes wrapped along one of the S^1 and n_p momentum carried along the S^1 direction.

In the 10D string theory the solution takes the form

$$ds_{10}^2 = \frac{1}{f_1}\left(-dt^2 + dy^2 + (f_p - 1)\,(dt + dy)^2\right) + f_5\left(dr^2 + r^2 d\Omega_3^2\right) + \sum_{a=1}^{4} dz^a dz_a\,, \tag{4.1}$$

where $r^2 = x_1^2 + x_2^2 + x_3^2 + x_4^2$ with $(t, x_1, x_2, x_3, x_4) \equiv (t, r, \Omega_3)$ as the coordinates of M^5, y as the S^1 circle and z_a as coordinates on T^4. The functions f_i and the coefficients c_i are:

$$f_i(r) = 1 + \frac{c_i n_i}{r^2}\,, i \in \{1, 5, p\}, \quad c_1 = \frac{4G_N^{(5)} R}{g_s \pi \alpha'}, \quad c_5 = \alpha' g_s, \quad c_p = \frac{4G_N^{(5)}}{\pi R}\,, \tag{4.2}$$

where $G_N^{(5)}$ is the 5D gravitational constant, g_s is the string coupling, α' is the Regge slope and R is the radius of S^1.

At high energies, this system can be identified with a classical extremal charged black hole[3] in five dimensions, as first recognized in [69]. The metric of the resulting 5D extremal black hole is given by:

$$ds_5^2 = -\frac{dt^2}{(f_1 f_5 f_p)^{2/3}} + (f_1 f_5 f_p)^{1/3}\left(dr^2 + r^2 d\Omega_3^2\right). \tag{4.3}$$

This solution has a horizon at $r = 0$ with nonzero area. The physical radius of the horizon and the area are given by:

$$R_h = (c_1 c_5 c_p\, n_1 n_5 n_p)^{1/6}\,, \tag{4.4}$$

$$A_h = 2\pi^2 R_h^3 = 8\pi G_N^{(5)} \sqrt{n_1 n_5 n_p}\,. \tag{4.5}$$

The Bekenstein-Hawking entropy then reads:

$$S_{Bek} = \frac{A_h}{4G_N^{(5)}} = 2\pi\sqrt{n_1 n_5 n_p}. \tag{4.6}$$

[2] M^5 refers to a five-dimensional compact manifold like T^5 or $K3 \times S^1$, T^N, represents an N dimensional torus, S^N represents an N dimensional sphere, and $K3$ represents a Calabi–Yau manifold.

[3] A non-extremal generalization of this solution can be obtained by introducing a non-extremality parameter r_0 and boost parameters α_i associated with each charge. For full expressions, see [67, 71].

4.2 The CFT Description of the D1D5 System

At low energies, the D1D5 system is described by a 1+1-dimensional supersymmetric gauge theory arising from open strings connecting the branes. The moduli space of this theory includes a Higgs branch, corresponding to configurations where the branes form bound states while preserving supersymmetry. In the infrared (IR) limit, the theory flows to a nonlinear sigma model with target space given by a smooth resolution of the symmetric product orbifold of $M = T^4$ or $K3$, where $N = n_1 n_5$. This results in a two-dimensional $\mathcal{N} = (4, 4)$ superconformal field theory (SCFT) that captures the interacting dynamics of the system. A free field realization of this theory can be constructed using $N = n_1 n_5$ copies of four bosons and fermions. See [67] for a detailed analysis.

While the D1D5 SCFT is not generically free, it becomes exactly solvable at a special point in its moduli space known as the *orbifold point*. At this point, the theory reduces to a free $\mathcal{N} = (4, 4)$ supersymmetric sigma model with target space $\mathrm{Sym}^N(M) = M^N/S_N$. Although the orbifold point lies far from the point in moduli space holographically dual to string theory on $\mathrm{AdS}_3 \times S^3 \times M$, it remains computationally tractable and retains the correct BPS spectrum. In particular, quantities protected by supersymmetry—such as black hole microstate counts—are invariant under moduli deformations and can thus be reliably computed at the orbifold point. We will make use of this free field realization to motivate the lifting program developed in Chapter 5.

Using the CFT description one can calculate the entropy of the D1D5 CFT, this was done by [3] and remarkably found to match the Bekenstein entropy of the 5D black hole.[4] We review the key features of the calculation below. At the orbifold point of the D1D5 SCFT, the central charge of the CFT is given by

$$c = 6 n_1 n_5 \,. \tag{4.7}$$

Adding a momentum charge n_p carried by left-moving excitations $L_0 = n_5$ gives us the D1D5P system described in the previous section. Now, Cardy's formula [72] gives the asymptotic density of states at large energy in a 2D CFT as:

$$\begin{aligned} S_{micro} &= 2\pi \sqrt{\frac{c\, L_0}{6}} \,. \\ &= 2\pi \sqrt{n_1 n_5 n_p} \,, \end{aligned} \tag{4.8}$$

which is exactly the S_{Bek} found in the previous section as (4.6).

[4] Note, at this low-energy limit, one can imagine the D1D5 system to be like system of gas particles which has entropy but due to weak gravity, cannot form black hole. But, one can show that this entropy remains protected as one moves away from this free orbifold point into the regime of strong coupling where we have black holes.

4.3 The Fuzzball Paradigm

In the above discussion, we counted black hole microstates by an indirect argument—using supersymmetry to relate the state count at weak coupling ($g_s \sim 0$, the CFT description) to the entropy at strong coupling ($g_s \sim 1$, the supergravity, black hole description). At weak coupling we could count states, but these did not form black holes. At strong coupling, we relied on the classical black hole metric and computed the area law entropy. But this metric has a horizon, and thus leads to the information paradox. To resolve this issue, we must explicitly construct the microstates at strong coupling and study their geometry.

This is the goal of the fuzzball program. [4, 5, 73–77]. In what follows, we present the 2-charge solution and highlight its key features.

4.3.1 The *naive* NS1-P solution

Consider the 3 charge metric of the previous section (4.1). Setting the n_5 charge to be zero, we find the metric to be of the form

$$ds_{10}^2 = \frac{1}{f_1}\left(-dudv + (f_p - 1)\, dv^2\right) + dr^2 + r^2 d\Omega_3^2 + \sum_{a=1}^{4} dz^a dz_a\,, \tag{4.9}$$

for $u = t - y, v = t + y$. This two-charge metric can also be viewed as the NS1-P solution, obtained via a sequence of T and S dualities.[5] We will refer to this solution as the **naive NS1-P metric**, as we will now argue that it does not correspond to a physical configuration of NS1 and P charges.

While the two-charge geometry above solves the low-energy supergravity equations away from $r = 0$, the presence of a singularity at the origin does not ensure that the solution is admissible in full string theory. In the bound state of NS1-P, the momentum P is carried by traveling waves on the *multiwound* NS1 string, with winding number $k = n_1$.

However, the fundamental string NS1 does not possess longitudinal vibration modes. Thus, all of the momentum must be carried by transverse oscillations. This necessarily causes the string to bend away from its central axis, implying that it cannot remain localized at $r = 0$ in the transverse space. We are therefore led to question the validity of the naive solution, which assumes that the NS1-P source sits at a point in the transverse space.

[5] If we retain only two charges in the D1-D5-P system, the resulting bound state is dual to the NS1-P configuration. This duality is useful for understanding the geometric structure of the D1-D5 system, since the NS1-P frame describes a fundamental string carrying left-moving vibrations.

4.3.2 The *true* NS1-P solution

Let us now find the true 2 charge solution with a transverse wave profile with momentum P on the NS1 string. There are n_1 strands of the long multiwound NS1 string carrying a momentum profile of $\vec{F}^s(v)$ where s labels each strand. The geometry can be found using the standard harmonic superposition method [70] and is given by[6]

$$ds_{10}^2 = \frac{1}{f_1}\left(-dudv + (f_p-1)\,dv^2 + 2A_i dx^i dv\right) + dr^2 + r^2 d\Omega_3^2 + \sum_{a=1}^{4} dz^a dz_a\,,$$
$$f_1 = 1 + \sum_s \frac{Q_1^s}{|\vec{x}-\vec{F}(v)|^2}\,, \quad f_p = 1 + \sum_s \frac{Q_1^s|\dot{\vec{F}}(v)|^2}{|\vec{x}-\vec{F}(v)|^2}\,, \quad A_i = -\sum_s \frac{Q_1^s \dot{\vec{F}}(v)}{|\vec{x}-\vec{F}(v)|^2}\,. \tag{4.10}$$

In the so called *black hole* limit of $n_1, n_p \gg 1$, we find

$$\sum_{s=1}^{n_1} \to \int_{s=0}^{n_1} ds = \int_{y=0}^{2\pi R n_1} \frac{ds}{dy} dy = \frac{1}{2\pi R}\int_{v=0}^{L_T} dv\,, \tag{4.11}$$

where $L_T = 2\pi R n_1$ is the total range of the y coordinate on the multiwound string. With these substitutions and $Q_1^{(s)} = \frac{Q_1}{n_1}$, we find our solution to be

$$ds_{10}^2 = \frac{1}{f_1}\left(-dudv + (f_p-1)\,dv^2 + 2A_i dx^i dv\right) + dr^2 + r^2 d\Omega_3^2 + \sum_{a=1}^{4} dz^a dz_a\,,$$
$$f_1 = 1 + \frac{Q_1}{L_T}\int_0^{L_T} \frac{dv}{|\vec{x}-\vec{F}(v)|^2}\,, \quad f_p = 1 + \frac{Q_1}{L_T}\int_0^{L_T} \frac{dv|\dot{F}(v)|^2}{|\vec{x}-\vec{F}(v)|^2}\,, \quad A_i = -\frac{Q_1}{L_T}\int_0^{L_T} \frac{dv\dot{F}_i(v)}{|\vec{x}-\vec{F}(v)|^2}\,. \tag{4.12}$$

4.3.3 The D1D5 versions

Using a string of S and T dualities, one arrives at the D1D5 solution for the above NS1-P solutions. We do not explicitly mention all the dualities here but refer the reader to [4] for a detailed analysis. We contrast the D1D5 versions of the *naive* and *true* NS1-P solutions below.

$$ds^2_{naive} = \frac{-dt^2+dy^2}{\sqrt{\left(1+\frac{Q_1'}{r^2}\right)\left(1+\frac{Q_5'}{r^2}\right)}} + \sqrt{\left(1+\frac{Q_1'}{r^2}\right)\left(1+\frac{Q_5'}{r^2}\right)}(dr^2 + r^2 d\Omega_3^2) + \sqrt{\frac{1+\frac{Q_1'}{r^2}}{1+\frac{Q_5'}{r^2}}} dz_a dz^a\,, \tag{4.13}$$

[6] We have used a shorthand $Q_1 = c_1 n_1$ to match with standard literature.

$$ds^2_{true} = \frac{1}{\sqrt{f_5 f_1}}\left(-(dt - A_i dx^i)^2 + (dy + B_i dx^i)^2\right) + \sqrt{f_5 f_1}(dr^2 + r^2 d\Omega_3^2) + \sqrt{\frac{f_1}{f_5}}\sum_{a=1}^{4} dz^a dz_a\,,$$

$$f_5 = 1 + \frac{\mu Q_1}{L_T}\int_0^{\mu L_T} \frac{dv}{|\vec{x} - \mu\vec{F}(v)|^2}\,, \quad f_1 = 1 + \frac{\mu Q_1}{L_T}\int_0^{\mu L_T} \frac{dv|\mu\dot{\vec{F}}(v)|^2}{|\vec{x} - \mu\vec{F}(v)|^2}\,,$$

$$A_i = -\frac{\mu Q_1}{L_T}\int_0^{\mu L_T} \frac{dv\mu\dot{F}_i(v)}{|\vec{x} - \vec{\mu}F(v)|^2}\,, \quad dB = -\star_4 dA\,, \tag{4.14}$$

where $\star_4$ is the duality operation in the 4-d transverse space (r, Ω_3) and μ is a parameter constructed out of the different moduli during the duality transformations. These geometries (4.14) represent horizonless, smooth solutions that carry the same charges as the naive 2-charge black hole. Unlike the standard black hole geometry—which would emerge from spherically averaging over all such microstates—each fuzzball has a unique structure in the cap region determined by its profile $\vec{F}(v)$. Far from the core, the geometries match the throat of the black hole, but near $r \sim 0$, they cap off smoothly without forming a horizon.

In Fig. 4.1, we schematically depict this transition from naive black hole geometry to horizonless fuzzball states. In the next section, we analyze the key lessons that emerge from these constructions.

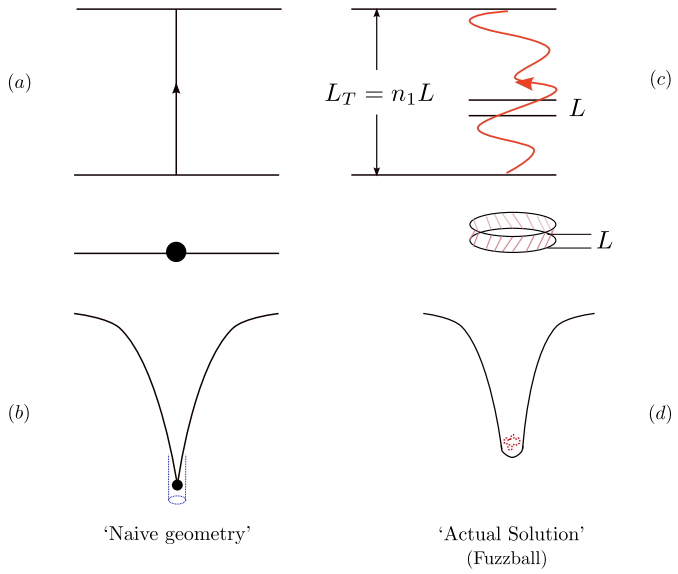

Figure 4.1: (a) If a string could carry momentum as a longitudinal wave, then it would generate a spherically symmetric geometry. (b) This 'naive' geometry would have a singular horizon at leading order, but α' corrections turn this singularity into a regular horizon. (c) The actual string of string theory has only transverse vibrations, which break spherical symmetry and cause the string to spread out over these transverse directions. (d) The resulting geometry is a 'fuzzball' with no horizon.

4.4 The Black Hole Information Paradox: Revisited

The fuzzball paradigm, emerging from explicit constructions in string theory, offers a novel resolution to the black hole information paradox. In this framework, black hole microstates correspond to horizonless, smooth geometries—termed fuzzballs—rather than the traditional singular solutions with horizons. The construction of large classes of such solutions, particularly for the two-charge and three-charge systems, challenges the standard black hole picture by demonstrating that horizonless geometries can reproduce the same charges and asymptotics as classical black holes.

Fuzzballs evade the paradox precisely because they lack horizons: the quantum information paradox arises from the presence of an event horizon, which leads to information loss in Hawking's semiclassical derivation. In contrast, fuzzballs radiate like any other quantum system, preserving unitarity. For example, non-extremal fuzzball solutions exhibit ergoregion emission spectra that match the predictions from the dual CFT and reproduce the expected thermal features, while remaining explicitly unitary. These matches provide compelling evidence that the traditional semiclassical black hole description emerges as a coarse-grained average over an ensemble of fuzzball microstates.

This perspective implies a significant shift in our understanding of black hole entropy. Although fuzzballs do not possess horizons, the area-entropy relation still holds when evaluated on surfaces enclosing the cap region where microstates differ. This suggests that the Bekenstein-Hawking entropy counts the number of orthogonal fuzzball geometries compatible with given macroscopic charges. Moreover, features such as the nontrivial fibration of compact directions, dipole charge structure, and deviations from spherical symmetry point to rich structure near the would-be horizon, supported by stringy and topological effects.

Despite this progress, many open questions remain. One of the most pressing challenges is understanding how black hole thermodynamics can be recovered when the classical geometry is replaced by a horizonless microstate. From the dual CFT perspective, it remains unclear which states remain BPS as we move away from the orbifold point, and to what extent they lift. More broadly, we may ask whether all black holes admit a complete description in terms of fuzzball microstates. What is the classification of non-BPS fuzzballs? What governs their dynamics under gravitational collapse? And by what mechanism does semiclassical geometry emerge from an ensemble of microstates?

Observationally, the possibility that astrophysical black holes are fuzzballs raises tantalizing prospects. Could echoes, horizon-scale structure, or subtle deviations from classical predictions offer evidence for underlying microstructure? Many of these phenomena are becoming increasingly accessible through current and future gravitational wave observations.

We explore two of these directions in the chapters that follow. In Chapter 5, we

analyze the lifting of D1D5P states away from the orbifold point and their implications for the microstate structure. In Chapter 6, we study the thermodynamics of horizonless Extremely Compact Objects, testing the emergence of black hole thermodynamics from regular, unitary systems.

Chapter 5

Lifting in D1D5P system

> *Our job in physics is to see things simply, to understand a great many complicated phenomena in a unified way, in terms of a few simple principles.*
>
> — S. Weinberg

In the previous section, we reviewed the essential ingredients of black holes in string theory and identified the D1D5 system in type IIB string theory as a particularly tractable and instructive setup for probing the black hole information paradox. In Section 4.2, we noted that the near-horizon dynamics of the D1D5 black hole is described by a $1+1$D conformal field theory, known as the D1D5 CFT, where the momentum charge n_p is carried by left-moving excitations[1]. This CFT possesses a special point in its moduli space, known as the orbifold point, where the theory admits a free-field description in terms of bosons and fermions living in twisted sectors.

At this orbifold point, states with purely left-moving (or purely right-moving) excitations are BPS[2] and preserve a fraction of the $\mathcal{N}=4$ supersymmetry. As the CFT is deformed away from the orbifold point toward the strongly coupled regime, for which there is a description in terms of a dual semiclassical gravity theory, some of the short multiplets formed from these BPS states join together into long multiplets and *lift*—acquiring anomalous corrections to their conformal dimensions. Only those states that remain unlifted (and thus BPS) throughout the moduli space contribute to protected quantities like the index. Given that the total number of such unlifted states (the set of microstates of the extremal black hole and hence the entropy) is captured by a supersymmetric index [3, 78], key questions arise:

> *Which extremal states at the orbifold point stay unlifted and thus remain BPS across the moduli space? Among the states that lift, how much does their conformal dimension shift upon lifting?*

[1] Without the loss of generality, we let the momentum charge be carried by left-movers.
[2] See [3] for a quick introduction to BPS states in black hole physics.

In this chapter, we review the progress we have made in addressing these questions. We examine specific families of D1D5 states that are BPS at the orbifold point but lift as we move away from this free point toward the supergravity regime. Using conformal perturbation theory, we compute the lifting at quadratic order in the coupling λ. The structure of these anomalous dimensions provides insight into how string states behave in the dual gravity description and helps illuminate the nature of fuzzball configurations representing black hole microstates.

5.1 Conformal perturbation theory on the cylinder

We begin by reviewing the deformation of the D1D5 CFT away from the orbifold point as given in [79].

5.1.1 CFT Setup

Consider a 2D conformal field theory on a cylinder with coordinate $w = \tau + i\sigma$, Hamiltonian H_0 and a normalized conformal field state $|\phi\rangle$ with dimensions $(h, 0)$. The energy of the state is $E = h + \bar{h} = h$ and suppose that it is nondegenerate. (We will relax this condition soon.) We place the state $|\phi\rangle$ on the the cylinder at $\tau = -T/2$ and the conjugate state $\langle\phi|$ at $\tau = T/2$ to get the transition amplitude[3]

$$A(T) = \langle\phi(\tfrac{T}{2})|\, e^{-H_0 T}\, |\phi(-\tfrac{T}{2})\rangle = e^{-hT}\,. \tag{5.1}$$

Now, suppose we perturb the Hamiltonian of the system H_0 as

$$H_0 \to H_0 + \delta H(\lambda)\,, \quad \frac{\delta H(\lambda)}{H_0} \ll 1\,, \tag{5.2}$$

where λ is a coupling constant. Then the transition amplitude of the perturbed system in the unperturbed basis is given by

$$A(T) + \delta A(T) = \langle\phi(\tfrac{T}{2})|\, e^{-(H_0+\delta H(\lambda))T}\, |\phi(-\tfrac{T}{2})\rangle = e^{-(h+2\delta h(\lambda))T} \approx e^{-hT}\,(1 - 2\delta h(\lambda) T)\,. \tag{5.3}$$

Thus, the change in the energy $\delta h(\lambda)$ can be read off from the coefficient of Te^{-hT} in $\delta A(T)$.

[3]The initial and final states are placed at finite τ in order to regularize the calculation. We will later send $T \to \infty$.

5.1.2 Degenerate states and perturbation

To generalize the setup and align it with our interests, we consider a set of n degenerate conformal field theory states $|\phi_a\rangle$, $a \in \{1, \ldots, n\}$, each with left-moving conformal dimension $(h, 0)$. In addition, we allow for the presence of other, possibly infinite, non-degenerate states $|\phi_\mu\rangle$ with well-defined scaling dimensions satisfying

$$\langle\phi_a|\phi_b\rangle = \delta_{ab}\,, \qquad \langle\phi_a|\phi_\mu\rangle = 0\,, \qquad a, b \in \{1, \ldots, n\}\,. \tag{5.4}$$

Under perturbation, the eigenbasis ϕ with $(h, 0)$ deforms to $\tilde{\phi}$ with $(h + \delta h_{a'}(\lambda), \delta h_{a'}(\lambda))$.[4] We differentiate the two types of operators in the following way. We label the deformations of $|\phi_a\rangle$ as $|\tilde{\phi}_{a'}(\lambda)\rangle$, $a' \in \{1, \ldots, n\}$ and all the new set of non degenerate operators with defined scaling dimensions as $|\tilde{\phi}_{\mu'}(\lambda)\rangle$, normalized similarly to (5.4) where λ is the coupling of the deformation. The energies of the unperturbed states $|\phi_{a'}\rangle$ and the perturbed states $|\tilde{\phi}_{a'}\rangle$ are therefore $E = h + \bar{h} = h$, $\tilde{E}_{a'} = h + 2\delta h_{a'}(\lambda)$ with expansions

$$\begin{aligned} \tilde{E}_{a'}(\lambda) &= E + \lambda E^{(1)}_{a'} + \lambda^2 E^{(2)}_{a'} + \cdots\,, \\ \tilde{E}_{\mu'}(\lambda) &= E_{\mu'} + \lambda E^{(1)}_{\mu'} + \lambda^2 E^{(2)}_{\mu'} + \cdots\,. \end{aligned} \tag{5.5}$$

Let us now consider the expansions of operators themselves. We can write

$$\begin{aligned} \phi_a &= \sum_{a'} C_{aa'}(\lambda)\, \tilde{\phi}_{a'}(\lambda) + \sum_{\mu'} D_{a\mu'}(\lambda)\, \tilde{\phi}_{\mu'}(\lambda)\,, \\ \phi_\mu &= \sum_{a'} F_{\mu a'}(\lambda)\, \tilde{\phi}_{a'}(\lambda) + \sum_{\mu'} G_{\mu\mu'}(\lambda)\, \tilde{\phi}_{\mu'}(\lambda)\,, \end{aligned} \tag{5.6}$$

where $C_{aa'}$, $D_{a\mu'}$, $F_{\mu a'}$, and $G_{\mu\mu'}$ are λ dependent expansion coefficients. Finally, we expand the coefficients above in powers of λ:

$$\begin{aligned} C_{aa'}(\lambda) &= C^{(0)}_{aa'} + \lambda C^{(1)}_{aa'} + \lambda^2 C^{(2)}_{aa'} + \cdots\,, \\ D_{a\mu'}(\lambda) &= D^{(0)}_{a\mu'} + \lambda D^{(1)}_{a\mu'} + \lambda^2 D^{(2)}_{a\mu'} + \cdots\,. \end{aligned} \tag{5.7}$$

Thus, in particular, ϕ_a can be expanded as[5]

$$\phi_a = \sum_{a'} \left(C^{(0)}_{aa'} + \lambda C^{(1)}_{aa'} + \lambda^2 C^{(2)}_{aa'} + \cdots\right) \tilde{\phi}_{a'} + \sum_{\mu'} \left(\lambda D^{(1)}_{a\mu'} + \lambda^2 D^{(2)}_{a\mu'} + \cdots\right) \tilde{\phi}_{\mu'}\,. \tag{5.8}$$

[4] The left and right dimensions must increase by the same amount, since$h - \bar{h}$ must always be an integer for the operator to be local.

[5] Note the absence of the term $D^{(0)}_{a\mu'}$ in this expression which can be understood by taking $\lambda \to 0$.

The orthonormality condition(5.4) gives at leading order

$$\sum_{a'} C^{(0)}_{aa'} C^{(0)*}_{ba'} = \delta_{ab} \ . \tag{5.9}$$

At last, to extract the change in energy $\delta h_{a'}(\lambda)$, we use the amplitude as in (5.3). Thus, we would compute an amplitude of the type

$$A_{ab}(T) \equiv \langle \phi_b(\tfrac{T}{2}) | e^{-(H_0+\delta H(\lambda))T} | \phi_a(-\tfrac{T}{2}) \rangle \ . \tag{5.10}$$

Substituting the expansions above into $A_{ab}(T)$ and using the orthonormality conditions, we find

$$\begin{aligned} A_{ab}(T) &= \langle \phi_b(\tfrac{T}{2}) | e^{-(H_0+\delta H(\lambda))T} | \phi_a(-\tfrac{T}{2}) \rangle \\ &= \sum_{a'} C^*_{ba'}(\lambda) C_{aa'}(\lambda) e^{-\tilde{E}_{a'}(\lambda)T} + \sum_{\mu'} D^*_{b\mu'}(\lambda) D_{a\mu'}(\lambda) e^{-\tilde{E}_{\mu'}(\lambda)T} \\ &= \sum_{a'} \left(C^{(0)*}_{ba'} + \lambda C^{(1)*}_{ba'} + \lambda^2 C^{(2)*}_{ba'} + \cdots \right) \left(C^{(0)}_{aa'} + \lambda C^{(1)}_{aa'} + \lambda^2 C^{(2)}_{aa'} + \cdots \right) e^{-\left(E + \lambda E^{(1)}_{a'} + \lambda^2 E^{(2)}_{a'} + \cdots\right)T} \\ &\quad + \sum_{\mu'} \left(\lambda D^{(1)*}_{b\mu'} + \lambda^2 D^{(2)*}_{b\mu'} + \cdots \right) \left(\lambda D^{(1)}_{a\mu'} + \lambda^2 D^{(2)}_{a\mu'} + \cdots \right) e^{-\left(E + \lambda E^{(1)}_{\mu'} + \lambda^2 E^{(2)}_{\mu'} + \cdots\right)T} . \end{aligned} \tag{5.11}$$

5.1.3 Extraction of anomalous dimensions

In general, amplitudes like $A_{ab}(T)$ are functions of the states ϕ_a, ϕ_b, the interval T, and the coupling λ. It is convenient to expand the amplitude in powers of λ to extract the anomalous dimension $\delta h_{a'}(\lambda)$:

$$A_{ab}(T) = A^{(0)}_{ab}(T) + \lambda A^{(1)}_{ab}(T) + \lambda^2 A^{(2)}_{ab}(T) + \cdots \ . \tag{5.12}$$

At $\mathcal{O}(\lambda)$, the Te^{-hT} term is

$$-Te^{-hT} \sum_{a'} C^{(0)*}_{ba'} E^{(1)}_{a'} C^{(0)}_{aa'} \, . \tag{5.13}$$

We now note that for the deformations we consider, the amplitude $A_{ab}(T)$ has no terms at $\mathcal{O}(\lambda)$. As we will see in the next subsection, this is because the deformation operator D that perturbs the theory away from the orbifold point lies in the twist-2 sector, while the states $|\phi_a\rangle$ and $|\phi_b\rangle$ belong to the untwisted sector. The three-point function $\langle \phi_b | \, D \, | \phi_a \rangle$ then vanishes due to orbifold group selection rules.

It follows that all first-order corrections $E^{(1)}_{a'}$ vanish. To see this explicitly, observe

that the $\mathcal{O}(\lambda)$ contribution to the amplitude expansion vanishes:

$$-Te^{-hT}\sum_{a'} C^{(0)*}_{ba'}\, E^{(1)}_{a'}\, C^{(0)}_{aa'} = 0 \qquad \forall\, a, b\,. \tag{5.14}$$

Let us define a diagonal matrix $E^{(1)}$ with entries

$$\left(E^{(1)}\right)_{a'b'} = E^{(1)}_{a'}\,\delta_{a'b'}\,, \tag{5.15}$$

so that the amplitude term becomes

$$\sum_{a'} C^{(0)*}_{ba'}\, E^{(1)}_{a'}\, C^{(0)}_{aa'} = \left(C^{(0)\dagger} E^{(1)}\, C^{(0)}\right)_{ba}\,. \tag{5.16}$$

Hence, we have

$$C^{(0)\dagger} E^{(1)}\, C^{(0)} = 0\,. \tag{5.17}$$

Since $C^{(0)}$ is unitary (by orthonormality of states (5.9)), the only solution to the above is

$$E^{(1)} = 0 \quad \Rightarrow \quad E^{(1)}_{a'} = 0 \quad \forall\, a'\,. \tag{5.18}$$

At $\mathcal{O}(\lambda^2)$, for the Te^{-hT} term, we are then left with (as $E^{(1)}_{a'} = 0\,, \forall\, a'$):

$$-Te^{-ET}\sum_{a'} C^{(0)*}_{ba'} E^{(2)}_{a'} C^{(0)}_{aa'}\,. \tag{5.19}$$

Hence to know the anomalous dimensions, we can compute the matrix $A^{(2)}$, look at the coefficient of $-Te^{-ET}$, then eigenvalues of $A^{(2)}$ yield $2\delta h_{a'}$ upto $\mathcal{O}(\lambda^2)$:

$$E^{(2)}_{a'} = 2\delta h_{a'}\,. \tag{5.20}$$

For practical reasons, instead of diagonalizing the entire matrix, we compute the expectation value

$$\sum_{a'} |\langle\tilde{\phi}_{a'}|\phi_1\rangle|^2 E^{(2)}_{a'}\,, \tag{5.21}$$

where $|\phi_1\rangle$ is the specific state of interest, e.g., $|\Phi^{(m)}\rangle$.

This approach allows us to probe the *lifting* behavior of specific stringy excitations, even when the full spectrum of degenerate states is too large to handle explicitly. We will elaborate this crucial point soon.

5.2 General expression for lifting at second order

We now derive the general formula for lifting using path integral techniques. Since the perturbation is specified as a deformation of the Lagrangian,

$$S_{\text{pert}} = S_0 + \lambda \int d^2w\, D(w, \bar{w})\,, \tag{5.22}$$

we compute the amplitude $A_{ab}(T)$ via insertions of D rather than Hamiltonian evolution. The CFT perturbation theory method 5.1.3 requires the computation of the second order lift from the integrated correlator

$$A^{(2)}_{ab}(T) = \frac{1}{2}\Big\langle \phi_b\big(\tfrac{T}{2}\big)\Big| \int d^2w_2 D(w_2, \bar{w}_2) \int d^2w_1 D(w_1, \bar{w}_1)\Big|\phi_a\big(-\tfrac{T}{2}\big)\Big\rangle\,, \tag{5.23}$$

where the factor of $1/2$ comes from the second order perturbation in the path integral and the range of the w_i integrals are

$$0 \le \sigma_i < 2\pi\ , \quad -\tfrac{T}{2} < \tau_i < \tfrac{T}{2}\ . \tag{5.24}$$

It is convenient to express the states in terms of cylinder modes (e.g., J^a_n) rather than local fields. Factoring out the time dependence, we define

$$|\phi_a(-\tfrac{T}{2})\rangle = e^{-\frac{hT}{2}}\,|\Phi_a\rangle\ , \qquad \langle\phi_b(\tfrac{T}{2})| = e^{-\frac{hT}{2}}\,\langle\Phi_b|\ , \tag{5.25}$$

where $|\Phi\rangle$ is built from modes with no explicit τ dependence. Thus, the amplitude simplifies to

$$A^{(2)}_{ab}(T) = \frac{1}{2}e^{-hT}\Big\langle \Phi_b\Big| \int d^2w_2 D(w_2, \bar{w}_2) \int d^2w_1 D(w_1, \bar{w}_1)\Big|\Phi_a\Big\rangle\,. \tag{5.26}$$

Since Φ_a and Φ_b have the same energy, the integrand depends only on $\Delta w = w_2 - w_1$. We wish to separate integration over Δw and the center-of-mass coordinate $s = \frac{1}{2}(w_1 + w_2)$.

Although the integration ranges do not factorize for finite T, in the limit $T \to \infty$, the suppression of intermediate states with $E_k \ge h + 2$ ensures that the contribution is dominated by small Δw.[6] Thus, setting $w_1 = 0$ and integrating over $w \equiv w_2$, we find

$$A^{(2)}_{ab}(T) \approx (2\pi T)\frac{1}{2}e^{-hT}\left\langle \Phi_b\left|\left(\int d^2w\, D(w, \bar{w})\right) D(0)\right|\Phi_a\right\rangle\ . \tag{5.27}$$

The factor $2\pi T$ comes from integrating over w_1.

It is convenient to write these two insertions of the deformation operator $D(w, \bar{w})$ in

[6] The suppression $E_k \ge h + 2$ is ensured because intermediate states must match the spin and allow a nonzero three-point function with D and ϕ_a, implying that the intermediate primary must have dimensions $(h + 1, 1)$, leading to $E_k = h + 2$. If we have descendants, $E_k \ge h + 2$.

different forms

$$D(w,\bar{w}) = \epsilon^{\dot{A}\dot{B}} G^{-}_{\dot{A},-\frac{1}{2}} \bar{G}^{-}_{\dot{B},-\frac{1}{2}} \sigma_2^{++}(w,\bar{w}) = \epsilon^{\dot{A}\dot{B}} G^{+}_{\dot{A},-\frac{1}{2}} \bar{G}^{+}_{\dot{B},-\frac{1}{2}} \sigma_2^{--}(w,\bar{w}) \ , \tag{5.28}$$

which are equivalent to (B.60) but with the explicit $SU(2)$ singlet structure obscured. In

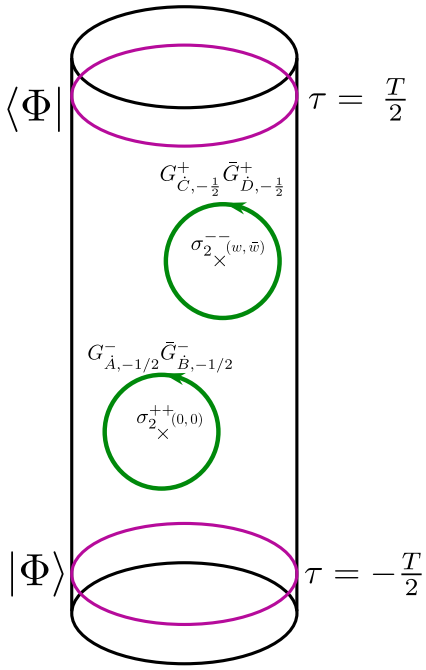

Figure 5.1: In the above figure, we depict the correlator from (5.30). In purple, we see the initial $|\Phi\rangle$ and final states $\langle\Phi|$ located at $\tau = -T/2$ and $\tau = T/2$ respectively. The green contours are the supersymmetry modes from the two deformation operators placed at $(0,0)$ and $(w,\bar{w})$.

the previous section on conformal perturbation theory 5.1, it was shown that the second order lift in energy is given by the coefficient of $-Te^{-hT}$ in the correlator $A^{(2)}(T)$ and so[7]

$$E^{(2)}\Big(|\Phi\rangle\Big) = -\pi\lambda^2 \lim_{T\to\infty} \frac{X(T)}{\langle\Phi|\Phi\rangle} \ , \tag{5.29}$$

where we define

$$X(T) \equiv \epsilon^{\dot{C}\dot{D}} \epsilon^{\dot{A}\dot{B}} \int d^2w \left\langle \Phi \middle| \Big(G^{+}_{\dot{C},-\frac{1}{2}} \bar{G}^{+}_{\dot{D},-\frac{1}{2}} \sigma_2^{--}\Big)(w,\bar{w}) \Big(G^{-}_{\dot{A},-\frac{1}{2}} \bar{G}^{-}_{\dot{B},-\frac{1}{2}} \sigma_2^{++}\Big)(0,0) \middle| \Phi \right\rangle \ , \tag{5.30}$$

with the initial and final states are located at $\tau = -\frac{T}{2}$ and $\tau = \frac{T}{2}$ respectively. The configuration of the amplitude in (5.30) is depicted in Figure 5.1.

We will consider the case where we excite only the left-moving part of the states. Since the right-moving part of the states we consider is just the NS vacuum on all copies, the right-moving part of the correlator in (5.30) will be determined simply by the $D \times D$ OPE

[7] We have at last taken $T \to \infty$ and also, explicitly divided the lift by the norm $\langle\Phi|\Phi\rangle$ to generalize to cases where the states are not normalized.

and thus will contribute a factor independent of the initial and final states of the form

$$\langle 0_{NS}|\Big(\bar{G}^{+}_{\dot{D},-\frac{1}{2}}\sigma_2^{-}\Big)(\bar{w})\Big(\bar{G}^{-}_{\dot{B},-\frac{1}{2}}\sigma_2^{+}\Big)(0)|0_{NS}\rangle = \frac{-\epsilon_{\dot{D}\dot{B}}}{4\sinh^2(\frac{\bar{w}}{2})} \ . \tag{5.31}$$

It is convenient to then write $X(T)$ as

$$\begin{aligned} X(T) &= \epsilon^{\dot{C}\dot{D}}\epsilon^{\dot{A}\dot{B}}\int d^2w\, A(w,0)\epsilon_{\dot{A}\dot{C}}\left(\frac{-\epsilon_{\dot{D}\dot{B}}}{4\sinh^2(\frac{\bar{w}}{2})}\right) \\ &= -\frac{1}{2}\epsilon^{\dot{C}\dot{D}}\epsilon^{\dot{A}\dot{B}}\epsilon_{\dot{D}\dot{B}}\epsilon_{\dot{C}\dot{A}}\int d^2w\, A(w,0)\,\partial_{\bar{w}}\Big(\coth(\tfrac{\bar{w}}{2})\Big) \\ &= \frac{i}{2}\int_C dw\, A(w,0)\coth(\tfrac{\bar{w}}{2}) \\ &\equiv I_{C_1} + I_{C_2} + I_{C_3} \ , \end{aligned} \tag{5.32}$$

where the contours C_1, C_2 and C_3 on the cylinder (depicted in Figure 5.2) are at $\tau = \frac{T}{2}, -\frac{T}{2}$ and around $|w| = \epsilon\,,\ \epsilon \to 0$ respectively and $A(w_2, w_1)$ is simply the non-integrated left-moving amplitude

$$A(w_2,w_1) \equiv \Big\langle \Phi\Big|\Big(G^{+}_{-,-\frac{1}{2}}\sigma_2^{-}\Big)(w_2)\Big(G^{-}_{+,-\frac{1}{2}}\sigma_2^{+}\Big)(w_1)\Big|\Phi\Big\rangle \ , \tag{5.33}$$

where specific $SU(2)_2$ indices on the G modes have been chosen for ease of computation.

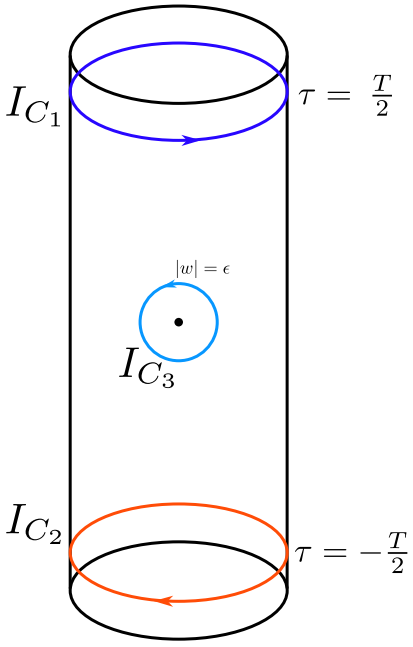

Figure 5.2: We show the three boundary contour integrals I_{C_1}, I_{C_2} and I_{C_3} defined in equations (5.34a), (5.34b) and (5.34c) respectively. Together these contour integrals yield the integrated amplitude in (5.32) required in the lift (5.29).

The three contour integrals in (5.32) are then

$$I_{C_1}(T) \equiv -\frac{1}{2}\int_0^{2\pi} d\sigma\, A(w,0)\coth(\tfrac{\bar{w}}{2})\ , \tag{5.34a}$$

$$I_{C_2}(T) \equiv \frac{1}{2}\int_0^{2\pi} d\sigma\, A(w,0)\coth(\tfrac{\bar{w}}{2})\ , \tag{5.34b}$$

$$I_{C_3} \equiv -\frac{i}{2}\oint_{|w|=\epsilon} dw\, A(w,0)\coth(\tfrac{\bar{w}}{2})\ , \tag{5.34c}$$

where the complex coordinates on the cylinder have been written as $w = \tau + i\sigma$ and $\bar{w} = \tau - i\sigma$. In I_{C_3} the cutoff ϵ should be taken to 0 at the end of the calculation. The computation thus boils down to evaluating the non-integrated left-moving amplitude $A(w,0)$ with the universal right-moving $D \times D$ OPE contribution factored out. We note that, as discussed in [79], the integral I_{C_3} contributes only a universal divergent piece $\sim \frac{1}{\epsilon}$ independently of the choice of external states which is removed by a counterterm in the action. Thus the integral I_{C_3} does not contribute to the lift (5.29).

5.2.1 The lifting method

The previous section provided the necessary tools to compute the lifting of D1D5 states. Before presenting the results for various classes of states in the following sections, we illustrate the complete detailed method using a single example. This will give the reader a concrete, hands-on understanding of the lifting procedure.

We compute the lift of the superdescendant state $|G\phi\rangle^{\alpha}_{\dot{A}(h,s)}$, chosen because it typifies the general level of computational complexity encountered in the states analyzed throughout this chapter. From Section 5.2 the key quantity we need to compute is the left-moving amplitude

$$A^{(1)(1)}_{h,s}(w_2,w_1) \equiv \langle\phi|G^{\beta}_{\dot{B},s}\left(G^{+}_{-,-\frac{1}{2}}\sigma_2^{-}\right)(w_2)\left(G^{-}_{+,-\frac{1}{2}}\sigma_2^{+}\right)(w_1)\, G^{\alpha}_{\dot{A},-s}|\phi\rangle\ , \tag{5.35}$$

where we have taken the descendant excitation to be on a definite copy, namely copy 1, for both the initial and final state. The general method of computing this amplitude will be similar to that employed in [20] with some modifications to account for the fact that we do not specify any explicit form of the superconformal primary state $|\phi\rangle$. The steps are as follows:

(1) The amplitude $A^{(1)(1)}_{h,s}(w_2,w_1)$ is on a doubly-covered cylinder due to the presence of twist operators σ_2. This operator joins and then splits the two copies of the untwisted initial and final states. This effect of the twist operators can be resolved by mapping the amplitude to the covering space. As shown in [80] and used in the context of lifting of states in [18–20, 79], the covering space map $z \to t$ for the case of two order-2

twist operators is given by

$$z(t) = \frac{(t+a)(t+b)}{t} \ , \tag{5.36}$$

where $z = e^w$ is the doubly-covered plane. The twist operator insertions on the plane at $z_1 = e^{w_1}$ and $z_2 = e^{w_2}$ are mapped to $t_1 = -\sqrt{ab}$ and $t_2 = \sqrt{ab}$ on the covering space. In our conventions the points $z = 0$ and $z = \infty$ on the first sheet of the doubly-covered plane map to $t = -a$ and $t = \infty$ on the covering space. Under this map the initial state transforms as

$$\begin{aligned} G^{\alpha}_{\dot{A},-s}|\phi\rangle &= \oint_{\tau\to-\infty} \frac{dw_3}{2\pi i}\, e^{-sw_3}\, G^{\alpha}_{\dot{A}}(w_3)|\phi\rangle \\ &= \lim_{\tilde{t}\to-a} \tilde{z}^h \left(\frac{d\tilde{t}}{d\tilde{z}}\right)^h \oint_{\tilde{t}} \frac{dt_3}{2\pi i}\, z_3^{-s+\frac{1}{2}} \left(\frac{dt_3}{dz_3}\right)^{\frac{1}{2}} G^{\alpha}_{\dot{A}}(t_3)\phi(\tilde{t}\,)|0_{NS}\rangle \ , \end{aligned} \tag{5.37}$$

and likewise the final state transforms as

$$\begin{aligned} \langle\phi|G^{\beta}_{\dot{B},s} &= -\oint_{\tau\to\infty} \frac{dw_4}{2\pi i}\, e^{sw_4} \langle\phi|G^{\beta}_{\dot{B}}(w_4) \\ &= -\lim_{t'\to\infty} z'^h \left(\frac{dt'}{dz'}\right)^h \oint_{t'} \frac{dt_4}{2\pi i}\, z_4^{s+\frac{1}{2}} \left(\frac{dt_4}{dz_4}\right)^{\frac{1}{2}} \langle 0_{NS}|\phi(t')G^{\beta}_{\dot{B}}(t_4) \ , \end{aligned} \tag{5.38}$$

where the negative sign accounts for the direction of the contour at ∞. Since the covering space map (5.36) is not conformal there will be an associated Liouville factor; this along with various conformal factors from the twist operators and spin fields are wrapped up into a "base amplitude" [79–81]

$$f_1 = \frac{a-b}{4\sqrt{ab}} \ , \tag{5.39}$$

that is independent of the external states.

(2) While this map resolves the geometric effect of the two twist operators, we are left with insertions of the spin fields $S^-(t_2)$ and $S^+(t_1)$. These can in turn be removed by performing a spectral flow of the amplitude by $\eta = -1$ and $\eta = +1$ units around t_1 and t_2 respectively. Under these spectral flows, the state at $t = -a$ transforms as

$$G^{\alpha}_{\dot{A}}(t_3)\phi(\tilde{t}\,)|0_{NS}\rangle \to \left(\frac{t_3-t_1}{t_3-t_2}\right)^{q_\alpha} G^{\alpha}_{\dot{A}}(t_3)\phi(\tilde{t}\,)|0_{NS}\rangle \ , \tag{5.40}$$

where q_α is the J^3_0 charge of $G^{\alpha}_{\dot{A},-s}$ and the state at $t = \infty$ transforms as

$$\langle 0_{NS}|\phi(t')G^{\beta}_{\dot{B}}(t_4) \to \left(\frac{t_4-t_1}{t_4-t_2}\right)^{q_\beta} \langle 0_{NS}|\phi(\tilde{t}\,)G^{\beta}_{\dot{B}}(t_4) \ . \tag{5.41}$$

While the G modes from the deformation operators do transform under the above

maps, their transformations do not depend on the external states under consideration and so they contribute a universal factor of (see Section (4.3) of [79])

$$f_2 = ab(a-b) \ . \tag{5.42}$$

(3) Following steps (1) and (2) the amplitude (5.35) is now given by

$$A^{(1)(1)}_{h,s} = -f_1 f_2 f_3 \oint_\infty \frac{dt_4}{2\pi i} \oint_{-a} \frac{dt_3}{2\pi i} \frac{z_4^{s+\frac{1}{2}}}{z_3^{s-\frac{1}{2}}} \left(\frac{dt_3}{dz_3}\right)^{\frac{1}{2}} \left(\frac{dt_4}{dz_4}\right)^{\frac{1}{2}} \left(\frac{t_3-t_1}{t_3-t_2}\right)^{q_\alpha} \left(\frac{t_4-t_1}{t_4-t_2}\right)^{q_\beta} \widetilde{C}^{\beta\alpha}_{\dot{B}\dot{A}}(t_4,t_3) \ , \tag{5.43}$$

where

$$f_3 \equiv \lim_{\substack{\tilde{t}\to -a \\ t'\to\infty}} \tilde{z}^h z'^h \left(\frac{d\tilde{t}}{d\tilde{z}}\right)^h \left(\frac{dt'}{dz'}\right)^h = \left(\frac{a}{a-b}\right)^h \ , \tag{5.44}$$

and $\widetilde{C}^{\beta\alpha}_{\dot{B}\dot{A}}$ is the correlator

$$\widetilde{C}^{\beta\alpha}_{\dot{B}\dot{A}}(t_4,t_3) \equiv \langle\phi|G^\beta_{\dot{B}}(t_4)G^+_-(t_2)G^-_+(t_1)G^\alpha_{\dot{A}}(t_3)|\phi\rangle \ . \tag{5.45}$$

At this point in the computation, one chooses how to compute such an $n-$point correlation function. In our works, we have employed three methods to compute this; the hybrid method [18], the series method [19] and the fields method [19, 20].

(4) The explicit dependence of the amplitude on w_1 and w_2 can then be recovered by using the relations

$$a = e^S \cosh^2\left(\frac{\Delta w}{4}\right) \quad , \quad b = e^S \sinh^2\left(\frac{\Delta w}{4}\right) \ , \tag{5.46}$$

where we define

$$S \equiv \frac{1}{2}(w_1+w_2) \quad , \quad \Delta w \equiv w_2 - w_1 \ . \tag{5.47}$$

This yields the amplitude $A^{(1)(1)}_{h,s}(w_2,w_1)$ where both the initial and final state have descendant excitations placed on copy 1. The left-moving copy symmetric amplitude required for the lift of the state is then given by

$$\begin{aligned} A_{h,s}(w,0) &\equiv {}^{\beta}_{(h,s)\dot{B}}\langle G\phi|\left(G^+_{-,-\frac{1}{2}}\sigma_2^-\right)(w)\left(G^-_{+,-\frac{1}{2}}\sigma_2^+\right)(0)|G\phi\rangle^{\alpha}_{\dot{A}(h,s)} \\ &= \frac{1}{2}\sum_{i,j=1}^{2} A^{(j)(i)}_{h,s}(w,0) \\ &= A^{(1)(1)}_{h,s}(w,0) + A^{(2)(1)}_{h,s}(w,0) \ , \end{aligned} \tag{5.48}$$

where we have used that $A^{(2)(2)} = A^{(1)(1)}$ and $A^{(1)(2)} = A^{(2)(1)}$ on general symmetry

grounds. The amplitude $A^{(2)(1)}$ can be obtained from $A^{(1)(1)}$ via the continuation

$$A^{(2)(1)}_{h,s}(w,0) = A^{(1)(1)}_{h,s}(w+2\pi i,0) \ , \tag{5.49}$$

which has the effect of interchanging the role of the two copies that the upper σ_2 twists.

(5) The norm of our descendant state can be found from the correlator

$${}^{\beta}_{(h,s)\dot{B}}\langle G\phi|G\phi\rangle^{\alpha}_{\dot{A}(h,s)} = \epsilon_{\dot{B}\dot{A}}\epsilon^{\beta\alpha}\left(s^2-\frac{1}{4}+h\right) \ , \tag{5.50}$$

where the quantum numbers of the conjugate state need to be opposite to the ket state and appropriate negative signs added as per the conjugation conventions of Appendix B.1.3. This definition of the Hermitian conjugate state should also be enforced on the final state of the amplitude (5.48) in order for it to be related to the lift of a particular state. The lift is then given by

$$E^{(2)}\left(|G\phi\rangle^{\alpha}_{\dot{A}(h,s)}\right) = \frac{\pi\lambda^2}{\left||G\phi\rangle^{\alpha}_{\dot{A}(h,s)}\right|^2}\lim_{T\to\infty}\int_0^{2\pi}d\sigma\, A_{h,s}(w,0)\coth\left(\tfrac{\bar{w}}{2}\right) \ , \tag{5.51}$$

where $w=\frac{T}{2}+i\sigma$ and $\bar{w}=\frac{T}{2}-i\sigma$ with $T\to\infty$ on this contour as given in (5.34a). Note that of the three integrals in (5.34) it was argued in Section 5.2 that I_{C_3} gives a vanishing contribution to the lift and for the states considered here we find that $\lim_{T\to\infty} I_{C_1}(T) = \lim_{T\to\infty} I_{C_2}(T)$ and so (5.51) contains only one integral.

5.3 Lifting of Superconformal Primaries

In this section, we present the lift of superconformal primaries in the D1-D5 orbifold CFT. We begin by defining these primaries within the $\mathcal{N}=4$ superconformal algebra and describe how the relevant physical states are constructed in the symmetric product theory. We then explain the necessity of symmetrization across copies and present the lift for this class of states. The explicit computation of the lift is omitted here for brevity, but all technical details can be found in our published work [18].

5.3.1 Superconformal Primaries: Definition

The superconformal primaries ϕ of the $\mathcal{N}=4$ superconformal algebra are defined, in the NS sector, by the mode conditions

$$L_n|\phi\rangle_{NS} = G^{\alpha}_{\dot{A},r}|\phi\rangle_{NS} = J^a_n|\phi\rangle_{NS} = 0 \quad , \quad n>0 \ , \ r\geq\frac{1}{2} \ . \tag{5.52}$$

For a superconformal primary of the full theory, these symmetry current modes should be global modes—for instance, the global Virasoro modes $L_n^{(g)}$ in the untwisted sector are given by the diagonal sum

$$L_n^{(g)} = \sum_{i=1}^{N} L_n^{(i)} \ , \tag{5.53}$$

where $L_n^{(i)}$ are the modes on the ith copy. A superconformal primary on a single copy would simply satisfy the conditions (5.52) with the modes on that particular copy. Under a spectral flow by $\eta = -1$ units to the R sector, the modes of the supercharges and $SU(2)$ currents transform as

$$G^{\pm}_{\dot{A},r} \longrightarrow G^{\pm}_{\dot{A},r\pm\frac{1}{2}} \quad , \quad J^{\pm}_n \longrightarrow J^{\pm}_{n\pm 1} \ , \tag{5.54}$$

and so we see that the superconformal primary conditions in the NS sector (5.52) become the R-sector superconformal primary conditions

$$L_n|\phi\rangle_R = G^{\alpha}_{\dot{A},n}|\phi\rangle_R = J^3_n|\phi\rangle_R = J^{\pm}_{n\pm1}|\phi\rangle_R = G^{-}_{\dot{A},0}|\phi\rangle_R = 0 \quad , \quad n > 0 \ . \tag{5.55}$$

We note that for the NS and R sectors on the *cylinder*, fermions have periodic boundary conditions in the R sector and anti-periodic boundary conditions in the NS sector. Mapping to the plane reverses these boundary conditions. These conditions dictate that fermions in the NS sector are half-integer modded and in the R sector are integer modded.

5.3.2 Superconformal Primaries: Building the state

The R sector states that we consider will be in the $k = 1$, untwisted sector of the orbifold theory (states of N singly-wound strings) where one copy (say copy 1) is excited into a left-moving superconformal primary state $|\phi\rangle_R^{[1](1)}$, with the right-moving part being the Ramond ground state $|\bar{0}^-\rangle_R^{[1](1)}$. This single-copy superconformal primary satisfies the conditions (5.55) for the single-copy modes and has dimension h_R and charge m_R. The remaining $N-1$ copies are in the Ramond-Ramond ground state $|0^-,\bar{0}^-\rangle_R^{[1](j)}$. To avoid overly cumbersome notation, we will drop the twist-sector label $[k]$ since we consider only the singly-twisted case at present. Hence, the class of states we consider is of the form

$$|\Phi\rangle_R^{(1)} \equiv |\phi,\bar{0}^-\rangle_R^{(1)}|0^-,\bar{0}^-\rangle_R^{(2)}\cdots|0^-,\bar{0}^-\rangle_R^{(N)} \ . \tag{5.56}$$

In order for this to be a physical state of the orbifold theory, it is necessary to then symmetrise over the choice of excited copy; with an appropriate normalisation factor this gives the state

$$|\Phi\rangle \equiv \frac{1}{\sqrt{N}}\sum_{i=1}^{N}\bigotimes_{j\neq i}^{N}|\phi,\bar{0}^-\rangle_R^{(i)}|0^-,\bar{0}^-\rangle_R^{(j)} = \frac{1}{\sqrt{N}}\sum_{i=1}^{N}|\Phi\rangle_R^{(i)} \ . \tag{5.57}$$

Due to the twist operators in (5.29) acting on pairs of copies and the fact that we are computing an expectation value, this forces the second twist operator to act on the same pair as the first in order to undo the twist. Therefore, at any intermediate step of the computation it is sufficient to work with only a particular ordered pair of copies, with the final lifting for generic values of N gaining an extra combinatoric factor. With the initial and final states being of the form (5.57), there are two distinct cases possible when choosing two copies to twist together. Either both copies are in the Ramond-Ramond ground state $|0^-, \bar{0}^-\rangle_R$ or one of the copies is in the superconformal primary state $|\phi, \bar{0}^-\rangle_R$. The former case would yield an expectation value that computes the lift of $|0^-, \bar{0}^-\rangle_R \otimes |0^-, \bar{0}^-\rangle_R$, which vanishes since all Ramond ground states are unlifted, leaving terms only of the latter type. Since we have only singly-wound strings, the first twist operator can only twist together two of these to form a doubly-wound component string (and cannot break apart component strings). This ensures that the covering space necessary to resolve the twist operators in the correlation function (5.29) will have genus 0.

We now discuss the combinatorial factor necessary for obtaining the general N copy-symmetric result of the lift. For the untwisted-sector state we consider, in which only one copy is excited, there will be a nonzero expectation value only when the first twist operator acts on a pair of copies that includes an excited copy. The second twist operator then has to act on this same pair in order to untwist them. The 'diagonal' terms are expectation values where the final state has the same copy excited as in the initial state. There are N different copies that could be excited and then $N-1$ choices of the second, vacuum, copy. Thus there are $N(N-1)$ diagonal terms. In our notation, these would be of the form $E^{(2)}_{(i)(i)}$ for some $1 \leq i \leq N$. The 'off-diagonal' terms have, for a given choice of excited copy in the initial state (N choices), a different copy excited in the final state ($N-1$ such choices). These choices of excited states then force the respective choice of vacuum copy in the initial and final states. Thus there are $N(N-1)$ off-diagonal terms. In the notation above, these would be of the form $E^{(2)}_{(j)(i)}$ for $i \neq j$. In both cases the remaining $N-2$ vacuum copies are spectator copies, playing no role in the lifting calculation. Along with the normalization factor in (5.57) (for the initial and final states), the total lift is then given in terms of the two-copy lift $E^{(2)}_{(1)(1)}(\Phi)$ as

$$E^{(2)}_{h,m}(\Phi) = \left(\frac{1}{\sqrt{N}}\right)^2 \Big(N(N-1) + N(N-1)\Big) E^{(2)}_{(1)(1)}(\Phi) = 2(N-1) E^{(2)}_{(1)(1)}(\Phi) \ . \quad (5.58)$$

We will proceed by computing the contribution to the lift from the particular diagonal term $E^{(2)}_{(1)(1)}$ and then will use (5.58) to get the full lift.[8]

[8]We note that while permutation invariance dictates that each of the diagonal terms $E^{(2)}_{(i)(i)}$ will contribute the same amount to the lift, and likewise for each of the $E^{(2)}_{(j)(i\neq j)}$, at this stage it is not at all clear that a diagonal and an off-diagonal term will contribute equally. This will be addressed at the end

5.3.3 Superconformal Primaries: Simplifying the set

We now give some comments on single-copy superconformal primary states that will significantly narrow down the possible values of dimension and charge that need to be considered. Our comments will be in the language of the NS sector, but these can all be mapped to the Ramond sector. Initially it appears that we can have arbitrary left-moving dimension h and J_0^3 charge m for the untwisted-sector state where one copy is excited to a left-moving superconformal primary and the remaining $N-1$ copies being the NS vacuum. However, this turns out not to be the case. Consider the norm

$$\left|\left|J_{-n}^{+}|\phi\rangle\right|\right|^2 \geq 0 \ , \tag{5.59}$$

for $n > 0$, which is positive definite in a unitary theory. From the commutator (B.2b) and the definition $J_n^{\pm} \equiv J_n^1 \pm iJ_n^2$, we find that for a superconformal primary

$$0 \leq \langle\phi|J_n^- J_{-n}^+|\phi\rangle = \langle\phi|(Nn - 2J_0^3)|\phi\rangle \ , \tag{5.60}$$

where we have used the conditions (5.52). For $|\phi\rangle$ being a state on a single copy (for which $N = 1$) with a J_0^3 charge of m, (5.60) then gives the set of constraints (one per value of n)

$$m \leq \frac{n}{2} \ . \tag{5.61}$$

Specifically, the most stringent constraint comes from $n = 1$ for which we find that $m \leq \frac{1}{2}$. Since the action of the modes $J_0^{\pm}$, which act as raising and lowering operators for the eigenvalue of J_0^3 within an $SU(2)_L$ multiplet, commutes with the superconformal primary conditions (5.52) the constraint (5.61) must be satisfied by all members of an $SU(2)_L$ multiplet. Labelling such multiplets by the eigenvalue of the $SU(2)_L$ quadratic Casimir j, since the range of m within a given multiplet is $m = -j, -j+1, \ldots, j-1, j$ we see that there are only two possibilities. Single-copy superconformal primaries are either in $j = \frac{1}{2}$ or $j = 0$ multiplets.

From (5.60), for a single-copy superconformal primary with $m = \frac{1}{2}$ we find

$$\langle\phi|J_1^- J_{-1}^+|\phi\rangle = 0 \quad \Longrightarrow \quad J_{-1}^+|\phi\rangle = 0 \ . \tag{5.62}$$

The state $|\phi\rangle$ thus satisfies

$$G_{\dot{A},-\frac{1}{2}}^{+}|\phi\rangle = \left[J_{-1}^{+}, G_{\dot{A},\frac{1}{2}}^{-}\right]|\phi\rangle = 0 \ , \tag{5.63}$$

which is exactly the condition for $|\phi\rangle$ to be chiral. Since chiral primaries are unlifted, this leaves us simply with $j = 0$ multiplets. It should be noted that this argument only

of the computation of $E^{(2)}_{(1)(1)}$ in Section 5.3.4, with its equality to $E^{(2)}_{(2)(1)}$ explicitly shown in [18].

holds true for superconformal primaries on a single copy, *i.e.* when $c = 6$. For instance, in higher twist sectors it is possible to have superconformal primaries with higher values of j.

5.3.4 Lift for superconformal primaries

Using the method described in Section 5.2 yields the diagonal two-copy contribution to the lift

$$E^{(2)}_{(1)(1)}(\Phi) = \frac{\lambda^2\pi^2}{2^{2h}}\frac{\Gamma(2h)}{\Gamma(h)^2} \ . \tag{5.64}$$

As discussed in Section 5.3.2, all of the diagonal two-copy contributions of the form $E^{(2)}_{(i)(i)}$ will be equal due to permutation invariance. Using the relation (5.58), the full lift is then given by

$$E^{(2)}_{h,0}(\Phi) = (N-1)\frac{\lambda^2\pi^2}{2^{2h-1}}\frac{\Gamma(2h)}{\Gamma(h)^2} \ . \tag{5.65}$$

The lift (5.65) interestingly does not depend on other details of the superconformal primary ϕ, just its dimension and charge. From a technical perspective, this has happened simply due to the choice of state (5.57) – specifically due to only exciting one copy above the Ramond ground state. Because of this, in the end we are left with a two-point function on the covering space, which does not depend on the details of the state. If more than one copy in the initial and final states was excited with the superconformal primary ϕ then there would be contributions to the lift where the first twist operator acts on two excited copies. These contributions would then yield a correlation function on the covering space of the schematic form $\sim \langle\phi^\dagger\phi^\dagger\phi\phi\rangle$ and hence the lift would depend on the details of the state.

One existing data point that the general formula (5.65) can be compared to was computed in [82]. In that paper the lifting of all states at level 1 was computed for the case of $N = 2$. One of these states is the normalised Ramond-sector state

$$|\widetilde{\phi}\rangle^{(\mathcal{A})}_R \equiv \frac{1}{2}d^{--(\mathcal{A})}_{-1}d^{+-(\mathcal{A})}_0|0^-,\bar{0}^-\rangle^{(1)}_R|0^-,\bar{0}^-\rangle^{(2)}_R \ . \tag{5.66}$$

The superscript $(\mathcal{A})$ denotes that these modes are anti-symmetrised over the copies in the state, *i.e.* in this case of $N = 2$

$$d^{\alpha A(\mathcal{A})}_n \equiv d^{\alpha A(1)}_n - d^{\alpha A(2)}_n \ . \tag{5.67}$$

The state (5.66) is the lowest-weight state of a short multiplet at the free point, which is then lifted at second order in λ. In total, four short multiplets of the free theory combine into a long multiplet of the deformed theory, for which the computed lift is $E^{(2)} = \pi^2\lambda^2$. The state (5.66) is the bottom member of this long multiplet, with the lowest A charge of -1. While not being of the form (5.57) of states we consider here, it can be related to

one by adding a global mode excitation (and normalising) to get

$$|\widetilde{\phi}\rangle_R \equiv \frac{1}{\sqrt{2}}\Big(|\widetilde{\phi}\rangle^{(\mathcal{A})} + |\widetilde{\phi}\rangle^{(g)}\Big) = \frac{1}{2\sqrt{2}}\Big(d_{-1}^{--(1)}d_0^{+-(1)} + d_{-1}^{--(2)}d_0^{+-(2)}\Big)|0^-,\bar{0}^-\rangle_R^{(1)}|0^-,\bar{0}^-\rangle_R^{(2)}\,, \tag{5.68}$$

where these global modes are defined analogously to (5.53). It was shown in Appendix D of [82] that such global modes are not lifted and so the lift of the state (5.68) is simply that of (5.66) multiplied by the extra normalisation factor for both the initial and final state: that is $E^{(2)}(\widetilde{\phi}_R) = \frac{1}{2}\pi^2\lambda^2$. The quantum numbers for the R-sector state (5.68) are $h_R = \frac{3}{2}$, $m_R = -1$. Spectral flowing to the NS sector using (B.15) with $\eta = 1$, we find

$$|\widetilde{\phi}\rangle_R \longrightarrow \frac{1}{2\sqrt{2}}\Big(d_{-\frac{1}{2}}^{--(1)}d_{-\frac{1}{2}}^{+-(1)} + d_{-\frac{1}{2}}^{--(2)}d_{-\frac{1}{2}}^{+-(2)}\Big)|0\rangle_{NS}^{(1)}|0\rangle_{NS}^{(2)}\,, \tag{5.69}$$

with dimension and charge $(h, m) = (1, 0)$. From (5.65) we then find

$$E_{1,0}^{(2)}\Big|_{N=2} = \frac{1}{2}\pi^2\lambda^2\,, \tag{5.70}$$

in agreement with the prediction from [82].

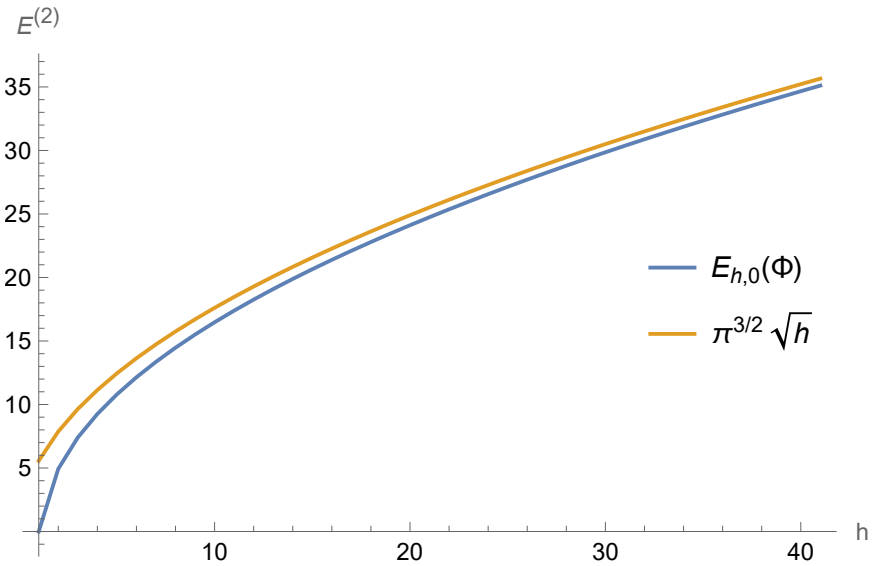

Figure 5.3: The second-order energy lift (5.65) for states of the form (5.57), with $N = 2$, as a function of the superconformal primary's dimension h. The plot shows the behavior of the lift for large h and an asymptotic $\sqrt{h}$ behavior is observed.

It is interesting to consider the large-dimension limit of (5.65). The asymptotic behaviour of the lift (5.65) can be easily found (see Figure 5.3 for a plot of the lift in the case of $N = 2$); using Stirling's approximation for the Gamma functions, we find

$$E_{h,0}^{(2)}(\Phi) \approx \lambda^2\pi^{\frac{3}{2}}\sqrt{h} + O\Big(h^{-\frac{1}{2}}\Big)\,. \tag{5.71}$$

An interesting observation is that all previously computed examples of lifting in the literature for which the large-dimension regime is accessible also have a $\sqrt{h}$ asymptotic behaviour [79, 83]. This functional behavior appears to be a universal property of lifting of D1-D5-P states, although with variable powers of π in the prefactor.

5.4 Lifting of Superconformal Descendants

In this section we will consider the lifting of descendants of superconformal primaries on a single copy as done in the previous Section 5.3. More precisely, let the state $|\phi\rangle$ be a superconformal primary on one copy of the seed $c = 6$ CFT, then $|\phi\rangle$ satisfies the conditions (5.52). Descendants of this primary are then found by acting with negative modes of the $\mathcal{N} = 4$ superconformal algebra given in Appendix B.1.1; namely acting with the current modes

$$\left\{ L_{-n} \ , \quad J^a_{-n} \ , \quad G^{\alpha}_{\dot{A},-s} \right\} , \tag{5.72}$$

for $n > 0$ and $s \geq \frac{1}{2}$. In actual fact, it is enough to study the lifting of descendants formed from acting with J and G modes.

5.4.1 Superconformal Descendants: Definition and states

Specifically we consider the following states

$$\begin{aligned} |G\phi\rangle^{\alpha}_{\dot{A}(h,s)} &\equiv \frac{1}{\sqrt{2}}\left(G^{\alpha(1)}_{\dot{A},-s}|\phi\rangle^{(1)}|0_{NS}\rangle^{(2)} + G^{\alpha(2)}_{\dot{A},-s}|0_{NS}\rangle^{(1)}|\phi\rangle^{(2)} \right) , \\ |J\phi\rangle^{+}_{(h,n)} &\equiv \frac{1}{\sqrt{2}}\left(J^{+(1)}_{-n}|\phi\rangle^{(1)}|0_{NS}\rangle^{(2)} + J^{+(2)}_{-n}|0_{NS}\rangle^{(1)}|\phi\rangle^{(2)} \right) , \end{aligned} \tag{5.73}$$

where ϕ has conformal dimension h and J^3_0 eigenvalue $j = 0$ and the factor of $\frac{1}{\sqrt{2}}$ is a copy normalization. The respective bra states are defined as

$$\begin{aligned} {}^{\beta}_{(h,s)\dot{B}}\langle G\phi| &\equiv \frac{1}{\sqrt{2}}\left({}^{(2)}_{NS}\langle 0|\ {}^{(1)}\langle\phi|G^{\beta(1)}_{\dot{B},s} + {}^{(2)}\langle\phi|\ {}^{(1)}_{NS}\langle 0|G^{\beta(2)}_{\dot{B},s} \right) , \\ {}^{-}_{(h,n)}\langle J\phi| &\equiv \frac{1}{\sqrt{2}}\left({}^{(2)}_{NS}\langle 0|\ {}^{(1)}\langle\phi|J^{-(1)}_{n} + {}^{(2)}\langle\phi|\ {}^{(1)}_{NS}\langle 0|J^{-(2)}_{n} \right) , \end{aligned} \tag{5.74}$$

where the Hermitian conjugate state of $|G\phi\rangle^{\alpha}_{\dot{A}(h,s)}$ should have opposite quantum numbers (see B.1.3 for our conventions). while these states are not currently normalized on an individual copy, this is taken into account in the lift formula (5.29). Since the method of lifting used here is for D1-D5-P states, the right-moving part of the states is necessarily the NS vacuum on all copies. The lift of single-copy superconformal primaries was previously computed in closed form in the previous section 5.3. The norm of our descendant states

can be found from the correlator

$$ {}^{\beta}_{(h,s)\dot{B}}\langle G\phi|G\phi\rangle^{\alpha}_{\dot{A}(h,s)} = \epsilon_{\dot{B}\dot{A}}\epsilon^{\beta\alpha}\Big(s^2 - \frac{1}{4} + h\Big) \ , \tag{5.75} $$

and

$$ {}^{-}_{(h,n)}\langle J\phi|J\phi\rangle^{+}_{(h,n)} = n \ , \tag{5.76} $$

where the quantum numbers of the conjugate state need to be opposite to the ket state and appropriate negative signs added as per the conjugation conventions of Appendix B.1.3. This definition of the Hermitian conjugate state should also be enforced on the final state of the amplitude (5.78) in order for it to be related to the lift of a particular state.

5.4.2 Lift for G descendant: $|G\phi\rangle^{\alpha}_{\dot{A}(h,s)}$

In this section we compute the lift of the superdescendant $|G\phi\rangle^{\alpha}_{\dot{A}(h,s)}$. From Section 5.2 the key quantity we need to compute is the left-moving amplitude

$$ A^{(1)(1)}_{h,s}(w_2,w_1) \equiv \langle\phi|G^{\beta}_{\dot{B},s}\Big(G^{+}_{-,-\frac{1}{2}}\sigma_2^{-}\Big)(w_2)\Big(G^{-}_{+,-\frac{1}{2}}\sigma_2^{+}\Big)(w_1)\,G^{\alpha}_{\dot{A},-s}|\phi\rangle \ , \tag{5.77} $$

where we have taken the descendant excitation to be on a definite copy, namely copy 1, for both the initial and final state. The strategy for computing this amplitude follows closely the method developed in [20], with modifications to accommodate the fact that we work with a general superconformal primary $|\phi\rangle$, without specifying its explicit form. We omit the intermediate steps of the calculation here and refer the reader to our detailed exposition in [19].

The left-moving copy symmetric amplitude required for the lift of the state (5.73) is then given by

$$ \begin{aligned} A_{h,s}(w,0) &\equiv {}^{\beta}_{(h,s)\dot{B}}\langle G\phi|\Big(G^{+}_{-,-\frac{1}{2}}\sigma_2^{-}\Big)(w)\Big(G^{-}_{+,-\frac{1}{2}}\sigma_2^{+}\Big)(0)|G\phi\rangle^{\alpha}_{\dot{A}(h,s)} \\ &= \frac{1}{2}\sum_{i,j=1}^{2} A^{(j)(i)}_{h,s}(w,0) \\ &= A^{(1)(1)}_{h,s}(w,0) + A^{(2)(1)}_{h,s}(w,0) \ , \end{aligned} \tag{5.78} $$

where we have used that $A^{(2)(2)} = A^{(1)(1)}$ and $A^{(1)(2)} = A^{(2)(1)}$ on general symmetry grounds. The amplitude $A^{(2)(1)}$ can be obtained from $A^{(1)(1)}$ via the continuation

$$ A^{(2)(1)}_{h,s}(w,0) = A^{(1)(1)}_{h,s}(w+2\pi i,0) \ , \tag{5.79} $$

which has the effect of interchanging the role of the two copies that the upper σ_2 twists.

The lift is then given by

$$E^{(2)}\Big(|G\phi\rangle^{\alpha}_{\dot{A}(h,s)}\Big) = \frac{\pi\lambda^2}{\Big||G\phi\rangle^{\alpha}_{\dot{A}(h,s)}\Big|^2}\lim_{T\to\infty}\int_0^{2\pi} d\sigma\, A_{h,s}(w,0)\coth\Big(\tfrac{\bar{w}}{2}\Big)\ , \tag{5.80}$$

where $w = \frac{T}{2} + i\sigma$ and $\bar{w} = \frac{T}{2} - i\sigma$ with $T \to \infty$ on this contour as given in (5.34a). Note that of the three integrals in (5.34) it was argued in Section 5.2 that I_{C_3} gives a vanishing contribution to the lift and for the states considered here we find that $\lim_{T\to\infty} I_{C_1}(T) = \lim_{T\to\infty} I_{C_2}(T)$ and so (5.80) contains only one integral. We now present plot of the lifts of different descendants.

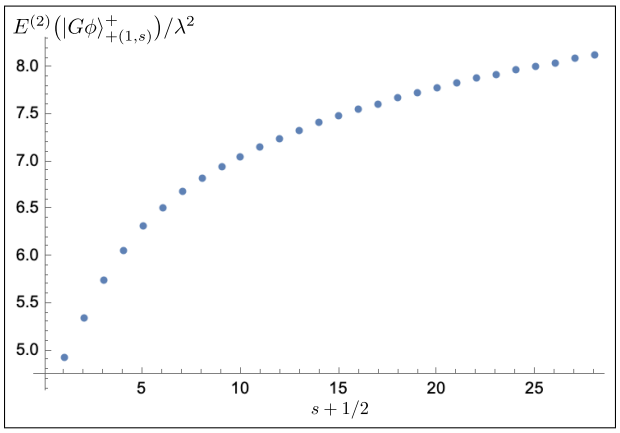

Figure 5.4: Plot of the lifts $E^{(2)}\Big(|G\phi\rangle^{+}_{+(1,s)}\Big)/\lambda^2$ for varying s. The plot fits to the curve: $3.5943 + 1.45554\sqrt{s+1/2} - 0.114676(s+1/2)$.

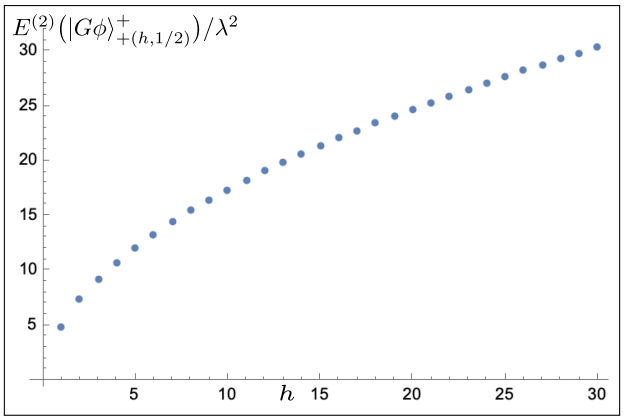

Figure 5.5: Plot of the lifts $E^{(2)}\Big(|G\phi\rangle^{+}_{+(h,1/2)}\Big)/\lambda^2$ for varying h. The plot fits to the curve: $-0.707422 + 5.7688\sqrt{h} - 0.0167021h$.

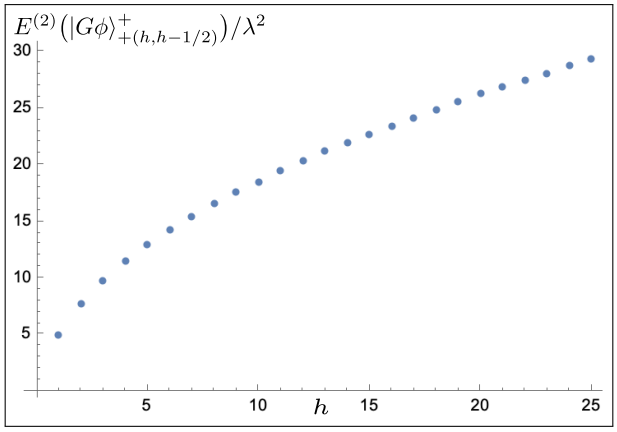

Figure 5.6: Plot of the lifts $E^{(2)}\Big(|G\phi\rangle^+_{+(h,h-1/2)}\Big)/\lambda^2$ for varying h. The plot fits to the curve: $-1.52527 + 6.68922\sqrt{h} - 0.104878h$.

5.4.3 Lift for J descendant: $|J\phi\rangle^+_{(h,n)}$

In this section we consider the lifting of J^+ descendants of a superconformal primary state $|\phi\rangle$; the copy-symmetric state is defined in (5.73). The lift of these descendant states is amenable to the same method used in Section 5.4.2.

As in (5.78) the copy symmetric amplitude is given by

$$\begin{aligned} A_{h,n}(w,0) &\equiv {}^-_{(h,n)}\langle J\phi|\Big(G^+_{-,-\frac{1}{2}}\sigma_2^-\Big)(w)\Big(G^-_{+,-\frac{1}{2}}\sigma_2^+\Big)(0)|J\phi\rangle^+_{(h,n)} \\ &= \frac{1}{2}\sum_{i,j=1}^{2} A^{(j)(i)}_{h,n}(w,0) \\ &= A^{(1)(1)}_{h,n}(w,0) + A^{(2)(1)}_{h,n}(w,0)\ , \end{aligned} \tag{5.81}$$

with $A^{(2)(1)}$ given in terms of $A^{(1)(1)}$ by (5.79). The lift is then given by

$$E^{(2)}\Big(|J\phi\rangle^+_{(h,n)}\Big) = \frac{\pi\lambda^2}{\Big||J\phi\rangle^+_{(h,n)}\Big|^2}\lim_{T\to\infty}\int_0^{2\pi} d\sigma\, A_{h,n}(w,0)\coth\Big(\tfrac{\bar{w}}{2}\Big)\ , \tag{5.82}$$

where $w = \frac{T}{2} + i\sigma$ and $\bar{w} = \frac{T}{2} - i\sigma$ with $T \to \infty$ on this contour as given in (5.34a) (noting again the comments below equation (5.80)).

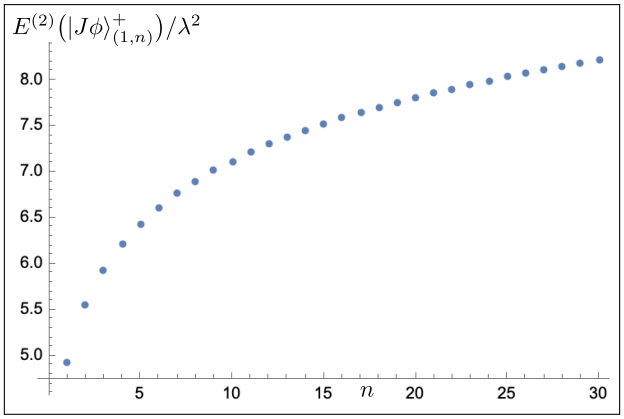

Figure 5.7: Plot of the lifts $E^{(2)}\left(|J\phi\rangle^{+}_{(1,n)}\right)/\lambda^2$ for varying n. The plot fits to the curve: $3.79158 + 1.39824\sqrt{n} - 0.109782n$.

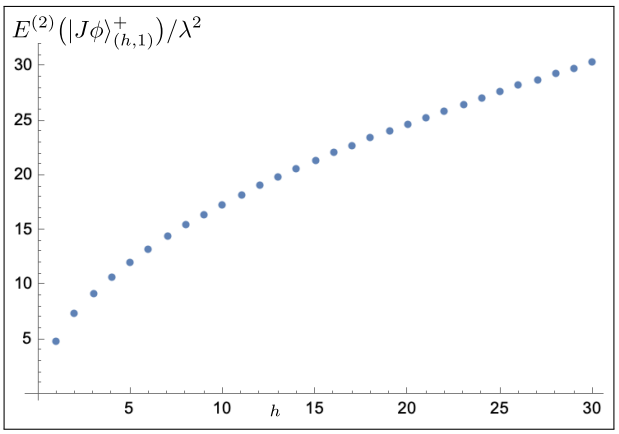

Figure 5.8: Plot of the lifts $E^{(2)}\left(|J\phi\rangle^{+}_{(h,1)}\right)/\lambda^2$ for varying h. The plot fits to the curve: $-0.820134 + 5.85066\sqrt{h} - 0.0292201h$.

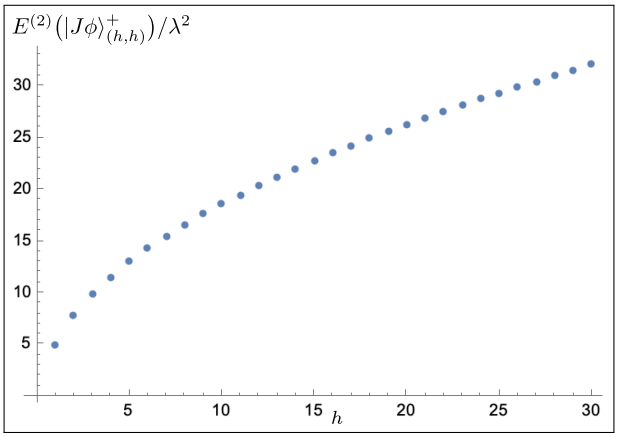

Figure 5.9: Plot of the lifts $E^{(2)}\left(|J\phi\rangle^{+}_{(h,h)}\right)/\lambda^2$ for varying n. The plot fits to the curve: $-1.35675 + 6.61605\sqrt{h} - 0.0935374h$.

5.5 Analytic form and asymptotic behavior

In the previous section, the lift of descendant states was computed via a six-point function on the covering space, requiring mode expansions and resummation of series using the $\mathcal{N} = 4$ algebra. However, this state-by-state approach is ill-suited for analyzing asymptotic behavior at large dimension or understanding how lifts depend on the distribution of dimension among current modes. To address this, in Section 4 of [19], we employ a method based on contour integrals and Ward identities, allowing us to derive compact analytic expressions for the lifts in terms of finite sums suitable for asymptotic analysis. Here, we present a schematic representation of the method in Figure 5.10[9], the explicit result and analyze its asymptotic behavior.

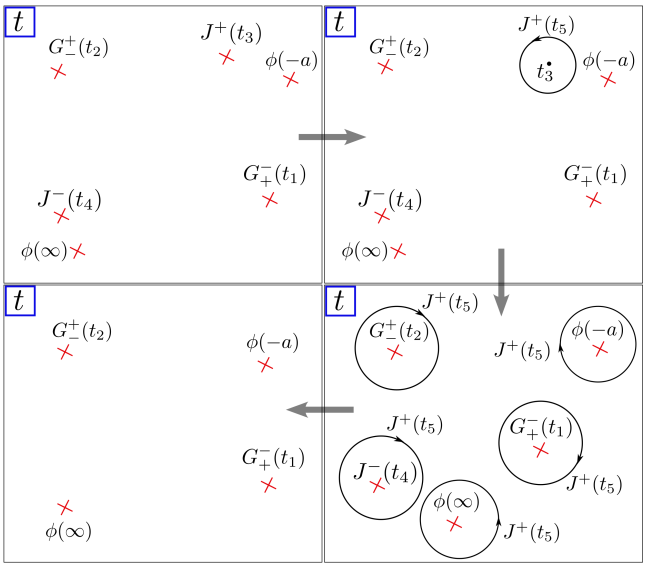

Figure 5.10: The general idea in deriving $|J\phi\rangle^+_{(h,n)}$ lifts using Ward identities is to start with the correlator (5.81) containing different insertions on the t-plane. Moving clockwise in the figure, trivially rewrite the field $J^+(t_3)$ as a contour integral centered around $t_5 = t_3$. Unwrapping this contour yields a sum of contours around each insertion on the t-plane. Different terms in the sum evaluate to different correlators one of which is shown as a 4-point insertion. Hence the descendant J^+ can be removed using this method leading to a different method of lifting computation.

5.5.1 Analytic expressions

It turns out that the lift is polynomial in h and we find that for a given value of n

$$E^{(2)}\Big(|J\phi\rangle^+_{(h,n>1)}\Big) = E^{(2)}_h\Big(\phi\Big)\left[1 + a_n \frac{P_n(h)}{(h+1)_{2n-2}}\right], \tag{5.83}$$

[9]We move from the w-cylinder to the z-plane and then to the covering space t-plane using techniques present in Section 5.2.1.

where $P_n(h)$ is a polynomial in h of degree $2n-4$ and $(x)_n$ is the Pochhammer symbol

$$(x)_n \equiv \frac{\Gamma(x+n)}{\Gamma(x)} \ . \tag{5.84}$$

The rational coefficients a_n in (5.83) for the first few values of n are

$$\left\{a_{n\geq 2}\right\} = \left\{ \frac{3}{4}, \frac{3}{8}, \frac{15}{32}, \frac{15}{128}, \frac{105}{256}, \frac{21}{512}, \cdots \right\} , \tag{5.85}$$

and the respective polynomials are

$$\begin{aligned}
P_2 &= 1 \ , \\
P_3 &= 8h^2 + 16h + 41 \ , \\
P_4 &= 16h^4 + 96h^3 + 578h^2 + 798h + 1305 \ , \\
P_5 &= 128h^6 + 1536h^5 + 16976h^4 + 64608h^3 + 237920h^2 + 268512h + 352107 \ , \\
P_6 &= 64h^8 + 1280h^7 + 22592h^6 + 163520h^5 + 1077776h^4 + 3208160h^3 + 9205198h^2 \\
&\qquad + 9091050h + 10377045 \ .
\end{aligned} \tag{5.86}$$

Given the knowledge of the form (5.83) for the lift of the $|J\phi\rangle^+_{(h,n)}$ states, we were able to find that the series method data of Section 5.4.2 for the lift of $|G\phi\rangle^+_{+(h,n)}$ follows a similar pattern of

$$E^{(2)}\Big(|G\phi\rangle^+_{+(h,n>1)}\Big) = E^{(2)}_h\Big(\phi\Big)\left[1 + b_n \frac{\widetilde{P}_n(h)}{(h+1)_{2(n-1)}(h+n^2-n)}\right] , \tag{5.87}$$

where the rational coefficients are

$$\left\{b_{n\geq 2}\right\} = \left\{ \frac{3}{4}, \frac{15}{16}, \frac{21}{16}, \frac{45}{256}, \frac{165}{256}, \frac{273}{1024}, \cdots \right\} , \tag{5.88}$$

and $b_1 = 0$ and $\widetilde{P}_n(h)$ are degree $2n-3$ polynomials in h of the form

$$\begin{aligned}
\widetilde{P}_2 &= h + 1 \ , \\
\widetilde{P}_3 &= 4h^3 + 16h^2 + 51h + 78 \ , \\
\widetilde{P}_4 &= 8h^5 + 72h^4 + 601h^3 + 2193h^2 + 3711h + 4905 \ , \\
\widetilde{P}_5 &= 128h^7 + 2048h^6 + 31952h^5 + 219392h^4 + 979664h^3 + 2908064h^2 + 3700845h + 4296180 \ , \\
\widetilde{P}_6 &= 64h^9 + 1600h^8 + 39952h^7 + 446320h^6 + 3690736h^5 + 19756240h^4 + 64904013h^3 \ , \\
&\qquad + 164470575h^2 + 176337585h + 185479875 \ .
\end{aligned} \tag{5.89}$$

We do not, however, have a derivation of this form for the lift of $|G\phi\rangle^+_{+(h,n)}$.

5.5.2 Asymptotic behavior

In our work [18], as mentioned in the previous section, the lift of a single-copy superconformal primary was found in a closed form—displayed in (5.65)—and it was observed that in the limit of large dimension the leading behavior of the lift was of the form

$$E_h^{(2)}\Big(\phi\Big) \approx \pi^{3/2}\lambda^2\sqrt{h}\ . \tag{5.90}$$

This $\sim\sqrt{h}$ behavior has also been hinted at in computations of lifts for which closed form expressions are not known, such as in [20] where the lift of states with excitations on one copy from two bosonic or fermionic modes was computed state by state. Looking at the lifts of states where one mode had a fixed and small mode number and the other was varied to, say, level 30 a square root behaviour was observed in the data. It is natural to then ask more nuanced questions: for a level-n descendant of a primary of dimension h, is the asymptotic behaviour of lifts the same as that of the primary and is the important quantity the total dimension $h_{tot} = h + n$ or are the dimensions of the primary and descendant excitation treated differently? If the latter case is true, it is interesting to then ask whether the partitioning of the descendant excitation dimension amongst different modes is important when it comes to the lift of the state. In this section we hope to answer exactly these questions.

Since the lifting formula of the descendant state $|J\phi\rangle^+_{(h,n)}$ is known exactly, albeit in terms of finite sums, we may derive a large dimension limit. Namely, consider the large h regime

$$h \gg n \sim O(1)\ . \tag{5.91}$$

Here, we find

$$E^{(2)}\Big(|J\phi\rangle^+_{(h,n)}\Big) \approx E_1 \approx \pi^{\frac{3}{2}}\lambda^2\sqrt{h}\ , \tag{5.92}$$

which exactly matches the leading asymptotic behaviour of the lift of superconformal primaries given in (5.90) and notably (5.92) is independent of the descendant excitation level n.

It turns out that more can be said about the asymptotic forms of the lifts of the descendant states $J^+_{-n}|\phi\rangle$ and $G^\alpha_{\dot{A},-s}|\phi\rangle$ that will shine a light on the questions raised at the beginning of this section. Firstly, and most simply, one can argue that the lifts of the lowest-level descendants ($n = 1$ and $s = \frac{1}{2}$ respectively) are exactly equal to the lift of the primary, *i.e.*

$$E^{(2)}\Big(|J\phi\rangle^+_{(h,1)}\Big) = E^{(2)}\Big(|G\phi\rangle^+_{+(h,1/2)}\Big) = E_h^{(2)}\Big(\phi\Big) = \pi^{\frac{3}{2}}\lambda^2\frac{\Gamma(h+\frac{1}{2})}{\Gamma(h)}\ . \tag{5.93}$$

The large h behaviour of these families is thus trivially also equal to that of ϕ, given in

(5.90).

Although the expressions (5.83) and (5.87) are not in closed form, it is possible to find a closed form for the subleading large h behaviour

$$\frac{E^{(2)}\Big(|J\phi\rangle^{+}_{(h,n)}\Big)}{E^{(2)}_{h}(\phi)} \approx 1 + \frac{n(n^2-1)}{8h^2} \ , \tag{5.94}$$

$$\frac{E^{(2)}\Big(|G\phi\rangle^{+}_{+(h,n)}\Big)}{E^{(2)}_{h}(\phi)} \approx 1 + \frac{n(n-1)(2n-1)}{8h^2} \ , \tag{5.95}$$

where again $n = s + \frac{1}{2}$ for the G descendant. The subleading term carries information about the descendant excitation, however, if the asymptotic behavior for large total dimension $h_{tot} = h + n$ was $\sim \sqrt{h_{tot}}$ as might be expected, then the subleading corrections should appear at order $1/h$ and not $1/h^2$ since for $h \gg n$

$$\sqrt{h+n} \approx \sqrt{h}\left(1 + \frac{n}{2h} + O\Big(h^{-2}\Big)\right) . \tag{5.96}$$

It therefore appears that the dimension of the primary and that of the descendant excitation are treated differently in the lift.

5.6 Lifting of single-copy two-mode states

5.6.1 The states

In this section, we consider untwisted sector states formed by acting with two modes of the free bosons and fermions of the orbifold theory on the NS-NS vacuum $|0\rangle^{(1)}_{NS}$ of a single copy, with all other copies in their ground state. These two-mode states fall into three classes:

$$\alpha_{B\dot{B},-m}\alpha_{A\dot{A},-n}|0_{NS}\rangle \quad , \quad \alpha_{B\dot{B},-m}d^{\alpha A}_{-s}|0_{NS}\rangle \quad , \quad d^{\beta B}_{-r}d^{\alpha A}_{-s}|0_{NS}\rangle \ , \tag{5.97}$$

which we define precisely below. We will compute the lifts for these three families separately.

Two-mode excitations are the simplest non-trivial states, since for single-mode states, $\alpha^{(1)}_{A\dot{A},-n}|0_{NS}\rangle$ and $d^{(1)\alpha A}_{-s}|0_{NS}\rangle$, the lift vanishes. In forming copy-symmetric states, a global mode[10] acts on the global NS-NS vacuum, whose lift is known to be zero [79]. This cancellation does not occur for states of the form (5.97) or for states built from more than two modes.

Since the lift computation only probes one pair of copies at a time,[11] it suffices to

[10] A global mode acts diagonally across copies, *i.e.*, $\mathcal{O}^{\text{global}}_{n} = \sum_{i=1}^{N}\mathcal{O}^{(i)}_{n}$, where $\mathcal{O}^{(i)}_{n}$ acts only on the ith copy.

[11] Twist-2 fields in the deformation operator act on a pair of copies, and the expectation value structure

consider a fixed ordered pair with one excited copy and one copy in the NS-NS vacuum. As discussed in Section 5.3.2, the extrapolation to general N is then purely combinatorial, yielding

$$E_N^{(2)}\Big(|\Phi\rangle\Big) = 2(N-1)E^{(2)}\Big(|\Phi\rangle\Big) \ , \tag{5.98}$$

where $E^{(2)}(|\Phi\rangle)$ denotes the two-copy lift.

5.6.2 Lifting of $|\alpha\alpha\rangle_{B\dot{B}A\dot{A}(m,n)}$

Firstly we consider the lift of states of the form

$$|\alpha\alpha\rangle_{B\dot{B}A\dot{A}(m,n)} \equiv \frac{1}{\sqrt{2}}\Big(\alpha^{(1)}_{B\dot{B},-m}\alpha^{(1)}_{A\dot{A},-n} + \alpha^{(2)}_{B\dot{B},-m}\alpha^{(2)}_{A\dot{A},-n}\Big)|0\rangle^{(1)}_{NS}|0\rangle^{(2)}_{NS} \ , \tag{5.99}$$

where the factor of $\frac{1}{\sqrt{2}}$ comes from the normalisation of the state over two copies. The norm of this state can be found from the following inner product

$$\begin{aligned}{}_{(m,n)D\dot{D}C\dot{C}}\langle\alpha\alpha|\alpha\alpha\rangle_{B\dot{B}A\dot{A}(m,n)} = mn\Big(\epsilon_{AC}\epsilon_{BD}\epsilon_{\dot{A}\dot{C}}\epsilon_{\dot{B}\dot{D}}\delta_{m,n} + \epsilon_{AD}\epsilon_{BC}\epsilon_{\dot{A}\dot{D}}\epsilon_{\dot{B}\dot{C}}\Big)H[m-1] \\ + 2m^2\epsilon_{AB}\epsilon_{CD}\epsilon_{\dot{A}\dot{B}}\epsilon_{\dot{C}\dot{D}}\delta_{m+n,0}H[-m-1] \ ,\end{aligned} \tag{5.100}$$

under the condition that for the bra state in (5.100) to be the Hermitian conjugate of the ket all $SU(2)$ indices should be opposite to those of the ket and additional negative signs are included as per the conjugation conventions given in Section B.1.3. In (5.100) we have used the discrete step function definition

$$H[n] \equiv \begin{cases} 1 & \text{for } n \geq 0 \\ 0 & \text{for } n < 0 \end{cases} \ . \tag{5.101}$$

The computation of the lift requires the following left-moving amplitude

$$A^{(1)(1)}_{m,n}(w_2,w_1) \equiv \langle 0_{NS}|\Big(\alpha^{(1)}_{D\dot{D},n}\alpha^{(1)}_{C\dot{C},m}\Big)\Big(G^+_{-,-\frac{1}{2}}\sigma^-\Big)(w_2)\Big(G^-_{+,-\frac{1}{2}}\sigma^+\Big)(w_1)\Big(\alpha^{(1)}_{B\dot{B},-m}\alpha^{(1)}_{A\dot{A},-n}\Big)|0_{NS}\rangle \ , \tag{5.102}$$

where we have chosen all of the α modes to act on copy 1 and have suppressed the $SU(2)_2$ indices on the left-hand side for easy of notation. The external states will need to be symmetrised over copy indices later. Clearly in order to have a non-vanishing initial state we require the condition

$$n > 0 \ . \tag{5.103}$$

As described in Section 5.2 the method of computing this amplitude is to map it from the (doubly covered) cylinder to the (doubly covered) plane, from which we map to the

forces both twist insertions to act on the same pair.

covering space[12] in order to geometrically resolve the effect of the two twist operator insertions. Under these two maps the initial state transforms as

$$\begin{aligned}\left(\alpha^{(1)}_{B\dot{B},-m}\alpha^{(1)}_{A\dot{A},-n}\right)_{-\infty} &= i^2\oint_{-\infty}\frac{dw_4}{2\pi i}\frac{dw_3}{2\pi i}\,e^{-mw_4}e^{-nw_3}\,\partial X_{B\dot{B}}(w_4)\partial X_{A\dot{A}}(w_3)\\ &= i^2\oint_{0}\frac{dz_4}{2\pi i}\frac{dz_3}{2\pi i}\,z_4^{-m}z_3^{-n}\,\partial X_{B\dot{B}}(z_4)\partial X_{A\dot{A}}(z_3)\\ &= i^2\oint_{-a}\frac{dt_4}{2\pi i}\frac{dt_3}{2\pi i}\,z_4(t_4)^{-m}z_3(t_3)^{-n}\,\partial X_{B\dot{B}}(t_4)\partial X_{A\dot{A}}(t_3)\ ,\end{aligned}\tag{5.104}$$

and likewise the final state transforms as

$$\begin{aligned}\left(\alpha^{(1)}_{D\dot{D},n}\alpha^{(1)}_{C\dot{C},m}\right)_{\infty} &= i^2\oint_{\infty}\frac{dw_5}{2\pi i}\frac{dw_6}{2\pi i}\,e^{mw_5}e^{nw_6}\,\partial X_{D\dot{D}}(w_6)\partial X_{C\dot{C}}(w_5)\\ &= i^2\oint_{\infty}\frac{dz_5}{2\pi i}\frac{dz_6}{2\pi i}\,z_5^{m}z_6^{n}\,\partial X_{D\dot{D}}(z_6)\partial X_{C\dot{C}}(z_5)\\ &= i^2\oint_{\infty}\frac{dt_5}{2\pi i}\frac{dt_6}{2\pi i}\,z_5(t_5)^{m}z_6(t_6)^{n}\,\partial X_{D\dot{D}}(t_6)\partial X_{C\dot{C}}(t_5)\ .\end{aligned}\tag{5.105}$$

On mapping to the covering space the order-2 twist fields are resolved, leaving behind spin fields $S_2^-(t_2)$ and $S_2^-(t_1)$ which can in turn be removed by spectrally flowing on the t-plane by $\eta=-1$ units around $t=t_1$ and by $\eta=1$ units around $t=t_2$. Since the α modes have no charge under J_0^3 these initial and final states transform trivially under these two spectral flows. The transformation of the σ fields inserted at w_1 and w_2 on the cylinder under these maps and spectral flows are universal to all of our lifting calculations and thus are packaged into the base amplitude

$$U(w_2,w_1)\equiv\langle 0_{NS}|\sigma^-(w_2)\sigma^+(w_1)|0_{NS}\rangle=\frac{1}{2\sinh\left(\frac{w_2-w_1}{2}\right)}\ ,\tag{5.106}$$

which was derived in [79], along with factors from the transformation of the G modes[13]. This leaves the amplitude (5.102) (up to the overall factors described above and the much simpler right-moving factor (5.31)) in terms of a correlation function of four contours of

[12] As found in [80] and used in the context of lifting in [79] the covering space map $z\to t$ for correlators containing two order-2 twist operators is given by $z(t)=\frac{(t+a)(t+b)}{t}$. The insertions of the two deformation operators on the plane $z_1=e^{w_1}$ and $z_2=e^{w_2}$ are mapped to the points $t_1=-\sqrt{ab}$ and $t_2=\sqrt{ab}$ on the cover. Our conventions are that the points $z=0$ and $z=\infty$ on the first sheet of the doubly-covered plane map to $t=-a$ and $t=\infty$ on the covering space.

[13] See Section (4.3) of [79] for a derivation of the transformation factors for the G modes coming from the two deformation operators under the maps to the t-plane and spectral flows. In total these factors are $\left[t_1t_2(t_1+a)(t_2+a)(t_1+b)(t_2+b)\right]^{\frac{1}{2}}$.

∂X fields and two insertions of G fields

$$A^{(1)(1)}_{m,n} \sim \oint_\infty \frac{dt_5}{2\pi i}\oint_\infty \frac{dt_6}{2\pi i}\oint_{-a}\frac{dt_4}{2\pi i}\oint_{-a}\frac{dt_3}{2\pi i}\frac{z_5(t_5)^m z_6(t_6)^n}{z_4(t_4)^m z_3(t_3)^n} \times \langle \partial X_{D\dot{D}}(t_6)\partial X_{C\dot{C}}(t_5)G^+_-(t_2)G^-_+(t_1)\partial X_{B\dot{B}}(t_4)\partial X_{A\dot{A}}(t_3)\rangle \ . \tag{5.107}$$

This covering space correlator can be computed straightforwardly by breaking the supercurrents into their free-field boson and fermion representation which for the cases we need are

$$G^+_-(t_2) = \psi^{+E}(t_2)\partial X_{E-}(t_2) \quad , \quad G^-_+(t_1) = \psi^{-F}(t_1)\partial X_{F+}(t_1) \ . \tag{5.108}$$

The correlator in (5.107) is then given by

$$\begin{aligned}\langle \partial X_{D\dot{D}}(t_6)\partial X_{C\dot{C}}(t_5)G^+_-(t_2)G^-_+(t_1)\partial X_{B\dot{B}}(t_4)\partial X_{A\dot{A}}(t_3)\rangle = \frac{1}{t_2-t_1}\Bigg[\\ \frac{\epsilon_{CD}\epsilon_{\dot{C}\dot{D}}}{(t_6-t_5)^2}\left(\frac{2\epsilon_{AB}\epsilon_{\dot{A}\dot{B}}}{(t_2-t_1)^2(t_4-t_3)^2}+\frac{\epsilon_{-\dot{B}}\epsilon_{+\dot{A}}\epsilon_{AB}}{(t_2-t_4)^2(t_1-t_3)^2}-\frac{\epsilon_{+\dot{B}}\epsilon_{-\dot{A}}\epsilon_{AB}}{(t_2-t_3)^2(t_1-t_4)^2}\right) \\ +\frac{\epsilon_{\dot{D}-}}{(t_6-t_2)^2}\left(\frac{\epsilon_{AB}\epsilon_{\dot{A}\dot{B}}\epsilon_{\dot{C}+}\epsilon_{CD}}{(t_5-t_1)^2(t_4-t_3)^2}+\frac{\epsilon_{BC}\epsilon_{\dot{B}\dot{C}}\epsilon_{\dot{A}+}\epsilon_{A,D}}{(t_5-t_4)^2(t_1-t_3)^2}+\frac{\epsilon_{AC}\epsilon_{\dot{A}\dot{C}}\epsilon_{\dot{B}+}\epsilon_{BD}}{(t_5-t_3)^2(t_1-t_4)^2}\right) \\ +\frac{-\epsilon_{\dot{D}+}}{(t_6-t_1)^2}\left(\frac{\epsilon_{AB}\epsilon_{\dot{A}\dot{B}}\epsilon_{\dot{C}-}\epsilon_{CD}}{(t_5-t_2)^2(t_4-t_3)^2}+\frac{\epsilon_{BC}\epsilon_{\dot{B}\dot{C}}\epsilon_{\dot{A}-}\epsilon_{AD}}{(t_5-t_4)^2(t_2-t_3)^2}+\frac{\epsilon_{AC}\epsilon_{\dot{A}\dot{C}}\epsilon_{\dot{B}-}\epsilon_{BD}}{(t_5-t_3)^2(t_2-t_4)^2}\right) \\ +\frac{\epsilon_{BD}\epsilon_{\dot{B}\dot{D}}}{(t_6-t_4)^2}\left(\frac{2\epsilon_{AC}\epsilon_{\dot{A}\dot{C}}}{(t_2-t_1)^2(t_5-t_3)^2}+\frac{\epsilon_{\dot{A}+}\epsilon_{\dot{C}-}\epsilon_{AC}}{(t_5-t_2)^2(t_1-t_3)^2}-\frac{\epsilon_{\dot{A}-}\epsilon_{\dot{C}+}\epsilon_{AC}}{(t_5-t_1)^2(t_2-t_3)^2}\right) \\ +\frac{\epsilon_{AD}\epsilon_{\dot{A}\dot{D}}}{(t_6-t_3)^2}\left(\frac{2\epsilon_{BC}\epsilon_{\dot{B}\dot{C}}}{(t_2-t_1)^2(t_5-t_4)^2}+\frac{\epsilon_{\dot{B}+}\epsilon_{\dot{C}-}\epsilon_{BC}}{(t_5-t_2)^2(t_1-t_4)^2}-\frac{\epsilon_{\dot{B}-}\epsilon_{\dot{C}+}\epsilon_{BC}}{(t_5-t_1)^2(t_2-t_4)^2}\right)\Bigg] \ .\end{aligned} \tag{5.109}$$

The four contour integrals in (5.107) can then be straightforwardly evaluated, yielding the amplitude $A^{(1)(1)}_{m,n}$. The equivalent amplitude with both the initial and final states being excited on copy 2 rather than copy 1 is then trivially obtained since by symmetry $A^{(2)(2)}_{m,n} = A^{(1)(1)}_{m,n}$. This then leaves the computation of the amplitudes with initial and final state excitations on different copies, *i.e.* $A^{(2)(1)}_{m,n} = A^{(1)(2)}_{m,n}$ (again by symmetry). As explained in [79] these correlators can be obtained by moving one of the deformation operators once around the doubly-covered cylinder on which the amplitude is defined. This has the effect of interchanging the two copies that are being twisted together. By writing the computed amplitude $A^{(1)(1)}_{m,n}$ back in terms of the coordinates on the cylinder $(w_2 = w, w_1 = 0)$ and mapping the insertion of the second deformation operator using $w \to w + 2\pi i$ we obtain $A^{(2)(1)}_{m,n}$. The sum of amplitudes

$$A_{m,n}(w_2, w_1) = \frac{1}{2}\sum_{i,j=1}^{2} A^{(i)(j)}_{m,n}(w_2, w_1) \ , \tag{5.110}$$

is then the copy-symmetric amplitude required for the lift, where the factor of $\frac{1}{2}$ comes from the normalisation over copy indices in the state (5.99). We then obtain the integrated amplitude $X(T)$ defined in (5.30) by integrating over the insertion points w_1, w_2. As argued in Section 5.2, the integrated amplitude can be written as a sum of three contour integrals $I_{C_1}, I_{C_2}, I_{C_3}$ defined in (5.34) with I_{C_3} having a vanishing contribution. It can also be shown that for the states we consider $\lim_{T\to\infty} I_{C_1}(T) = \lim_{T\to\infty} I_{C_2}(T)$ and so this step can be reduced to essentially one independent contour integral leaving

$$E^{(2)}\Big(|\alpha\alpha\rangle_{B\dot{B}A\dot{A}(m,n)}\Big) = \frac{\pi\lambda^2}{\Big||\alpha\alpha\rangle_{B\dot{B}A\dot{A}(m,n)}\Big|^2} \lim_{T\to\infty} \int_0^{2\pi} d\sigma\, A_{m,n}(w,0) \coth(\tfrac{\bar{w}}{2}) \ , \tag{5.111}$$

where $w = \frac{T}{2} + i\sigma$ and $\bar{w} = \frac{T}{2} - i\sigma$ with $T \to \infty$ on this contour. For generic $SU(2)$ doublet indices on the α modes in the amplitude (5.102) it is not directly related to the second order lift of a particular state of the form (5.99). Only when the final state is the Hermitian conjugate of the initial state (as defined in Appendix B.1.3) can we use the relation (5.111) to obtain a lift.

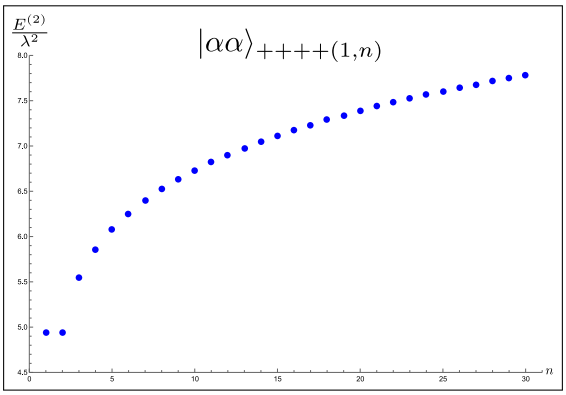

Figure 5.11: Plot of the lifts $E^{(2)}(|\alpha\alpha\rangle_{++++(1,n)})/\lambda^2$ for varying n. The plot fits to the curve: $-0.0974563\, n + 1.28434\sqrt{n} + 3.62389$.

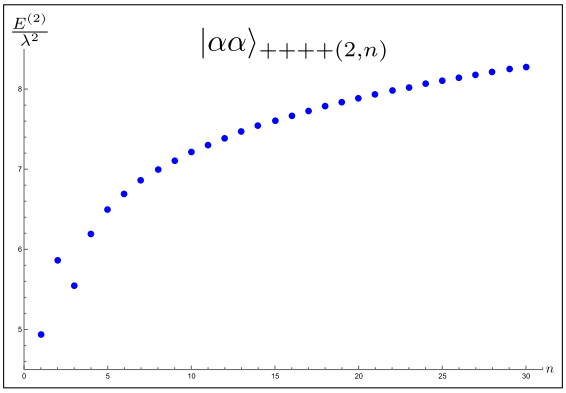

Figure 5.12: Plot of the lifts $E^{(2)}(|\alpha\alpha\rangle_{++++(2,n)})/\lambda^2$ for varying n. The plot fits to the curve: $-0.119293\, n + 1.47589\sqrt{n} + 3.71017$.

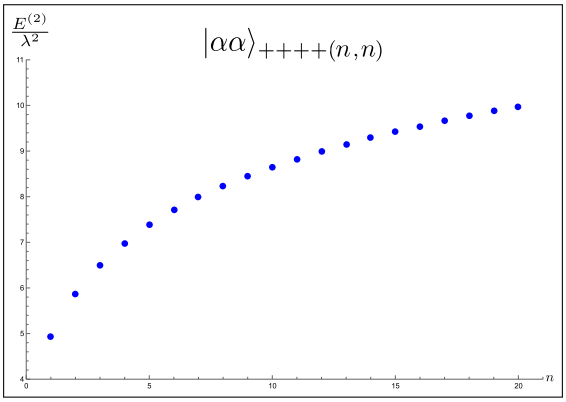

Figure 5.13: Plot of the lifts $E^{(2)}(|\alpha\alpha\rangle_{++++(n,n)})/\lambda^2$ for varying n. The plot fits to the curve: $-0.211721\ n + 2.57926\sqrt{n} + 2.62963$.

5.6.3 Lifting of $|\alpha d\rangle^{\alpha A}_{B\dot{B}(m,s)}$

Next we consider the lift of states of the form

$$|\alpha d\rangle^{\alpha A}_{B\dot{B}(m,s)} \equiv \frac{1}{\sqrt{2}}\left(\alpha^{(1)}_{B\dot{B},-m} d^{(1)\alpha A}_{-s} + \alpha^{(2)}_{B\dot{B},-m} d^{(2)\alpha A}_{-s}\right)|0\rangle^{(1)}_{NS}|0\rangle^{(2)}_{NS} \ , \tag{5.112}$$

where the norm is given by

$${}^{\delta D}_{(m,s)C\dot{C}}\langle \alpha d|\alpha d\rangle^{\alpha A}_{B\dot{B}(m,s)} = m\,\epsilon_{BC}\epsilon_{\dot{B}\dot{C}}\epsilon^{\alpha\delta}\epsilon^{AD} H[m-1]H\left[s-\tfrac{1}{2}\right] \ , \tag{5.113}$$

with appropriate choices of $SU(2)$ indices as per Appendix B.1.3. The computation of the lift requires the following left-moving amplitude

$$A^{(1)(1)}_{m,s}(w_2,w_1) \equiv \langle 0_{NS}|\left(d^{(1)\delta D}_{s}\alpha^{(1)}_{C\dot{C},m}\right)\left(G^{+}_{-,-\frac{1}{2}}\sigma^{-}\right)(w_2)\left(G^{-}_{+,-\frac{1}{2}}\sigma^{+}\right)(w_1)\left(\alpha^{(1)}_{B\dot{B},-m}d^{(1)\alpha A}_{-s}\right)|0_{NS}\rangle \ , \tag{5.114}$$

where we have chosen all of the modes to act on copy 1. In order to have a non-vanishing state we clearly require

$$n > 0 \quad \text{and} \quad s \geq \frac{1}{2} \ , \tag{5.115}$$

since the d and α modes commute and so neither should annihilate the NS vacuum. In mapping to the covering space and removing the spin fields that appear there via spectral flow transformations, the initial and final states transform similarly to the $|\alpha\alpha\rangle$ states in (5.104) and (5.105), however, the d modes gain extra factors due to their non-zero charge

under J_0^3. The initial state therefore transforms as

$$\begin{aligned}\left(\alpha^{(1)}_{B\dot{B},-m}d^{(1)\alpha A}_{-s}\right)_{-\infty} &= i\oint_{-\infty}\frac{dw_4}{2\pi i}\oint_{-\infty}\frac{dw_3}{2\pi i}\,e^{-mw_4}e^{-sw_3}\,\partial X_{B\dot{B}}(w_4)\psi^{\alpha A}(w_3)\\ &= i\oint_0\frac{dz_4}{2\pi i}\oint_0\frac{dz_3}{2\pi i}\,z_4^{-m}z_3^{-s-\frac{1}{2}}\partial X_{B\dot{B}}(z_4)\psi^{\alpha A}(z_3)\\ &= i\oint_{-a}\frac{dt_4}{2\pi i}\oint_{-a}\frac{dt_3}{2\pi i}\left(\frac{dz_3}{dt_3}\right)^{\frac{1}{2}}\frac{\partial X_{B\dot{B}}(t_4)\psi^{\alpha A}(t_3)}{z_4(t_4)^m z_3(t_3)^{s+\frac{1}{2}}}\\ &\longrightarrow i\oint_{-a}\frac{dt_4}{2\pi i}\oint_{-a}\frac{dt_3}{2\pi i}\left(\frac{dz_3}{dt_3}\right)^{\frac{1}{2}}\left(\frac{t_3-t_1}{t_3-t_2}\right)^{q_\alpha}\frac{\partial X_{B\dot{B}}(t_4)\psi^{\alpha A}(t_3)}{z_4(t_4)^m z_3(t_3)^{s+\frac{1}{2}}}\ ,\end{aligned}\tag{5.116}$$

where the spectral flow transformations were made in the final line with q_α being the eigenvalue of J_0^3 for the state created by the fermion mode $d^{\alpha A}_{-s}$. Likewise the final state transforms as

$$\begin{aligned}\left(d^{(1)\delta D}_{s}\alpha^{(1)}_{C\dot{C},m}\right)_{\infty} &= i\oint_{\infty}\frac{dw_5}{2\pi i}\oint_{\infty}\frac{dw_6}{2\pi i}\,e^{mw_5}e^{sw_6}\,\psi^{\delta D}(w_6)\partial X_{C\dot{C}}(w_5)\\ &= i\oint_{\infty}\frac{dz_5}{2\pi i}\oint_{\infty}\frac{dz_6}{2\pi i}\,z_5^{m}z_6^{s-\frac{1}{2}}\,\psi^{\delta D}(z_6)\partial X_{C\dot{C}}(z_5)\\ &= i\oint_{\infty}\frac{dt_5}{2\pi i}\oint_{\infty}\frac{dt_6}{2\pi i}\,z_5(t_5)^m z_6(t_6)^{s-\frac{1}{2}}\left(\frac{dz_6}{dt_6}\right)^{\frac{1}{2}}\psi^{\delta D}(t_6)\partial X_{C\dot{C}}(t_5)\\ &\longrightarrow i\oint_{\infty}\frac{dt_5}{2\pi i}\oint_{\infty}\frac{dt_6}{2\pi i}\,z_5(t_5)^m z_6(t_6)^{s-\frac{1}{2}}\left(\frac{dz_6}{dt_6}\right)^{\frac{1}{2}}\left(\frac{t_6-t_1}{t_6-t_2}\right)^{q_\delta}\psi^{\delta D}(t_6)\partial X_{C\dot{C}}(t_5)\ .\end{aligned}\tag{5.117}$$

This leaves the amplitude (5.114) (up to overall factors) as a correlation function of two contours of ∂X fields, two contours of ψ fields and two insertions of G fields

$$\begin{aligned}A^{(1)(1)}_{m,s} \sim \oint_{\infty}\frac{dt_5}{2\pi i}\oint_{\infty}\frac{dt_6}{2\pi i}\oint_{-a}\frac{dt_4}{2\pi i}\oint_{-a}\frac{dt_3}{2\pi i}\frac{z_5(t_5)^m z_6(t_6)^{s-\frac{1}{2}}}{z_4(t_4)^m z_3(t_3)^{s+\frac{1}{2}}}\left(\frac{dz_6}{dt_6}\right)^{\frac{1}{2}}\left(\frac{dz_3}{dt_3}\right)^{\frac{1}{2}}\left(\frac{t_6-t_1}{t_6-t_2}\right)^{q_\delta}\\ \times\left(\frac{t_3-t_1}{t_3-t_2}\right)^{q_\alpha}\langle\psi^{\delta D}(t_6)\partial X_{C\dot{C}}(t_5)G^+_-(t_2)G^-_+(t_1)\partial X_{B\dot{B}}(t_4)\psi^{\alpha A}(t_3)\rangle\ .\end{aligned}\tag{5.118}$$

This covering space correlator can be computed straightforwardly by breaking the supercurrents into the free-field bosons and fermions via (5.108), yielding

$$\begin{aligned}\langle\psi^{\delta D}(t_6)\partial X_{C\dot{C}}(t_5)G^+_-(t_2)G^-_+(t_1)\partial X_{B\dot{B}}(t_4)\psi^{\alpha A}(t_3)\rangle = \frac{\epsilon_{\dot{C}-}\epsilon_{+\dot{B}}}{(t_5-t_2)^2(t_1-t_4)^2}\Bigg[\frac{\epsilon^{\delta+}\epsilon^{-\alpha}\delta^D_C\delta^A_B}{(t_6-t_2)(t_1-t_3)}\\ -\frac{\epsilon^{\delta-}\epsilon^{+\alpha}\delta^D_B\delta^A_C}{(t_6-t_1)(t_2-t_3)}+\frac{\epsilon^{\delta\alpha}\epsilon^{AD}\epsilon_{CB}}{(t_6-t_3)(t_2-t_1)}\Bigg]+\frac{\epsilon_{\dot{C}+}\epsilon_{2\dot{B}}}{(t_5-t_1)^2(t_2-t_4)^2}\Bigg[\frac{\epsilon^{\delta+}\epsilon^{-\alpha}\delta^A_C\delta^D_B}{(t_6-t_2)(t_1-t_3)}\\ -\frac{\epsilon^{\delta-}\epsilon^{+\alpha}\delta^D_C\delta^A_B}{(t_6-t_1)(t_2-t_3)}-\frac{\epsilon^{\delta\alpha}\epsilon^{AD}\epsilon_{CB}}{(t_6-t_3)(t_2-t_1)}\Bigg]+\frac{\epsilon_{CB}\epsilon_{\dot{C}\dot{B}}}{(t_5-t_4)^2(t_2-t_1)^2}\Bigg[\frac{\epsilon^{\delta+}\epsilon^{-\alpha}\epsilon^{AD}}{(t_6-t_2)(t_1-t_3)}\\ +\frac{\epsilon^{\delta-}\epsilon^{+\alpha}\epsilon^{AD}}{(t_6-t_1)(t_2-t_3)}+\frac{2\epsilon^{\delta\alpha}\epsilon^{AD}}{(t_6-t_3)(t_2-t_1)}\Bigg]\,.\end{aligned} \tag{5.119}$$

The remainder of the lifting computation is exactly as described in Section 5.6.2 with the final lift given by

$$E^{(2)}\left(|\alpha d\rangle^{\alpha A}_{B\dot{B}(m,s)}\right)=\frac{\pi\lambda^2}{\left||\alpha d\rangle^{\alpha A}_{B\dot{B}(m,s)}\right|^2}\lim_{T\to\infty}\int_0^{2\pi}d\sigma\,A_{m,s}(w,0)\coth(\tfrac{\bar{w}}{2})\,, \tag{5.120}$$

where $w=\frac{T}{2}+i\sigma$ and $\bar{w}=\frac{T}{2}-i\sigma$ with $T\to\infty$ on this contour and $A_{m,s}(w_2,w_1)$ is the copy-symmetrised amplitude defined analogously to (5.110). For generic $SU(2)$ doublet indices on the α and d modes in the amplitude (5.114) it is not directly related to the second order lift of a particular state of the form (5.112). Only when the final state is the Hermitian conjugate of the initial state (as defined in Appendix B.1.3) can we use the relation (5.120) to obtain a lift.

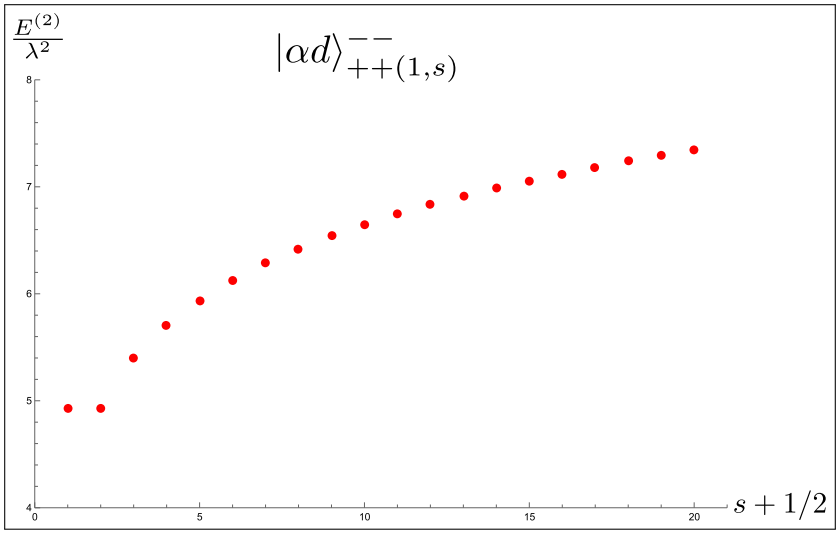

Figure 5.14: Plot of the lifts $E^{(2)}\left(|\alpha d\rangle^{--}_{++(1,s)}\right)/\lambda^2$ for varying s. The plot fits to the curve: $-0.0187122(s+1/2)+0.590457\sqrt{s+1/2}+4.20151$.

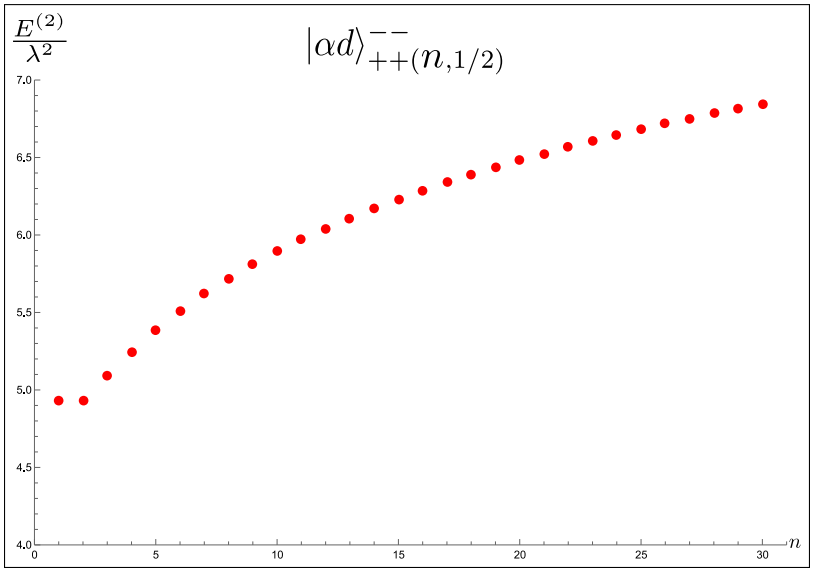

Figure 5.15: Plot of the lifts $E^{(2)}\Big(|\alpha d\rangle^{--}_{++(n,1/2)}\Big)/\lambda^2$ for varying n. The plot fits to the curve: $-0.0909845\, n + 1.25023\sqrt{n} + 3.58201$.

Below we do not list the diagonal elements of the lift matrix for large mode numbers of $|\alpha d\rangle^{--}_{++(m,s)}$ because there are relations between the diagonal elements of the lift matrix of states $|\alpha\alpha\rangle_{++++(m,n)}$ and $|\alpha d\rangle^{--}_{++(m,s)}$. These relations force the diagonal elements of the lift matrix of $|\alpha d\rangle^{--}_{++(m,s)}$ to be the same as those of $|\alpha\alpha\rangle_{++++(m,n)}$. We study these relations in Section 5.7.

5.6.4 Lifting of $|dd\rangle^{\beta B\alpha A}_{(r,s)}$

Lastly, we consider the lift of normalized states of the form

$$|dd\rangle^{\beta B\alpha A}_{(r,s)} \equiv \frac{1}{\sqrt{2}}\Big(d^{(1)\beta B}_{-r}d^{(1)\alpha A}_{-s} + d^{(2)\beta B}_{-r}d^{(2)\alpha A}_{-s}\Big)|0\rangle^{(1)}_{NS}|0\rangle^{(2)}_{NS}\ , \tag{5.121}$$

where the norm is given by

$$\begin{aligned}{}^{\delta D\gamma C}_{(r,s)}\langle dd|dd\rangle^{\beta B\alpha A}_{(r,s)} = \Big(&\epsilon^{\alpha\beta}\epsilon^{\gamma\delta}\epsilon_{AB}\epsilon_{CD}\delta_{r+s,1} - \epsilon^{\alpha\gamma}\epsilon^{\beta\delta}\epsilon_{AC}\epsilon_{BD}\delta_{r,s} \\ &+ \epsilon^{\alpha\delta}\epsilon^{\beta\gamma}\epsilon_{AD}\epsilon_{BC}H\Big[r-\tfrac{1}{2}\Big]\Big)H\Big[s-\tfrac{1}{2}\Big]\ ,\end{aligned} \tag{5.122}$$

with appropriate choices of $SU(2)$ indices as per Appendix B.1.3. The computation of the lift requires the following left-moving amplitude

$$A^{(1)(1)}_{r,s}(w_2,w_1) \equiv \langle 0_{NS}|\Big(d^{(1)\delta D}_s d^{(1)\gamma C}_r\Big)\Big(G^+_{-,-\frac{1}{2}}\sigma^-\Big)(w_2)\Big(G^-_{+,-\frac{1}{2}}\sigma^+\Big)(w_1)\Big(d^{(1)\beta B,}_{-r}d^{(1)\alpha A}_{-s}\Big)|0_{NS}\rangle\ , \tag{5.123}$$

where we have chosen all of the modes to act on copy 1. In order to have a non-vanishing state we require

$$s \geq \frac{1}{2} \,. \tag{5.124}$$

In mapping to the covering space and removing the spin fields that appear there the initial state transforms as

$$\begin{aligned}
\left(d^{(1)\beta B}_{-r} d^{(1)\alpha A}_{-s}\right)_{-\infty} &= \oint_{-\infty} \frac{dw_4}{2\pi i} \oint_{-\infty} \frac{dw_3}{2\pi i}\, e^{-rw_4} e^{-sw_3}\, \psi^{\beta B}(w_4)\psi^{\alpha A}(w_3) \\
&= \oint_0 \frac{dz_4}{2\pi i} \oint_0 \frac{dz_3}{2\pi i}\, z_4^{-r-\frac{1}{2}} z_3^{-s-\frac{1}{2}}\, \psi^{\beta B}(z_4)\psi^{\alpha A}(z_3) \\
&= \oint_{-a} \frac{dt_4}{2\pi i} \oint_{-a} \frac{dt_3}{2\pi i} \left(\frac{dz_4}{dt_4}\right)^{\frac{1}{2}} \left(\frac{dz_3}{dt_3}\right)^{\frac{1}{2}} \frac{\psi^{\beta B}(t_4)\psi^{\alpha A}(t_3)}{z_4(t_4)^{r+\frac{1}{2}} z_3(t_3)^{s+\frac{1}{2}}} \\
&\longrightarrow \oint_{-a} \frac{dt_4}{2\pi i} \oint_{-a} \frac{dt_3}{2\pi i} \left(\frac{dz_4}{dt_4}\right)^{\frac{1}{2}} \left(\frac{dz_3}{dt_3}\right)^{\frac{1}{2}} \left(\frac{t_4-t_1}{t_4-t_2}\right)^{q_\beta} \left(\frac{t_3-t_1}{t_3-t_2}\right)^{q_\alpha} \frac{\psi^{\beta B}(t_4)\psi^{\alpha A}(t_3)}{z_4(t_4)^{r+\frac{1}{2}} z_3(t_3)^{s+\frac{1}{2}}} \,,
\end{aligned} \tag{5.125}$$

where the spectral flow transformation was made in the final line and q_α and q_β correspond to the values of the J_0^3 charge of $d^{\alpha A}_{-s}$ and $d^{\beta B}_{-r}$ respectively. Likewise the final state transforms as

$$\begin{aligned}
\left(d^{(1)\delta D}_{s} d^{(1)\gamma C}_{r}\right)_{\infty} &= \oint_{\infty} \frac{dw_5}{2\pi i} \oint_{\infty} \frac{dw_6}{2\pi i} e^{rw_5} e^{sw_6}\, \psi^{\delta D}(w_6)\psi^{\gamma C}(w_5) \\
&= \oint_{\infty} \frac{dz_5}{2\pi i} \oint_{\infty} \frac{dz_6}{2\pi i} z_5^{r-\frac{1}{2}} z_6^{s-\frac{1}{2}}\, \psi^{\delta D}(z_6)\psi^{\gamma C}(z_5) \\
&= \oint_{\infty} \frac{dt_5}{2\pi i} \oint_{\infty} \frac{dt_6}{2\pi i} z_5(t_5)^{r-\frac{1}{2}} z_6(t_6)^{s-\frac{1}{2}} \left(\frac{dz_6}{dt_6}\right)^{\frac{1}{2}} \left(\frac{dz_5}{dt_5}\right)^{\frac{1}{2}} \psi^{\delta D}(t_6)\psi^{\gamma C}(t_5) \\
&\longrightarrow \oint_{\infty} \frac{dt_5}{2\pi i} \oint_{\infty} \frac{dt_6}{2\pi i} \left(\frac{dz_6}{dt_6}\right)^{\frac{1}{2}} \left(\frac{dz_5}{dt_5}\right)^{\frac{1}{2}} \left(\frac{t_6-t_1}{t_6-t_2}\right)^{q_\delta} \left(\frac{t_5-t_1}{t_5-t_2}\right)^{q_\gamma} \frac{\psi^{\delta D}(t_6)\psi^{\gamma C}(t_5)}{z_5(t_5)^{\frac{1}{2}-r} z_6(t_6)^{\frac{1}{2}-s}} \,.
\end{aligned} \tag{5.126}$$

This leaves the amplitude (5.123) (up to overall factors) as a correlation function of four contours of ψ fields and two insertions of G fields

$$\begin{aligned}
A^{(1)(1)}_{r,s} \sim \oint_{\infty} \frac{dt_5}{2\pi i} \oint_{\infty} \frac{dt_6}{2\pi i} \oint_{-a} \frac{dt_4}{2\pi i} \oint_{-a} \frac{dt_3}{2\pi i} \frac{z_5(t_5)^{r-\frac{1}{2}} z_6(t_6)^{s-\frac{1}{2}}}{z_4(t_4)^{r+\frac{1}{2}} z_3(t_3)^{s+\frac{1}{2}}} \left(\frac{dz_6}{dt_6}\right)^{\frac{1}{2}} \left(\frac{dz_5}{dt_5}\right)^{\frac{1}{2}} \left(\frac{dz_4}{dt_4}\right)^{\frac{1}{2}} \left(\frac{dz_3}{dt_3}\right)^{\frac{1}{2}} \\
\times \left(\frac{t_6-t_1}{t_6-t_2}\right)^{q_\delta} \left(\frac{t_5-t_1}{t_5-t_2}\right)^{q_\gamma} \left(\frac{t_4-t_1}{t_4-t_2}\right)^{q_\beta} \left(\frac{t_3-t_1}{t_3-t_2}\right)^{q_\alpha} \langle \psi^{\delta D}(t_6)\psi^{\gamma C}(t_5) G^+_-(t_2) G^-_+(t_1) \psi^{\beta B}(t_4)\psi^{\alpha A}(t_3)\rangle \,.
\end{aligned} \tag{5.127}$$

This covering space correlator can be computed straightforwardly by breaking the supercurrents into the free-field bosons and fermions via (5.108) and using the fact that the only bosonic fields in this correlator are from the supercurrents and so they must Wick

contract together. The correlator is then given by

$$\begin{aligned}\langle\psi^{\delta D}(t_6)\psi^{\gamma C}(t_5)G^+_-(t_2)G^-_+(t_1)\psi^{\beta B}(t_4)\psi^{\alpha A}(t_3)\rangle = \frac{-1}{(t_2-t_1)^2}\Bigg[\\ -\frac{\epsilon^{CD}\epsilon^{\gamma\delta}}{t_6-t_5}\left(\frac{2\epsilon^{AB}\epsilon^{\alpha\beta}}{(t_2-t_1)(t_4-t_3)}-\frac{\epsilon^{\beta+}\epsilon^{\alpha-}\epsilon^{AB}}{(t_2-t_4)(t_1-t_3)}+\frac{\epsilon^{\alpha+}\epsilon^{\beta-}\epsilon^{AB}}{(t_2-t_3)(t_1-t_4)}\right) \\ +\frac{\epsilon^{\delta+}}{t_6-t_2}\left(\frac{\epsilon^{AB}\epsilon^{\alpha\beta}\epsilon^{\gamma-}\epsilon^{CD}}{(t_5-t_1)(t_4-t_3)}-\frac{\epsilon^{BC}\epsilon^{\beta\gamma}\epsilon^{\alpha-}\epsilon^{AD}}{(t_5-t_4)(t_1-t_3)}+\frac{\epsilon^{AC}\epsilon^{\alpha\gamma}\epsilon^{\beta-}\epsilon^{BD}}{(t_5-t_3)(t_1-t_4)}\right) \\ +\frac{\epsilon^{\delta-}}{t_6-t_1}\left(\frac{\epsilon^{AB}\epsilon^{\alpha\beta}\epsilon^{\gamma+}\epsilon^{CD}}{(t_5-t_2)(t_4-t_3)}-\frac{\epsilon^{BC}\epsilon^{\beta\gamma}\epsilon^{\alpha+}\epsilon^{AD}}{(t_5-t_4)(t_2-t_3)}+\frac{\epsilon^{AC}\epsilon^{\alpha\gamma}\epsilon^{\beta+}\epsilon^{BD}}{(t_5-t_3)(t_2-t_4)}\right) \\ +\frac{\epsilon^{BD}\epsilon^{\beta\delta}}{t_6-t_4}\left(\frac{2\epsilon^{AC}\epsilon^{\alpha\gamma}}{(t_2-t_1)(t_5-t_3)}+\frac{\epsilon^{\alpha+}\epsilon^{\gamma-}\epsilon^{AC}}{(t_5-t_1)(t_2-t_3)}+\frac{\epsilon^{\alpha-}\epsilon^{\gamma+}\epsilon^{AC}}{(t_5-t_2)(t_1-t_3)}\right) \\ -\frac{\epsilon^{AD}\epsilon^{\alpha\delta}}{t_6-t_3}\left(\frac{2\epsilon^{BC}\epsilon^{\beta\gamma}}{(t_2-t_1)(t_5-t_4)}+\frac{\epsilon^{\beta+}\epsilon^{\gamma-}\epsilon^{BC}}{(t_5-t_1)(t_2-t_4)}+\frac{\epsilon^{\beta-}\epsilon^{\gamma+}\epsilon^{BC}}{(t_5-t_2)(t_1-t_4)}\right)\Bigg] .\end{aligned} \tag{5.128}$$

Again, all of the remaining steps in the lifting computation are identical to that described in Section 5.6.2

$$E^{(2)}\left(|dd\rangle^{\beta B\alpha A}_{(r,s)}\right) = \frac{\pi\lambda^2}{\left||dd\rangle^{\beta B\alpha A}_{(r,s)}\right|^2}\lim_{T\to\infty}\int_0^{2\pi} d\sigma\, A_{r,s}(w,0)\coth(\tfrac{\bar{w}}{2}) \ , \tag{5.129}$$

where $w = \frac{T}{2} + i\sigma$ and $\bar{w} = \frac{T}{2} - i\sigma$ with $T \to \infty$ on this contour and $A_{r,s}(w_2, w_1)$ is the copy-symmetrised amplitude defined analogously to (5.110). For generic $SU(2)$ doublet indices on the d modes in the amplitude (5.123) it is not directly related to the second order lift of a particular state of the form (5.121). Only when the final state is the Hermitian conjugate of the initial state (as defined in Appendix B.1.3) can we use the relation (5.129) to obtain a lift.

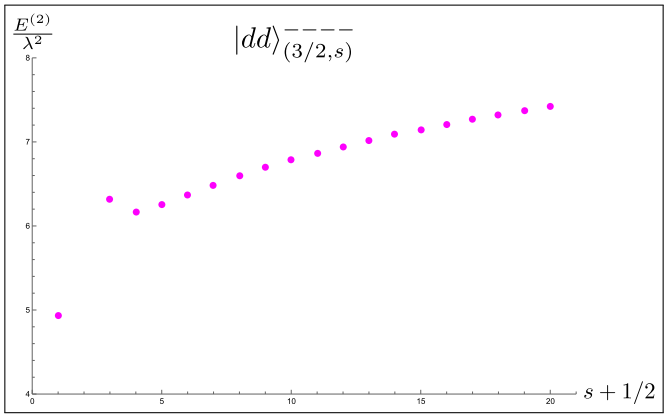

Figure 5.16: Plot of the lifts $E^{(2)}\left(|dd\rangle^{----}_{(3/2,s)}\right)/\lambda^2$ for varying s. The plot fits to the curve: $-0.41026\ (s+1/2) + 3.40665\sqrt{s+1/2} + 0.216748$.

5.7 Relations between lifts

From the low-level lift matrices in our work [20], it is clear that there exists some patterns and symmetries in the lifts of these families of two-mode states. In this section we explore some of the relations between lifts of the states considered in Section 5.6 that emerge from the action of the $\mathcal{N} = 4$ current algebra modes.

5.7.1 L_{-1} relations

We first consider the relations between lifts due to the action of the stress tensor mode L_{-1} on the initial and final states in the amplitude in (5.30). In what follows, we show that there exist a set of simple relations between the lift of a state and the lift of its L_{-1} descendant involving only a multiplicative factor.

Let us consider a state $|\psi\rangle$ and its L_{-1} descendant $|\psi\rangle$ defined as[14]

$$|\phi\rangle \equiv L_{-1}\,|\psi\rangle \ , \tag{5.130}$$

where $|\psi\rangle$ has conformal dimension h_ψ. The stress tensor mode can expressed as a contour integral of the stress tensor field $T(w)$ around the cylinder as

$$L_{-1} = \frac{1}{2\pi i}\oint dw\, T(w)\, e^{-w} \ , \tag{5.131}$$

which we will use in the amplitude required in the lift (5.29) (this was defined as $X(T)$ in (5.30), however, in this section we will use the notation $A(\phi)$)

$$\begin{aligned} A(\phi) &= \langle\phi| \int d^2w_2\, D(w_2,\bar{w_2}) \int d^2w_1\, D(w_1,\bar{w_1})\, |\phi\rangle \\ &= \langle\psi|\, L_1 \int d^2w_2\, D(w_2,\bar{w_2}) \int d^2w_1\, D(w_1,\bar{w_1})\, L_{-1}|\psi\rangle \ . \end{aligned} \tag{5.132}$$

The general steps in the derivation of these relations between lifts is given pictorially in Figure 5.17. As shown in Figure 5.17(a)-(c), the first step is to deform the L_{-1} contour in the amplitude (5.132) which yields a contour encircling the first deformation operator insertion and one wrapped around the cylinder between the two D insertions. We now show that the first of these terms actually vanishes. The contour integral I_L of the stress tensor around the insertion of $D(w_1)$ can be evaluated by using the OPE

$$T(w)D(w_1) \sim \frac{D(w_1)}{(w-w_1)^2} + \frac{\partial_{w_1} D(w_1)}{(w-w_1)} + \text{reg} \ , \tag{5.133}$$

[14] One subtlety here is that the descendant state we actually consider is the single-copy descendant $|\phi\rangle^{(1)}|0\rangle^{(2)}_{NS} = L^{(1)}_{-1}|\psi\rangle^{(1)}|0\rangle^{(2)}_{NS}$, however, in this case this is exactly equal to a global L_{-1} mode acting on $|\psi\rangle \equiv |\psi\rangle^{(1)}|0\rangle^{(2)}_{NS}$. This fact is the reason that we consider only L_{-1} modes here.

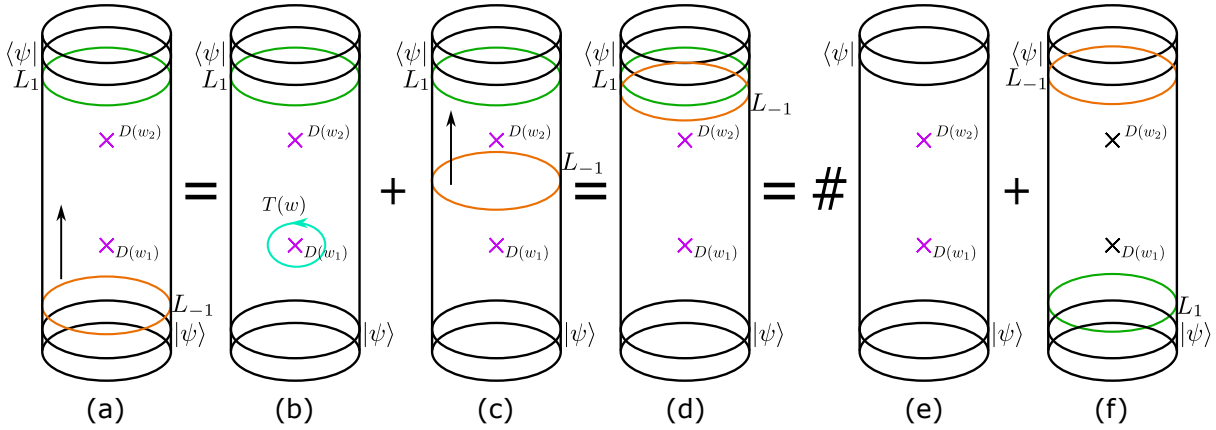

Figure 5.17: The general tactic in deriving these relations between lifts will be to start with the correlator (5.132) containing descendants of $|\psi\rangle$ as initial and final states (a), deform the contour of the L_{-1} mode through the insertions of the deformation operators (b)-(d) and then commute the L_{-1} mode with the L_1 mode from the final state. This leaves (up to constant coefficients) a correlator that computes the lift of the state $|\psi\rangle$ (e) and one that computes the lift of the state $L_1|\psi\rangle$ (f). We have suppressed the trivial right-moving part throughout.

yielding

$$\begin{aligned} I_L &= \frac{1}{2\pi i}\int d^2w_1 \oint_{w_1} dw\, e^{-w}\, T(w)D(w_1) \\ &= \frac{1}{2\pi i}\int d^2w_1 \oint_{w_1} dw\, e^{-w_1}\Big(1-(w-w_1)+\cdots\Big)T(w)D(w_1) \\ &= \frac{1}{2\pi i}\int d^2w_1 e^{-w_1}\oint_{w_1} dw\left(\frac{D(w_1)}{(w-w_1)^2}+\frac{\partial_{w_1}D(w_1)}{(w-w_1)}-\frac{D(w_1)}{(w-w_1)}\right) \\ &= \int d^2w_1 e^{-w_1}\Big(\partial_{w_1}D(w_1)-D(w_1)\Big)=0\ , \end{aligned} \tag{5.134}$$

where (5.133) was used in the third line and the final integrand is simply a total derivative of $e^{-w_1}D(w_1)$. This argument can be exactly repeated when deforming the L_{-1} contour past the $D(w_2)$ insertion. The correlator (5.132) containing descendant initial and final states is thus equal to the correlator represented by Figure 5.17(d), *i.e.*

$$\begin{aligned} A(\phi) &= \langle\psi|\, L_1L_{-1}\int d^2w_2\, D(w_2,\bar{w}_2)\int d^2w_1\, D(w_1,\bar{w}_1)\,|\psi\rangle \\ &= \langle\psi|\,\Big(2h_\psi + L_{-1}L_1\Big)\int d^2w_2 D(w_2,\bar{w}_2)\int d^2w_1 D(w_1,\bar{w}_1)\,|\psi\rangle\ , \end{aligned} \tag{5.135}$$

where the two terms in the last line are displayed in Figure 5.17(e) and (f). If the state ψ is chosen to be a global conformal primary (that is $L_1|\psi\rangle = 0$) then the second term in (5.135) (depicted in Figure 5.17(f)) vanishes and we are left with a relation between amplitudes given by

$$A(\phi) = 2h_\psi A(\psi)\ . \tag{5.136}$$

Promoting this relation between amplitudes to a precise relation between lifts is discussed in Appendix B.5 and we will do this for some explicit cases in Section 5.7.3 using the data of Section 5.6.

5.7.2 $G^{\alpha}_{\dot{A},-\frac{1}{2}}$ relations

It turns out that very similar relations also exist between a state $|\tilde{\psi}\rangle$ and its $G_{-1/2}$ descendant. Much of the derivation follows along the same lines as in Section 5.7.1 with some added complexities from there being multiple choices of G modes. Again, we show that there exist simple relations that link the lifts of different two-mode states of the kind discussed in Section 5.6. One key difference with the relations of Section 5.7.1 is that these relate the lifts of states in different families (*i.e.* between the $\alpha\alpha$, αd and dd families of states).

Let us consider a superdescendant of a state $|\tilde{\psi}\rangle$, defined as

$$|\widetilde{\phi}\,\rangle^{\alpha}_{\dot{A}} \equiv G^{\alpha}_{\dot{A},-\frac{1}{2}}|\widetilde{\psi}\,\rangle \ , \tag{5.137}$$

where $|\widetilde{\psi}\,\rangle$ has dimension $h_{\widetilde{\psi}}$ and J^3_0 charge $m_{\widetilde{\psi}}$ and the G mode can expressed as a contour integral of a G field as

$$G^{\alpha}_{\dot{A},-1/2} = \frac{1}{2\pi i}\oint_{C_\tau} dw\, e^{-\frac{1}{2}w}\, G^{\alpha}_{\dot{A}}(w) \ , \tag{5.138}$$

where the contour C_τ wraps the cylinder at a fixed τ coordinate. Then the amplitude (5.30) we wish to compute for the lift (5.29) is

$$\begin{aligned} A^{\beta\alpha}_{\dot{B}\dot{A}}(\widetilde{\phi}) &= {}^{\beta}_{\dot{B}}\langle\widetilde{\phi}\,| \int d^2w_2\, D(w_2,\bar{w}_2) \int d^2w_1\, D(w_1,\bar{w}_1)|\widetilde{\phi}\,\rangle^{\alpha}_{\dot{A}} \\ &= \langle\widetilde{\psi}\,|G^{\beta}_{\dot{B},1/2} \int d^2w_2\, D(w_2,\bar{w}_2) \int d^2w_1\, D(w_1,\bar{w}_1)\, G^{\alpha}_{\dot{A},-1/2}|\widetilde{\psi}\,\rangle \ , \end{aligned} \tag{5.139}$$

where it is understood that once a choice of the state (5.137) is made, the bra state in the amplitude (5.139) is fixed to be its Hermitian conjugate. For now, however, we keep the indices of the G modes unfixed. Following the same steps as displayed in Figure 5.17 the contour of $G^{\alpha}_{\dot{A}}(w)$ (defined in (5.138)) that was acting on the initial state in Figure 5.17(a) can be deformed through the two D insertions, with the terms containing contour integrals $I^{\alpha}_{\dot{A}}$ of a G field around a D insertion vanishing (see Figure 5.17(b) for one of these terms).

The first of these terms, around $D(w_1)$, is given by

$$\begin{aligned} I^\alpha_{\dot A} &= \frac{1}{2\pi i}\int d^2w_1 \oint_{C_{w_1}} dw\, e^{-\frac{1}{2}w}\, G^\alpha_{\dot A}(w) D(w_1) \\ &= \frac{1}{2\pi i}\int d^2w_1\, e^{-\frac{1}{2}w_1} \oint_{C_{w_1}} dw \sum_{k=0}^{\infty} \frac{(-1)^k}{2^k k!}(w-w_1)^k\, G^\alpha_{\dot A}(w) D(w_1) \\ &= \int d^2w_1\, e^{-\frac{1}{2}w_1} \sum_{k=0}^{\infty} \frac{(-1)^k}{2^k k!}\, G^\alpha_{\dot A, k-\frac{1}{2}} D(w_1)\ , \end{aligned} \tag{5.140}$$

where the contour C_{w_1} is centred around w_1 and in the last line we used that on such contours the modes on the cylinder are defined as

$$G^\alpha_{\dot A, s} = \oint_{C_{w_1}} \frac{dw}{2\pi i}\,(w-w_1)^{s+\frac{1}{2}}\, G^\alpha_{\dot A}\ . \tag{5.141}$$

As stated in (5.28) the deformation operator can be written in multiple equivalent ways; to analyse (5.140) further it is simplest to choose the representation of D containing a twist operator with $SU(2)_L$ index equal to that of the $G^\alpha_{\dot A,-\frac{1}{2}}$ mode of the starting descendant state (5.137). For instance, for the choice $\alpha = +$ the integral (5.140) becomes

$$\begin{aligned} I^+_{\dot A} &= \epsilon^{\dot C\dot D}\bar G^-_{\dot D,-\frac{1}{2}} \int d^2w_1\, e^{-\frac{1}{2}w_1} \sum_{k=0}^{\infty} \frac{(-1)^k}{2^k k!}\, G^+_{\dot A,k-\frac{1}{2}} G^-_{\dot C,-\frac{1}{2}} \sigma_2^{++}(w_1,\bar w_1) \\ &= \epsilon^{\dot C\dot D}\bar G^-_{\dot D,-\frac{1}{2}} \int d^2w_1\, e^{-\frac{1}{2}w_1} \sum_{k=0}^{\infty} \frac{(-1)^k}{2^k k!} \left(\left\{ G^+_{\dot A,k-\frac{1}{2}}, G^-_{\dot C,-\frac{1}{2}} \right\} + G^-_{\dot C,-\frac{1}{2}} G^+_{\dot A,k-\frac{1}{2}} \right) \sigma_2^{++}(w_1,\bar w_1) \\ &= -\bar G^-_{\dot A,-\frac{1}{2}} \int d^2w_1\, e^{-\frac{1}{2}w_1} \sum_{k=0}^{\infty} \frac{(-1)^k}{2^k k!} \left(k J^3_{k-1} + L_{k-1} \right) \sigma_2^{++}(w_1,\bar w_1) \\ &= -\bar G^-_{\dot A,-\frac{1}{2}} \int d^2w_1\, e^{-\frac{1}{2}w_1} \left[L_{-1} - \frac{1}{2}\left(J^3_0 + L_0 \right) \right] \sigma_2^{++}(w_1,\bar w_1) \\ &= -\bar G^-_{\dot A,-\frac{1}{2}} \int d^2w_1\, e^{-\frac{1}{2}w_1} \left(\partial_{w_1} - \frac{1}{2} \right) \sigma_2^{++}(w_1,\bar w_1) = 0\ , \end{aligned} \tag{5.142}$$

where in the third line we use the fact that σ_2^{++} is chiral and in the forth line we use that it is killed by positive J^3 and L modes. The integral (5.142) vanishes since the integrand in the final line forms a total derivative. The argument for the case of $I^-_{\dot A}$ follows almost identically using the representation $D(w_1,\bar w_1) = \epsilon^{\dot C\dot D} G^+_{\dot C,-\frac{1}{2}} \bar G^+_{\dot D,-\frac{1}{2}} \sigma_2^{--}(w_1,\bar w_1)$ instead. We thus conclude that terms of the form shown in Figure 5.17(b) with a G contour encircling the insertion of a deformation operator vanish. This leaves us with the amplitude shown

in Figure 5.17(d)

$$\begin{aligned} A^{\beta\alpha}_{\dot{B}\dot{A}}(\widetilde{\phi}) &= \langle\widetilde{\psi}\,|G^{\beta}_{\dot{B},1/2}G^{\alpha}_{\dot{A},-1/2}\int d^2w_2\,D(w_2,\bar{w}_2)\int d^2w_1\,D(w_1,\bar{w}_1)|\widetilde{\psi}\rangle \\ &= \epsilon_{\dot{B}\dot{A}}\langle\widetilde{\psi}\,|\Big(\big(\sigma^{aT}\big)^{\beta}_{\ \gamma}\epsilon^{\gamma\alpha}J^a_0+\epsilon^{\beta\alpha}L_0\Big)\int d^2w_2\,D(w_2,\bar{w}_2)\int d^2w_1\,D(w_1,\bar{w}_1)|\widetilde{\psi}\rangle \\ &\quad-\langle\widetilde{\psi}\,|G^{\alpha}_{\dot{A},-1/2}G^{\beta}_{\dot{B},1/2}\int d^2w_2\,D(w_2,\bar{w}_2)\int d^2w_1\,D(w_1,\bar{w}_1)|\widetilde{\psi}\rangle\ , \end{aligned} \tag{5.143}$$

where the two terms in the last line are those displayed in Figure 5.17(e) and (f). If the state $\widetilde{\psi}$ is chosen to satisfy $G^{\beta}_{\dot{B},\frac{1}{2}}|\widetilde{\psi}\,\rangle=0$ then the second term in (5.143) vanishes and we are left with a simple relation between amplitudes. Clearly to relate the amplitude (5.139) to that required in the computation of lifts it is necessary for the quantum numbers of the G mode in the bra state to be opposite to those of the G mode in the ket (an additional overall negative sign may also be required as per the conjugation conventions given in Appendix B.1.3). With this being the case our relations read

$$A^{\beta\alpha}_{\dot{B}\dot{A}}(\widetilde{\phi})=K^{\beta\alpha}_{\dot{B}\dot{A}}A(\widetilde{\psi})\ , \tag{5.144}$$

where

$$K^{\beta\alpha}_{\dot{B}\dot{A}}\equiv\epsilon_{\dot{B}\dot{A}}\Big(m_{\widetilde{\psi}}\big(\sigma^3\big)^{\beta}_{\ \gamma}\epsilon^{\gamma\alpha}+h_{\widetilde{\psi}}\epsilon^{\beta\alpha}\Big)\ . \tag{5.145}$$

5.7.3 Using lifting relations to perform checks

We will now use the above-derived relations to explain some of the symmetries and properties of the lifting matrices computed in Section 5.6. Let us begin by showing the lifting matrices of the various states. The $|\alpha\alpha\rangle_{++++(m,n)}$ lift matrix is:

increasing n →

$$\begin{pmatrix}
\frac{\pi^2}{2} & \frac{\pi^2}{2} & \frac{9\pi^2}{16} & \frac{19\pi^2}{32} & \frac{5045\pi^2}{8192} & \frac{10377\pi^2}{16384} & \frac{42469\pi^2}{65536} \\
\frac{\pi^2}{2} & \frac{19\pi^2}{32} & \frac{9\pi^2}{16} & \frac{2569\pi^2}{4096} & \frac{10775\pi^2}{16384} & \frac{44469\pi^2}{65536} & \frac{22771\pi^2}{32768} \\
\frac{9\pi^2}{16} & \frac{9\pi^2}{16} & \frac{2697\pi^2}{4096} & \frac{5001\pi^2}{8192} & \frac{44205\pi^2}{65536} & \frac{23061\pi^2}{32768} & \frac{24275979\pi^2}{33554432} \\
\frac{19\pi^2}{32} & \frac{2569\pi^2}{4096} & \frac{5001\pi^2}{8192} & \frac{92751\pi^2}{131072} & \frac{42555\pi^2}{65536} & \frac{47798349\pi^2}{67108864} & \frac{99368101\pi^2}{134217728} \\
\frac{5045\pi^2}{8192} & \frac{10775\pi^2}{16384} & \frac{44205\pi^2}{65536} & \frac{42555\pi^2}{65536} & \frac{200592615\pi^2}{268435456} & \frac{183067725\pi^2}{268435456} & \frac{1597261925\pi^2}{2147483648} \\
\frac{10377\pi^2}{16384} & \frac{44469\pi^2}{65536} & \frac{23061\pi^2}{32768} & \frac{47798349\pi^2}{67108864} & \frac{183067725\pi^2}{268435456} & \frac{3351953103\pi^2}{4294967296} & \frac{1524951729\pi^2}{2147483648} \\
\frac{42469\pi^2}{65536} & \frac{22771\pi^2}{32768} & \frac{24275979\pi^2}{33554432} & \frac{99368101\pi^2}{134217728} & \frac{1597261925\pi^2}{2147483648} & \frac{1524951729\pi^2}{2147483648} & \frac{444727449481\pi^2}{549755813888}
\end{pmatrix} \tag{5.146}$$

increasing m ↓

The $|\alpha d\rangle_{++(n,s)}$ lifting matrix is:

increasing s →

$$\begin{pmatrix}
\frac{\pi^2}{2} & \frac{\pi^2}{2} & \frac{35\pi^2}{64} & \frac{37\pi^2}{64} & \frac{9859\pi^2}{16384} & \frac{10171\pi^2}{16384} & \frac{333847\pi^2}{524288} \\
\frac{\pi^2}{2} & \frac{19\pi^2}{32} & \frac{19\pi^2}{32} & \frac{1283\pi^2}{2048} & \frac{10663\pi^2}{16384} & \frac{175711\pi^2}{262144} & \frac{179969\pi^2}{262144} \\
\frac{33\pi^2}{64} & \frac{39\pi^2}{64} & \frac{2697\pi^2}{4096} & \frac{2697\pi^2}{4096} & \frac{358269\pi^2}{524288} & \frac{368643\pi^2}{524288} & \frac{48290217\pi^2}{67108864} \\
\frac{17\pi^2}{32} & \frac{2563\pi^2}{4096} & \frac{5525\pi^2}{8192} & \frac{92751\pi^2}{131072} & \frac{92751\pi^2}{131072} & \frac{48833787\pi^2}{67108864} & \frac{99898097\pi^2}{134217728} \\
\frac{8935\pi^2}{16384} & \frac{10495\pi^2}{16384} & \frac{361355\pi^2}{524288} & \frac{378645\pi^2}{524288} & \frac{200592615\pi^2}{268435456} & \frac{200592615\pi^2}{268435456} & \frac{6562949705\pi^2}{8589934592} \\
\frac{9141\pi^2}{16384} & \frac{171381\pi^2}{262144} & \frac{184155\pi^2}{262144} & \frac{24675753\pi^2}{33554432} & \frac{204097593\pi^2}{268435456} & \frac{3351953103\pi^2}{4294967296} & \frac{3351953103\pi^2}{4294967296} \\
\frac{298417\pi^2}{524288} & \frac{348943\pi^2}{524288} & \frac{47941229\pi^2}{67108864} & \frac{50147797\pi^2}{67108864} & \frac{6632510507\pi^2}{8589934592} & \frac{6804589421\pi^2}{8589934592} & \frac{444727449481\pi^2}{549755813888}
\end{pmatrix}$$

increasing m ↓ (5.147)

and lastly, the $|dd\rangle^{----}_{(r,s)}$ lifting matrix is:

increasing s →

$$\begin{pmatrix}
- & \frac{\pi^2}{2} & \frac{\pi^2}{2} & \frac{33\pi^2}{64} & \frac{17\pi^2}{32} & \frac{8935\pi^2}{16384} & \frac{9141\pi^2}{16384} \\
\frac{\pi^2}{2} & - & \frac{41\pi^2}{64} & \frac{5\pi^2}{8} & \frac{10383\pi^2}{16384} & \frac{661\pi^2}{1024} & \frac{344545\pi^2}{524288} \\
\frac{\pi^2}{2} & \frac{41\pi^2}{64} & - & \frac{2959\pi^2}{4096} & \frac{11437\pi^2}{16384} & \frac{367977\pi^2}{524288} & \frac{23281\pi^2}{32768} \\
\frac{33\pi^2}{64} & \frac{5\pi^2}{8} & \frac{2959\pi^2}{4096} & - & \frac{409209\pi^2}{524288} & \frac{24603\pi^2}{32768} & \frac{50412795\pi^2}{67108864} \\
\frac{17\pi^2}{32} & \frac{10383\pi^2}{16384} & \frac{11437\pi^2}{16384} & \frac{409209\pi^2}{524288} & - & \frac{221622483\pi^2}{268435456} & \frac{212700391\pi^2}{268435456} \\
\frac{8935\pi^2}{16384} & \frac{661\pi^2}{1024} & \frac{367977\pi^2}{524288} & \frac{24603\pi^2}{32768} & \frac{221622483\pi^2}{268435456} & - & \frac{7408688711\pi^2}{8589934592} \\
\frac{9141\pi^2}{16384} & \frac{344545\pi^2}{524288} & \frac{23281\pi^2}{32768} & \frac{50412795\pi^2}{67108864} & \frac{212700391\pi^2}{268435456} & \frac{7408688711\pi^2}{8589934592} & -
\end{pmatrix}$$

increasing r ↓ (5.148)

L_{-1} mode on $|\alpha\alpha\rangle_{++++(1,1)}$

In the lifting matrix of the states $|\alpha\alpha\rangle_{++++(m,n)}$ shown above in (5.146) it is clear that the lifts of the first two states of the top row are both equal to $\frac{\pi^2}{2}$. This equality can be explained by considering the L_{-1} descendant of the level 1 state

$$L_{-1}|\alpha\alpha\rangle_{++++(1,1)} = 2|\alpha\alpha\rangle_{++++(2,1)} \ . \tag{5.149}$$

By using the relation (B.67) we find that the lifts are related by

$$E^{(2)}\Big(|\alpha\alpha\rangle_{++++(2,1)}\Big) = E^{(2)}\Big(|\alpha\alpha\rangle_{++++(1,1)}\Big) \ , \tag{5.150}$$

where on the left-hand side we used the fact that

$$E^{(2)}\Big(x|\phi\rangle\Big) = E^{(2)}\Big(|\phi\rangle\Big) \ , \tag{5.151}$$

for any constant x.

L_{-1} mode on $|dd\rangle^{----}_{(3/2,1/2)}$

In the lifting matrix of the states $|dd\rangle^{----}_{(r,s)}$ shown in (5.148) we see that the lifts in the second and third entries of the first row are equal to $\frac{\pi^2}{2}$. This equality can be explained by considering the L_{-1} descendant of the level 2 state

$$L_{-1}|dd\rangle^{----}_{(3/2,1/2)} = |dd\rangle^{----}_{(5/2,1/2)} + |dd\rangle^{----}_{(3/2,3/2)} = |dd\rangle^{----}_{(5/2,1/2)} \ , \tag{5.152}$$

where the state $|dd\rangle^{----}_{(3/2,3/2)}$ vanishes due to repeated fermion modes. By applying the relation (B.67) we find that

$$E^{(2)}\Big(|dd\rangle^{----}_{(5/2,1/2)}\Big) = E^{(2)}\Big(|dd\rangle^{----}_{(3/2,1/2)}\Big) \ . \tag{5.153}$$

We note that for the relation (B.67) to be applicable here it is necessary that the initial state is annihilated by L_1

$$L_1|dd\rangle^{----}_{(3/2,1/2)} = |dd\rangle^{----}_{(1/2,1/2)} + |dd\rangle^{----}_{(3/2,-1/2)} = 0 \ , \tag{5.154}$$

due to each state vanishing.

$G^-_{-,\frac{1}{2}}$ mode on $|\alpha\alpha\rangle_{++++(n,n)}$

There are also lifts in different families that are equal; by comparing the lifting matrices (5.146) and (5.147) one sees that the lifts of the diagonal states are equal. We reproduce the relevant shallow lift matrices below: see

$$E^{(2)}\Big(|\alpha\alpha\rangle_{++++(m,n)}\Big) = \lambda^2 \begin{pmatrix} \frac{\pi^2}{2} & \frac{\pi^2}{2} & \frac{9\pi^2}{16} & \frac{19\pi^2}{32} & \frac{5045\pi^2}{8192} \\ \frac{\pi^2}{2} & \frac{19\pi^2}{32} & \frac{9\pi^2}{16} & \frac{2569\pi^2}{4096} & \frac{10775\pi^2}{16384} \\ \frac{9\pi^2}{16} & \frac{9\pi^2}{16} & \frac{2697\pi^2}{4096} & \frac{5001\pi^2}{8192} & \frac{44205\pi^2}{65536} \\ \frac{19\pi^2}{32} & \frac{2569\pi^2}{4096} & \frac{5001\pi^2}{8192} & \frac{92751\pi^2}{131072} & \frac{42555\pi^2}{65536} \\ \frac{5045\pi^2}{8192} & \frac{10775\pi^2}{16384} & \frac{44205\pi^2}{65536} & \frac{42555\pi^2}{65536} & \frac{200592615\pi^2}{268435456} \end{pmatrix} \ , \tag{5.155}$$

and

$$E^{(2)}\Big(|\alpha d\rangle^{--}_{++(n,s)}\Big) = \lambda^2 \begin{pmatrix} \frac{\pi^2}{2} & \frac{\pi^2}{2} & \frac{35\pi^2}{64} & \frac{37\pi^2}{64} & \frac{9859\pi^2}{16384} \\ \frac{\pi^2}{2} & \frac{19\pi^2}{32} & \frac{19\pi^2}{32} & \frac{1283\pi^2}{2048} & \frac{10663\pi^2}{16384} \\ \frac{33\pi^2}{64} & \frac{39\pi^2}{64} & \frac{2697\pi^2}{4096} & \frac{2697\pi^2}{4096} & \frac{358269\pi^2}{524288} \\ \frac{17\pi^2}{32} & \frac{2563\pi^2}{4096} & \frac{5525\pi^2}{8192} & \frac{92751\pi^2}{131072} & \frac{92751\pi^2}{131072} \\ \frac{8935\pi^2}{16384} & \frac{10495\pi^2}{16384} & \frac{361355\pi^2}{524288} & \frac{378645\pi^2}{524288} & \frac{200592615\pi^2}{268435456} \end{pmatrix} . \tag{5.156}$$

This matching of lifts can be explained by considering the superdescendants

$$G^{-}_{-,\frac{1}{2}}|\alpha\alpha\rangle_{++++(n,n)} = 2in|\alpha d\rangle^{--}_{++(n,n-1/2)} \ , \tag{5.157}$$

and using the relation (B.71) and (5.151) one finds that

$$E^{(2)}\Big(|\alpha d\rangle^{--}_{++(n,n-1/2)}\Big) = E^{(2)}\Big(|\alpha\alpha\rangle_{++++(n,n)}\Big) \ . \tag{5.158}$$

Once again, in order to apply the relation (B.71) it was important that the initial state is annihilated by the current mode in the bra descendant state; *i.e.* in this case that

$$G^{+}_{+,-\frac{1}{2}}|\alpha\alpha\rangle_{++++(n,n)} = 0 \ , \tag{5.159}$$

which is due to the choice of $SU(2)$ indices.

Relations between lifts of $|\alpha d\rangle$ states

Next we look at relationships between the lifts of the $|\alpha d\rangle^{--}_{++(m,s)}$ family of states, as computed in Section 5.6.3, for which we display a shallow lifting matrix of $E^{(2)}\left(|\alpha d\rangle^{--}_{++(m,s)}\right)/\lambda^2$:

$$\begin{pmatrix}
\frac{\pi^2}{2} & \frac{\pi^2}{2} & \frac{35\pi^2}{64} & \frac{37\pi^2}{64} & \frac{9859\pi^2}{16384} & \frac{10171\pi^2}{16384} & \frac{333847\pi^2}{524288} \\
\frac{\pi^2}{2} & \frac{19\pi^2}{32} & \frac{19\pi^2}{32} & \frac{1283\pi^2}{2048} & \frac{10663\pi^2}{16384} & \frac{175711\pi^2}{262144} & \frac{179969\pi^2}{262144} \\
\frac{33\pi^2}{64} & \frac{39\pi^2}{64} & \frac{2697\pi^2}{4096} & \frac{2697\pi^2}{4096} & \frac{358269\pi^2}{524288} & \frac{368643\pi^2}{524288} & \frac{48290217\pi^2}{67108864} \\
\frac{17\pi^2}{32} & \frac{2563\pi^2}{4096} & \frac{5525\pi^2}{8192} & \frac{92751\pi^2}{131072} & \frac{92751\pi^2}{131072} & \frac{48833787\pi^2}{67108864} & \frac{99898097\pi^2}{134217728} \\
\frac{8935\pi^2}{16384} & \frac{10495\pi^2}{16384} & \frac{361355\pi^2}{524288} & \frac{378645\pi^2}{524288} & \frac{200592615\pi^2}{268435456} & \frac{200592615\pi^2}{268435456} & \frac{6562949705\pi^2}{8589934592} \\
\frac{9141\pi^2}{16384} & \frac{171381\pi^2}{262144} & \frac{184155\pi^2}{262144} & \frac{24675753\pi^2}{33554432} & \frac{204097593\pi^2}{268435456} & \frac{3351953103\pi^2}{4294967296} & \frac{3351953103\pi^2}{4294967296}
\end{pmatrix} \tag{5.160}$$

This lifting matrix displays some interesting patterns that we will now explore. Firstly there is the equality of lifts on the diagonal with those on the first off diagonal on the upper-half triangle. This can be understood by considering the application of two G modes to a diagonal term (for which $s = m - \frac{1}{2}$) since

$$G^-_{-,-1/2}G^+_{+,-1/2}|\alpha d\rangle^{--}_{++(m,m-1/2)} = i\,G^-_{-,-1/2}|\alpha\alpha\rangle_{++++(m,m)} = 2im|\alpha d\rangle^{--}_{++(m,m+1/2)}\ . \tag{5.161}$$

We can then use the relation (B.71) at each step of (5.161) to obtain the simple equality

$$E^{(2)}\left(|\alpha d\rangle^{--}_{++(m,m-1/2)}\right) = E^{(2)}\left(|\alpha d\rangle^{--}_{++(m,m+1/2)}\right)\ . \tag{5.162}$$

The use of these two relations is justified due to the fact that $G^-_{-,\frac{1}{2}}|\alpha d\rangle^{--}_{++(m,m-1/2)} = 0$ and $G^+_{+,\frac{1}{2}}|\alpha\alpha\rangle_{++++(m,m)} = 0$ and that at each step in (5.161) only one state is created and hence (B.71) could be straightforwardly applied.

Secondly, there is also a single pair of equal lifts in the first column of the lifting matrix (5.160) (in black circles) which can be understood from the action of L_{-1} on the level-3/2 state in this family

$$L_{-1}|\alpha d\rangle^{--}_{++(1,1/2)} = |\alpha d\rangle^{--}_{++(2,1/2)} + |\alpha d\rangle^{--}_{++(1,3/2)}\ . \tag{5.163}$$

The L_{-1} relation between lifts (B.67) can then be applied, since the condition $L_1|\alpha d\rangle^{--}_{++(1,1/2)} = 0$ holds, yielding

$$E^{(2)}\Big(L_{-1}|\alpha d\rangle^{--}_{++(1,1/2)}\Big) = E^{(2)}\Big(|\alpha d\rangle^{--}_{++(1,1/2)}\Big) \ . \tag{5.164}$$

Due to the descendant state (5.163) being a sum of two basis states the lifting relation (5.164) cannot be immediately extrapolated to a relation between elements of the lifting matrix (5.160). Using the identity (B.74) with $|\phi_1\rangle = |\alpha d\rangle^{--}_{++(2,1/2)}$ and $|\phi_2\rangle = |\alpha d\rangle^{--}_{++(1,3/2)}$ along with the fact that $E^{(2)}(\phi_1;\phi_2) = 0$ and $\langle\phi_1|\phi_2\rangle = 0$ here, (B.71) then gives

$$E^{(2)}\Big(|\alpha d\rangle^{--}_{++(2,1/2)}\Big) = \frac{1}{2}\left[3E^{(2)}\Big(|\alpha d\rangle^{--}_{++(1,1/2)}\Big) - E^{(2)}\Big(|\alpha d\rangle^{--}_{++(1,3/2)}\Big)\right] \ . \tag{5.165}$$

Using the previously derived relation (5.162) with $m = 1$ we then obtain

$$E^{(2)}\Big(|\alpha d\rangle^{--}_{++(2,1/2)}\Big) = E^{(2)}\Big(|\alpha d\rangle^{--}_{++(1,1/2)}\Big) \ , \tag{5.166}$$

as seen from the lifting matrix (5.160).

5.8 Chapter Summary

Understanding the BPS spectrum of the D1-D5 CFT is relevant to identifying and studying the states dual to microstates of certain extremal black holes. BPS states are classified very simply at the locus of moduli space where the theory has a description in terms of a free orbifold theory, in terms of states with purely left- or right-moving excitations above the NS-NS vacuum. However, away from this special region their classification is unknown. This is because multiple short multiplets of the free theory can group together into a long multiplet of the general theory and so 'lift'. Thus, members of those free-theory short multiplets are not in fact BPS. Progress towards identifying the BPS states that can be the duals of black hole microstates can be made by looking at the lifting of various families of states of the free orbifold theory in order to understand general patterns in which states lift and by how much.

In this chapter, we studied the lifting of various families of D1-D5-P states at second order in the deformation parameter, focusing on untwisted sector states where a single copy of the $c = 6$ seed CFT is excited.

First, we computed the lift for states created by acting with a single left-moving superconformal primary on one copy. Remarkably, the resulting anomalous dimension depends only on the conformal dimension h of the primary, and not on the details of the primary itself. The functional form of the lift was compactly expressed as 2^{-2h} multiplied by the reciprocal of the Euler beta function $B(h,h)$ (see Eq. (5.65)). All such superconformal primaries, provided they are not chiral primaries, satisfy $j = m = 0$. The

calculation used a hybrid method, combining direct evaluation of twist operator correlators and the Gava-Narain method, exploiting the fact that the covering space remained genus zero for these correlators. In the large h limit, the lift exhibits a $\sqrt{h}$ growth, consistent with prior observations in the literature [79, 83].

We then extended the analysis to descendant states, focusing on two families: descendants created by the action of $G^{\alpha}_{\dot{A},-s}$ and by J^{+}_{-n} modes acting on a single superconformal primary. The lift in these cases was found by expressing it as a finite number of nested sums, whose structure depended on the descendant level and primary dimension. Explicit lifting matrices were computed up to level 7, and detailed tables were generated for various 1-parameter subfamilies. Using Ward identities on the covering space, an exact expression for the lift of $J^{+}_{-n}|\phi\rangle$ states was derived, again showing leading $\sqrt{h}$ growth in the large h limit.

Interestingly, we found that the lift of descendant states depends on the partitioning of excitation energy among descendant modes, with different scaling behaviors even at subleading orders. For example, the $O(h^{-2})$ term scales as n^3 or m^4 depending on the mode structure. These findings further strengthened the conjecture that lifts universally grow as $\sim \sqrt{h}$ at large dimensions, but also revealed that the detailed structure of excitations matters beyond the leading term.

Finally, we studied states constructed from two oscillator excitations on a single copy of the seed CFT. The lift was computed through contour integrals over the relevant mode numbers, and explicit values were obtained for many examples, again showing the $\sqrt{h}$ behavior at large h. These calculations were carried out at general N using a method that sees only two copies at a time, with the full N dependence reinstated combinatorially.

Across all the studied families—superconformal primaries, descendants, and two-mode excitations—the large-h behavior appears universal. Although no closed-form expression was available in every case, the $\sqrt{h}$ scaling was consistently observed, suggesting a deep and possibly universal feature of the lifting mechanism in the D1-D5 CFT.

Chapter 6

The Universality of Black Hole Thermodynamics

> *The supreme task of the physicist is to arrive at those universal elementary laws from which the cosmos can be built up by pure deduction.*
>
> — A. Einstein

Having explored black holes through the lens of string theory—particularly the D1D5 system—we now turn to a potential consequence of this framework: the existence of horizonless geometries even in the semiclassical regime, and their universal thermodynamic behavior.

The universal thermodynamic behavior of black holes is often attributed to the presence of a *horizon* in the black hole geometry. Bekenstein's argument for black hole entropy [2] began with the idea that the entropy of matter falling through a horizon is 'lost' to the outside world. Although using quantum fields in curved spacetime, one can formulate the field of black hole thermodynamics. Yet this traditional picture, where the black hole possesses a smooth horizon, leads to a profound conflict: the black hole information paradox, as discussed in Sections 3.4 and 4.4.

The fuzzball program resolves this paradox by reimagining black holes as horizonless geometries—microstate solutions that cap off smoothly before a horizon can form. This gives rise to a new puzzle:

> *How do fuzzballs—despite lacking a traditional horizon—reproduce the thermodynamic behavior that, in earlier derivations, crucially depended on the presence of one?*

This question lies at the heart of recent developments in string theory and quantum gravity, and understanding horizonless objects like fuzzballs has significant implications for fields such as astronomy, astrophysics, and cosmology. Within string theory, there

is compelling evidence that a typical fuzzball's surface lies only a Planck-scale distance ($l_P \sim 10^{-35}\,\mathrm{m}$) outside what would have been the horizon of a classical black hole with the same mass. This means one can consider objects that are extremely compact and ask:

> *Can we then assert that any semiclassical horizonless extremely compact object with a radius approaching that of a classical black hole must exhibit the thermodynamic behavior predicted by Hawking for a black hole?*

The answer is yes, and understanding why this is true constitutes the central focus of this chapter.

6.1 Extremely Compact Objects

In this section, we outline the structure of an Extremely Compact Object (ECO), assuming spherical symmetry to leading order. While the ECO's interior may contain microscopic, non-symmetric features, we approximate its external gravitational field as static and spherically symmetric. For simplicity and to highlight universal behavior, we restrict our attention to the simplest class of ECOs—those characterized solely by a mass M measured at infinity, with zero angular momentum and charge. We will assume that the mass M of the ECO satisfies[1]

$$\frac{M}{m_p} \gg 1\,, \tag{6.2}$$

where m_p is Planck mass.

6.1.1 Geometric Setup and the First ECO Condition

An ECO is characterized by a radius slightly larger than the Schwarzschild radius corresponding to mass M. In this regime, the surface experiences a strong inward gravitational pull, making equilibrium configurations impossible for simple matter distributions. The Buchdahl theorem [84] in $3+1$ dimensions shows that a static, spherically symmetric perfect fluid with radius R (with monotonically decreasing pressure) cannot support itself against collapse if $R < \frac{9}{4}GM$.

In string theory, however, fuzzballs evade this conclusion. As shown in [85], the compact and noncompact dimensions are non-trivially tensored, altering the gravitational dynamics. More recently, constructions of solitonic stars have been developed in string

[1] We set the constants as

$$G_N^{(d)} = l_p^{d-1}\,, \quad m_p = \frac{1}{l_p}\,. \tag{6.1}$$

theory [86–90], allowing horizonless configurations that can be made arbitrarily close to the Schwarzschild radius.

Our ECO will be described by a radius $r = R_{\rm ECO}$. We will make no assumptions about the structure in the region $r < R_{\rm ECO}$; this can be a region with significant quantum gravitational effects, non-trivial extra dimensions, solitonic bubbles, etc. But in the region $r > R_{\rm ECO}$ we require usual semiclassical dynamics to hold to sufficient accuracy for all our purposes and here we take the metric ansatz in $D = d + 1$ spacetime dimensions as[2]

$$ds^2 = -e^{2\alpha(r)}dt^2 + e^{2\beta(r)}dr^2 + r^2 d\Omega_{d-1}^2 \,. \tag{6.3}$$

The vacuum solution known as the Tangherlini solution [91] of the Einstein field equations, Section 2.1.2, in $D = d + 1$ dimensions is

$$ds_D^2 = -\left(1 - \frac{\mu GM}{r^{d-2}}\right) dt^2 + \left(1 - \frac{\mu GM}{r^{d-2}}\right)^{-1} dr^2 + r^2 d\Omega_{d-1}^2 \,, \tag{6.4}$$

where we define the horizon radius r_0 by

$$r_0^{d-2} = \mu GM \,, \quad \mu = \frac{16\pi}{(d-1)\Omega_{d-1}} \,. \tag{6.5}$$

It is easy to see that this reduces to the familiar Schwarzschild (2.4) for $D = 4$.

The requirement that the ECO be extremely compact says that $R_{\rm ECO}$ should be only a little larger than the horizon radius for the same mass M. For the black hole metric (6.4), we can describe the near-horizon region using Rindler coordinates. We define

$$\eta = \frac{d-2}{r_0} t \,, \quad \rho = 2\sqrt{\frac{r_0(r - r_0)}{d-2}} \tag{6.6}$$

The near-horizon geometry then becomes Rindler space$(1,1) \times S^{d-1}$ with the Rindler metric as in (2.15). We wish to consider ECOs with $R_{\rm ECO}$ slightly larger than r_0. To keep track of physical variables, it is convenient to recast the compactness requirement on $R_{\rm ECO}$ through the proper radius $s_{\rm ECO}$.[3] From (6.6) we see that

$$s_{\rm ECO} = 2\sqrt{\frac{r_0(R_{\rm ECO} - r_0)}{d-2}} \tag{6.7}$$

An ECO is characterized by $s_{\rm ECO} \ll r_0$. For fuzzballs, $s_{\rm ECO} \sim l_p$, but our analysis extends to a wider range, determined later. Note that $s_{\rm ECO}$ uses the black hole metric (6.4)

[2] In this chapter, we consider $d \geq 3$. In $2 + 1$ dimensional gravity, mass M does not yield an asymptotically flat spacetime, a scenario excluded from our present discussion and the $1 + 1$ dimensional dilaton gravity case warrants separate treatment which we refer the reader to section 7 of [17].

[3] Adopting a notational convention consistent with the ECO literature, we denote the ECO's proper radius as $s_{\rm ECO}$. Similarly, from this point onward we will use all proper distance as s, switching from ρ; this is to reserve ρ for energy densities, explicitly alerting the reader whenever potential ambiguity arises.

merely to quantify the difference between $R_{\rm ECO}$ and r_0, as the actual metric near $R_{\rm ECO}$ can deviate significantly from the vacuum solution. This leads us to list the first ECO condition:[4]

ECO 1: Semiclassical physics holds outside the radius $r = R_{\rm ECO}$, and this radius $R_{\rm ECO}$ is close to the horizon radius r_0, with

$$s_{\rm ECO} \ll s_c \,, \tag{6.8}$$

where s_c describes the 'compactness' of an ECO. We will find for the universality of black hole thermodynamics to hold, this scale must be

$$s_c \sim \left(\frac{M}{m_p}\right)^{\frac{2}{(d-2)(d+1)}} l_p \sim \left(\frac{r_0}{l_p}\right)^{\frac{2}{d+1}} l_p \,. \tag{6.9}$$

6.1.2 Gravitational Redshift and the Second ECO Condition

The essential property of a black hole is the infinite redshift that we get at the black hole horizon. Any extremely compact object that replaces a black hole should be characterized by a very large (though not infinite) redshift at its surface $R_{\rm ECO}$. Let us note what the scale of this redshift should be. The redshift parameter $q(r)$ is defined as

$$q(r) \equiv \frac{1}{\sqrt{-g_{tt}(r)}} \,. \tag{6.10}$$

In the Rindler region, for the black hole metric (6.4), we have

$$q(r) \approx \frac{2r_0}{(d-2)s(r)} \,. \tag{6.11}$$

Using the above equation, we can calculate the redshift at the ECO surface $r = R_{\rm ECO}$. Since the ECO is required to have $s_{\rm ECO} \ll s_c$, we place the following requirement:

ECO 2: The redshift at $r = R_{\rm ECO}$ satisfies

$$q(R_{\rm ECO}) \gg \left(\frac{r_0}{l_p}\right)^{\frac{d-1}{d+1}} \sim \left(\frac{M}{m_p}\right)^{\frac{(d-1)}{(d-2)(d+1)}} \,. \tag{6.12}$$

6.1.3 Minimal Exterior Energy and the Third ECO Condition

It may appear reasonable to require that the spacetime in the region $r > R_{\rm ECO}$ has zero stress-energy and thus a metric of the black hole form (6.4). But the ECO has in general a nonzero temperature $T_{\rm ECO}$, and radiation corresponding to this temperature will fill up the region near the ECO. We have in mind temperatures of order the Hawking temperature

[4] A quick implication of this condition follows that we present in A.2.

(3.35), and it is true that the radiation energy density at this temperature is very small at $r \gg R_{\rm ECO}$. But the energy density of this radiation can be very large close to $R_{\rm ECO}$ due to the large redshift in this region, and contribute a total mass that is $O(M)$. Thus we have to consider the more general ansatz (6.3) for the metric in the region just outside $r = R_{\rm ECO}$.

To clarify this point, let us estimate the distance s from the horizon radius r_0 upto which this radiation density is appreciable. Suppose the temperature of the ECO as seen at infinity is $T_{\rm ECO}$. The radiated quanta suffer a redshift as they move out of the gravitational potential of the ECO. Thus the effective temperature of the radiation at a radius r, measured in a local orthonormal frame with time direction along t, is

$$T_{\rm ECO}(r) = q(r) T_{\rm ECO}\,, \tag{6.13}$$

where $q(r)$ is the redshift parameter (6.10). Using (6.11) for the value of $q(r)$ in the Rindler region for the black hole metric (6.4), we find that the temperature at a distance s from the horizon radius r_0 is

$$T_{\rm ECO}(s) \approx \frac{2r_0}{(d-2)s} T_{\rm ECO}\,. \tag{6.14}$$

Assuming that $T_{\rm ECO}$ is of the same order as the Hawking temperature $T_{\rm H} \sim \frac{1}{r_0}$, we have

$$T_{\rm ECO}(s) \sim \frac{1}{s}\,. \tag{6.15}$$

Thus we see that at small s, the local temperature is very high, and in fact this temperature reaches planck scale at planck distance $s \sim l_p$ from the horizon radius. The energy density of a massless quantum field at temperature T is

$$\rho = a T^{d+1}\,, \tag{6.16}$$

where a is a constant of order unity, depending on the dimension d and the spin of the quantum field.[5] This raises a pressing issue:

> *If there is nonzero stress energy outside R_{ECO}, then how should we capture the compactness of the ECO through the compactness condition (6.8) on R_{ECO}?*

Note that the energy density of thermal radiation will typically fall off as a power law as we go out from the ECO. Thus we cannot ask that it be exactly zero at some given distance from the ECO surface, but we can ask that its effects not be relevant if we are sufficiently far from the ECO surface.[6]

[5] For a scalar field in 3+1 dimensions, $a = \frac{\pi^2}{30}$.

[6] There is a singular solution that formally satisfies ECO 1 and ECO 2, but which we exclude from our

We do this by requiring that outside the compactness scale s_c, the geometry is close to the metric of the black hole:

ECO 3: At distances $s > s_c$ (6.9) from the black hole horizon radius r_0, the geometry is well approximated by the black hole metric (6.4).

In Section 6.3.4 we will check that it is consistent to impose condition ECO 3; i.e., we will verify that the stress-tensor of the thermal radiation near the ECO surface does not significantly distort the black hole metric at distances $s \gtrsim s_c$ from the horizon radius r_0.

To summarize, the ECO conditions are

ECO 1: Semiclassical physics holds outside the radius $r = R_{\rm ECO}$, and this radius $R_{\rm ECO}$ is close to the horizon radius r_0, with

$$s_{\rm ECO} \ll s_c\,, \quad s_c \sim \left(\frac{M}{m_p}\right)^{\frac{2}{(d-2)(d+1)}} l_p \sim \left(\frac{r_0}{l_p}\right)^{\frac{2}{d+1}} l_p\,. \tag{6.17}$$

ECO 1.1: In the region $r > R_{\rm ECO}$ we must have everywhere

$$1 - \frac{\mu G M(r)}{r^{d-2}} > 0\,. \tag{6.18}$$

ECO 2: The redshift at $r = R_{\rm ECO}$ satisfies

$$q(R_{\rm ECO}) \gg \left(\frac{r_0}{l_p}\right)^{\frac{d-1}{d+1}} \sim \left(\frac{M}{m_p}\right)^{\frac{(d-1)}{(d-2)(d+1)}}\,. \tag{6.19}$$

ECO 3: At distances $s > s_c$ (6.9) from the black hole horizon radius r_0, the geometry is well approximated by the black hole metric (6.4).

6.2 The vacuum stress-energy near an ECO

Even at zero temperature, quantum fields in the ECO's background metric induce a nonvanishing vacuum stress-energy outside the surface. As we'll see, for temperatures near the Hawking temperature, this vacuum energy is comparable to the thermal stress-energy and thus plays a crucial role in our analysis.

We will begin by recalling the computation of vacuum energy for the Schwarzschild hole. We will then note that an ECO has, to leading order, the *same* vacuum energy as

definition of an ECO. As discussed in Section 6.3, this is the so-called 'truncated isothermal star,' which consists of an isothermal photon gas in the region $0 < r < R$, with the density truncated at $r = R$. The energy density and the redshift $q(r)$ diverges as $r \to 0$. One could define a surface just outside $r = 0$ with large redshift and small radius, apparently satisfying ECO 1 and ECO 2. However, such an object is not an ECO for our purposes, since the majority of the mass lies *outside* the high-redshift surface. To exclude this case, we impose ECO 3.

a black hole. Taking into account the thermal radiation just outside the ECO, we will obtain the total stress energy in this near-surface region.

6.2.1 The vacuum stress-tensor near a black hole horizon

The vacuum energy in a spacetime depends in general on the choice of the quantum state for the fields. In a black hole spacetime, as seen in Section 3.2.3, some commonly considered states are the Unruh $|0\rangle_U$ vacuum, the Hartle-Hawking vacuum $|0\rangle_{HH}$ and the Boulware vacuum $|0\rangle_B$. In 3+1 dimensions the vacuum energy for these states was computed in [92], using methods developed in [93–98]. This computation is in general quite complicated, but there is a simple way to get the answer for the quantity we need: the vacuum stress energy for the Boulware vacuum to leading order close to the horizon.

In the Hartle-Hawking vacuum, the black hole is in equilibrium with its radiation. The geometry is smooth at the horizon, and there is no flux into or out of the horizon. Thus to leading order the stress-energy tensor is zero around the horizon.[7] We can understand this vanishing of the stress energy by going to Rindler coordinates (6.6) near the horizon. Then the Hartle-Hawking vacuum is like the Minkowski vacuum, which has a vanishing stress tensor. Now consider the Boulware vacuum $|0\rangle_B$. This vacuum state is obtained by requiring

$$\hat{a}_{\{l\},k}\,|0\rangle_B = 0\,, \tag{6.20}$$

for the operator modes of the massless scalar field. The field in terms of field modes that satisfy $\Box\hat{\phi} = 0$ is given by

$$\hat{\phi} = \sum_{\{l\},k}\left(\,\hat{a}_{\{l\},k}\,f_{\{l\},k}(r)Y_{\{l\}}(\{\Phi\})e^{-i\omega_{\{l\},k}\,t} + \hat{a}^{\dagger}_{\{l\},k}\,f^{*}_{\{l\},k}(r)Y^{*}_{\{l\}}(\{\Phi\})e^{i\omega_{\{l\},k}\,t}\,\right). \tag{6.21}$$

To understand the nature of this state, consider the near horizon Rindler region. In this region the modes $f_{\{l\},k}(r)$ are Rindler modes and the Boulware vacuum is the Rindler vacuum. In Rindler coordinates, the Minkowski vacuum appears to be populated with Rindler excitations. Since the Minkowski vacuum has vanishing stress tensor, the stress tensor of the Rindler vacuum is given by the *negative* of the stress tensor of thermal radiation at the Hawking temperature.

The Hawking temperature of the Tangherlini black hole (6.4) at infinity in $d+1$ dimensions is

$$T_{\rm H} = \frac{d-2}{4\pi r_0}\,, \tag{6.22}$$

[7] Here by 'leading order' we mean that we are ignoring contributions of order $\langle T^{\mu}{}_{\nu}\rangle \sim 1/r_0^{d+1}$ which arise from the energy density of quanta with wavelength $\lambda \sim r_0$, and terms arising from the anomaly; these terms are regular at the horizon.

and local temperature at s in terms of the coordinate r is

$$T_{\rm H}(r) = q(r)\, T_{\rm H} = \frac{1}{4\pi}\sqrt{\frac{d-2}{r_0(r-r_0)}}\,, \tag{6.23}$$

where the final expression is found using (6.11) and (6.22) for the Rindler region. The stress tensor of the Boulware vacuum is then

$$T^{\mu}{}_{\nu} = \text{diag}\{-\rho(r), p(r), \cdots, p(r)\}\,, \tag{6.24}$$

with

$$\rho(r) = -aT_{\rm H}(r)^{d+1}\,, \quad p(r) = \frac{\rho(r)}{d}\,. \tag{6.25}$$

6.2.2 The stress tensor near an ECO

We now argue that for an ECO with $T_{\rm ECO} = 0$, the stress tensor just outside $R_{\rm ECO}$ closely matches that of the Boulware vacuum (6.24) and (6.25). The ECO's compactness ensures that its exterior modes $f_{l,k}(r)$ oscillate rapidly for $r > R_{\rm ECO}$, enabling the construction of local wavepackets. These yield a good approximation of the local stress tensor, making the interior mode structure irrelevant to the exterior stress-energy.

Here we show that a typical scalar field outside an ECO has wavemodes with many many oscillations mimicking the black hole scenario where a scalar field has infinite oscillations.

Consider the wavemodes $f_{\{l\},k}(r)$ of a scalar field in the black hole metric in $d+1$ dimensions which have the following form

$$f_{\{l\},k}(r) = \frac{\chi_{\{l\},k(r)}}{r^{\frac{d-1}{2}}}\,. \tag{6.26}$$

The functions $\chi_{\{l\},k}(r)$ satisfy the equation

$$-\frac{d^2}{dr^{*2}}\,\chi_{\{l\},k}(r) + V_{eff}(r)\chi_{\{l\},k}(r) = \omega^2\chi_{\{l\},k}(r) \tag{6.27}$$

where r^* is the Tortoise coordinate for $d+1$ dimensions from Section 2.2.1, $\omega = |k|$ is the energy of the wave and $L^2 = l(l+d-2)$ with $l = 0, 1, 2, \ldots$ is the value of the quadratic Casimir describing angular momentum. The effective potential is found to be

$$V_{eff}(r) \equiv \left(1 - \frac{r_0^{d-2}}{r^{d-2}}\right)\left[\frac{(d-1)^2}{4}\frac{r_0^{d-2}}{r^d} + \frac{L^2 + \frac{1}{4}(d-1)(d-3)}{r^2}\right]\,. \tag{6.28}$$

In the near horizon region, $V_{eff}(r) \to 0$, and we have

$$-\frac{d^2}{dr^{*2}}\,\chi_{\{l\},k}(r) = \omega^2 \chi_{\{l\},k}(r)\,, \tag{6.29}$$

which has an exponential solution $e^{\pm i\omega r^*}$. Suppose we look at the region $r_0 + \epsilon < r \lesssim 2r_0$, for $\epsilon \ll r_0$ or the corresponding range for r^*, $\frac{r_0}{d-2}\ln\left(\frac{\epsilon}{r_0}\right) < r^* < 0$, then the phase of χ is seen to oscillate a number of times n given by

$$n \approx \frac{\omega}{2\pi}\frac{r_0}{d-2}\ln\left(\frac{r_0}{\epsilon}\right)\,. \tag{6.30}$$

Note that $\omega r_0 \sim 1$, since the energy of the typical quantum emitted is of order the black hole temperature $\sim 1/r_0$. For ϵ/r_0 small, we find that the number of oscillations near the horizon is $n \gg 1$. As we approach the horizon, we have $\epsilon \to 0$ and the number of oscillations becomes infinite. We depict these oscillations in Figure 6.1(a).

Now consider the computation of the stress tensor for an ECO. We should first expand the field $\hat{\phi}$ in terms of field modes that satisfy $\Box\hat{\phi} = 0$ in the metric produced by the ECO

$$\hat{\phi} = \sum_{\{l\},k}\left(\,\hat{b}_{\{l\},k}\,g_{\{l\},k}(r)Y_{\{l\}}(\{\Phi\})e^{-i\omega_{\{l\},k}\,t} + \hat{b}^\dagger_{\{l\},k}\,g^*_{\{l\},k}(r)Y^*_{\{l\}}(\{\Phi\})e^{i\omega_{\{l\},k}\,t}\,\right). \tag{6.31}$$

Consider the situation where the ECO is at temperature $T_{\rm ECO} = 0$. Then the quantum field $\hat{\phi}$ will be in its lowest energy state $|\Psi_{{\rm ECO},T_{\rm ECO}=0}\rangle$ in the background geometry created by the ECO. This state is described by

$$\hat{b}_{\{l\},k}\,|\Psi_{{\rm ECO},T_{\rm ECO}=0}\rangle = 0\,. \tag{6.32}$$

A priori, the modes $g_{\{l\},k}(r)$ will depend on the metric in the outside region $r > R_{\rm ECO}$ as well as the metric in the inside region $r < R_{\rm ECO}$; in fact they are required to satisfy a smoothness condition at $r = 0$ which is in the region $r < R_{\rm ECO}$. But due to the compactness of the ECO, the modes $g_{\{l\},k}(r)$ will have a large number of oscillations $n_{\rm ECO}$ in the region $R_{\rm ECO} < r < 2r_0$ similar to a black hole. By condition ECO 1, we have $s_{ECO} \ll s_c$, where s_c is the compactness length scale s_c defined in (6.9). From (6.30) we find

$$n_{\rm ECO} \gg \frac{\omega}{2\pi}\frac{2r_0}{(d-2)}\ln\left(\frac{2}{(d-2)^{\frac{1}{2}}}\frac{r_0}{s_c}\right) \sim \omega r_0 \ln\left(\frac{M}{m_p}\right) \sim \ln\left(\frac{M}{m_p}\right)\,, \tag{6.33}$$

where in the last step we have again set $\omega r_0 \sim 1$ since we have in mind a temperature for the ECO which is of order the black hole temperature. This large number of oscillations is depicted in Figure 6.1(b). Due to this large number of oscillations of $g_{\{l\},k}(r)$ in the region just outside $R_{\rm ECO}$, any computation using these modes can be captured equally well by local wavepackets built from these modes. Thus we can compute the quantity

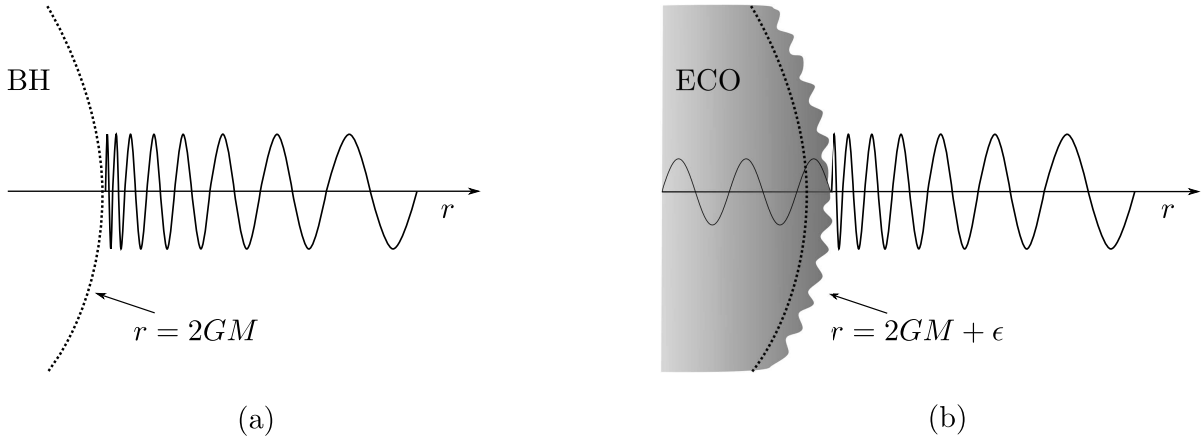

(a) (b)

Figure 6.1: (a) In the black hole geometry, a wavemode oscillates an infinite number of times as it approaches the horizon. (b) In the ECO geometry, the wavemode oscillates a large number of times $n \gg 1$ before entering the ECO surface at $R_{\rm ECO}$.

$\langle \Psi_{{\rm ECO},T_{\rm ECO}=0}| \hat{\phi}(x)\, \hat{\phi}(y) \,|\Psi_{{\rm ECO},T_{\rm ECO}=0}\rangle$, to a good approximation, by using the form of the modes $g_{\{l\},k}(r)$ in the region $r > R_{\rm ECO}$. If we assume that this region is just given by the Schwarzschild geometry (6.4) with mass M, then the wavepackets made from modes $g_{\{l\},k}(r)$ in the region $r > R_{\rm ECO}$ will be approximately the same as wavepackets made from modes $f_{\{l\},k}(r)$ in the black hole geometry. In this approximation, we will get the same value for the stress tensor in the ECO as we had in the black hole. Thus, in the region $r > R_{\rm ECO}$, we will have

$$T^{\mu}{}_{\nu} = {\rm diag}\{-\rho(r), p(r), \cdots, p(r)\}\,, \tag{6.34}$$

with

$$\rho(r) = -a\, T_{\rm H}(r)^{d+1}\,, \quad p(r) = \frac{\rho(r)}{d}\,. \tag{6.35}$$

6.2.3 The ECO at a general temperature T

As shown above, an ECO at $T_{\rm ECO} = 0$ exhibits a negative energy density near its surface, mirroring the Boulware vacuum. This relied on approximating the exterior geometry as Schwarzschild. We now extend this approximation to ECOs with $T_{\rm ECO} \neq 0$, postponing discussion of deviations from Schwarzschild at $r > R_{\rm ECO}$ to later.

At a radius r, the redshift for an ECO at $T_{\rm ECO} \neq 0$ results in a local temperature

$$T_{\rm ECO}(r) = q(r) T_{\rm ECO}\,, \tag{6.36}$$

where $q(r)$ is given by (6.11). This radiation generates a stress tensor of the form (6.34)

with

$$\rho(r) = a\, T_{\rm ECO}(r)^{d+1}\,, \quad p(r) = \frac{\rho(r)}{d}\,. \tag{6.37}$$

Taking into account the vacuum stress-energy (6.36) and (6.37), we find that, with the above mentioned approximations, the total stress tensor in the region just outside the ECO is of the form (6.36) with

$$\rho(r) = a\, \left(T_{\rm ECO}^{d+1} - T_{\rm H}^{d+1}\right) q(r)^{d+1}\,, \quad p(r) = \frac{\rho(r)}{d}\,. \tag{6.38}$$

6.3 Using the Tolman-Oppenheimer-Volkoff equation

In this section, we analyze ECOs with $T_{\rm ECO} \neq T_{\rm H}$ using the Tolman-Oppenheimer-Volkoff (TOV) equation, which self-consistently couples the metric to the stress tensor. We motivate the use of a perfect fluid stress tensor show how the energy density links to redshift in this framework. The analysis splits into cases with $\rho < 0$ and $\rho > 0$, paralleling the $T_{\rm ECO} < T_{\rm H}$ and $T_{\rm ECO} > T_{\rm H}$ regimes discussed in Section A.3. We find that the only non-singular solution in the semiclassical region $r > R_{\rm ECO}$ is $\rho = p = 0$, corresponding to $T_{\rm ECO} = T_{\rm H}$ by (6.38).

6.3.1 Assumptions for the TOV equation

We adopt the spherically symmetric ansatz (6.3) for the region $r > R_{\rm ECO}$. In the near-surface region, the high redshift (required by ECO 2) implies a very high local temperature. Consequently, typical quantum fields with $m \ll m_p$ behave effectively as massless. We make the following modeling assumptions:

1. **Perfect Fluid Form:**
   The stress tensor of the thermal gas is taken to be that of a perfect fluid aligned with the t, r, and angular directions:

$$T^{\mu}{}_{\nu}{}^{\rm radiation} = \mathrm{diag}\{-\rho^{\rm r}(r), p^{\rm r}(r), \ldots, p^{\rm r}(r)\}\,. \tag{6.39}$$

2. **Equation of State for Radiation:**
   Due to the high temperature, the thermal gas satisfies the massless field equation of state:

$$p^{\rm r}(r) = \frac{\rho^{\rm r}(r)}{d}\,. \tag{6.40}$$

3. **Vacuum Stress Tensor Form:**
   In analogy with the black hole case, the vacuum stress tensor near the ECO surface

is also assumed to have the perfect fluid form:

$$T^{\mu}{}_{\nu}{}^{\text{vacuum}} = \text{diag}\{-\rho^{\text{v}}(r), p^{\text{v}}(r), \ldots, p^{\text{v}}(r)\}\,. \tag{6.41}$$

4. **Equation of State for Vacuum:**
   Following the behavior of the Rindler vacuum near a black hole horizon, we assume:

$$p^{\text{v}}(r) = \frac{\rho^{\text{v}}(r)}{d}\,. \tag{6.42}$$

These assumptions are justified by the fact that in the high-redshift near-surface region, both thermal and vacuum contributions become comparable (see Section 6.2), and both take the same functional form as in the near-horizon limit of black holes. Since the metric outside the ECO is not the metric of a black hole, a priori we have to solve the analog of equation (6.27) for the field modes in the ECO geometry, and then compute the vacuum stress energy from those modes. This is a difficult computation, and so we assume (6.41) as a heuristic extrapolation motivated by the properties of the vacuum stress tensor in the black hole geometry. It is important to note that we are not specifying the *value* of $\rho^{\text{v}}(r)$ for the vacuum stress tensor; we are just assuming that the vacuum energy stress tensor is **diagonal, isotropic** and **traceless**.[8] The form (6.41) is consistent to leading order with the expected properties of the vacuum stress tensor. Assuming (6.41), (6.42) for the vacuum stress energy, the total stress energy (radiation+vacuum) in the near-surface region also has the form

$$T^{\mu}{}_{\nu} = \text{diag}\{-\rho(r), p(r), p(r), \ldots, p(r)\}\,, \tag{6.43}$$

with the pressure

$$p = \frac{\rho(r)}{d}. \tag{6.44}$$

Our goal now is to solve the Tolman-Oppenheimer-Volkoff (TOV) equations with such a stress tensor in the region just outside $r = R_{\text{ECO}}$.

6.3.2 Approximating the TOV equation

From the estimates of Appendix A.3, we note that we are interested in the situation where the stress tensor in the region $r > R_{\text{ECO}}$ falls off rapidly with increasing $r - r_0$. Since

[8] In the Section 7 of [17], we have worked with the 1+1 dimensional system, where we know the vacuum energy explicitly in the fully backreacted geometry of the ECO.

$R_{\rm ECO}$ is very close to the value r_0, we will be able to use the approximation

$$r \approx r_0 \,. \tag{6.45}$$

in many of the terms in the TOV equation. This approximation will allow us to simplify the equation. We will find that this approximate equation has no solution which yields an ECO. We will then re-examine the approximations we made in simplifying the TOV equation, and find that these approximations become invalid only when we are outside the compactness scale s_c defined in (6.9). Thus we will conclude that if an ECO satisfies condition ECO1, then there must be vanishing (at leading order) of the stress tensor (6.43) at $r > R_{\rm ECO}$. As we saw in Section 6.3.1, the vanishing of this stress tensor happens when $T_{\rm ECO} = T_{\rm H}$ and the geometry in the region just outside $r > R_{\rm ECO}$ becomes the geometry of the traditional black hole with a vacuum around the horizon.

Before proceeding to obtain the approximate form of the TOV equation valid near $r \approx r_0$, we note what is known about the exact TOV equation, for the case where the stress tensor is given by (6.43), (6.44). The Einstein equations can be reduced to a single nonlinear second order equation called the Emden-Chandrasekhar equation [99]. This equation has an analytically known solution which is singular at the origin. For the $3+1$ dimensional case, the solution has the form.

$$\rho = \frac{Q_1}{r^2}, \quad e^{2\alpha} = Q_2 r, \quad e^{2\beta} = Q_3 \,, \tag{6.46}$$

where Q_i are positive constants. The solution regular at the origin cannot be solved for analytically, but its asymptotic form has been developed as a power series. The singular solution is discarded when we consider the context of stellar structure, where the 'truncated isothermal sphere' can be used to model the core of a star. In our problem, we have the opposite situation, where the region $r < R_{\rm ECO}$ is a quantum gravitational region *not* described by isothermal semiclassical physics, while the region $r > R_{\rm ECO}$ can take the form of an isothermal region, truncated at some radius r_{max}. Thus the singular solution (6.46) is also an allowed solution in the region $R_{\rm ECO} < r < r_{max}$.

This singular solution shows the relevance of our condition ECO3, which says that there should not be too much matter far from the ECO surface. Take the singular isothermal solution (6.46), truncated at some large radius R. Choose a small radius $r = \epsilon$, and replace the singular region in its interior by some unspecified quantum dynamics. Now if we let $R_{\rm ECO} = \epsilon$, we see that, formally, such a solution will satisfy the conditions ECO1, ECO2. Condition ECO1 says that $r_{\rm ECO}$ be not much larger than r_0, and here we have $R_{\rm ECO} = \epsilon \ll r_0$. Condition ECO2 requires a high redshift at $r = R_{\rm ECO}$, and from(6.46) we see that $q(\epsilon) = e^{-\beta(\epsilon)}$ is indeed large. But note that almost all the mass of this object is outside $r = R_{\rm ECO}$. To exclude such a case from our analysis we had imposed the condition

ECO3.

While we cannot solve the isothermal TOV equation exactly, we will find that we have a high energy density in the region very close to $r = r_0$. In this situation we can get an approximation to the TOV equation that we can solve in closed form, and this solution will yield a more rigorous derivation of the heuristic estimates of section A.3.

Preliminary steps

For the metric ansatz (6.3), the conservation law $T^{r\mu}{}_{;\mu} = 0$ gives

$$\alpha' = -\frac{p'}{p+\rho}\,, \tag{6.47}$$

where a prime denotes $\frac{d}{dr}$. Setting $p = \frac{\rho}{d}$ from (6.44) gives us

$$\alpha' = -\frac{1}{(d+1)}\frac{\rho'}{\rho}\,. \tag{6.48}$$

The solution to this equation is

$$e^{2\alpha} = \frac{C_2}{|\rho|^{\frac{2}{d+1}}}\,, \tag{6.49}$$

where $C_2 > 0$ is a constant.

The Einstein equation $G_{tt} = 8\pi G T_{tt}$ gives the g_{rr} coefficient $e^{2\beta(r)}$ through (A.9),(A.10). From (A.10) we find

$$M'(r) = \Omega_{d-1} r^{d-1} \rho(r)\,. \tag{6.50}$$

With the approximation (6.45), this becomes

$$M'(r) \approx \Omega_{d-1} r_0^{d-1} \rho(r)\,. \tag{6.51}$$

Approximating the TOV equation

The TOV equation in $d+1$ dimensions reads

$$r^{d-1} p'(r) = -\frac{(d-2)\mu}{2} G M(r) \rho(r) \left(1 + \frac{p(r)}{\rho(r)}\right) \left(1 + \frac{16\pi p(r)\, r^d}{\mu(d-2)(d-1)M(r)}\right) \left(1 - \frac{\mu G M(r)}{r^{d-2}}\right)^{-1}\,. \tag{6.52}$$

We simplify this equation using the approximation (6.45):

(a) Using our assumed equation of state $p = \frac{1}{d}\rho$ we get

$$-r^{d-1}p'(r) = -\frac{1}{d}r^{d-1}\rho'(r) \approx -\frac{1}{d}r_0^{d-1}\rho'(r)\,. \tag{6.53}$$

(b) We have

$$1 + \frac{p(r)}{\rho(r)} = \frac{d+1}{d}\,. \tag{6.54}$$

(c) We have

$$1 + \frac{16\pi p(r)\, r^d}{\mu(d-2)(d-1)M(r)} = 1 + \frac{16\pi\rho(r)\, r^d}{\mu d(d-2)(d-1)M(r)} \approx 1 + \frac{16\pi\rho(r)\, r_0^d}{\mu d(d-2)(d-1)M(r)}\,. \tag{6.55}$$

We also note that if we were to distribute a mass M uniformly over a radius r_0, we would get a density

$$\rho_{\text{uniform}} \sim \frac{M}{r_0^d}\,. \tag{6.56}$$

By contrast, in the example of section A.3.2, we had taken $s_{\text{ECO}} \sim l_p$, and found that the energy of radiation in a planck width shell was also order $\sim M$. So, in that example the energy density $\rho(r)$ near the ECO would be higher than ρ_{uniform} by a factor $r_0/l_p \gg 1$. More generally, we assume that the energy density near the surface of the ECO is much higher than ρ_{uniform}, which implies that

$$p \sim \rho \gg \frac{M}{r_0^d}\,. \tag{6.57}$$

Thus we make the approximation

$$1 + \frac{16\pi\rho(r)\, r_0^d}{\mu d(d-2)(d-1)M(r)} \approx \frac{16\pi\rho(r)\, r_0^d}{\mu d(d-2)(d-1)M(r)}\,. \tag{6.58}$$

(d) We have

$$\left(1 - \frac{\mu G M(r)}{r^{d-2}}\right)^{-1} \approx \left(1 - \frac{\mu G M(r)}{r_0^{d-2}}\right)^{-1}\,. \tag{6.59}$$

With these approximations, and using (6.51) to express ρ, the TOV equation (6.52)

reduces to

$$\left(1-\frac{\mu G M(r)}{r_0^{d-2}}\right)M''(r) = -\frac{\mu G}{2r_0^{d-2}}\frac{(d+1)}{d}(M'(r))^2\,, \tag{6.60}$$

In what follows we will call this the approximate TOV equation.

Solving the approximate TOV equation

Let us write

$$u(r) = 1-\frac{\mu G M(r)}{r_0^{d-2}}\,. \tag{6.61}$$

Then (6.60) becomes

$$u(r)u''(r) = \frac{(d+1)}{2d}\left(u'(r)\right)^2\,. \tag{6.62}$$

The solution to this equation is

$$u'(r) = C_3\, u(r)^{\frac{d+1}{2d}}\,, \tag{6.63}$$

and a final integration gives

$$u(r) = \left(\frac{(d-1)}{2d}C_3(r-r_1)\right)^{\frac{2d}{d-1}}\,. \tag{6.64}$$

Thus we have

$$1-\frac{\mu G M(r)}{r_0^{d-2}} = \left(\frac{(d-1)}{2d}C_3(r-r_1)\right)^{\frac{2d}{d-1}}\,. \tag{6.65}$$

Range of validity of the approximation

We have obtained the approximate TOV equation (6.60) for the near-surface region of the ECO. This approximation will be good for a range

$$R_{\rm ECO} < r \lesssim r_{max}\,. \tag{6.66}$$

We will now obtain an estimate for r_{max}.

1. Recall that in eq. (6.57) we had set

$$\frac{p(r)r_0^d}{M(r)} \gg 1\,. \tag{6.67}$$

This inequality is expected to hold close to the ECO surface, since $p(r) \sim \rho(r) \sim T_{\rm ECO}^{d+1}(r) \sim T_{\rm H}^{d+1}(r)$, and $T_{\rm H}(r)$ is large near the ECO surface due to the large redshift $q(r)$.

To get a rough estimate of scales, we use the expression (6.11) for $q(r)$ for the black hole geometry to get

$$p(r) \sim T_{\rm H}^{d+1} q(r)^{d+1} \sim \frac{1}{r_0^{d+1}} \left(\frac{r_0}{r-r_0}\right)^{\frac{d+1}{2}} \sim \frac{1}{r_0^{\frac{d+1}{2}} (r-r_0)^{\frac{d+1}{2}}} \,. \tag{6.68}$$

We also have

$$M(r) \sim M \sim \frac{r_0^{d-2}}{G} = \frac{r_0^{d-2}}{l_p^{d-1}} \,. \tag{6.69}$$

Thus,

$$\frac{p(r) r_0^d}{M(r)} \sim \frac{l_p^{d-1}}{(r-r_0)^{\frac{d+1}{2}} r_0^{\frac{d-3}{2}}} \,. \tag{6.70}$$

We find that $\frac{p(r) r_0^d}{M(r)} \sim 1$ at

$$(r-r_0) \sim \left(\frac{l_p^{d-1}}{r_0^{\frac{d-3}{2}}}\right)^{\frac{2}{d+1}} \,. \tag{6.71}$$

Using the relation (6.6) to write this value of $r - r_0$ in terms of the proper distance s from r_0 in the black hole metric, we find

$$s \sim M^{\frac{2}{(d-2)(d+1)}} l_p \,. \tag{6.72}$$

Thus, we find that for the condition (6.67) to hold, the value of r_{max} defined in (6.66) is given by the same distance scale s_c (eq. (6.9)) that was used to define the compactness of the ECO in condition ECO1.

2. In (6.60) we needed to evaluate the derivative of $\frac{M(r)}{r}$, but we approximated this by the derivative of $\frac{M(r)}{r_0}$; thus we were ignoring the variation of the value of r in the near surface region. Writing

$$\frac{d}{dr}\left(\frac{M(r)}{r}\right) = \frac{1}{r}\frac{dM(r)}{dr} - \frac{M(r)}{r^2} \,, \tag{6.73}$$

we see that this approximation is valid as long as the ratio between the two terms

on the RHS satisfies

$$z(r) \equiv \left(\frac{M(r)}{r^2}\right)\left(\frac{1}{r}\frac{dM(r)}{dr}\right)^{-1} \ll 1\,. \tag{6.74}$$

Using (6.50) and the same estimates for $\rho(r)$ that we used for $p(r)$ in (6.68), we find

$$z(r) \sim \frac{(r-r_0)^{\frac{d+1}{2}} M}{r_0^{\frac{d-1}{2}}}\,. \tag{6.75}$$

Thus $z(r) \sim 1$ at

$$(r-r_0) \sim \left(\frac{r_0^{\frac{d-1}{2}}}{M}\right)^{\frac{2}{d+1}} \sim \left(\frac{l_p^{d-1}}{r_0^{\frac{d-3}{2}}}\right)^{\frac{2}{d+1}}\,. \tag{6.76}$$

This is the same distance scale that appeared (6.71), so we again find that r_{max} is the radius given by the compactness scale s_c.

Thus in the discussion below, we will set

$$r_{max} - r_0 = \left(\frac{l_p^{d-1}}{r_0^{\frac{d-3}{2}}}\right)^{\frac{2}{d+1}}\,. \tag{6.77}$$

Since the radius $r \sim r_{max}$ is at the compactness scale s_c, we see by condition ECO3 that the redshift factor at r_{max} must be of the same order as the redshift factor predicted by the black hole geometry. Thus

$$q(r_{max}) \sim \left(\frac{r_0}{l_p}\right)^{\frac{d-1}{d+1}} \sim \left(\frac{M}{m_p}\right)^{\frac{(d-1)}{(d-2)(d+1)}}\,. \tag{6.78}$$

6.3.3 Analyzing the approximate TOV solution

First, consider the power $\frac{2d}{d-1}$ appearing on the RHS of (6.65). We are considering $d \geq 3$. For $d = 3$, this power is an odd integer 3, while for all higher d it is a fraction. The LHS of (6.65) must be a positive real number by the requirement (6.17), so we need

$$C_3(r - r_1) > 0\,, \tag{6.79}$$

throughout the domain (6.66) where our approximate solution is valid. This gives us two possibilities, which we study in turn.

The case $C_3 > 0,\ r_1 < R_{\mathbf{ECO}}$:

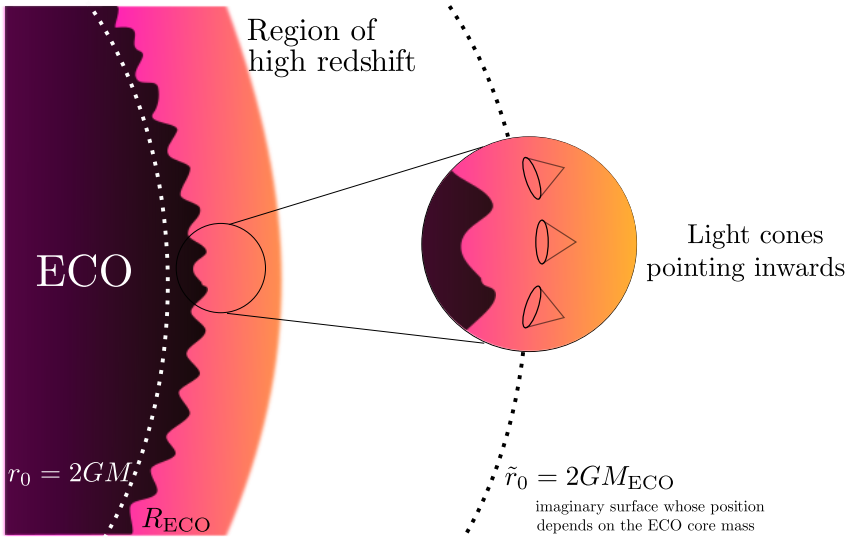

Figure 6.2: The argument for an ECO with $T_{\rm ECO} < T_{\rm H}$ and a surface $r = R_{\rm ECO}$ that is just a planck length outside the horizon radius. The region just outside $R_{\rm ECO}$ has a large negative energy density due to the negative vacuum energy. Thus the core of the ECO (the region depicted with a jagged boundary) must have a mass significantly more than M. Since the radius of this core is very close to the horizon radius r_0 for mass M, this core must be inside its own horizon; this fact is depicted in the magnified region by light cones that point inwards. Thus such an ECO cannot exist as a time-independent configuration.

One possibility is that we have $C_3 > 0$, and $r_1 < R_{\rm ECO}$, which gives (6.79) throughout the domain (6.66). Using (6.65) we find

$$\rho(r) = -\frac{d}{8\pi G r_0}\left(\frac{(d-1)}{2d}|C_3|\right)^{\frac{2d}{d-1}}(r-r_1)^{\frac{d+1}{d-1}}\,. \tag{6.80}$$

We see that $\rho(r) < 0$. Thus this situation is similar to the case $T_{\rm ECO} < T_{\rm H}$ which had $\rho(r) < 0$ in our heuristic analysis of section A.3. We present a schematic description of this case in the above Figure 6.2. From (6.49) we find

$$e^{2\alpha(r)} = \frac{C_2}{|\rho|^{\frac{2}{d+1}}} = C_2\left(\frac{d}{8\pi G r_0}\left(\frac{(d-1)}{2d}|C_3|\right)^{\frac{2d}{d-1}}\right)^{-\frac{2}{d+1}}(r-r_1)^{-\frac{2}{(d-1)}}\,. \tag{6.81}$$

Note that $e^{2\alpha(r)}$ determines the redshift factor

$$q(r) = (-g_{tt}(r))^{-\frac{1}{2}} = e^{-\alpha(r)} = C_2^{-\frac{1}{2}}\left(\frac{d}{8\pi G r_0}\left(\frac{(d-1)}{2d}|C_3|\right)^{\frac{2d}{d-1}}\right)^{\frac{1}{d+1}}(r-r_1)^{\frac{1}{d-1}}\,. \tag{6.82}$$

We see that since $r > r_1$, the redshift factor $q(r)$ *increases* as we move r to larger values. Thus $q(r)$ will keep increasing monotonically until at least the location $r = r_{max}$ where

our near-surface approximation (6.45) to the TOV equation fails. Thus

$$q(R_{ECO}) < q(r_{max}) \sim \left(\frac{M}{m_p}\right)^{\frac{(d-1)}{(d-2)(d+1)}} , \tag{6.83}$$

where in the second step we have recalled (6.78). Thus we see that we do not satisfy the high redshift condition (6.12).

The case $C_3 < 0,\ r_1 > R_{\mathbf{ECO}}$:

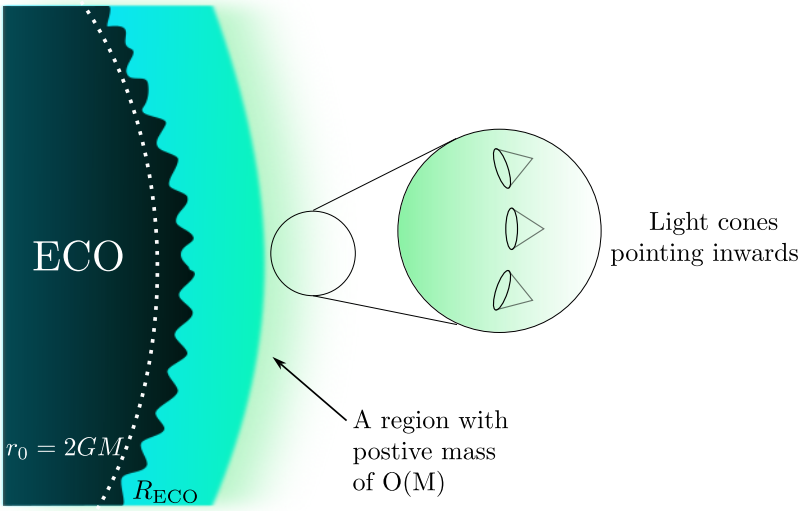

Figure 6.3: The argument for an ECO with $T_{\rm ECO} > T_{\rm H}$, and an surface at $R_{\rm ECO}$ where the redshift is very high. This high redshift implies that $R_{\rm ECO}$ is a very small distance outside the horizon radius $\tilde{r}_0$ corresponding to the mass inside $R_{\rm ECO}$. The region just outside $R_{\rm ECO}$ has a large positive energy density due to the thermal radiation. A thin shell of this radiation, depicted as the outer band, has a significant amount of mass. Then the total mass in the region inside the outer boundary r_{outer} of this shell is such that the corresponding horizon radius $r_{0,outer}$ is larger than r_{outer}. Thus we again find that such an ECO cannot exist as a time-independent configuration.

Now consider the possibility that

$$C_3 < 0, \qquad r_1 > R_{\rm ECO}\,. \tag{6.84}$$

We write $\rho(r)$ as

$$\rho(r) = \frac{d}{8\pi G r_0}\left(\frac{(d-1)}{2d}|C_3|\right)^{\frac{2d}{d-1}}(r_1 - r)^{\frac{d+1}{d-1}}\,. \tag{6.85}$$

We see that $\rho(r) > 0$. Thus this situation is similar to the case $T_{\rm ECO} > T_{\rm H}$ which had $\rho(r) > 0$ in our heuristic analysis of section A.3. We present a schematic description of this case in the above Figure 6.2.

Note that the LHS of (6.65) is required to not vanish anywhere, but the RHS vanishes at $r = r_1$. We avoid an inconsistency only if r_1 is sufficiently large that values $r \approx r_1$ lie outside the range where the near-surface approximation (6.45) of the TOV equation is valid. Recall that r_{max} is the same order as the compactness scale s_c, and that outside this compactness scale the standard black hole geometry is expected to be a reasonable approximation to the geometry. Noting that the solution (6.65) is a power law in the near-surface region, we state the requirement that r_1 be significantly outside the range $r_0 < r < r_{max}$ by requiring

$$r_1 - r_{max} \gtrsim r_{max} - r_0 \,. \tag{6.86}$$

Even though we say that r_1 is far outside the compactness scale s_c, we will take $r_1 - r_0 \ll r_0$, and will use this approximation to simplify some relations; taking a larger r_1 does not change the argument that follows.

Again, using (6.49) we have

$$q(r) = (-g_{tt}(r))^{\frac{1}{2}} = e^{-\alpha(r)} = C_2^{-\frac{1}{2}} \left(\frac{d}{8\pi G r_0} \left(\frac{(d-1)}{2d} |C_3| \right)^{\frac{2d}{d-1}} \right)^{\frac{1}{d+1}} (r_1 - r)^{\frac{1}{d-1}} \,. \tag{6.87}$$

In the standard black hole geometry,

$$q(r) \approx \left(\frac{(d-2)(r-r_0)}{r_0} \right)^{-\frac{1}{2}} \,. \tag{6.88}$$

The expression (6.87) holds for $R \lesssim r_{max}$ while by condition ECO3, the expression (6.88) holds for $r \gtrsim r_{max}$. Thus at $r \sim r_{max}$ both expressions should have approximately the same value. Thus we must have

$$C_2^{-\frac{1}{2}} \left(\frac{d}{8\pi G r_0} \left(\frac{(d-1)}{2d} |C_3| \right)^{\frac{2d}{d-1}} \right)^{\frac{1}{d+1}} (r_1 - r_{max})^{\frac{1}{d-1}} \approx \left(\frac{(d-2)(r_{max} - r_0)}{r_0} \right)^{-\frac{1}{2}} \,. \tag{6.89}$$

Thus the constants C_2, C_3 in the above relation satisfy

$$C_2^{-\frac{1}{2}} \left(\frac{d}{8\pi G r_0} \left(\frac{(d-1)}{2d} |C_3| \right)^{\frac{2d}{d-1}} \right)^{\frac{1}{d+1}} \approx \left(\frac{r_0}{(d-2)(r_{max} - r_0)} \right)^{\frac{1}{2}} \frac{1}{(r_1 - r_{max})^{\frac{1}{d-1}}} \,. \tag{6.90}$$

Then the redshift at $r = R_{\rm ECO}$ is given by (using eq.(6.87))

$$q(R_{\rm ECO}) \approx \left(\frac{r_0}{(d-2)(r_{max} - r_0)} \right)^{\frac{1}{2}} \left(\frac{r_1 - R_{\rm ECO}}{r_1 - r_{max}} \right)^{\frac{1}{d-1}} \,. \tag{6.91}$$

We now wish to use the intuition that r_1 is 'large' in the sense (6.86). We have

$$\frac{r_1 - R_{\rm ECO}}{r_1 - r_{max}} = 1 + \frac{r_{max} - R_{\rm ECO}}{r_1 - r_{max}} < 1 + \frac{r_{max} - r_0}{r_1 - r_{max}} < 1 + \frac{r_{max} - r_0}{r_{max} - r_0} = 2\,, \tag{6.92}$$

where in the last step we have used the relation $(r_1 - r_{max}) \gtrsim (r_{max} - r_0)$. Then (6.91) gives

$$q(R_{\rm ECO}) \sim \left(\frac{r_0}{(d-2)(r_{max} - r_0)}\right)^{\frac{1}{2}} \sim \left(\frac{r_0}{l_p}\right)^{\frac{d-1}{d+1}}\,. \tag{6.93}$$

Since condition ECO2 requires a redshift much larger than this at the ECO surface (eq. (6.12)), we conclude that we again do not find an acceptable solution to the approximate TOV equation (6.60).

6.3.4 Checking the consistency of condition ECO3

The goal of condition ECO3 was to exclude situations where there is a significant amount of matter outside the radius $R_{\rm ECO}$; having such matter would conflict with the notion that our object is 'extremely compact'. But we have noted that there is a certain amount of stress energy outside $R_{\rm ECO}$ that is unavoidable, since this stress-energy results from the state of quantum fields at temperature $T_{\rm ECO}(r)$ in the near-surface region. We should therefore check that the stress-energy of this thermal gas is low enough at $s \gtrsim s_c$ so that we can indeed require that the geometry in this region is close to the black hole geometry. In this section we will check that such is the case, using estimates from the analysis above.

For the ECO geometry (6.3), the metric coefficient $e^{2\beta(r)}$ is given by (eq. A.9))

$$e^{-2\beta(r)} = 1 - \frac{\mu G M(r)}{r^{d-2}}\,, \tag{6.94}$$

with

$$M(r) = M - E_{rad}(r)\,. \tag{6.95}$$

Here $E_{rad}(r)$ is the energy contributed by the radiation in the region $r < r' \lesssim 2r_0$, where (as in the above sections) we have truncated our thermal gas at a scale $2r_0$. Following the lines of the computation leading to (A.25) we have

$$E_{rad}(r) \sim \frac{r_0^{\frac{d-3}{2}}}{(r - r_0)^{\frac{d-1}{2}}}\,. \tag{6.96}$$

In the black hole metric we have

$$e^{-2\beta_{\rm H}(r)} = 1 - \frac{\mu G M}{r^{d-2}} \,. \tag{6.97}$$

Then we have, (still assuming $r \lesssim 2r_0$)

$$\frac{e^{-2\beta(r)}}{e^{-2\beta_{\rm H}(r)}} = 1 + \frac{\mu G E_{rad}(r)}{r^{d-2} - \mu G M} = 1 + \frac{\mu G E_{rad}(r)}{r^{d-2} - r_0^{d-2}} \approx 1 + \frac{\mu G E_{rad}(r)}{(d-2) r_0^{d-3}(r - r_0)} \,. \tag{6.98}$$

Using arguments similar to the ones leading to (A.25) to estimate $E_{rad}(r)$, we find

$$\frac{\mu G E_{rad}(r)}{(d-2) r_0^{d-3}(r - r_0)} \sim \frac{l_p^{d-1}}{r_0^{\frac{d-3}{2}} (r - r_0)^{\frac{d+1}{2}}} \,. \tag{6.99}$$

For the ECO geometry to approximate the black hole geometry we need that the above quantity be $\lesssim 1$. This yields the requirement which is

$$(r - r_0) \gtrsim \left(\frac{l_p^{d-1}}{r_0^{\frac{d-3}{2}}} \right)^{\frac{2}{d+1}} \,. \tag{6.100}$$

From (6.71),(6.72) we see that this is just the condition $s \gtrsim s_c$. Thus the coefficient of g_{rr} in the ECO geometry satisfies the constraint ECO3.

The coefficient $\alpha(r)$ in the ECO geometry (6.3) is given through the equation

$$\frac{(d-1)\alpha'(r) e^{-2\beta(r)}}{r} = -\frac{(d-1)(d-2)(e^{-2\beta(r)} - 1)}{2r^2} + 8\pi G p(r) \,. \tag{6.101}$$

Using (A.9), this is

$$\frac{(d-1)\alpha'(r) e^{-2\beta(r)}}{r} = \frac{(d-1)(d-2)\mu G M(r)}{2r^d} + 8\pi G p(r) \,. \tag{6.102}$$

For the black hole, we have (i) $e^{-2\beta_{\rm H}(r)} = 1 - \frac{\mu G M}{r_0^{d-2}}$, (ii) $M(r) = M$, and (iii) $p = 0$. Then we get

$$\alpha'_{\rm H}(r) = \frac{(d-2)\mu G M}{2r^{d-1}(1 - \frac{\mu G M}{r^{d-2}})} \,, \tag{6.103}$$

which gives

$$e^{2\alpha_{\rm H}(r)} = 1 - \frac{\mu G M}{r^{d-2}} \,. \tag{6.104}$$

From the discussion above we have seen that $e^{-2\beta(r)}$ can be approximated by its black hole value for $s \gtrsim s_c$. On the RHS, again using estimates for E_{rad} similar to the one in

(A.25), we find that for $s \gtrsim s_c$,

$$1 - \frac{M(r)}{M} = \frac{E_{rad}(r)}{M} \sim \frac{l_p^{d-1}}{r_0^{\frac{d-1}{2}}(r-r_0)^{\frac{d-1}{2}}} \sim \frac{l_p^{d-1}}{s^{d-1}} \lesssim \frac{l_p^{d-1}}{s_c^{d-1}} \sim \left(\frac{l_p}{r_0}\right)^{\frac{2(d-1)}{d+1}} \ll 1\,. \tag{6.105}$$

Thus in the first term on the RHS of (6.102) we can write $M(r) \approx M$. To see if $\alpha(r) \approx \alpha_{\rm H}(r)$, we just need to check that the last term on the RHS of (6.102) can be ignored compared to the first term on the RHS; i.e., we need

$$\frac{p(r)r^d}{M} \lesssim 1\,. \tag{6.106}$$

But using the analysis leading to (6.71), we find that this inequality holds for $s \gtrsim s_c$.

To summarize, the thermal energy of quantum fields in the region $s \gtrsim s_c$ is small enough that the geometry in this region can be approximated by the black hole geometry. In particular, in this region the redshift in the ECO geometry is of the same order as its value in the black hole geometry. Thus it is consistent to impose condition ECO3 in our definition of an ECO to disallow additional sources of stress-energy outside $R_{\rm ECO}$.

6.4 Chapter Summary

In this chapter, we have argued that *Extremely Compact Objects* (ECOs)—compact configurations with radii just outside the black hole horizon—must exhibit the same thermodynamic properties as a semiclassical black hole of the same mass. Specifically, we demonstrated that their **temperature** T must coincide with those of the corresponding black hole.

This result is significant because semiclassical black holes, while possessing elegant thermodynamic properties, rely on the existence of an event horizon—a feature that ultimately leads to information loss via Hawking evaporation. In contrast, string theory suggests that black holes are composed of *fuzzballs*—horizonless microstates—which resolve the information paradox. However, this raises the question: if fuzzballs have no horizon, is there any reason to expect them to reproduce the thermodynamics of the semiclassical black hole?

Entropic arguments suggest that fuzzballs possess a surface located at a proper distance $s \sim l_p$ outside the would-be horizon. Similar conclusions apply to other compact models such as boson stars [100], strange stars [101], Q-balls [102], and quark stars [103]. Although these objects are typically less compact than fuzzballs, if they satisfy certain compactness conditions, they too would fall within the ECO class and exhibit the same universal thermodynamics (see [104] for a detailed discussion).

Our main result is that for any ECO with a surface located at a proper distance

$$s_{\rm ECO} \ll \left(\frac{M}{m_p}\right)^{\frac{2}{(d-2)(d+1)}} \tag{6.107}$$

outside the horizon radius r_0, the temperature $T_{\rm ECO}$ must match the Hawking temperature $T_{\rm H}$, up to exponentially small corrections in s. This conclusion follows from an analysis of the *Tolman-Oppenheimer-Volkoff (TOV) equation* near the ECO surface. The near-surface region contains a high-density thermal bath of radiation, whose energy density and temperature are amplified by the large redshift. The presence of a negative vacuum energy contribution—analogous to Casimir energy—is assumed to match, to leading order, the vacuum energy of the local Rindler vacuum. We find that if the sum of radiation and vacuum energies does not vanish, the resulting backreaction on the geometry prevents a consistent static solution. A cancellation occurs precisely when $T_{\rm ECO} = T_{\rm H}$, ensuring equilibrium.

This result thus offers a compelling resolution: while information loss is avoided due to the absence of a horizon in microstates (resolving the paradox), the thermodynamic properties of black holes are still universally reproduced by horizonless ECOs.

We have not explicitly analyzed the dynamical process by which an ECO equilibrates to $T_{\rm H}$ if initially starts out of equilibrium. However, we conjecture the following mechanism: if $T_{\rm ECO} > T_{\rm H}$, the structure at $r < r_{\rm ECO}$ absorbs energy and expands, decreasing the local radiation temperature until equilibrium is reached. Conversely, if $T_{\rm ECO} < T_{\rm H}$, the structure contracts and transfers energy to the surrounding thermal bath, raising its temperature toward $T_{\rm H}$. Equilibrium is achieved when the redshifted surface temperature matches $T_{\rm H}$, allowing for a stable, time-independent ECO configuration.

Our analysis also opens directions for further exploration. While we defined $\eta_T = T_{\rm ECO}/T_{\rm H}$ and showed that consistent static solutions require $\eta_T = 1$, small deviations $\Delta T = T_{\rm ECO} - T_{\rm H}$ could be nonzero yet parametrically small. It would be interesting to quantify how such deviations scale with $s_{\rm ECO} \to 0$.

In this chapter, we restricted to non-rotating, uncharged ECOs. Extending this analysis to charged and rotating black holes, particularly in the extremal limit, remains an important open direction. We hope to address these cases in future work.

Finally, recent studies [105, 106] have proposed observational probes of near-horizon quantum structure. These developments offer exciting prospects for linking the theoretical structure of ECOs and fuzzballs to astrophysical data, bringing quantum gravity into contact with experiment.

Chapter 7

Future Outlook and Discussion

We are trying to prove ourselves wrong as quickly as possible, because only in that way can we find progress.

— R. P. Feynman

The results presented in this thesis open several avenues for future research. From probing the structure of black hole microstates via conformal field theory to exploring the universal thermodynamics of horizonless objects, each chapter points to deeper questions at the intersection of gravity, quantum theory, and high-energy phenomenology. Future work may extend these ideas to charged and rotating microstates, incorporate higher-derivative corrections from string theory, and explore observational signatures of quantum structure near black hole horizons. We now reflect on the broader implications of the results presented in this thesis and outline possible directions they suggest.

7.1 Charged ECOs

An important future direction is the extension of our universality arguments to charged Extremely Compact Objects (ECOs). In this context, we derived a generalized compactness scale s_c which sets the upper bound for how close the ECO surface must lie relative to the would-be horizon of a Reissner–Nordström-like geometry. This scale depends not only on the mass M and Planck scale m_p, but also crucially on the charge Q of the object. Specifically, in $d+1$ dimensions, the scale is given by

$$s_c = \frac{1}{m_p^{\frac{2}{(d-2)(d+1)}}} \left(\frac{\left(\frac{\mu}{2} M + \sqrt{\frac{\mu^2}{4} M^2 - \nu \frac{Q^2}{G}} \right)^{\frac{d}{d-2}}}{\sqrt{\frac{\mu^2}{4} M^2 - \nu \frac{Q^2}{G}}} \right)^{\frac{1}{d+1}} l_p \tag{7.1}$$

and the condition for universality of thermodynamics becomes $s_{\rm ECO} \ll s_c$. This generalizes the uncharged result and shows how charge modifies the required compactness of ECOs.

In $3+1$ dimensions, this condition simplifies to

$$s_c = \frac{1}{m_p^{\frac{1}{2}}} \frac{\left(M + \sqrt{M^2 - \frac{Q^2}{G}}\right)^{\frac{3}{4}}}{(M^2 - \frac{Q^2}{G})^{\frac{1}{8}}} l_p \,. \tag{7.2}$$

This formulation raises several compelling questions. How does the inclusion of electric or magnetic charge influence the near-surface stress-energy tensor and the vacuum polarization effects? Can a charged ECO with $s_{\rm ECO} \ll s_c$ still achieve thermodynamic universality with a semiclassical charged black hole? Addressing these issues will be crucial in understanding the role of charge in horizonless black hole microstructure, and we hope to pursue these extensions in future work.

7.2 ECOs in Higher Derivative Gravity

Another intriguing avenue for future work lies in understanding how higher-derivative corrections to Einstein gravity affect the universal thermodynamic properties of Extremely Compact Objects (ECOs). In particular, modifications such as Gauss-Bonnet (GB) and Einstein-dilaton-Gauss-Bonnet (EdGB) gravity provide a well-motivated framework to study such effects, as they naturally arise in low-energy limits of string theory and effective field theories of gravity. In these models, we find that the compactness scale s_c—which determines how close an ECO's surface must lie to the would-be horizon—receives corrections that scale as α/r_0^2 in EGB gravity ($D > 4$) and as α^2/r_0^4 in EdGB gravity ($D = 4$), where α is the higher-curvature coupling and r_0 is the classical horizon radius. These corrections imply that the compactness requirements for ECOs are relaxed or tightened depending on the sign and size of the coupling, thereby modifying the conditions under which thermodynamic universality holds. Importantly, observational bounds on $\sqrt{\alpha}$ from gravitational wave data suggest values up to a few kilometers, indicating that these effects could be significant for astrophysical black hole candidates. Understanding how such corrections influence the stress-energy balance near the ECO surface, the back-reaction problem, and the emergence of thermodynamic equilibrium—especially whether $T_{\rm ECO} = T_H$ continues to hold in these modified gravity theories—constitutes a promising direction for future exploration. These investigations would help refine our understanding of black hole microstructure and potentially yield testable predictions linking modified gravity theories with observational signatures in gravitational wave astronomy.

7.3 Electromagnetic Entrapment in Different Spacetimes

The strong gravitational environment near black holes profoundly alters the behavior of electromagnetic fields. In our work [88], we showed that a neutral configuration of charges placed in a region of high redshift—characterized by a large g_{tt}—produces an electromagnetic field that is tightly localized and vanishes just outside the redshifted region. This *electromagnetic entrapment* gives rise to smooth, horizonless geometries that are indistinguishable from Schwarzschild black holes except in an infinitesimal region near the would-be horizon, where the trapped electromagnetic structure becomes manifest.

To further generalize this mechanism, we wish to extend classical analyses of electrostatics in Schwarzschild spacetimes [107–109] to arbitrary $(d+1)$-dimensional spherically symmetric backgrounds. We wish to ask if the key requirement for entrapment is tied to specific geometry or to the presence of sufficiently high gravitational redshift. This direction resonates with the fuzzball paradigm, which replaces the classical horizon with rich structure supported by stringy or quantum ingredients. A more general question is whether non-supersymmetric, classical gauge fields alone may be sufficient to generate such structures.

7.4 The VECRO Hypothesis

A promising direction for future research lies in understanding the cosmological implications of fuzzball-type structures through the concept of Virtual Extended Compression Resistant Objects (VECROs) [110]. If fuzzballs represent the true microstates of black holes in string theory, then the vacuum wavefunctional of quantum gravity should include virtual fluctuations of these geometries—manifesting as VECROs. These objects, by their very construction, resist compression and can stretch or deform depending on the background spacetime curvature. This dynamical behavior modifies the local vacuum energy, potentially influencing the large-scale dynamics of the universe. Notably, it has been proposed that the stretching of VECROs during the radiation–matter equality era could help resolve the Hubble tension, i.e., the discrepancy between early- and late-time measurements of the Hubble constant [111–113]. Moreover, suitably constructed models of VECRO-induced vacuum energy may offer insights into the cosmological constant problem, one of the deepest puzzles in fundamental physics. Future efforts will focus on formulating precise models of VECRO potentials, analyzing their backreaction on cosmological evolution, and exploring their observational consequences, thereby bridging black hole microphysics with early-universe cosmology.

7.5 Lifting and Chaos

Another natural extension of our current work involves broadening the class of states for which lifting is computed in the D1-D5 CFT. Thus far, our analysis has primarily focused on states where a singly wound string is excited within a system of N strings. A promising direction is to consider excitations of multiwound strings—those with winding number $k > 1$—which naturally introduce a richer set of superconformal primaries, including those with higher angular momentum j. These more general configurations open the door to computing lifts for a larger family of states, potentially uncovering new universal patterns and scaling behaviors. Additionally, it would be compelling to examine whether techniques developed in recent studies of candidate black hole microstates in supersymmetric string theories can inform the lifting behavior in these extended settings.

A complementary and equally exciting line of investigation arises from a recent conjecture [114] that *BPS* states represented by horizonless geometries may exhibit distinct chaotic properties compared to their horizon-full counterparts. This aligns closely with our research on fuzzball microstates and opens a novel window to test the fuzzball paradigm through dynamical diagnostics. Specifically, studying the degree of chaos—quantified via tools such as out-of-time-order correlators or spectral form factors—in various lifted states could provide new evidence supporting or falsifying the conjecture. Together, these directions promise to deepen our understanding of microstate structure, universality, and the signatures of quantum gravity in holographic settings.

7.6 Rotating ECOs, Kerr Uniqueness and Observations

Another compelling direction for future research lies in developing a generalized back-reaction framework for rotating Extremely Compact Objects (ECOs), building on the techniques we have established for static, spherically symmetric geometries. Extending our thermodynamic analysis to the rotating case could help address one of the longstanding challenges in general relativity: constructing a smooth, horizonless interior solution that matches onto the Kerr metric at large distances. If ECOs truly exhibit universal thermodynamic behavior, then the surface gravity at their boundary must be constant, enabling a consistent matching with Kerr geometry. This could open a novel pathway for validating semiclassical quantum effects in rotating backgrounds and yield potential observational signatures—such as deviations from Kerr multipole moments—that could be probed by next-generation black hole imaging and gravitational wave interferometers.

In tandem, a second important frontier is the study of corrections to Einstein's equations in gravitational wave signals arising from ECO merger events. Unlike classical

black holes, ECOs possess a finite surface located a proper distance $\sim \sqrt{M\, l_p}$ from the would-be horizon. This additional scale could leave distinct imprints on the post-merger waveform, including late-time echoes or deviations from the expected ring-down spectrum. A detailed analysis of such merger events could offer a robust observational test of the ECO paradigm and provide conclusive evidence for the existence of horizonless compact objects in the universe. Together, these two lines of research promise to further our understanding of both the theoretical structure and empirical viability of black hole microstructure.

7.7 Closing Remarks

The investigations presented in this thesis offer a multifaceted view of black holes and their possible replacements by horizonless, quantum-corrected structures. From the universality of thermodynamic behavior in ECOs to the detailed lifting patterns in the D1-D5 CFT, and from electromagnetic entrapment to potential observational probes, each thread reinforces the possibility that spacetime near what we once called horizons is far richer and more structured than previously imagined. Our future directions aim to expand these insights—exploring rotation, gravitational waves, chaos, and cosmological consequences—with the hope of grounding speculative models in testable frameworks.

At its core, this journey reflects a deeper philosophical lesson: that nature, even in its most extreme and opaque regimes, may still obey universal principles and that by pursuing consistency to its logical end, we uncover not only technical clarity but also conceptual elegance. In peeling back the veil of classical horizons, we may be glimpsing a more complete quantum architecture of spacetime—one where gravity, thermodynamics, and quantum theory are not in tension but in resonance. In doing so, we circle back to the theme that began this journey. By going "through the horizon and back," we have lifted the veil on black hole thermodynamics, revealing how unitarity, symmetry, and quantum structure might coexist in harmony. The horizon, once seen as a limit to understanding, now becomes a window into the deepest architecture of spacetime—an invitation to look more closely, think more deeply, and believe that even the most enigmatic features of the universe may yield to careful reasoning and universal principles.

Appendix A

Gravity Appendix

Most of the material in this appendix is adapted from our papers [16, 17]. Only the sections relevant to the present discussion have been included.

A.1 Surface gravity κ

Consider a particle with four velocity u^μ in $3+1$ dimensions with constant r, θ, ϕ. The tangent vector of such an observer is

$$\chi^\mu = \frac{dx^\mu}{dt}\,, \quad \chi^\mu = (1,0,0,0) \tag{A.1}$$

which is related to its four velocity by

$$u^\mu = (-\chi^2)^{-1/2}\chi^\mu\,. \tag{A.2}$$

Now, the energy E_∞ of the particle per unit mass as seen from infinity by an asymptotic observer is $E_\infty = -\chi_\mu u^\mu$. If this particle is held still using a rope by the asymptotic observer, then the force per unit mass exerted on the rope is $F^\mu_\infty = -\nabla^\mu E_\infty$. In terms of the particles variables, we find

$$F^\mu_\infty = -\nabla^\mu(-\chi_\alpha u^\alpha) = -\nabla^\mu(-\chi_\alpha\chi^\alpha)^{1/2}\,. \tag{A.3}$$

Surface gravity κ at a point P is defined as the norm of the force per unit mass exerted on the rope extended by an asymptotic observer attached to a particle located at the point P.

$$\kappa = (F_{\mu\infty}F^\mu_\infty)^{1/2}\ . \tag{A.4}$$

So, for static spherically symmetric spacetimes, it becomes (see. for eg. 2.2)

$$\kappa = \frac{1}{2}\partial_r(-g_{tt})\,. \tag{A.5}$$

κ also measures the in-affinity of a parameter used to measure the spacetime coordinates of a particle. In this way, it can be defined using Killing vectors. See [24] for a detailed analysis.

A.2 A relation following from condition ECO 1

The condition ECO 1 says that semiclassical dynamics is a good approximation at $r > R_{\rm ECO}$. From the discussion of section 6.2.2, we see that there will in general be a nonvanishing energy density $T^t{}_t = -\rho$ in this region. We can then use the ansatz (6.4) for the metric, and solve the equation $G_{tt} = 8\pi G T_{tt}$ with this energy density. In 3+1 dimensions we get

$$e^{-2\beta(r)} = 1 - \frac{2GM(r)}{r}\,. \tag{A.6}$$

For a star, we have

$$M(r) = \int_0^r dr\, 4\pi r^2 \rho(r)\,. \tag{A.7}$$

For an ECO, the region $0 < r < R_{\rm ECO}$ can have large quantum gravitational effects, and thus may not be well approximated as a smooth manifold. Thus we do not wish to integrate over r in this region. But we can compute $M(r)$ by integrating the mass density *outside* the ECO, using the fact that the mass as seen from infinity is M:

$$M(r) = M - \int_r^\infty dr\, 4\pi r^2 \rho(r)\,. \tag{A.8}$$

In $d+1$ dimensions, we have

$$e^{-2\beta(r)} = 1 - \frac{\mu G M(r)}{r^{d-2}}, \quad \mu = \frac{16\pi}{(d-1)\,\Omega_{d-1}}\,, \tag{A.9}$$

with

$$M(r) = M - \int_r^\infty dr\, \Omega_{d-1} r^{d-1} \rho(r)\,. \tag{A.10}$$

The regularity of the ECO solution thus yields the following requirement. In the region $r > R_{\rm ECO}$ we must have everywhere

$$1 - \frac{\mu G M(r)}{r^{d-2}} > 0\,. \tag{A.11}$$

A.3 A heuristic argument for the relation $T_{\rm ECO} \approx T_{\rm H}$

It can be shown that *if* we are given that $T_{\rm ECO} = T_{\rm H}$, then the entropy and radiation rates of the ECO will agree with the corresponding quantities for the black hole. We now pass on to our main task: arguing that an ECO that satisfies our conditions ECO 1-ECO 3 cannot have an arbitrary temperature, but rather must have $T_{\rm ECO} \approx T_{\rm H}$. It will be clear from our discussion that the approximation in this relation will become better as we take the distance $s_{\rm ECO}$ to be smaller.

In this section, we will make our first pass at arguing for this equality of temperatures, in the process obtaining the compactness condition (6.8). In this first pass, we will not be completely consistent in our approximations, in the following sense. We will need to use the energy density of the radiation near the surface of the ECO. This energy density at a radius r depends on the value of the redshift at r. This redshift, in turn, is affected by the energy density of the radiation itself. But in the analysis of this section, we will ignore this feedback of the radiation on the metric, assuming instead the redshift implied by the usual black hole metric in the region $r > R_{\rm ECO}$. In the next section, we will remedy this inaccuracy by solving the Tolman-Oppenheimer-Volkoff equation in the region near $r = R_{\rm ECO}$.

A.3.1 The energy of radiation near the ECO

Consider the near-surface region outside $R_{\rm ECO}$, described by the condition $r - R_{\rm ECO} \ll r_0$. As we saw in section 6.2.2, the effective potential V_{eff} traps the radiation from the ECO in this near-surface region, so that we have a thermal gas of quanta at some local temperature $T_{\rm ECO}(r)$ which depends on r. Far from the ECO we just have outgoing radiation in low l harmonics, so the energy density is very low. Thus we will take the thermal distribution of the near-surface region to be truncated so that it is nonvanishing only in the the region $r \lesssim 2r_0$; in fact as we will see the energy density is appreciable only very close to $r = R_{\rm ECO}$.

This radiation in the region $R_{\rm ECO} < r < 2r_0$ has a total energy which we will call $E_{\rm rad}$. Note that due to the negative vacuum energy in the region outside the ECO, $E_{\rm rad}$ will be positive if $T_{\rm ECO} > T_{\rm H}$ and $E_{\rm rad}$ will be negative if $T_{\rm ECO} < T_{\rm H}$.

Now consider the mass function $M(r)$ defined in (A.10). Since the mass at infinity is

M, we will have

$$M(R_{\rm ECO}) = M - E_{\rm rad}\,. \tag{A.12}$$

The quantity $M(R_{\rm ECO})$ can be thought of as the mass contained inside the 'core' of the ECO – the region which contains any nontrivial quantum gravitational dynamics. Recall that the horizon radius r_0 of a black hole is related to its mass M by the relation (6.5). Correspondingly, we define a radius $\tilde{r}_0$ through

$$\tilde{r}_0^{d-2} = \mu G M(R_{\rm ECO})\,, \tag{A.13}$$

where the radius $\tilde{r}_0$ would be the radius of a black hole with mass $M(R_{\rm ECO})$ if we had a Schwarzschild geometry with mass $M(R_{\rm ECO})$. The equation (6.17) requires

$$1 - \frac{\mu G M(R_{\rm ECO})}{R_{\rm ECO}^{d-2}} > 0\,, \tag{A.14}$$

so that

$$\tilde{r}_0 < R_{\rm ECO}\,. \tag{A.15}$$

Thus $\tilde{r}_0$ is a radius that is inside a region that we will not directly address. Nevertheless, the coordinate separation $R_{\rm ECO} - \tilde{r}_0$ will play an important role in the discussion below. We will generally find that $\tilde{r}_0 - r_0 \ll r_0$ and so in many steps below we will use the approximation

$$\tilde{r}_0 \approx r_0\,, \tag{A.16}$$

to simplify our expressions.

Consider the geometry generated by a mass $M(R_{\rm ECO})$ confined within the radius $r = R_{\rm ECO}$, and no energy density at $r > R_{\rm ECO}$. For $r > R_{\rm ECO}$ the metric for this geometry is of the Schwarzschild form

$$ds^2 = -\Big(1 - \Big(\frac{\tilde{r}_0}{r}\Big)^{d-2}\Big)dt^2 + \frac{dr^2}{1 - \Big(\frac{\tilde{r}_0}{r}\Big)^{d-2}} + r^2 d\Omega_{d-1}^2\,. \tag{A.17}$$

As noted above, in the actual ECO, there is a nonzero energy density ρ in the region $r > R_{\rm ECO}$. But we will be ignoring the deformation of the metric due to this ρ in some of steps below; in these steps we will refer to the metric (A.17).

With the metric (A.17), the redshift at a radius r is given by

$$\tilde{q}(r) = (-g_{tt}(r))^{-\frac{1}{2}} \approx \frac{\tilde{r}_0^{\frac{1}{2}}}{(d-2)^{\frac{1}{2}}(r-\tilde{r}_0)^{\frac{1}{2}}} \approx \frac{r_0^{\frac{1}{2}}}{(d-2)^{\frac{1}{2}}(r-\tilde{r}_0)^{\frac{1}{2}}}\,. \tag{A.18}$$

Here we have added a tilde to the variable q to denote the fact that this redshift $\tilde{q}$

corresponds to the redshift in the geometry with horizon radius $\tilde{r}_0$. The energy density at radius r is then

$$\rho(r) = a\left(T_{\rm ECO}^{d+1} - T_{\rm H}^{d+1}\right)\,\tilde{q}(r)^{d+1}\,. \tag{A.19}$$

The total energy of this radiation in the region $R_{\rm ECO} < r < \infty$ is

$$\begin{aligned}
E_{\rm rad} \approx & \int_{r=R_{\rm ECO}}^{\Lambda} dr\,\Omega_{d-1}\,r^{d-1}\,\rho(r)\,,\\
\approx & \; a\left(T_{\rm ECO}^{d+1} - T_{\rm H}^{d+1}\right)\,\Omega_{d-1}\int_{r=R_{\rm ECO}}^{\Lambda} dr\,r^{d-1}\,\tilde{q}(r)^{d+1}\,,\\
\approx & \; a\left(T_{\rm ECO}^{d+1} - T_{\rm H}^{d+1}\right)\,\Omega_{d-1}\int_{r=R_{\rm ECO}}^{\Lambda} dr\,r_0^{d-1}\left(\frac{r_0}{(d-2)(r-\tilde{r}_0)}\right)^{\frac{d+1}{2}}\,,\\
\approx & \; a\left(T_{\rm ECO}^{d+1} - T_{\rm H}^{d+1}\right)\,\frac{2\,\Omega_{d-1}}{(d-2)^{\frac{d+1}{2}}(d-1)}\,\frac{r_0^{\frac{3d-1}{2}}}{(R_{\rm ECO}-\tilde{r}_0)^{\frac{d-1}{2}}}\,,
\end{aligned} \tag{A.20}$$

a where $\Lambda = 2r_0$ is the cutoff we had chosen for our thermal bath and where we are ignoring the energy of the outgoing modes at $r \gtrsim 2r_0$.

We will also be interested in the energy of a thin shell outside $r = R_{\rm ECO}$. Note that the energy density (A.19) falls off as a power of $r - \tilde{r}_0$. We write

$$\Delta r \equiv R_{\rm ECO} - \tilde{r}_0\,. \tag{A.21}$$

and define our thin shell as

$$R_{\rm ECO} < r < R_{\rm ECO} + \Delta r. \tag{A.22}$$

The energy of such a shell will be

$$E_{\rm rad}^{\rm shell} = \left(1 - \frac{1}{2^{\frac{d-1}{2}}}\right)E_{\rm rad}\,. \tag{A.23}$$

It will be helpful to write

$$T_{\rm ECO} = \eta_{\rm T}\,T_{\rm H}\,. \tag{A.24}$$

Noting the expression (6.22) for $T_{\rm H}$, we then get

$$\begin{aligned}
aE_{\rm rad} = & \; a\left(\eta_{\rm T}^{d+1} - 1\right)\frac{2(d-2)^{\frac{d+1}{2}}\Omega_{d-1}}{(4\pi)^{d+1}(d-1)}\,\frac{r_0^{\frac{d-3}{2}}}{(R_{\rm ECO}-\tilde{r}_0)^{\frac{d-1}{2}}}\,,\\
\equiv & \; \frac{C_1\,r_0^{\frac{d-3}{2}}}{(R_{\rm ECO}-\tilde{r}_0)^{\frac{d-1}{2}}}\,,
\end{aligned} \tag{A.25}$$

a where C_1 is a dimensionless constant of order unity. Note that $C_1 > 0$ for $T_{\rm ECO} > T_{\rm H}$, and $C_1 < 0$ for $T_{\rm ECO} < T_{\rm H}$. We will have $C_1 = 0$ if $T_{\rm ECO} = T_{\rm H}$; i.e., $\eta_{\rm T} = 1$. Our goal will be to show that this is the only allowed value for $\eta_{\rm T}$ for an ECO.

A.3.2 An outline of the argument

Let us first sketch the nature of the argument, before moving onto more detailed estimates. Let the spacetime be 3+1 dimensional for simplicity. We consider the cases $T_{\rm ECO} < T_H$ and $T_{\rm ECO} > T_H$ in turn.

The case $T_{\rm ECO} < T_H$

Let us start with a simple case, depicted in Figure 6.2. Suppose $T_{\rm ECO} = 0$. Suppose further that the ECO surface, which is at $r = R_{\rm ECO}$, is only a planck distance outside the horizon radius $r_0 = 2GM$; i.e., $s_{ECO} = l_p$ which gives $(R_{\rm ECO} - \tilde{r}_0) \sim l_p^2/r_0$. The vacuum energy density outside $R_{\rm ECO}$ is negative and order planck scale just outside the surface $r = R_{\rm ECO}$. We find from (A.25)

$$E_{\rm rad} \sim -\frac{1}{(R_{\rm ECO} - \tilde{r}_0)} \sim -\frac{r_0}{l_p^2} \sim -M\,, \tag{A.26}$$

where we have used the fact that in 3+1 dimensions, $G = l_p^2$. Thus the vacuum energy outside the core of the ECO is negative and of the same order as the mass M seen at infinity.

For concreteness, let us assume that $E_{\rm rad} = -\frac{1}{2}M$. Then from (A.12), we have

$$M(R_{\rm ECO}) = M - E_{\rm rad} = \frac{3}{2}M\,. \tag{A.27}$$

Now consider the validity of the relation (6.17) at $r = R_{\rm ECO}$. Recall that $R_{\rm ECO} \approx 2GM$. Thus we have

$$1 - \frac{2GM(R_{\rm ECO})}{R_{\rm ECO}} \approx 1 - \frac{3GM}{2GM} = -\frac{1}{2} < 0\,. \tag{A.28}$$

This contradicts the requirement (6.17), which was required for regularity of the geometry.

Put another way, the vacuum energy outside the ECO contributes a negative value $-\frac{1}{2}M$ to the overall mass, which means the mass of the core has to be $\frac{3}{2}M$ to yield a total mass M at infinity. The Schwarzschild radius for this mass $\frac{3}{2}M$ is $3GM$, so that the core of the ECO is deep inside its own horizon radius. Recall that in classical general relativity, any particle inside a horizon must move towards smaller values of r by the inward pointing structure of light cones inside the horizon. Noting that semiclassical dynamics was required to hold at $r \geq R_{\rm ECO}$, we conclude that the particles at the surface

$r = R_{\rm ECO}$ cannot stay at a fixed radius $R_{\rm ECO}$; instead, the core of the ECO must collapse. Thus we conclude that we cannot have such an ECO with $T_{\rm ECO} = 0$.

The argument does not change in any significant way if we take some other temperature $T_{\rm ECO} < T_{\rm H}$. Suppose we take $T_{\rm ECO} = \frac{1}{2} T_{\rm H}$. Then $\eta_{\rm T} = \frac{1}{2}$ in (A.24), as compared to the value $\eta_{\rm T} = 0$ for the case $T_{\rm ECO} = 0$. Using (A.25), we see that the energy $E_{\rm rad}(\eta_{\rm T} = \frac{1}{2})$ is smaller than $E_{\rm rad}(\eta_{\rm T} = 0)$ by a factor

$$\frac{E_{\rm rad}(\eta_{\rm T} = \frac{1}{2})}{E_{\rm rad}(\eta_{\rm T} = 0)} = \frac{1 - \left(\frac{1}{2}\right)^4}{1} = \frac{15}{16}\,, \tag{A.29}$$

but this does not affect the nature of the argument we had outlined above for the case $T_{\rm ECO} = 0$.

The case $T_{\rm ECO} > T_H$

Now consider the case $T_{\rm ECO} > T_{\rm H}$, which is depicted in Figure 6.3. Condition ECO 2 requires a high redshift at the surface R_{ECO}, which leads to a high local temperature for the radiation. Let us assume for our example that this temperature is planck scale. Then the energy density at the ECO surface is also planck scale. The energy of radiation outside $R_{\rm ECO}$ is $E_{\rm rad} \sim M$.

For concreteness, let us assume that $E_{\rm rad} = \frac{1}{2}M$. Then the mass of the core of the ECO is $M(R_{\rm ECO}) = \frac{1}{2}M$. Note that the horizon radius corresponding to this mass $M(R_{\rm ECO})$ is $\tilde{r}_0 = GM$. Now we observe that in order to get the required high redshift at R_{ECO}, the mass inside $R_{\rm ECO}$ had to be compact enough to generate this high redshift. More precisely, we need the surface $R_{\rm ECO}$ to be $\sim l_p$ outside the radius $\tilde{r}_0 = GM$; thus we write $R_{\rm ECO} \approx GM$.

Now consider a shell of radiation, with width l_p, just outside the ECO surface. Thus the outer boundary of this shell r_{outer} is very close to $R_{\rm ECO}$, which was very close to $\tilde{r}_0 = GM$. Thus $r_{outer} \approx GM$.

By (A.23), the energy of the shell is $E^{shell}_{rad} = \frac{1}{2}E_{rad} = 0.25M$. Thus the total mass inside the radius r_{outer} is is $M(r_{outer}) = 0.5M + 0.25M = 0.75M$. Now consider the validity of the relation (6.17) at $r = R_{\rm ECO}$. We have

$$1 - \frac{2GM(r_{outer})}{r_{outer}} \approx 1 - \frac{1.5GM}{GM} = -0.5 < 0\,, \tag{A.30}$$

which contradicts the requirement (6.17).

In other words, the core of the ECO had to be very compact to yield a high redshift at $R_{\rm ECO}$. We then find that a thin shell just outside this core adds enough mass so that the system given by core+shell is inside its own horizon radius; thus such an ECO cannot exist.

A.3.3 Defining a useful scale Δr_{crit}

Let us review the quantities which played a role in the above arguments. The difference $r_0 - \tilde{r}_0$ described the difference between the Schwarzschild radius r_0 for the mass M of the ECO, and the the Schwarzschild radius $\tilde{r}_0$ of the core of the ECO. This difference stems from the fact that a part $E_{\rm rad}$ of the mass M of the ECO is carried by the radiation surrounding the core of the ECO. The energy $E_{\rm rad}$ in turn depends on

$$\Delta r \equiv (R_{\rm ECO} - \tilde{r}_0)\,. \tag{A.31}$$

A very small value of $(R_{\rm ECO} - \tilde{r}_0)$ gives a very large $E_{\rm rad}$ and thus a very large $r_0 - \tilde{r}_0$. Conversely, a very large $(R_{\rm ECO} - \tilde{r}_0)$ gives a very small $E_{\rm rad}$ and thus a very small $r_0 - \tilde{r}_0$.

Given the above, it will be useful to define a critical value Δr_{crit} for $R_{\rm ECO} - \tilde{r}_0$, such the corresponding radiation energy $E_{\rm rad}$ shifts the horizon radius by an amount which is again $r_0 - \tilde{r}_0 = \Delta r_{crit}$. Recalling that the horizon radius satisfies $r_0^{d-2} = \mu G M$, we note that small shifts of this radius are given by $\delta r_0 \approx \frac{\mu G \delta M}{(d-2) r_0^{d-3}}$. Setting $\delta M = -E_{\rm rad}$, we find that

$$|r_0 - \tilde{r}_0| \approx \frac{\mu G |E_{\rm rad}|}{(d-2) r_0^{d-3}} \approx \frac{\mu G |C_1|}{(\Delta r)^{\frac{d-1}{2}} (d-2) r_0^{\frac{d-3}{2}}}\,, \tag{A.32}$$

where we have used the expression for $E_{\rm rad}$ from (A.25). We define the critical separation Δr_{crit} as the value of Δr when this shift $|r_0 - \tilde{r}_0|$ equals Δr defined in (A.31). Thus we have

$$\Delta r_{crit} = \frac{\mu G |C_1|}{(\Delta r_{crit})^{\frac{d-1}{2}} (d-2)\, r_0^{\frac{d-3}{2}}}\,. \tag{A.33}$$

which gives

$$\Delta r_{crit} = \left(\frac{\mu G |C_1|}{(d-2)\, r_0^{\frac{d-3}{2}}} \right)^{\frac{2}{d+1}}\,. \tag{A.34}$$

To get an idea of the scale Δr_{crit}, we write it in terms of a proper distance s_{crit} using the relation (6.6) between coordinate distance from the horizon and proper distance from the horizon. Then we get

$$s_{crit} \sim \left(\frac{M}{m_p} \right)^{\frac{2}{(d-2)(d+1)}} l_p \sim s_c\,, \tag{A.35}$$

where the compactness scale s_c was defined in (6.9).

A.3.4 The argument for $T_{\mathbf{ECO}} < T_{\mathbf{H}}$

Let us assume that $T_{\rm ECO} < T_{\rm H}$, so that $\eta_{\rm T} < 1$. As noted above, a crucial role in the argument is played by the quantity $\Delta r = R_{\rm ECO} - \tilde{r}_0$. We will consider separately the following two possibilities:

(a) $\Delta r \ll \Delta r_{crit}$:

Since $\eta_{\rm T} < 1$, we have $E_{\rm rad} < 0$. Further,

$$|E_{\rm rad}| = \frac{|C_1|\, r_0^{\frac{d-3}{2}}}{(R_{\rm ECO} - \tilde{r}_0)^{\frac{d-1}{2}}} \gg \frac{|C_1|\, r_0^{\frac{d-3}{2}}}{(\Delta r_{crit})^{\frac{d-1}{2}}} \,. \tag{A.36}$$

Since $E_{\rm rad} < 0$, we have $\tilde{r}_0 > r_0$. From (A.32) we have

$$(\tilde{r}_0 - r_0) = \frac{\mu G |E_{\rm rad}|}{(d-2)\, r_0^{d-3}} \gg \frac{\mu G |C_1|}{(\Delta r_{crit})^{\frac{d-1}{2}} (d-2)\, r_0^{\frac{d-3}{2}}} \sim \Delta r_{crit} \,, \tag{A.37}$$

where the last relation follows from using the definition (A.33) of Δr_{crit}.

Now, since $R_{\rm ECO} > \tilde{r}_0$, we find that

$$R_{\rm ECO} - r_0 = (R_{\rm ECO} - \tilde{r}_0) + (\tilde{r}_0 - r_0) > (\tilde{r}_0 - r_0) \gg \Delta r_{crit} \,, \tag{A.38}$$

where in the last step we have used (A.37). Given that the separation Δr_{crit} corresponds to the proper distance scale s_c by (A.35), we see that our ECO is not sufficiently compact to satisfy condition ECO 1.

(b) $\Delta r \gtrsim \Delta r_{crit}$:

In this situation the redshift at the ECO surface is, using (6.11)

$$q(R_{\rm ECO}) \approx \frac{r_0^{\frac{1}{2}}}{(d-2)^{\frac{1}{2}} (R_{\rm ECO} - \tilde{r}_0)^{\frac{1}{2}}} \lesssim \frac{r_0^{\frac{1}{2}}}{(\Delta r_{crit})^{\frac{1}{2}}} \sim \left(\frac{r_0}{l_p}\right)^{\frac{d-1}{d+1}} \,. \tag{A.39}$$

This violates the condition ECO 2 (eq. (6.12)) which requires that we have a higher redshift than (A.39) at $R_{\rm ECO}$.

Thus we find that for $T_{\rm ECO} < T_{\rm H}$, we cannot get an ECO satisfying the conditions ECO 1-ECO 3.

A.3.5 The estimate for $T_{\mathbf{ECO}} > T_{\mathbf{H}}$

Now we consider the case $T_{\rm ECO} > T_{\rm H}$, so that $\eta_{\rm T} > 1$. Again we proceed to examine the two possibilities:

(a) $\Delta r \ll \Delta r_{crit}$:

Since $\eta_T > 1$, we have $E_{\rm rad} > 0$. Further,

$$E_{\rm rad} = \frac{C_1\, r_0^{\frac{d-3}{2}}}{(R_{\rm ECO} - \tilde{r}_0)^{\frac{d-1}{2}}} \gg \frac{C_1\, r_0^{\frac{d-3}{2}}}{(\Delta r_{crit})^{\frac{d-1}{2}}} \,. \tag{A.40}$$

Since $E_{\rm rad} > 0$, we have $r_0 > \tilde{r}_0$, and

$$(r_0 - \tilde{r}_0) = \frac{\mu G E_{\rm rad}}{(d-2) r_0^{d-3}} \gg \frac{\mu G |C_1|}{(\Delta r_{crit})^{\frac{d-1}{2}} (d-2)\, r_0^{\frac{d-3}{2}}} \sim \Delta r_{crit} \,. \tag{A.41}$$

Now consider the thin shell outside $r = R_{\rm ECO}$ with coordinate width Δr as defined in (A.22). We have from (A.23)

$$E_{\rm rad}^{\rm shell} = \left(1 - \frac{1}{2^{\frac{d-1}{2}}}\right) \frac{C_1\, r_0^{\frac{d-3}{2}}}{(R_{\rm ECO} - \tilde{r}_0)^{\frac{d-1}{2}}} \gg \frac{C_1\, r_0^{\frac{d-3}{2}}}{(\Delta r_{crit})^{\frac{d-1}{2}}} \,. \tag{A.42}$$

Let us define $\tilde{r}_{0,outer}$ as the Schwarzschild radius corresponding to the mass within radius r_{outer}; i.e., we define $r_{0,outer}$ through the condition $r_{0,outer}^{d-2} \equiv \mu G M(r_{outer})$. Then we have

$$r_{0,outer} - \tilde{r}_0 \approx \frac{\mu G E_{\rm rad}^{\rm shell}}{(d-2) r_0^{d-3}} \gg \frac{\mu G |C_1|}{(\Delta r_{crit})^{\frac{d-1}{2}} (d-2)\, r_0^{\frac{d-3}{2}}} \sim \Delta r_{crit} \,, \tag{A.43}$$

where in the last step we have used (A.33). Now recall that we had chosen the coordinate width of the shell as described in (A.22), which says

$$r_{outer} - R_{\rm ECO} = R_{\rm ECO} - \tilde{r}_0 \,. \tag{A.44}$$

Thus since $\Delta r = (R_{\rm ECO} - \tilde{r}_0) \ll \Delta r_{crit}$, we find

$$r_{outer} - R_{\rm ECO} \ll \Delta r_{crit} \,. \tag{A.45}$$

On the other hand, from (A.43) we have

$$r_{0,outer} - \tilde{r}_0 \gg \Delta r_{crit} \,. \tag{A.46}$$

Subtracting (A.45) from (A.46) we get

$$(r_{0,outer} - r_{outer}) + (R_{\rm ECO} - \tilde{r}_0) \gg \Delta r_{crit} \,. \tag{A.47}$$

Again using $(R_{\rm ECO} - \tilde{r}_0) \ll \Delta r_{crit}$ we find

$$(r_{0,outer} - r_{outer}) \gg \Delta r_{crit}\,. \tag{A.48}$$

Thus we find that

$$r_{outer} < r_{0,outer}\,. \tag{A.49}$$

This is a violation of equation (6.8), since it implies

$$1 - \frac{\mu G M(r_{outer})}{r_{outer}^{d-2}} = 1 - \frac{r_{0,outer}^{d-2}}{r_{outer}^{d-2}} < 0\,. \tag{A.50}$$

(b) $\Delta r \gtrsim \Delta r_{crit}$:

The argument here will be the same as the one for the case $T_{\rm ECO} < T_{\rm H}$. The redshift at the ECO surface is, using (6.11)

$$q(R_{\rm ECO}) \approx \frac{r_0^{\frac{1}{2}}}{(d-2)^{\frac{1}{2}}(R_{\rm ECO} - \tilde{r}_0)^{\frac{1}{2}}} \lesssim \frac{r_0^{\frac{1}{2}}}{(\Delta r_{crit})^{\frac{1}{2}}} \sim \left(\frac{r_0}{l_p}\right)^{\frac{d-1}{d+1}}\,. \tag{A.51}$$

This violates the condition ECO 2 (eq. (6.12)) which requires that we have a higher redshift at $R_{\rm ECO}$.

Thus we find that for $T_{\rm ECO} > T_{\rm H}$, we cannot get an ECO satisfying the conditions ECO 1-ECO 3.

Appendix B

CFT Appendix

Most of the material in this appendix is adapted from our papers [18–20]. Only the sections relevant to the present discussion have been included.

B.1 The $\mathcal{N} = 4$ superconformal algebra

We follow the notation in the appendix A of [79]. The indices $\alpha = (+, -)$ and $\bar{\alpha} = (+, -)$ correspond to the subgroups $SU(2)_L$ and $SU(2)_R$ arising from rotations on S^3. The indices $A = (+, -)$ and $\dot{A} = (+, -)$ correspond to the subgroups $SU(2)_1$ and $SU(2)_2$ arising from rotations in T^4. We use the convention

$$\epsilon_{+-} = 1 \quad , \quad \epsilon^{+-} = -1 \ . \tag{B.1}$$

B.1.1 Commutation relations

The commutation relations for the small $\mathcal{N} = 4$ superconformal algebra are

$$\Big[L_m, L_n\Big] = \frac{c}{12} m(m^2-1)\delta_{m+n,0} + (m-n)L_{m+n} \ , \tag{B.2a}$$

$$\Big[J^a_m, J^b_n\Big] = \frac{c}{12} m\, \delta^{ab}\delta_{m+n,0} + i\epsilon^{ab}{}_c\, J^c_{m+n} \ , \tag{B.2b}$$

$$\Big\{G^\alpha_{\dot{A},r}, G^\beta_{\dot{B},s}\Big\} = \epsilon_{\dot{A}\dot{B}}\left[\epsilon^{\alpha\beta}\frac{c}{6}\Big(r^2 - \frac{1}{4}\Big)\delta_{r+s,0} + \Big(\sigma^{aT}\Big)^\alpha_\gamma\, \epsilon^{\gamma\beta}(r-s)J^a_{r+s} + \epsilon^{\alpha\beta}L_{r+s}\right] \ , \tag{B.2c}$$

$$\Big[J^a_m, G^\alpha_{\dot{A},r}\Big] = \frac{1}{2}\Big(\sigma^{aT}\Big)^\alpha_\beta\, G^\beta_{\dot{A},m+r} \ , \tag{B.2d}$$

$$\Big[L_m, G^\alpha_{\dot{A},r}\Big] = \Big(\frac{m}{2} - r\Big)G^\alpha_{\dot{A},m+r} \ , \tag{B.2e}$$

$$\Big[L_m, J^a_n\Big] = -nJ^a_{m+n} \ , \tag{B.2f}$$

with the right-moving modes satisfying an analogous set of relations. We will not have need for the full contracted large $\mathcal{N} = 4$ superconformal algebra of the D1-D5 CFT, but this can nonetheless be found in Appendix A of [82] or Appendix A.4 of [79] with the

same conventions. We do, however, give our conventions for the realisation of part of this algebra in terms of the free fermions $\psi^{\alpha A}$ with modes $d_r^{\alpha A}$, and the free bosons $\partial X_{A\dot{A}}$ with modes $\alpha_{A\dot{A},n}$. The mode expansions are given by

$$\partial X_{A\dot{A}}(z) = -i\sum_n z^{-n-1}\,\alpha_{A\dot{A},n}\ , \tag{B.3a}$$

$$\psi^{\alpha A}(z) = \sum_r z^{-r-1/2}\,d_r^{\alpha A}\ , \tag{B.3b}$$

and the brackets are

$$\Big[\alpha_{A\dot{A},n}, \alpha_{B\dot{B},m}\Big] = -n\frac{c}{6}\epsilon_{AB}\,\epsilon_{\dot{A}\dot{B}}\,\delta_{n+m,0}\ , \tag{B.4a}$$

$$\Big\{d_r^{\alpha A}, d_s^{\beta B}\Big\} = -\frac{c}{6}\epsilon^{\alpha\beta}\epsilon^{AB}\delta_{r+s,0}\ , \tag{B.4b}$$

and likewise for the right-moving fields.

B.1.2 Relations involving the twist operator $\sigma_2^{\alpha\bar{\alpha}}$

In the main lifting calculation of Section 5.6, we will have need of the following relations involving the twist operator $\sigma^{\alpha\bar{\alpha}}$ and the supersymmetry modes

$$\begin{aligned} G^{+(0)}_{\dot{A},-\frac{1}{2}}\sigma^{+\bar{\alpha}} = 0 \quad &, \quad G^{-(0)}_{\dot{A},-\frac{1}{2}}\sigma^{-\bar{\alpha}} = 0\ , \\ \bar{G}^{+(0)}_{\dot{A},-\frac{1}{2}}\sigma^{\alpha+} = 0 \quad &, \quad \bar{G}^{-(0)}_{\dot{A},-\frac{1}{2}}\sigma^{\alpha-} = 0\ . \end{aligned} \tag{B.5}$$

On top of these, we also have the relations

$$G^{-(0)}_{\dot{A},-\frac{1}{2}}\sigma^{+\bar{\alpha}} = -G^{+(0)}_{\dot{A},-\frac{1}{2}}\sigma^{-\bar{\alpha}} \quad , \quad \bar{G}^{-(0)}_{\dot{A},-\frac{1}{2}}\sigma^{\alpha+} = -\bar{G}^{+(0)}_{\dot{A},-\frac{1}{2}}\sigma^{\alpha-}\ . \tag{B.6}$$

These can be proved by the following chain of logic

$$G^{-(0)}_{\dot{A},-\frac{1}{2}}\sigma^{+\bar{\alpha}} = \Big[J_0^{-(0)}, G^{+(0)}_{\dot{A},-\frac{1}{2}}\Big]\sigma^{+\bar{\alpha}} = J_0^{-(0)}G^{+(0)}_{\dot{A},-\frac{1}{2}}\sigma^{+\bar{\alpha}} - G^{+(0)}_{\dot{A},-\frac{1}{2}}J_0^{-(0)}\sigma^{+\bar{\alpha}} = -G^{+(0)}_{\dot{A},-\frac{1}{2}}\sigma^{-\bar{\alpha}}\ , \tag{B.7}$$

where in the last step we use (B.6) and $J_0^{-(0)}\sigma^{+\bar{\alpha}} = \sigma^{-\bar{\alpha}}$. In all of the above, the superscript (0) refers to the fact that these are the supersymmetry modes of the undeformed theory's generators.

B.1.3 Rules for Hermitian conjugation

Suppose we consider an amplitude on the cylinder, in the NS sector, with the form

$$A = {}_{NS}\langle 0|\,\mathcal{O}^\dagger\Big(\tau = T, \sigma = 0\Big)\mathcal{O}\Big(\tau = -T, \sigma = 0\Big)|0\rangle_{NS}\ . \tag{B.8}$$

Then we should have $A \geq 0$. This requirement helps determine the way Hermitian conjugates are defined in our CFT. Note that contractions between $su(2)$ indices are done using antisymmetric tensors like $\epsilon_{\alpha\beta}$, and this fact gives rise to certain negative signs in the definitions of Hermitian conjugates. For the supercharges, we use the following rules

$$\begin{aligned} \Big(G^+_+(\tau,\sigma)\Big)^\dagger &= -G^-_-(-\tau,\sigma) \quad , \quad \Big(G^+_-(\tau,\sigma)\Big)^\dagger = G^-_+(-\tau,\sigma) \ , \\ \Big(\bar{G}^+_+(\tau,\sigma)\Big)^\dagger &= -\bar{G}^-_-(-\tau,\sigma) \quad , \quad \Big(\bar{G}^+_-(\tau,\sigma)\Big)^\dagger = \bar{G}^-_+(-\tau,\sigma) \ , \end{aligned} \tag{B.9}$$

while for the degree-2 twist operators, our conventions are

$$\Big(\sigma^{--}(\tau,\sigma)\Big)^\dagger = -\sigma^{++}(-\tau,\sigma) \quad , \qquad \Big(\sigma^{-+}(\tau,\sigma)\Big)^\dagger = \sigma^{+-}(-\tau,\sigma) \ . \tag{B.10}$$

With these choices, we find for the Gava-Narain type operators

$$\bar{G}^{+(P)\dagger}_{+,0} = -\bar{G}^{-(P)}_{-,0} \quad , \qquad \bar{G}^{+(P)\dagger}_{-,0} = \bar{G}^{-(P)}_{+,0} \ . \tag{B.11}$$

We also use a set of 'notational conventions' regarding the twist operators that drastically help in writing out the computations. A twist operator acts on both the left and right sectors, since it is a geometric deformation of the 2-dimensional spacetime on which the CFT lives. Thus strictly speaking, we cannot separate an operator like $\sigma^{\alpha\bar{\alpha}}$ into a σ^α for the left-mover and a $\bar{\sigma}^{\bar{\alpha}}$ for the right-mover. However, we would still like such a separation for ease of writing out expressions and to then be able to combine left- and right-moving terms consistently at the end. Attempting such a consistent separation encounters a difficulty with the signs to be used in Hermitian conjugation. This can be seen by considering the expression (B.8) with $\mathcal{O} = \sigma^+$. Suppose we choose a Hermitian conjugation convention of $(\sigma^+)^\dagger = \sigma^-$. We would then find that ${}_{NS}\langle 0|\, \sigma^-(T,0)\, \sigma^+(-T,0)\, |0\rangle_{NS} > 0$. However, since the OPE has the form

$$\sigma^\alpha(z)\, \sigma^\beta(0) \sim \frac{\epsilon^{\alpha\beta}}{z} \ , \tag{B.12}$$

we would expect ${}_{NS}\langle 0|\, \sigma^+(T,0)\, \sigma^-(-T,0)\, |0\rangle_{NS} < 0$. This contradicts the fact that $(\sigma^-)^\dagger = \sigma^+$. It turns out that there is no consistent choice of Hermitian conjugation for a 'left' part of the twist operator. For our purposes, however, we never require the use of Hermitian conjugations of the split twist operators and so we can neglect this issue here. This leaves us two options for conventions that yield consistent recombined formulae. We can either use the slightly unnatural-looking conventions

$$\langle \sigma^+ \sigma^- \rangle = 1 \quad , \quad \langle \bar{\sigma}^+ \bar{\sigma}^- \rangle = -1 \ , \tag{B.13}$$

or the left/right symmetric conventions

$$\langle \sigma^+ \sigma^- \rangle = 1 \quad , \quad \langle \bar{\sigma}^+ \bar{\sigma}^- \rangle = 1 \ . \tag{B.14}$$

We choose the latter option, however, in doing so it is also necessary to add the prescription that when the left and right parts are brought back together, an extra minus sign should be included per usage of one of the above inner products.

B.2 Transformation rules under spectral flow

In this appendix we derive the conditions for an operator $\mathcal{O}(w_0)$, with J^3 charge m, to transform under a spectral flow, at $\tilde{w}$ and by η units, as

$$\mathcal{O}(w_0) \to \left(e^{w_0} - e^{\tilde{w}}\right)^{-\eta m} \mathcal{O}(w_0) \ , \tag{B.15}$$

as discussed in Section B.15. Given a particular representation of the $\mathcal{N} = 4$ superconformal algebra (B.2), specified by the value of the central charge and the dimension and J^3 charge of the ground state, the currents will be written in terms of a set of fundamental fields $\{\mathcal{O}^{(i)}\}$. In general this will be a mixture of bosons and fermions. In this paper we have in mind the $c = 6$ representation with ground-state dimension and charge $h = m = 0$, in which case we have four free bosons $\partial X_{A\dot{A}}$ and four free fermions $\psi^{\alpha A}$ with periodicities relevant for the NS algebra. Thus in this representation $i = 1, \ldots, 8$. Spectral flow then acts on these fundamental fields by changing the periodicity of the fermions in the manner of (B.15). Since the fundamental bosons have $m = 0$, we can then write that collectively for the fundamental fields

$$\mathcal{O}^{(i)}(w_0) \to \left(e^{w_0} - e^{\tilde{w}}\right)^{-\eta m_i} \mathcal{O}^{(i)}(w_0) \ . \tag{B.16}$$

B.2.1 Operators on the cylinder

An arbitrary field in the spectrum $\mathcal{O}_{\text{cyl}}(w_0)$ on the cylinder will be made out of a number of modes $\mathcal{O}^{(i)}_{-n_i}$ of the fundamental fields $\mathcal{O}^{(i)}_{\text{cyl}}(w_0)$, schematically written in the form

$$\mathcal{O}_{\text{cyl}}(w_0) = \sum_b C^b_{i_1,\ldots,i_p} \, \mathcal{O}^{(i_1)}_{-n_1} \cdots \mathcal{O}^{(i_p)}_{-n_p} \ , \tag{B.17}$$

for some set of coefficients $C^b_{i_1,\ldots,i_p}(w_0)$. The mode expansions of the fundamental fields can be written as

$$\mathcal{O}^{(i)}_{\text{cyl}}(w_0) = \sum_n (-i)^{N_i} \, w_0^{n-h_i} \, \mathcal{O}^{(i)}_{-n} \ , \tag{B.18}$$

with N_i being 0 or 1 if $\mathcal{O}^{(i)}$ is fermionic or bosonic respectively. In (B.18) $n \in \mathbb{Z}$ or $n \in \mathbb{Z} + \frac{1}{2}$ depending on the choice[1] of $\mathcal{O}^{(i)}$. We will therefore look at the effect of spectral flow on a composite field by studying the effect on one term in (B.17), or more precisely, on the combination of modes

$$\mathcal{O}^{\{i\}}_{\{n\}} \equiv \mathcal{O}^{(i_1)}_{-n_1} \cdots \mathcal{O}^{(i_p)}_{-n_p} \ . \tag{B.19}$$

A given mode in B.19 can be written as a contour integral of its field around the insertion point w_0

$$\mathcal{O}^{(i)}_{-n} = \oint_{C_{w_0}} \frac{dw}{2\pi i} \, (w - w_0)^{h_i - n - 1} \, i^{N_i} \, \mathcal{O}^{(i)}_{\rm cyl}(w) \ , \tag{B.20}$$

which transforms under spectral flow (around $w = -\infty$) by η units as

$$\mathcal{O}^{(i)}_{-n} \to \mathcal{O}^{\eta(i)}_{-n} \equiv \oint_{C_{w_0}} \frac{dw}{2\pi i} \, (w - w_0)^{h_i - n - 1} \, i^{N_i} \, e^{-\eta m_i w} \, \mathcal{O}^{(i)}_{\rm cyl}(w) \ , \tag{B.21}$$

where (B.16) has been used with $\tilde{w} = -\infty$. This spectrally flowed mode can then be written as

$$\begin{aligned} \mathcal{O}^{\eta(i)}_{-n} &= e^{-\eta m_i w_0} \oint_{C_{w_0}} \frac{dw}{2\pi i} \, (w - w_0)^{h_i - n - 1} \, i^{N_i} \, e^{-\eta m_i (w - w_0)} \, \mathcal{O}^{(i)}_{\rm cyl}(w) \\ &= e^{-\eta m_i w_0} \sum_{k \geq 0} \frac{(-\eta m_i)^k}{k!} \oint_{C_{w_0}} \frac{dw}{2\pi i} \, (w - w_0)^{h_i + k - n - 1} \, i^{N_i} \, \mathcal{O}^{(i)}_{\rm cyl}(w) \\ &= e^{-\eta m_i w_0} \sum_{k \geq 0} \frac{(-\eta m_i)^k}{k!} \mathcal{O}^{(i)}_{-n+k} \ . \end{aligned} \tag{B.22}$$

Considering now the spectral flow of the product of the p modes given in (B.19), each mode transforms in the same manner leading to

$$\mathcal{O}^{\{i\}}_{\{n\}} \to \mathcal{O}^{\eta\{i\}}_{\{n\}} = e^{-\eta m w_0} \sum_{k_1, \ldots, k_p \geq 0} \frac{(-\eta)^K}{k_1! \cdots k_p!} \, m_{i_1}^{k_1} \cdots m_{i_p}^{k_p} \, \mathcal{O}^{(i_1)}_{-n_1 + k_1} \cdots \mathcal{O}^{(i_p)}_{-n_p + k_p} \ , \tag{B.23}$$

where $m = \sum_{j=1}^{p} m_{i_j}$ and $K = \sum_{j=1}^{p} k_j$. In order to write $\mathcal{O}^{\eta\{i\}}_{\{n\}}$ in terms of an operator acting on $\mathcal{O}^{\{i\}}_{\{n\}}$, we will have use for the action of J^3_1 on a mode of a fundamental field

$$J^3_1 \, \mathcal{O}^{(i)}_{-n} |0\rangle_{NS} = m_i \, \mathcal{O}^{(i)}_{-n+1} |0\rangle_{NS} \ , \tag{B.24}$$

which can then be easily generalised to

$$\left(J^3_1\right)^k \mathcal{O}^{(i)}_{-n} |0\rangle_{NS} = (m_i)^k \, \mathcal{O}^{(i)}_{-n+k} |0\rangle_{NS} \ . \tag{B.25}$$

[1] In the NS sector of the theory fermions are anti-periodic on the cylinder and periodic on the plane, with the reverse being true in the R sector. This leads to fermions having half-integer modes in the NS sector and integer modes in the R sector.

One further generalisation of (B.25) is to the case

$$(J_1^3)^k \, \mathcal{O}^{\{i\}}_{\{n\}} |0\rangle_{NS} = \left(J_1^3\right)^k \mathcal{O}^{(i_1)}_{-n_1} \cdots \mathcal{O}^{(i_p)}_{-n_p} |0\rangle_{NS} \ . \tag{B.26}$$

For $p = 1$ this is exactly (B.25), whereas for $p = 2$ we find

$$\begin{aligned}
\left(J_1^3\right)^k \mathcal{O}^{(i_1)}_{-n_1} \mathcal{O}^{(i_2)}_{-n_2} |0\rangle_{NS} &= \left(J_1^3\right)^{k-1} \left[J_1^3, \mathcal{O}^{(i_1)}_{-n_1} \mathcal{O}^{(i_2)}_{-n_2}\right] |0\rangle_{NS} \\
&= \left(J_1^3\right)^{k-1} \left(m_{i_1} \mathcal{O}^{(i_1)}_{-n_1+1} \mathcal{O}^{(i_2)}_{-n_2} + m_{i_2} \mathcal{O}^{(i_1)}_{-n_1} \mathcal{O}^{(i_2)}_{-n_2+1}\right) |0\rangle_{NS} \\
&= \sum_{k_1=0}^{k} {}^k C_{k_1} \, m_{i_1}^{k_1} m_{i_2}^{k-k_1} \, \mathcal{O}^{(i_1)}_{-n_1+k_1} \mathcal{O}^{(i_2)}_{-n_2+k-k_1} |0\rangle_{NS} \ .
\end{aligned} \tag{B.27}$$

By analogy with the multinomial theorem one finds the general p case to be

$$(J_1^3)^k \, \mathcal{O}^{\{i\}}_{\{n\}} |0\rangle_{NS} = {\sum_{k_1,\ldots,k_p \geq 0}}' \prod_{j=1}^{p} \frac{k!}{k_j!} \, m_{i_j}^{k_j} \, \mathcal{O}^{(i_j)}_{-n_j+k_j} |0\rangle_{NS} \ , \tag{B.28}$$

where the primed sum is defined as the sum over non-negative $k_1, \ldots, k_p$ subject to the constraint $k_1 + \cdots + k_p = k$. We then immediately find that

$$\begin{aligned}
e^{-\eta J_1^3} \, \mathcal{O}^{\{i\}}_{\{n\}} |0\rangle_{NS} &= \sum_{k=0}^{\infty} \frac{(-\eta)^k}{k!} (J_1^3)^k \, \mathcal{O}^{\{i\}}_{\{n\}} |0\rangle_{NS} \\
&= \sum_{k=0}^{\infty} \frac{(-\eta)^k}{k!} {\sum_{k_1,\ldots,k_p \geq 0}}' \prod_{j=1}^{p} \frac{k!}{k_j!} \, m_{i_j}^{k_j} \, \mathcal{O}^{(i_j)}_{-n_j+k_j} |0\rangle_{NS} \ .
\end{aligned} \tag{B.29}$$

By considering a p-dimensional lattice of points describing the possible values of the k_j, the primed sum is over a $(p-1)$-dimensional sub-lattice defined by the constraint equation $\sum_j k_j = k$ for some fixed k. The $(p-1)$-dimensional sub-lattices for different values of k have vanishing overlap and so the union of these sub-lattices is equivalent to the p-dimensional lattice. We can thus make the replacement

$$\sum_{k \geq 0} {\sum_{k_1,\ldots,k_p \geq 0}}' \longrightarrow \sum_{k_1,\ldots,k_p \geq 0} \ , \tag{B.30}$$

in (B.29). By comparison with the first line of (B.23) we therefore find

$$\mathcal{O}^{\{i\}}_{\{n\}} |0\rangle_{NS} \to \mathcal{O}^{\eta\{i\}}_{\{n\}} |0\rangle_{NS} = e^{-\eta m w_0} e^{-\eta J_1^3} \, \mathcal{O}^{\{i\}}_{\{n\}} |0\rangle_{NS} \ , \tag{B.31}$$

and so the field (B.17) on the cylinder transforms as

$$\mathcal{O}_{\rm cyl}(w_0) \to e^{-\eta m w_0} e^{-\eta J_1^3} \, \mathcal{O}_{\rm cyl}(w_0) \ . \tag{B.32}$$

Therefore, if the field on the cylinder is to transform in the manner of (B.15) for all η (with $\tilde{w} = -\infty$) it is sufficient that it satisfies the condition

$$J_1^3 \, \mathcal{O}_{\text{cyl}}(w_0) = 0 \ . \tag{B.33}$$

B.2.2 Operators on the plane

In the lifting calculation of Section 5.3.4, we also require the analogous condition to (B.33) for the plane. This is because once the component amplitudes in (5.35) are mapped to the covering space (the t-plane) we are left with amplitudes of the form $\langle \mathcal{O} S^- S^+ \mathcal{O} \rangle$ with $S^\pm$ being spin fields. These spin field insertions can then be resolved by appropriate spectral flows around each of them. Knowledge of the transformation of the operators $\mathcal{O}$ under spectral flow is then necessary.

Instead of finding the most general condition for a field in the spectrum to transform with a simple phase factor, we focus on the two special cases required in the main body of this paper. Those cases are when $\mathcal{O}$ is either a superconformal primary ϕ or is of the form $G^+_{-,-\frac{1}{2}}\phi$. We proceed in the following steps, firstly for $\mathcal{O} = \phi$:

(1) The correlator on the t-plane $\langle \phi(\infty) S^-(t_2) S^+(t_1) \phi(-a) \rangle$ is mapped to the t'-plane, where the two are related by

$$t' = \frac{t - t_1}{t - t_2} \quad , \quad \frac{dt'}{dt} = \frac{t_1 - t_2}{(t - t_2)^2} = \frac{(t'-1)^2}{t_1 - t_2} \ . \tag{B.34}$$

This gives the correlator $f_1 \langle \phi(1) S^-(\infty) S^+(0) \phi(T) \rangle$.

(2) The t'-plane is mapped to the w'-cylinder, with

$$t' = e^{w'} \ , \tag{B.35}$$

giving the correlator $f_1 f_2 \langle \phi(0) S^-(\infty) S^+(-\infty) \phi(\log T) \rangle$.

(3) Due to the insertions of the spin fields on the cylinder being at $w' = \pm\infty$, they are equivalent to the whole cylinder being in the Ramond sector. Now on the w'-cylinder we spectral flow by $\eta = -1$ at $w = -\infty$. This gives the correlator $f_1 f_2 f_3 \langle \phi(0) \phi(\log T) \rangle$.

(4) We now map back to the t'-plane yielding $f_1 f_2 f_3 f_4 \langle \phi(1) \phi(T) \rangle$.

(5) And then to the original t-plane giving the correlator $f_1 f_2 f_3 f_4 f_5 \langle \phi(\infty) \phi(-a) \rangle$.

(6) This final correlator can then be compared with the 'naïve' plane spectral flow transformation of the t-plane correlator. For a spectral flow around $t = \tilde{t}$ by η units,

this would be

$$\mathcal{O}(t_0) \to (t_0 - \tilde{t}\,)^{-\eta m}\mathcal{O}(t_0)\ , \tag{B.36}$$

by analogy with (B.15). For this t-plane correlator, we would need a spectral flow by $\eta = -1$ around $t = t_1$ under which, using (B.36), the operators transform as

$$S^+(t_1) \to \mathbb{I}\ , \tag{B.37a}$$
$$S^-(t_2) \to (t_2 - t_1)^{-1/2} S^-(t_2)\ , \tag{B.37b}$$
$$\phi(-a) \to (-a - t_1)^m \phi(-a)\ , \tag{B.37c}$$
$$\phi(\infty) = \lim_{t\to\infty} t^{2h}\phi(t) \to \lim_{t\to\infty} t^{2h}(t - t_1)^m \phi(t)\ . \tag{B.37d}$$

This is then followed by a spectral flow by $\eta = +1$ around $t = t_2$ under which

$$S^-(t_2) \to \mathbb{I}\ , \tag{B.38a}$$
$$\phi(-a) \to (-a - t_2)^{-m}\phi(-a)\ , \tag{B.38b}$$
$$\phi(t) \to (t - t_2)^{-m}\phi(t)\ , \tag{B.38c}$$

giving, in total

$$\begin{aligned}\langle\phi(\infty)S^-(t_2)S^+(t_1)\phi(-a)\rangle \longrightarrow \lim_{t\to\infty}(t_2 - t_1)^{-\frac{1}{2}}\, t^{2h}\frac{(-a - t_1)^m}{(-a - t_2)^m}\frac{(t - t_1)^m}{(t - t_2)^m}\langle\phi(t)\phi(-a)\rangle \\ = (t_2 - t_1)^{-\frac{1}{2}}\left(\frac{a + t_1}{a + t_2}\right)^m \langle\phi(\infty)\phi(-a)\rangle\ .\end{aligned} \tag{B.39}$$

We proceed through steps (1) to (5) above and compare the result with (B.39) in step (6). We require the result that a conformal primary of dimension h transforms under the map $z \to z'$ homogeneously as

$$\mathcal{O}(z) \to \widetilde{\mathcal{O}}(z') = \left(\frac{dz'}{dz}\right)^{-h}\mathcal{O}(z)\ , \tag{B.40}$$

and that a spin field transforms like a dimension $h = \frac{1}{4}$ primary. For ease of notation we define $\widetilde{\mathcal{O}}(z') \equiv \mathcal{O}(z')$. Therefore, one finds that from the map to the t'-plane in step (1)

we have the transformations

$$\phi(t=\infty) = \lim_{t\to\infty} t^{2h}\frac{(t_1-t_2)^h}{(t-t_2)^{2h}}\,\phi(t'=1) = (t_1-t_2)^h\phi(t'=1)\ , \tag{B.41a}$$

$$\phi(t=-a) = \frac{(t_1-t_2)^h}{(-a-t_2)^{2h}}\,\phi(t'=T)\ , \tag{B.41b}$$

$$\begin{aligned} S^-(t_2) = \lim_{t'\to\infty}\left(\frac{(t'-1)^2}{t_1-t_2}\right)^{\frac{1}{4}} S^-(t') &= \lim_{t'\to\infty}(t')^{\frac{1}{2}}(t_2-t_1)^{-\frac{1}{4}}(-1)^{\frac{1}{4}}S^-(t') \\ &= (t_2-t_1)^{-\frac{1}{4}}(-1)^{\frac{1}{4}}S^-(\infty)\ , \end{aligned} \tag{B.41c}$$

$$S^+(t_1) = \lim_{t\to t_1}\left(\frac{t_1-t_2}{(t-t_2)^2}\right)^{\frac{1}{4}} S^+(t'=0) = (t_2-t_1)^{-\frac{1}{4}}(-1)^{-\frac{1}{4}}S^+(t'=0)\ , \tag{B.41d}$$

where $T \equiv \frac{a+t_1}{a+t_2}$. In total this step gives the factor

$$f_1 = \frac{(t_2-t_1)^{2h-\frac{1}{2}}}{(a+t_2)^{2h}}\ . \tag{B.42}$$

In step (2), the map to the w'-cylinder we have the transformations

$$\phi(t'=1) = \phi(w'=0)\ , \tag{B.43a}$$

$$\phi(t'=T) = T^{-h}\phi(w'=\log T)\ , \tag{B.43b}$$

$$S^-(t'=\infty) = \lim_{t',w'\to\infty}(t')^{\frac{1}{2}}(t')^{-\frac{1}{4}}S^-(w') = \lim_{w'\to\infty}\left(e^{w'}\right)^{\frac{1}{4}}S^-(w') = \lim_{w'\to\infty}\left(e^{w'}\right)^{-\frac{1}{4}}S^-(w'=\infty)\ , \tag{B.43c}$$

$$S^+(t'=0) = \lim_{t'\to\infty}(t')^{-\frac{1}{4}}S^+(w') = \lim_{w'\to-\infty}\left(e^{w'}\right)^{-\frac{1}{4}}S^+(w') = \lim_{w'\to\infty}\left(e^{w'}\right)^{\frac{1}{4}}S^+(w'=-\infty)\ . \tag{B.43d}$$

So we have the overall factor from step (2) as

$$f_2 = T^{-h}\ . \tag{B.44}$$

We now spectral flow on the cylinder by $\eta=-1$ around $w'=-\infty$, removing the spin fields and giving the transformations (using (B.15))

$$\phi(w'=0) \to \phi(w'=0)\ , \tag{B.45a}$$

$$\phi(w'=\log T) \to e^{m\log T}\phi(w'=\log T) = T^m\phi(w'=\log T)\ . \tag{B.45b}$$

These transformations are justified because $J_1^3\phi=0$ on the cylinder for a superconformal primary. Therefore we have the step (3) factor

$$f_3 = T^m\ . \tag{B.46}$$

Mapping back to the t'-plane we get

$$\phi(w'=0) = \lim_{w'\to 0}(t')^h \phi(t') = \phi(t'=1) \ , \tag{B.47a}$$

$$\phi(w'=\log T) = T^h \phi(t'=T) \ , \tag{B.47b}$$

and so the step (4) factor

$$f_4 = T^h \ . \tag{B.48}$$

Finally mapping to the t-plane gives us

$$\phi(t'=1) = \lim_{t'\to 1}\left(\frac{(t-t_2)^2}{t_1-t_2}\right)^h \phi(t) = \lim_{t\to\infty} t^{2h}(t_1-t_2)^{-h}\phi(t) = (t_1-t_2)^{-h}\phi(t=\infty) \ , \tag{B.49a}$$

$$\phi(t'=T) = \left(\frac{(-a-t_2)^2}{t_1-t_2}\right)^h \phi(t=-a) \ , \tag{B.49b}$$

giving the step (5) factor

$$f_5 = \left(\frac{-a-t_2}{t_1-t_2}\right)^{2h} \ . \tag{B.50}$$

Multiplying the factors from each step, we have

$$f_1 f_2 f_3 f_4 f_5 = \frac{(t_2-t_1)^{2h-\frac{1}{2}}}{(a+t_2)^{2h}} T^{-h} T^m T^h \left(\frac{-a-t_2}{t_1-t_2}\right)^{2h} = T^m (t_2-t_1)^{-\frac{1}{2}} = \left(\frac{a+t_1}{a+t_2}\right)^m (t_2-t_1)^{-\frac{1}{2}}. \tag{B.51}$$

Thus we see that this is precisely equal to the 'naïve' t-plane spectral flow of the correlator from step (6) above. This then concludes that: a superconformal primary transforms under spectral flow on the plane by the simple phase relation B.36.

In our paper we also need the transformation rule for $G^+_{-,-\frac{1}{2}}\phi$ which is not a superconformal primary but does satisfy $J_1^3\, G^+_{-,-\frac{1}{2}}\phi = 0$ on the cylinder. So we can again use its cylinder transformation under spectral flow to derive its plane transformation. It is first important to start on the w-cylinder and map to the z-plane via $w \to z(w) = e^w$ and then from the z-plane to the t-plane in order to check that the initial and final states on the w-cylinder yield two insertions of $G^+_{-,-\frac{1}{2}}\phi$ on the covering space. Under the map

$w \to z$, using (B.40) we have

$$\begin{aligned}\left(G^+_{-,-\frac{1}{2}}\phi\right)(w=-\infty) &= \lim_{w\to-\infty}\oint_{C_w}\frac{d\tilde{w}}{2\pi i}\,G^+_-(\tilde{w})\phi(w) = \lim_{z\to 0} z^h\oint_{C_z}\frac{d\tilde{z}}{2\pi i}\,\tilde{z}^{\frac{1}{2}}G^+_-(\tilde{z})\phi(z)\\ &= \lim_{z\to 0} z^{h+\frac{1}{2}}\left(G^+_{-,-\frac{1}{2}}\phi\right)(z=0)\ ,\end{aligned} \tag{B.52}$$

$$\begin{aligned}\left(G^-_{+,\frac{1}{2}}\phi\right)(w=\infty) &= \lim_{w\to\infty}\left(e^w\right)^{2h+1}\oint_{C_w}\frac{d\tilde{w}}{2\pi i}\,G^+_-(\tilde{w})\phi(w) = \lim_{z\to\infty} z^{3h+1}\oint_{C_z}\frac{d\tilde{z}}{2\pi i}\,\tilde{z}^{\frac{1}{2}}G^+_-(\tilde{z})\phi(z)\\ &= \lim_{z\to\infty} z^{h+\frac{1}{2}}\left(G^-_{+,\frac{1}{2}}\phi\right)(z=\infty)\ .\end{aligned} \tag{B.53}$$

Thus when mapping the correlator from the w-cylinder to the z-plane the zero and diverging factors above cancel and the G modes remain the same. Then under the map $z \to t(z)$, where

$$z(t) = \frac{(t+a)(t+b)}{t} \quad , \quad \frac{dz}{dt} = \frac{(t-t_1)(t-t_2)}{t^2}\ , \tag{B.54}$$

with $t_1 = -\sqrt{ab}$ and $t_2 = \sqrt{ab}$, we have firstly (the fields are taken to be on the first sheet, $z = 0^{(1)}$ and $z = \infty^{(1)}$ respectively)

$$\begin{aligned}\left(G^+_{-,-\frac{1}{2}}\phi\right)(z=0^{(1)}) &= \lim_{t\to-a}\left(\frac{dt}{dz}\right)^h\oint_{C_t}\frac{d\tilde{t}}{2\pi i}\left(\frac{\tilde{t}^{\,2}}{(\tilde{t}-t_1)(\tilde{t}-t_2)}\right)^{\frac{1}{2}}G^+_-(\tilde{t})\phi(t)\\ &= \lim_{t\to-a}\frac{a^2}{(a+t_1)^h(a+t_2)^h}\oint_{C_t}\frac{d\tilde{t}}{2\pi i}\,\frac{t}{\sqrt{t^2-ab}}\Big[1+O(\tilde{t}-t)\Big]G^+_-(\tilde{t})\phi(t)\\ &= \frac{-a^3}{a^{h+\frac{1}{2}}(a-b)^{h+\frac{1}{2}}}\left(G^+_{-,-\frac{1}{2}}\phi\right)(t=-a)\ ,\end{aligned} \tag{B.55}$$

and secondly

$$\begin{aligned}\left(G^-_{+,\frac{1}{2}}\phi\right)(z=\infty^{(1)}) &= \lim_{t\to\infty}\Big(z(t)\Big)^{2h+1}\left(\frac{dt}{dz}\right)^h\oint_{C_t}\frac{d\tilde{t}}{2\pi i}\left(\frac{d\tilde{t}}{d\tilde{z}}\right)^{\frac{1}{2}}G^+_-(\tilde{t})\phi(t)\\ &= \lim_{t\to\infty}\frac{[(t+a)(t+b)]^{2h+1}}{t[(t-t_1)(t-t_2)]^h}\oint_{C_t}\frac{d\tilde{t}}{2\pi i}\left(\frac{\tilde{t}^{\,2}}{(\tilde{t}-t_1)(\tilde{t}-t_2)}\right)^{\frac{1}{2}}G^+_-(\tilde{t})\phi(t)\\ &= \lim_{t\to\infty} t^{2h+1}\oint_{C_t}\frac{d\tilde{t}}{2\pi i}\,\frac{t}{\sqrt{t^2-ab}}\Big[1+O(\tilde{t}-t)\Big]G^+_-(\tilde{t})\phi(t)\\ &= \left(G^-_{+,\frac{1}{2}}\phi\right)(t=\infty)\ .\end{aligned} \tag{B.56}$$

So on the t-plane we still have only the one G mode around each ϕ. This is clearly a special case due to ϕ being a superconformal primary. Now we can repeat the steps (1) to (6) of the argument above with $G\phi$ instead of ϕ. From the case done in detail above, we see that all of the Jacobians picked up by the two ϕ cancel. The same will hold for

$G\phi$ since it is also a conformal primary and will have just a shifted Jacobian (B.40) with $h \to h + \frac{1}{2}$. The Jacobians and spectral flow transformations of the spin fields will be the same as before, leaving us just to calculate the spectral flow transformations of the $G\phi$ on the w'-cylinder.

Since $J_1^3\, G^+_{-,-\frac{1}{2}}\phi = 0$ we can again use the simple transformation on the cylinder under spectral flow, giving for step (3)

$$\Big(G^+_{-,-\frac{1}{2}}\phi\Big)(w'=0) \to \Big(G^+_{-,-\frac{1}{2}}\phi\Big)(w'=0)\ , \tag{B.57}$$

$$\Big(G^+_{-,-\frac{1}{2}}\phi\Big)(w'=\log T) \to e^{(m+\frac{1}{2})\log T}\Big(G^+_{-,-\frac{1}{2}}\phi\Big)(w'=\log T) = T^{m+\frac{1}{2}}\Big(G^+_{-,-\frac{1}{2}}\phi\Big)(w'=\log T)\ . \tag{B.58}$$

Putting all of the factors together gives the t-plane correlator

$$\begin{aligned}\langle\Big(G^-_{+,\frac{1}{2}}\phi\Big)(\infty)S^-(t_2)S^+(t_1)\Big(G^+_{-,-\frac{1}{2}}\phi\Big)(-a)\rangle &= T^{m+\frac{1}{2}}(t_2-t_1)^{-\frac{1}{2}}\langle\Big(G^-_{+,\frac{1}{2}}\phi\Big)(\infty)\Big(G^+_{-,-\frac{1}{2}}\phi\Big)(-a)\rangle \\ &= \left(\frac{a+t_1}{a+t_2}\right)^{m+\frac{1}{2}}(t_2-t_1)^{-\frac{1}{2}}\langle\Big(G^-_{+,\frac{1}{2}}\phi\Big)(\infty)\Big(G^+_{-,-\frac{1}{2}}\phi\Big)(-a)\rangle\ ,\end{aligned} \tag{B.59}$$

which is again exactly the 'naïve' spectral flow on the plane given by (B.39) with $m \to m+\frac{1}{2}$. This then concludes that: for a superconformal primary ϕ, the field $G^+_{-,-\frac{1}{2}}\phi$ also transforms under spectral flow on the plane by the simple phase relation (B.36).

B.3 Choice of the deformation operator

Before proceeding to calculating lifts for specific states, let us review our choice of the deformation operator. As seen in Section 4.2, the deformation of the CFT off the orbifold point is given by adding a deformation operator D to the Lagrangian where D has conformal dimensions $(h,\bar{h}) = (1,1)$ in order to be marginal. There are 20 exactly marginal operators of the theory to choose from; 16 of these correspond to T^4 shape and complex structure moduli, while the remaining 4 are superdescendants of the twist-2 chiral/anti-chiral primaries $\sigma^{\alpha\bar{\alpha}}$ of the orbifold theory. The former set of moduli are in a sense 'trivial deformations', whereas the latter four are 'non-trivial'— they break the higher-spin symmetry found at the orbifold point and move the theory towards the region with a semi-classical gravity description. A choice of D that is a singlet under all of the $SU(2)$ symmetries at the orbifold point is

$$D = \frac{1}{4}\epsilon^{\dot{A}\dot{B}}\epsilon_{\alpha\beta}\epsilon_{\bar{\alpha}\bar{\beta}}\, G^{\alpha}_{\dot{A},-\frac{1}{2}}\bar{G}^{\bar{\alpha}}_{\dot{B},-\frac{1}{2}}\sigma^{\beta\bar{\beta}}\ . \tag{B.60}$$

Here G and $\bar{G}$ are respectively the left- and right-moving supercharge modes at the *orbifold point*, *i.e.* at $\lambda = 0$. This choice of deformation operator is the projection onto the singlet representation of $SU(2)_2$; the remaining three non-trivial deformation operators form the triplet projection. The $SO(4)_I$-invariant operator (B.60) corresponds to turning on the dual string tension. The operator $\sigma^{\alpha\bar{\alpha}}$ is made by adding R-charge to the bare twist operator σ_2 to form a chiral/anti-chiral primary. In the particular case of $k = 2$, this is done using only spin fields [81] to give

$$\sigma^{\alpha\bar{\alpha}} = S_2^{\alpha}\bar{S}_2^{\bar{\alpha}}\sigma_2 \ . \tag{B.61}$$

These spin fields change the fermion boundary conditions around their insertion points.[2]

B.4 Choice of ground states

Consider the Ramond sector of the theory. On a k-twisted component string, the ground state is degenerate in both the left and right sectors. There are 4 Ramond ground states for the left sector per value of k, which we denote as

$$|0^-\rangle_R^{[k]} \quad , \quad |0^+\rangle_R^{[k]} = d_0^{++[k]}d_0^{+-[k]}|0^-\rangle_R^{[k]} \quad , \quad |0\rangle_R^{[k]} = d_0^{++[k]}|0^-\rangle_R^{[k]} \quad , \quad |\tilde{0}\rangle_R^{[k]} = d_0^{+-[k]}|0^-\rangle_R^{[k]} \ , \tag{B.62}$$

where the $d_n^{\alpha A}$ are the Ramond-sector modes of the canonical free fermions of the orbifold CFT. Our conventions for the anti-commutator for these fermion modes is given in (B.4b). A similar set of 4 Ramond ground states exist for the right sector. The superscript $[k]$ denotes that these states are in the k-twisted sector of the theory. Thus for any component string (*i.e.* for each twisted sector), there are 16 Ramond-Ramond ground states. We will label these ground states as $|L, R\rangle_R^{[k]}$ where $L = 0^-, 0^+, 0, \tilde{0}$ and $R = \bar{0}^-, \bar{0}^+, \bar{0}, \bar{\tilde{0}}$. The Ramond-Ramond ground state dimensions are $h = \bar{h} = \frac{c}{24}$ and with the conventions of Section B.2, they are related by a spectral flow of $\eta = +1$ to chiral primaries in the NS sector. The Ramond ground state $|0^-\rangle_R^{[1]}$ is then the spectral flow of the NS vacuum $|0\rangle_{NS}$, having $h = m = 0$. While we use only the first of the Ramond ground states given in (B.62) for the particular lifting computation described in this thesis, we hope to return to the more general problem for arbitrary ground states in future work (see Section 7).

[2]The operator σ_2 twists together two copies, i and j, of the $c = 6$ seed CFT, which in an S_N-invariant form is written as $\sigma_2 = \sum_{\substack{i,j=1 \\ j<i}}^{N} \sigma_{(ij)}$.

B.5 Mapping amplitude relations to lift relations

In Section 5.7 we found interesting relations between amplitudes of certain states and those of their descendants (see (5.136) and (5.144)). Here we describe how to map those amplitude relations to relations between the lifts of states. Consider the following simplified form of the definition of lift given in (5.29)

$$E^{(2)}(\phi) = \kappa \frac{A(\phi)}{\langle\phi|\,|\phi\rangle} \ , \tag{B.63}$$

where κ is a constant and $A(\phi)$ is an amplitude related to (5.30) with initial and final states being ϕ. Taking, for instance, the amplitude relation

$$A(\phi) = 2h_\psi A(\psi) \ , \tag{B.64}$$

obtained in Section 5.7.1 by considering the states $|\psi\rangle$ and $|\phi\rangle = L_{-1}\,|\psi\rangle$ and using (B.63) we find that at the level of lifts

$$E^{(2)}(\phi) = 2h_\psi \frac{\langle\psi|\,|\psi\rangle}{\langle\phi|\,|\phi\rangle}\, E^{(2)}(\psi) \ . \tag{B.65}$$

Since the norm of the descendant state is given by

$$\langle\phi|\phi\rangle = \langle\psi|L_1L_{-1}|\psi\rangle = 2\langle\psi|L_0|\psi\rangle = 2h_\psi\langle\psi|\psi\rangle \ , \tag{B.66}$$

we can simplify (B.65) to give the lifting relation

$$E^{(2)}(\phi) = E^{(2)}(\psi) \ , \tag{B.67}$$

i.e. that the lift of a state satisfying $L_1|\psi\rangle = 0$ is equal to the lift of its L_{-1} descendant. Equally one can start with the amplitude relation

$$A^{\beta\alpha}_{\dot B\dot A}(\widetilde\phi) = K^{\beta\alpha}_{\dot B\dot A} A(\widetilde\psi) \ , \tag{B.68}$$

with $K^{\beta\alpha}_{\dot B\dot A}$ defined in (5.145) obtained by considering the states $|\widetilde\psi\,\rangle$ and $|\widetilde\phi\,\rangle^\alpha_{\dot A} = G^\alpha_{\dot A,-\frac12}|\widetilde\psi\,\rangle$. This can be recast in terms of lifts using (B.63) and imposing that the index β is opposite to α and $\dot B$ opposite to $\dot A$, giving

$$E^{(2)}\big(\widetilde\phi^{\,\alpha}_{\dot A}\big) = K^\alpha_{\dot A}\, \frac{\langle\widetilde\psi\,|\widetilde\psi\,\rangle}{{}^\alpha_{\dot A}\langle\widetilde\phi\,|\widetilde\phi\,\rangle^\alpha_{\dot A}}\, E^{(2)}\big(\widetilde\psi\big) \ , \tag{B.69}$$

where there is no implied summation over the repeated indices α and $\dot A$ and $K^\alpha_{\dot A}$ is defined as $K^{\beta\alpha}_{\dot B\dot A}$ with the above conditions imposed on β and $\dot B$. Since the norm of the descendant

state is given by (there no sum over repeated indices)

$$ {}^{\alpha}_{\dot{A}}\langle\widetilde{\phi}\,|\widetilde{\phi}\rangle^{\alpha}_{\dot{A}} = \langle\widetilde{\psi}\,|\Big(G^{\alpha}_{\dot{A},-\frac{1}{2}}\Big)^{\dagger}G^{\alpha}_{\dot{A},-\frac{1}{2}}|\widetilde{\psi}\,\rangle = K^{\alpha}_{\dot{A}}\langle\widetilde{\psi}\,|\widetilde{\psi}\,\rangle \ , \tag{B.70} $$

we can simplify (B.69) to give the lifting relation

$$ E^{(2)}(\widetilde{\phi}^{\alpha}_{\dot{A}}) = E^{(2)}(\widetilde{\psi}) \ , \tag{B.71} $$

i.e. that the lift of a state satisfying $\Big(G^{\alpha}_{\dot{A},-\frac{1}{2}}\Big)^{\dagger}|\widetilde{\psi}\,\rangle = 0$ is equal to the lift of its $G^{\alpha}_{\dot{A},-\frac{1}{2}}$ descendant.

Given a chosen basis of states for which the lift is being computed, *i.e.* the set used in this paper

$$ \left\{ |\alpha\alpha\rangle_{B\dot{B}A\dot{A}(m,n)} \ , \quad |\alpha d\rangle^{\alpha A}_{B\dot{B}(n,s)} \ , \quad |dd\rangle^{\beta B\alpha A}_{r,s} \right\} , \tag{B.72} $$

the descendant states $|\phi\rangle$ and $|\widetilde{\phi}\rangle^{\alpha}_{\dot{A}}$ can generally be written as a sum of basis states. The lift of the descendant state (the left-hand side of the relations (B.67) and (B.71)) can not then be immediately written in terms of the lifts of basis states from (B.72), which are the data points computed in Section 5.6.

In the case that the descendant state is a sum of two basis states, *i.e.* if we have

$$ |\phi\rangle = |\phi_1\rangle + |\phi_2\rangle \ , \tag{B.73} $$

where $|\phi_1\rangle$ and $|\phi_2\rangle$ are states in the set (B.72), then we have

$$ \begin{aligned} E^{(2)}(\phi) &= E^{(2)}(\phi_1+\phi_2) \\ &= \kappa\,\frac{A(\phi_1+\phi_2)}{\langle\phi_1+\phi_2|\phi_1+\phi_2\rangle} \\ &= \kappa\,\frac{A(\phi_1)+A(\phi_2)+2A(\phi_1;\phi_2)}{\langle\phi_1|\phi_1\rangle+\langle\phi_2|\phi_2\rangle+2\langle\phi_1|\phi_2\rangle} \\ &= \frac{\langle\phi_1|\phi_1\rangle E^{(2)}(\phi_1)+\langle\phi_2|\phi_2\rangle E^{(2)}(\phi_2)+2\sqrt{\langle\phi_1|\phi_1\rangle\langle\phi_2|\phi_2\rangle}\,E^{(2)}(\phi_1;\phi_2)}{\langle\phi_1|\phi_1\rangle+\langle\phi_2|\phi_2\rangle+2\langle\phi_1|\phi_2\rangle} \ . \end{aligned} \tag{B.74} $$

Here $A(\phi_f;\phi_i)$ is a generalization of the integrated amplitude $A(\phi)$ used in lifting computations where the initial and final states are not necessarily equal, with $A(\phi_i;\phi_i) = A(\phi_i)$ and $E^{(2)}(\phi_f;\phi_i)$ is the associated lift-like quantity defined analogously to (B.63) as

$$ E^{(2)}(\phi_f;\phi_i) \equiv \kappa\,\frac{A(\phi_f;\phi_i)}{\sqrt{\langle\phi_f|\,|\phi_f\rangle\,\langle\phi_i|\,|\phi_i\rangle}} \ . \tag{B.75} $$

Thus in the case that the descendant state splits as (B.73) then (B.74) can be used as the left-hand side of the relations (B.67) and (B.71). This argument can easily be generalized

to the case of $|\phi\rangle = \sum_{k=1}^{K} |\phi_k\rangle$ with the states $|\phi_k\rangle$ being in the set (B.72).

Bibliography

[1] S. W. Hawking, "Particle Creation by Black Holes," *Commun. Math. Phys.* **43** (1975) 199–220.

[2] J. D. Bekenstein, "Black holes and the second law," *Lett. Nuovo Cim.* **4** (1972) 737–740.

[3] A. Strominger and C. Vafa, "Microscopic origin of the Bekenstein-Hawking entropy," *Phys. Lett. B* **379** (1996) 99–104, arXiv:hep-th/9601029.

[4] S. D. Mathur, "The Fuzzball proposal for black holes: An Elementary review," *Fortsch. Phys.* **53** (2005) 793–827, arXiv:hep-th/0502050.

[5] S. D. Mathur and M. Mehta, "The Fuzzball Paradigm," arXiv:2412.09495 [hep-th].

[6] S. D. Mathur, A. Saxena, and Y. K. Srivastava, "Constructing 'hair' for the three charge hole," *Nucl. Phys. B* **680** (2004) 415–449, arXiv:hep-th/0311092.

[7] O. Lunin, "Adding momentum to D-1 - D-5 system," *JHEP* **04** (2004) 054, arXiv:hep-th/0404006.

[8] S. Giusto, S. D. Mathur, and A. Saxena, "Dual geometries for a set of 3-charge microstates," *Nucl. Phys. B* **701** (2004) 357–379, arXiv:hep-th/0405017.

[9] S. Giusto, S. D. Mathur, and A. Saxena, "3-charge geometries and their CFT duals," *Nucl. Phys. B* **710** (2005) 425–463, arXiv:hep-th/0406103.

[10] V. S. Rychkov, "D1-D5 black hole microstate counting from supergravity," *JHEP* **01** (2006) 063, arXiv:hep-th/0512053.

[11] V. Jejjala, O. Madden, S. F. Ross, and G. Titchener, "Non-supersymmetric smooth geometries and D1-D5-P bound states," *Phys. Rev. D* **71** (2005) 124030, arXiv:hep-th/0504181.

[12] V. Cardoso, O. J. C. Dias, J. L. Hovdebo, and R. C. Myers, "Instability of non-supersymmetric smooth geometries," *Phys. Rev. D* **73** (2006) 064031, arXiv:hep-th/0512277.

[13] B. D. Chowdhury and S. D. Mathur, "Radiation from the non-extremal fuzzball," *Class. Quant. Grav.* **25** (2008) 135005, arXiv:0711.4817 [hep-th].

[14] B. D. Chowdhury and S. D. Mathur, "Pair creation in non-extremal fuzzball geometries," *Class. Quant. Grav.* **25** (2008) 225021, arXiv:0806.2309 [hep-th].

[15] B. Chakrabarty, D. Turton, and A. Virmani, "Holographic description of non-supersymmetric orbifolded D1-D5-P solutions," *JHEP* **11** (2015) 063, arXiv:1508.01231 [hep-th].

[16] S. D. Mathur and M. Mehta, "The universality of black hole thermodynamics," *Int. J. Mod. Phys. D* **32** no. 14, (2023) 2341003, arXiv:2305.12003 [hep-th].

[17] S. D. Mathur and M. Mehta, "The universal thermodynamic properties of extremely compact objects," *Class. Quant. Grav.* **41** no. 23, (2024) 235011, arXiv:2402.13166 [hep-th].

[18] B. Guo, M. R. R. Hughes, S. D. Mathur, and M. Mehta, "Universal lifting in the D1-D5 CFT," *JHEP* **10** (2022) 148, arXiv:2208.07409 [hep-th].

[19] M. R. R. Hughes, S. D. Mathur, and M. Mehta, "Lifting of superconformal descendants in the D1-D5 CFT," *JHEP* **04** (2024) 129, arXiv:2311.00052 [hep-th].

[20] M. R. R. Hughes, S. D. Mathur, and M. Mehta, "Lifting of two-mode states in the D1-D5 CFT," arXiv:2309.03321 [hep-th].

[21] R. d'Inverno, *Introducing Einstein's relativity*. 1992.

[22] C. W. Misner, K. S. Thorne, and J. A. Wheeler, *Gravitation*. W. H. Freeman, San Francisco, 1973.

[23] S. W. Hawking and G. F. R. Ellis, *The Large Scale Structure of Space-Time*. Cambridge Monographs on Mathematical Physics. Cambridge University Press, 1973.

[24] R. M. Wald, *General Relativity*. Chicago Univ. Pr., Chicago, USA, 1984.

[25] S. M. Carroll, *Spacetime and Geometry: An Introduction to General Relativity*. Cambridge University Press, 7, 2019.

[26] M. Blau, "Lecture notes on general relativity," 2017. http://www.blau.itp.unibe.ch/newlecturesGR.pdf. Accessed April 22, 2025.

[27] K. Schwarzschild, "On the Gravitational Field of a Mass Point According to Einstein's Theory," *Abh. Konigl. Preuss. Akad. Wissenschaften Jahre 1906,92, Berlin,1907* **1916** (Jan., 1916) 189–196. https://ui.adsabs.harvard.edu/abs/1916AbhKP1916..189S.

[28] A. Fabbri and J. Navarro-Salas, *Modeling Black Hole Evaporation*. Published by Imperial College Press and distributed by World Scientific Publishing Co., 2005. https://www.worldscientific.com/doi/abs/10.1142/p378.

[29] J. R. Oppenheimer and H. Snyder, "On continued gravitational contraction," *Phys. Rev.* **56** (Sep, 1939) 455–459. https://link.aps.org/doi/10.1103/PhysRev.56.455.

[30] T. Regge and J. A. Wheeler, "Stability of a schwarzschild singularity," *Phys. Rev.* **108** (1957) 1063–1069.

[31] A. S. Eddington, "A Comparison of Whitehead's and Einstein's Formulæ," *Nature* **113** no. 2832, (Feb., 1924) 192. https://ui.adsabs.harvard.edu/abs/1924Natur.113..192E.

[32] D. Finkelstein, "Past-Future Asymmetry of the Gravitational Field of a Point Particle," *Physical Review* **110** no. 4, (May, 1958) 965–967. https://ui.adsabs.harvard.edu/abs/1958PhRv..110..965F.

[33] M. D. Kruskal, "Maximal extension of schwarzschild metric," *Phys. Rev.* **119** (Sep, 1960) 1743–1745. https://link.aps.org/doi/10.1103/PhysRev.119.1743.

[34] G. Szekeres, "On the singularities of a riemannian manifold," *Publ. Math. Debrecen* **7** (1960) 285–301. http://old.phys.huji.ac.il/~barak_kol/Courses/Black-holes/reading-papers/Szekeres.pdf.

[35] H. Reissner, "Über die eigengravitation des elektrischen feldes nach der einsteinschen theorie," *Annalen der Physik* **355** no. 9, (1916) 106–120.

[36] G. Nordström, "On the Energy of the Gravitation field in Einstein's Theory," *Koninklijke Nederlandse Akademie van Wetenschappen Proceedings Series B Physical Sciences* **20** (Jan., 1918) 1238–1245. https://ui.adsabs.harvard.edu/abs/1918KNAB...20.1238N.

[37] R. P. Kerr, "Gravitational field of a spinning mass as an example of algebraically special metrics," *Phys. Rev. Lett.* **11** (1963) 237–238.

[38] M. Visser, "The kerr spacetime: A brief introduction," 2008. https://arxiv.org/abs/0706.0622.

[39] R. Penrose and R. M. Floyd, "Extraction of Rotational Energy from a Black Hole," *Nature Physical Science* **229** no. 6, (Feb., 1971) 177–179. https://ui.adsabs.harvard.edu/abs/1971NPhS..229..177P.

[40] Y. B. Zel'Dovich, "Generation of Waves by a Rotating Body," *Soviet Journal of Experimental and Theoretical Physics Letters* **14** (Aug., 1971) 180.

[41] M. Bañados, C. Teitelboim, and J. Zanelli, "Black hole in three-dimensional spacetime," *Physical Review Letters* **69** no. 13, (Sept., 1992) 1849–1851. http://dx.doi.org/10.1103/PhysRevLett.69.1849.

[42] G. D. Birkhoff, *Relativity and Modern Physics*. Harvard University Press, 1923.

[43] W. Israel, "Event horizons in static vacuum space-times," *Phys. Rev.* **164** (Dec, 1967) 1776–1779. https://link.aps.org/doi/10.1103/PhysRev.164.1776.

[44] D. C. Robinson, "Uniqueness of the kerr black hole," *Phys. Rev. Lett.* **34** (1975) 905–906.

[45] P. O. Mazur, "Proof of uniqueness of the kerr-newman black hole solution," *J. Phys. A* **15** (1982) 3173–3180.

[46] H. M. z. Hagen, "On the analyticity of static vacuum solutions of einstein's equations," *Mathematical Proceedings of the Cambridge Philosophical Society* **67** no. 2, (1970) 415–421.

[47] R. Ruffini and J. A. Wheeler, "Introducing the black hole," *Phys. Today* **24** no. 1, (1971) 30.

[48] J. D. Bekenstein, "Black hole hair: twenty–five years after," 1996. https://arxiv.org/abs/gr-qc/9605059.

[49] W. Israel, "Event horizons in static electrovac space-times," *Commun. Math. Phys.* **8** (1968) 245–260.

[50] B. Carter, "Axisymmetric black hole has only two degrees of freedom," *Phys. Rev. Lett.* **26** (1971) 331–333.

[51] R. M. Wald, "Final states of gravitational collapse," *Phys. Rev. Lett.* **26** (Jun, 1971) 1653–1655. https://link.aps.org/doi/10.1103/PhysRevLett.26.1653.

[52] N. E. Mavromatos, "Eluding the no-hair conjecture for black holes," 1996. https://arxiv.org/abs/gr-qc/9606008.

[53] S. W. Hawking, "Black holes in general relativity," *Commun. Math. Phys.* **25** (1972) 152–166.

[54] N. D. Birrell and P. C. W. Davies, *Quantum Fields in Curved Space*. Cambridge Monographs on Mathematical Physics. Cambridge Univ. Press, Cambridge, UK, 2, 1984.

[55] S. A. Fulling, *Aspects of Quantum Field Theory in Curved Spacetime*. London Mathematical Society Student Texts. Cambridge University Press, 1989.

[56] R. M. Wald, *Quantum Field Theory in Curved Space-Time and Black Hole Thermodynamics*. Chicago Lectures in Physics. University of Chicago Press, Chicago, IL, 1995.

[57] L. E. Parker and D. J. Toms, *Quantum Field Theory in Curved Spacetime: Quantized Fields and Gravity*. Cambridge University Press, 2009.

[58] S. D. Mathur, "Gian course on the black hole information paradox." https://www.asc.ohio-state.edu/mathur.16/gian/bhdivershortft.pdf, 2018. Short review on black hole information paradox.

[59] P. Di Francesco, P. Mathieu, and D. Senechal, *Conformal Field Theory*. Graduate Texts in Contemporary Physics. Springer-Verlag, New York, 1997.

[60] M. R. Gaberdiel, "An introduction to conformal field theory," *Rept. Prog. Phys.* **63** (2000) 607–667, arXiv:hep-th/9910156.

[61] P. Ginsparg, "Applied conformal field theory," in *Fields, Strings and Critical Phenomena (Les Houches, 1988)*, E. Brézin and J. Zinn-Justin, eds., pp. 1–168. North-Holland, 1990. arXiv:hep-th/9108028.

[62] R. Blumenhagen and E. Plauschinn, *Introduction to conformal field theory: with applications to String theory*, vol. 779. 2009.

[63] J. M. Bardeen, B. Carter, and S. W. Hawking, "The four laws of black hole mechanics," *Commun. Math. Phys.* **31** (1973) 161–170.

[64] J. D. Bekenstein, "Black holes and entropy," *Phys. Rev. D* **7** (1973) 2333–2346.

[65] J. D. Bekenstein, "Generalized second law of thermodynamics in black hole physics," *Phys. Rev. D* **9** (1974) 3292–3300.

[66] M. Heusler, *Black Hole Uniqueness Theorems*. Cambridge Lecture Notes in Physics. Cambridge University Press, 1996.

[67] J. R. David, G. Mandal, and S. R. Wadia, "Microscopic formulation of black holes in string theory," *Physics Reports* **369** no. 6, (Nov., 2002) 549–686. http://dx.doi.org/10.1016/S0370-1573(02)00271-5.

[68] J. M. Maldacena, "The Large N limit of superconformal field theories and supergravity," *Adv. Theor. Math. Phys.* **2** (1998) 231–252, arXiv:hep-th/9711200.

[69] C. G. Callan and J. M. Maldacena, "D-brane approach to black hole quantum mechanics," *Nucl. Phys. B* **472** (1996) 591–610, arXiv:hep-th/9602043.

[70] D. Youm, "Black holes and solitons in string theory," *Physics Reports* **316** no. 1–3, (Aug., 1999) 1–232. http://dx.doi.org/10.1016/S0370-1573(99)00037-X.

[71] M. Cvetic, "Non-extreme black holes from non-extreme intersecting m-branes," *Nuclear Physics B* **478** no. 1–2, (Oct., 1996) 181–198. http://dx.doi.org/10.1016/0550-3213(96)00411-7.

[72] J. L. Cardy, "Operator Content of Two-Dimensional Conformally Invariant Theories," *Nucl. Phys. B* **270** (1986) 186–204.

[73] S. D. Mathur, "Tunneling into fuzzball states," *Gen. Rel. Grav.* **42** (2010) 113–118, arXiv:0805.3716 [hep-th].

[74] B. Guo, S. Hampton, and S. D. Mathur, "Can we observe fuzzballs or firewalls?," *JHEP* **07** (2018) 162, arXiv:1711.01617 [hep-th].

[75] I. Kanitscheider, K. Skenderis, and M. Taylor, "Fuzzballs with internal excitations," *JHEP* **06** (2007) 056, arXiv:0704.0690 [hep-th].

[76] B. D. Chowdhury and A. Virmani, "Modave Lectures on Fuzzballs and Emission from the D1-D5 System," in *5th Modave Summer School in Mathematical Physics*. 1, 2010. arXiv:1001.1444 [hep-th].

[77] I. Bena, E. J. Martinec, S. D. Mathur, and N. P. Warner, "Fuzzballs and Microstate Geometries: Black-Hole Structure in String Theory," arXiv:2204.13113 [hep-th].

[78] J. M. Maldacena, G. W. Moore, and A. Strominger, "Counting BPS black holes in toroidal Type II string theory," arXiv:hep-th/9903163.

[79] S. Hampton, S. D. Mathur, and I. G. Zadeh, "Lifting of D1-D5-P states," *JHEP* **01** (2019) 075, arXiv:1804.10097 [hep-th].

[80] O. Lunin and S. D. Mathur, "Correlation functions for M**N / S(N) orbifolds," *Commun. Math. Phys.* **219** (2001) 399–442, arXiv:hep-th/0006196.

[81] O. Lunin and S. D. Mathur, "Metric of the multiply wound rotating string," *Nucl. Phys. B* **610** (2001) 49–76, arXiv:hep-th/0105136.

[82] B. Guo and S. D. Mathur, "Lifting of level-1 states in the D1D5 CFT," *JHEP* **03** (2020) 028, arXiv:1912.05567 [hep-th].

[83] B. Guo and S. Hampton, "Partial Spectral Flow in the D1D5 CFT," arXiv:2112.10573 [hep-th].

[84] H. A. Buchdahl, "General relativistic fluid spheres," *Phys. Rev.* **116** (Nov, 1959) 1027–1034. https://link.aps.org/doi/10.1103/PhysRev.116.1027.

[85] S. D. Mathur, "What prevents gravitational collapse in string theory?," *Int. J. Mod. Phys. D* **25** no. 12, (2016) 1644018, arXiv:1609.05222 [hep-th].

[86] I. Bah, P. Heidmann, and P. Weck, "Schwarzschild-like topological solitons," *JHEP* **08** (2022) 269, arXiv:2203.12625 [hep-th].

[87] P. Heidmann, "Non-BPS floating branes and bubbling geometries," *JHEP* **02** (2022) 162, arXiv:2112.03279 [hep-th].

[88] P. Heidmann and M. Mehta, "Electromagnetic Entrapment in Gravity," arXiv:2312.11607 [hep-th].

[89] P. Heidmann, "Half the Schwarzschild Entropy From Strominger and Vafa," arXiv:2312.12496 [hep-th].

[90] I. Bah and P. Heidmann, "Geometric Resolution of Schwarzschild Horizon," arXiv:2303.10186 [hep-th].

[91] F. R. Tangherlini, "Schwarzschild field in n dimensions and the dimensionality of space problem," *Il Nuovo Cimento* **27** (1963) 636–651.

[92] P. Candelas, "Vacuum Polarization in Schwarzschild Space-Time," *Phys. Rev. D* **21** (1980) 2185–2202.

[93] W. G. Unruh, "Notes on black hole evaporation," *Phys. Rev. D* **14** (1976) 870.

[94] D. G. Boulware, "Quantum Field Theory in Schwarzschild and Rindler Spaces," *Phys. Rev. D* **11** (1975) 1404.

[95] J. B. Hartle and S. W. Hawking, "Path Integral Derivation of Black Hole Radiance," *Phys. Rev. D* **13** (1976) 2188–2203.

[96] S. M. Christensen, "Vacuum Expectation Value of the Stress Tensor in an Arbitrary Curved Background: The Covariant Point Separation Method," *Phys. Rev. D* **14** (1976) 2490–2501.

[97] S. A. Fulling, "Alternative Vacuum States in Static Space-Times with Horizons," *J. Phys. A* **10** (1977) 917–951.

[98] S. M. Christensen and S. A. Fulling, "Trace Anomalies and the Hawking Effect," *Phys. Rev. D* **15** (1977) 2088–2104.

[99] S. Chandrasekhar, *An Introduction to the Study of Stellar Structure*. Dover Books on Astronomy Series. Dover Publications, Incorporated, 2012. https://books.google.com/books?id=joWn8s2BF04C.

[100] M. Colpi, S. L. Shapiro, and I. Wasserman, "Boson stars: Gravitational equilibria of self-interacting scalar fields," *Phys. Rev. Lett.* **57** (Nov, 1986) 2485–2488. https://link.aps.org/doi/10.1103/PhysRevLett.57.2485.

[101] C. Alcock, E. Farhi, and A. Olinto, "Strange Stars," **310** (Nov., 1986) 261.

[102] S. R. Coleman, "Q-balls," *Nucl. Phys. B* **262** no. 2, (1985) 263. [Addendum: Nucl.Phys.B 269, 744 (1986)].

[103] J. J. Drake *et al.*, "Is RXJ1856.5-3754 a quark star?," *Astrophys. J.* **572** (2002) 996–1001, arXiv:astro-ph/0204159.

[104] V. Cardoso and P. Pani, "Testing the nature of dark compact objects: a status report," *Living Rev. Rel.* **22** no. 1, (2019) 4, arXiv:1904.05363 [gr-qc].

[105] W. Z. Chua and N. Afshordi, "Electromagnetic albedo of quantum black holes," *Journal of High Energy Physics* **2021** no. 7, (July, 2021) . http://dx.doi.org/10.1007/JHEP07(2021)006.

[106] D. R. Mayerson, "Fuzzballs and Observations," *Gen. Rel. Grav.* **52** no. 12, (2020) 115, arXiv:2010.09736 [hep-th].

[107] E. T. Copson, "On electrostatics in a gravitational field," *Proceedings of the Royal Society of London. Series A* **118** (1928) 184–194. http://doi.org/10.1098/rspa.1928.0044.

[108] R. S. Hanni and R. Ruffini, "Lines of force of a point charge near a schwarzschild black hole," *Phys. Rev. D* **8** (Nov, 1973) 3259–3265. https://link.aps.org/doi/10.1103/PhysRevD.8.3259.

[109] B. Linet, "Electrostatics and magnetostatics in the schwarzschild metric," *Journal of Physics A: Mathematical and General* **9** no. 7, (Jul, 1976) 1081. https://dx.doi.org/10.1088/0305-4470/9/7/010.

[110] S. D. Mathur, "The VECRO hypothesis," arXiv:2001.11057 [hep-th].

[111] S. D. Mathur, "The elastic vacuum," *Int. J. Mod. Phys. D* **30** no. 14, (2021) 2141001, arXiv:2105.06963 [hep-th].

[112] S. D. Mathur, "The secret structure of the gravitational vacuum," *Int. J. Mod. Phys. D* **33** no. 15, (2024) 2440002, arXiv:2405.08945 [hep-th].

[113] S. D. Mathur, "Space cannot stretch too \it fast," arXiv:2505.10368 [hep-th].

[114] Y. Chen, H. W. Lin, and S. H. Shenker, "BPS chaos," *SciPost Phys.* **18** no. 2, (2025) 072, arXiv:2407.19387 [hep-th].